

AFFDL-TR-77-79, Vol I

# Flaw Growth in Complex Structure Volume I — Technical Discussion

Lockheed-California Company  
A Division of Lockheed Corporation  
Burbank, California 91520

DECEMBER 1977

Final Report

May 1975 — September 1977

Distribution Statement

Approved for public release; distribution unlimited.

Prepared for

Air Force Flight Dynamics Laboratory  
Air Force Systems Command  
Wright-Patterson AFB, Ohio 45433

20071128032

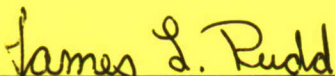
AD-A056372

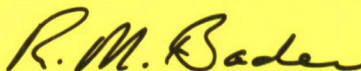
## NOTICE

When Government drawings, specifications, or other data are used for any purpose other than in connection with a definitely related Government procurement operation, the United States Government thereby incurs no responsibility nor any obligation whatsoever; and the fact that the government may have formulated, furnished, or in any way supplied the said drawings, specifications, or other data, is not to be regarded by implication or otherwise as in any manner licensing the holder or any other person or corporation, or conveying any rights or permission to manufacture, use, or sell any patented invention that may in any way be related thereto.

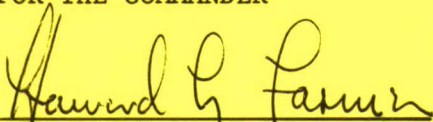
This report has been reviewed by the Information Office (IO) and is releasable to the National Technical Information Service (NTIS). At NTIS, it will be available to the general public, including foreign nations.

This technical report has been reviewed and is approved for publication.

  
\_\_\_\_\_  
JAMES L. RUDD  
Project Engineer

  
\_\_\_\_\_  
ROBERT M. BADER, Chief  
Structural Integrity Branch  
Structural Mechanics Division

FOR THE COMMANDER

  
\_\_\_\_\_  
HOWARD L. FARMER, Colonel, USAF  
Chief, Structural Mechanics Division

Copies of this report should not be returned unless return is required by security considerations, contractual obligations, or notice on a specific document.

| REPORT DOCUMENTATION PAGE   |                       | READ INSTRUCTIONS<br>BEFORE COMPLETING FORM   |
|---|-----------------------|---|
| 1. REPORT NUMBER<br>AFFDL-TR-77-79, Vol I   | 2. GOVT ACCESSION NO. | 3. RECIPIENT'S CATALOG NUMBER   |
| 4. TITLE (and Subtitle)<br>FLAW GROWTH IN COMPLEX STRUCTURE<br>FINAL REPORT, VOLUME I<br>TECHNICAL DISCUSSION   |                       | 5. TYPE OF REPORT<br>Technical - Final<br>PERIOD COVERED<br>May 1975 - September 1977 |
|   |                       | 6. PERFORMING ORG. REPORT NUMBER<br>LR 28272, Vol. I                                  |
| 7. AUTHOR(s)<br>T. R. Brussat and S. T. Chiu, Lockheed-California Company, and M. Creager, Del West Engineering, Chatsworth, California   |                       | 8. CONTRACT OR GRANT NUMBER(s)<br>F33615-75-C-3090                                    |
| 9. PERFORMING ORGANIZATION NAME AND ADDRESS<br>LOCKHEED-CALIFORNIA COMPANY<br>BURBANK, CALIFORNIA 91520   |                       | 10. PROGRAM ELEMENT, PROJECT, TASK AREA & WORK UNIT NUMBERS<br>486U-02-09             |
| 11. CONTROLLING OFFICE NAME AND ADDRESS<br>Air Force Flight Dynamics Laboratory<br>Air Force Systems Command, (FBE)<br>Wright-Patterson AFB, Ohio 45433   |                       | 12. REPORT DATE<br>December 1977  |
|   |                       | 13. NUMBER OF PAGES   |
| 14. MONITORING AGENCY NAME & ADDRESS (if different from Controlling Office)   |                       | 15. SECURITY CLASS. (of this report)<br><br>UNCLASSIFIED                              |
|   |                       | 15a. DECLASSIFICATION/DOWNGRADING SCHEDULE  |
| 16. DISTRIBUTION STATEMENT (of this Report)   |                       |   |
| 17. DISTRIBUTION STATEMENT (of the abstract entered in Block 20, if different from Report)  |                       |   |
| 18. SUPPLEMENTARY NOTES   |                       |   |
| 19. KEY WORDS (Continue on reverse side if necessary and identify by block number)<br>Fracture Mechanics, Fatigue, Structure, Testing, Damage Tolerance, Crack Propagation, Analysis, Stress Intensity Factors, Stress Severity Factors, Fasteners, Friction, Joints, Crack Arrest, Spectrum Loading, Crack Retardation   |                       |   |
| 20. ABSTRACT (Continue on reverse side if necessary and identify by block number)<br>Fatigue crack growth testing and analysis were conducted to evaluate the effects of initial flaw location and multiplicity on fatigue crack growth life and element failure sequence in multiple element, mechanically fastened metallic structure. The test program, which included 68 precracked structural specimens consisting of 26 joints and 42 stringer-reinforced panels, is described in detail. Stress intensity factor analyses and stress severity factor equations and the results of baseline static, fatigue, crack growth, and fracture tests are |                       |   |

## 20. ABSTRACT

presented for use in making crack growth predictions for the structural specimens. Procedures are described for machining, precracking, assembling and testing the structural specimens. The test results and corresponding analytical results are presented and compared. With respect to the test results for precracked joints the following effects are discussed: fastener torque, faying surface friction, friction under the fastener head, single and multiple initial flaws, fretting, transverse bending, flush-head and protruding-head fasteners, and spectrum loading effects. With respect to the results for precracked stringer-reinforced panels, the following are discussed: longitudinal splice versus continuous skin, initial flaw locations, single or multiple initial flaws, presence of continuing damage flaws, crack growth in a tee or angle stringer, transverse bending, load shedding effects, crack repair with a torqued Hi-lok in a stop-drilled hole, spectrum loading, fracture surface marking, stress level, and crack path. A specimen-by-specimen tabulation of the test data and graphic comparison to the predicted crack growth are contained in Volume II. Volume III is a concise summary of the program.

## FOREWORD

This experimental and analytical research program reported herein was the responsibility of the Structural Methods Group of the Lockheed-California Company from 12 May 1975 to 12 Sept. 1977. The work was performed for the Air Force Flight Dynamics Laboratory to fulfill the objectives of Contract F33615-75-C-3093.

J. L. Rudd was the AFFDL technical monitor, and his continuous interest in every detail was of great technical benefit to the program.

The care that was taken in specimen preparation and testing led to a reliable set of test results. Specimen fabrication and precracking were coordinated by W. P. Renslen with assistance from W. F. Kerwin, both of Del West Engineering. Testing, under the direction of D. E. Pettit, was carried out by the Lockheed Rye Canyon Fatigue Laboratory personnel including F. M. Pickel, D. Black, C. J. Looper, L. Reed, L. Silvas and C. L. Spratt.

Special thanks are in order for W. G. Browne, who provided continuous guidance in budget management and program administration throughout the course of the program. E. K. Walker, J. C. Wordsworth, and J. C. Ekvall are thanked for their valuable contributions in the area of program management as well as their technical consultation. Others in the Stress Department who made significant technical contributions were L. Bakow, W. L. Rakness, P. Schall and R. C. Smith. R. J. Van Ness and the Publication Services Department are appreciated for coordinating the layout, typing and artwork for the final report.

## TABLE OF CONTENTS

| Section |   | Page |
|---------|---|------|
| I       | INTRODUCTION  | 1    |
| 1.      | BACKGROUND  | 1    |
| 2.      | PROGRAM OBJECTIVES  | 5    |
| 3.      | SUMMARY OF THE FINAL REPORT                                   | 6    |
| II      | TEST PROGRAM  | 8    |
| 1.      | INTRODUCTION  | 8    |
| 2.      | SPECIMENS AND INITIAL DAMAGE FOR PHASE I TESTS                | 11   |
| 2.1     | Precracked Joints   | 11   |
| 2.2     | Stringer Reinforced Specimens                                 | 18   |
| 3.      | PHASE II TESTS  | 22   |
| 3.1     | Flight-Simulation Spectrum Tests                              | 22   |
| 3.2     | Joint Tests for Fastener Head Effects and Two-Bay Panel Tests | 25   |
| 4.      | STRAIN GAGING   | 27   |
| 5.      | BASELINE TEST SUMMARY   | 27   |
| III     | ANALYSIS METHODS  | 31   |
| 1.      | BACKGROUND  | 31   |
| 1.1     | Summary of Analysis Approach                                  | 31   |
| 1.2     | Continuing Damage for a Crack Growing Along a Row of Holes    | 34   |
| 1.3     | Some Observations on the Notch Root Neighborhood              | 40   |
| 2.      | PREDICTING THE REINITIATION OF AN ARRESTED CRACK              | 43   |
| 2.1     | Modified Stress Severity Factor Equation                      | 44   |
| 2.2     | Stress Concentration Factor $k_{tb}$ for Fastener Load        | 45   |
| 2.3     | Stress Concentration Factor $k_{tg}$ for Remote Loading       | 49   |
| 2.4     | Baseline Fatigue Data Required                                | 52   |
| 2.5     | Cumulative Damage Computation of Crack Initiation Times       | 52   |

## TABLE OF CONTENTS (Continued)

| Section |  | Page |
|---------|--|------|
| 3.      | STRESS INTENSITY FACTOR ANALYSIS                     | 53   |
| 3.1     | The Fundamental $K_I$ Solutions                      | 54   |
| 3.2     | Correction Factors for Adjacent Holes and Edges      | 56   |
| 3.2.1   | Crack at or Near a Free Edge                         | 56   |
| 3.2.2   | Crack in a Finite Width Strip                        | 57   |
| 3.2.3   | Crack Approaching a Hole                             | 59   |
| 3.3     | Corner Flaw at a Hole                                | 61   |
| 3.3.1   | Transition Criterion                                 | 61   |
| 3.3.2   | Experimental Verification                            | 62   |
| 3.4     | Fastener Load Effects on $K_I$                       | 65   |
| 3.4.1   | Fastener Loads Near the Crack                        | 65   |
| 3.4.2   | Fastener Load at the Crack Origin                    | 67   |
| 3.4.3   | Correction for Fastener Tilting                      | 70   |
| 4.      | FASTENER LOAD ANALYSIS IN STRUCTURAL JOINT SPECIMENS | 72   |
| 4.1     | Approach   | 72   |
| 4.2     | Computation of Effective Fastener Stiffness          | 73   |
| 4.3     | Computation of Fastener Loads Using NASTRAN          | 75   |
| 4.3.1   | Modeling Techniques                                  | 75   |
| IV      | BASELINE TEST RESULTS                                | 78   |
| 1.      | TENSILE TESTS  | 78   |
| 2.      | FATIGUE CRACK INITIATION TESTS                       | 79   |
| 2.1     | The S-N Curve for the 3/16 Inch Sheet                | 85   |
| 2.2     | Material Comparisons                                 | 86   |
| 2.3     | Fatigue Tests of Fastener Specimens                  | 89   |
| 3.      | FATIGUE CRACK PROPAGATION TESTS                      | 91   |
| 4.      | FRACTURE TESTS                                       | 99   |
| 4.1     | R-Curve Test Procedure                               | 99   |
| 4.2     | Test Results   | 104  |
| 5.      | MARKING CYCLE TESTS                                  | 105  |
| 6.      | PREDICTED AND ACTUAL BASELINE SPECTRUM DATA          | 107  |

## TABLE OF CONTENTS (Continued)

| Section | Page  |
|---------|---|
| V       | CRACK GROWTH PREDICTIONS                                    |
|         | 112   |
| 1.      | DOUBLE LAP JOINT SPECIMENS                                  |
|         | 112   |
| 1.1     | Modeling for the Double Lap Shear Joint Specimen            |
|         | 112   |
| 1.2     | Stress Intensities for the Double Lap Shear Joint Specimens |
|         | 118   |
| 1.2.1   | Crack in the First Ligament                                 |
|         | 118   |
| 1.2.2   | Double Unsymmetric Cracking at the Precracked Hole          |
|         | 121   |
| 2.      | SINGLE LAP JOINT SPECIMENS                                  |
|         | 122   |
| 3.      | TEE-REINFORCED CONTINUOUS SKIN SPECIMENS                    |
|         | 125   |
| 3.1     | Stress Intensity Factors for the Skin                       |
|         | 127   |
| 3.2     | Stress Intensity Factor in the Tee Stringer                 |
|         | 127   |
| 3.3     | Crack Reinitiation  |
|         | 131   |
| 4.      | TEE-REINFORCED SPLIT-SKIN SPECIMENS                         |
|         | 132   |
| 5.      | EDGE-STRINGER SPECIMENS                                     |
|         | 133   |
| 5.1     | Initial Outside Crack in the Angle Stringer                 |
|         | 134   |
| 5.2     | Initial Outside Crack in Skin                               |
|         | 136   |
| 5.3     | Initial Inside Crack in the Angle Stringer                  |
|         | 137   |
| 5.4     | Initial Inside Crack in the Skin                            |
|         | 139   |
| 6.      | CRACK GROWTH LIFE PREDICTIONS FOR SPECTRUM LOADING          |
|         | 140   |
| VI      | SPECIMEN FABRICATION AND TEST PROCEDURES                    |
|         | 144   |
| 1.      | FABRICATION OF TEST SPECIMENS                               |
|         | 144   |
| 1.1     | Joints  |
|         | 145   |
| 1.2     | Stringer-Reinforced Panels                                  |
|         | 147   |
| 2.      | TEST PROCEDURES   |
|         | 153   |
| 2.1     | Crack Length Monitoring                                     |
|         | 154   |
| 2.2     | Control and Measurement of Transverse Deflections           |
|         | 155   |
| VII     | TEST RESULTS FOR PRECRACKED JOINTS                          |
|         | 161   |
| 1.      | TEST OBSERVATIONS FROM PHASE I                              |
|         | 161   |
| 1.1     | Double Lap Joint Tests                                      |
|         | 163   |
| 1.2     | Single Lap Joint Tests                                      |
|         | 173   |

# TABLE OF CONTENTS (Continued)

| Section    | Page   |
|------------|--|
| 2.         | DISCUSSION OF RESULTS FROM PHASE I 179   |
| 2.1        | Insensitivity to Initial Flaw Conditions 183                                     |
| 2.2        | Effects of Fastener-Head Friction on Crack Arrest 186                            |
| 2.3        | Faying Surface Friction Effects 192  |
| 2.4        | Effects of Faying Surface Sealant, Environment,<br>and Compressive Stressing 198 |
| 3.         | PHASE II TESTS OF JOINTS 201   |
| 3.1        | Fastener Head Investigation in Single Lap Joints 201                             |
| 3.2        | Spectrum Tests of Joint Specimens 204  |
| 4.         | SUMMARY OF CONCLUSIONS FROM TESTS OF JOINTS 210                                  |
| VIII       | STRINGER-REINFORCED PANELS 213   |
| 1.         | CENTER STRINGER SPECIMENS 213  |
| 1.1        | Panel Strains and Lateral Deflections 213  |
| 1.2        | Test Results, Continuous Skin Specimens 214                                      |
| 1.3        | Test Results, Split Skin Specimens 225   |
| 1.4        | Empirical Stress Intensity Analysis for the<br>Tee Stringer 232                  |
| 1.5        | Spectrum Tests (Phase II) 232  |
| 2.         | EDGE STRINGER SPECIMEN 240   |
| 2.1        | Strain Gage Survey 240   |
| 2.2        | Discussion of Results 242  |
| 3.         | TWO-BAY SPECIMENS 247  |
| 3.1        | Strain Gage Results 247  |
| 3.2        | Discussion of Test Results 251   |
| 4.         | SUMMARY OF CONCLUSIONS FROM TESTS OF STRINGER-<br>REINFORCED PANELS 256          |
| APPENDIX A | SUMMARY OF MIL-A-83444 261   |
| APPENDIX B | SPECIMEN DRAWINGS 267  |
| APPENDIX C | FATIGUE TESTS OF CONTINUING DAMAGE FLAWS 274                                     |
|            | REFERENCES 288   |

## LIST OF FIGURES

| Figure |  | Page |
|--------|--|------|
| 1      | Section View (Looking Spanwise) of Upper Skin, Front Spar Cap, and Shear Web                         | 3    |
| 2      | Double Lap Joint Specimen with 0.188-Inch Doublers   | 12   |
| 3      | Double Lap Joint Specimen with 0.094-Inch Doublers   | 13   |
| 4      | Single Lap Joint Specimen  | 14   |
| 5      | Summary of Initial Damage Conditions, Double Lap Joint Specimens                                     | 15   |
| 6      | Summary of Initial Damage Conditions, Single Lap Joint Specimens                                     | 16   |
| 7      | Two-Bay Stringer-Reinforced Specimen   | 19   |
| 8      | The 80-Flight Spectrum Loading Sequence  | 24   |
| 9      | Crack Growth Prediction Method   | 32   |
| 10     | Test Specimen Configuration from Reference 9   | 35   |
| 11     | Test Data from Reference 9   | 37   |
| 12     | Actual and Estimated Crack Reinitiation Periods  | 38   |
| 13     | Elliptical Hole in a Plate   | 40   |
| 14     | Notch Root Neighborhood, Long Elliptical Notch   | 42   |
| 15     | Equivalent Crack and Notch Problems  | 47   |
| 16     | Crack Arrested at a Circular Hole  | 49   |
| 17     | Stress Concentration Factors for Common Notch Configurations   | 51   |
| 18     | Uniform Tension Applied to a Through-Thickness Crack at a Circular Hole                              | 55   |
| 19     | Two Approximately Equivalent Cases (if $a \ll R_o$ )   | 55   |
| 20     | Cracked Semi-Infinite Plate  | 58   |
| 21     | Eccentrically Cracked Strip in Uniform Tension   | 58   |
| 22     | Crack Approaching a Hole   | 60   |
| 23     | Corner Flaw at a Hole in a Plate   | 63   |
| 24     | Corner Crack Tangent to Back Surface   | 63   |
| 25     | Comparison of Experimental and Theoretical Stress Intensity Factors for a Transitioning Corner Crack | 64   |

# LIST OF FIGURES (Continued)

| Figure |  | Page |
|--------|--|------|
| 26     | Point Force in the Cracked Plane of Thickness $t$  | 66   |
| 27     | Stress Intensity Factor for a Crack at a Loaded Hole   | 68   |
| 28     | Four Similar Problems. (Unknown Solution to Problem A is Estimated from Known Solutions to the Others.)          | 69   |
| 29     | Profile Model of the Double Lap Shear Joint Specimen   | 74   |
| 30     | Details of Fastener System Model with a Square Cut-Out   | 76   |
| 31     | $k_t = 3.1$ Coupon   | 82   |
| 32     | Modified CT Specimen   | 82   |
| 33     | High Load Transfer Specimen  | 83   |
| 34     | Reversed and 1-1/2 Dogbone Specimens   | 84   |
| 35     | S-N Curve for 3/16 Inch 7075-T6 Aluminum Sheet, $R = 0.1$  | 87   |
| 36     | Comparison of Fatigue Lives for Various Thicknesses and Product Forms  | 88   |
| 37     | Fatigue Crack Growth Data, 0.188-Inch 7075-T6 Aluminum Sheet, Longitudinal Grain Direction, $R = 0.1$            | 94   |
| 38     | Fatigue Crack Growth Data, 0.188 Inch 7075-T6 Aluminum Sheet, Transverse Grain Direction, $R = 0.1$              | 95   |
| 39     | Fatigue Crack Growth Data, 0.375 Inch 7075-T6 Aluminum Plate, Longitudinal Grain Direction, $R = 0.1$            | 96   |
| 40     | Fatigue Crack Growth Data, 0.094 Inch 7075-T6 Aluminum Sheet, Longitudinal Grain Direction, $R = 0.1$            | 97   |
| 41     | Fatigue Crack Growth Data, 0.188 Inch 7075-T6 Aluminum Tee Extrusion, Two Grain Directions, $R = 0.1$            | 98   |
| 42     | Fatigue Crack Growth Data, 0.25 Inch 7075-T651 Aluminum Angle Extrusion, Longitudinal Grain Direction, $R = 0.1$ | 100  |
| 43     | Summary of Fatigue Crack Growth Data, 7075-T6 Aluminum, $R = 0.1$  | 101  |
| 44     | Compliance Method for R-Curve Testing  | 102  |
| 45     | Typical R-Curve Test Set-Up  | 105  |
| 46     | R-Curves for 7075-T6 Sheet Material  | 106  |
| 47     | Baseline Spectrum Crack Growth Rates for 80-Flight Loading Sequence  | 108  |
| 48     | Baseline Spectrum Crack Initiation Lives for 80-Flight Loading Sequence  | 109  |

## LIST OF FIGURES (Continued)

| Figure |   | Page |
|--------|---|------|
| 49     | NASTRAN Finite Element Model for the Face Plate of the Double Lap Joint                                 | 113  |
| 50     | Typical Distribution of Normalized Fastener Loads for the Double Lap Joint Specimen                     | 116  |
| 51     | Anticipated Crack Configuration in Row 2 of the Double Lap Joint Specimens                              | 119  |
| 52     | Remote Load Factor $\gamma_{RE}$ for K for Single Lap Joint Specimen                                    | 124  |
| 53     | Stress Intensity Correction Factor $\gamma_{FO}$ for Fastener Loads on the Crack Line                   | 126  |
| 54     | Inside Cracks and Outside Cracks in the Stringer  | 128  |
| 55     | Estimate of Correction Factor $\gamma_{SF}$ for Effect of Tee-Stringer Flange on Crack in Stringer Base | 130  |
| 56     | Dimensions for Outside Cracks, Edge Stringer Specimens  | 135  |
| 57     | Dimensions for Inside Cracks, Edge Stringer Specimens   | 138  |
| 58     | Fatigue-Induced 0.05-Inch Near-Circular Corner Flaws at Drilled Holes in 7075-T6 Aluminum Sheet         | 148  |
| 59     | Stringer Configurations for Precracking   | 149  |
| 60     | Precracking of the Angle by Pin Loading   | 152  |
| 61     | Single Lap Joint Specimen, Showing Lateral Constraint   | 156  |
| 62     | Center-Stringer Specimen in Fatigue Test Machine  | 157  |
| 63     | Test Setup, Two-Bay Specimens (Same as for Edge-Stringer Specimen)                                      | 159  |
| 64     | Total Test Lives for Precracked Single Lap and Double Lap Joint Specimens                               | 162  |
| 65     | Crack Growth Across the First Ligament, Thick Double Lap Joint Specimens 4.6A-1 and 4.6A-2              | 164  |
| 66     | Crack Growth Across the First Ligament, Thick Double Lap Joint Specimens 4.6A-3, 4.6A-4, and 4.6A-12    | 165  |
| 67     | Crack Growth Across the First Ligament, Thick Double Lap Joint Specimens 4.6A-5 and 4.6A-6              | 166  |
| 68     | Crack Growth Across First Ligament, Thick Double Lap Joint Specimens 4.6A-7 and 4.6A-8                  | 167  |
| 69     | Crack Growth Across First Ligament, Thin Double Lap Joint Specimens                                     | 168  |
| 70     | Gap-Opening Displacement Range in the Thick Double Lap Joints   | 170  |

# LIST OF FIGURES (Continued)

| Figure |  | Page |
|--------|--|------|
| 71     | Strain Gage Results, Double Lap Joint Specimen 4.6A-8  | 171  |
| 72     | Crack Growth Results, Single Lap Joint Specimens   | 174  |
| 73     | Predicted and Actual Crack Growth Lives, Single Lap Joint Specimens                              | 175  |
| 74     | Strain Gage Results, Single Lap Joint Specimen 4.7-3   | 177  |
| 75     | Strain Gage Results, Single Lap Joint Specimen 4.7-7   | 178  |
| 76     | Comparison of Arrest Times at the Torqued, Interference-Fit Fastener in the Precrack Path        | 180  |
| 77     | Crack Growth History in the Collar-Side Doubler of Specimen 4.6A-5                               | 181  |
| 78     | Specimen 4.6A-5. Cracked Collar and Fretting-Induced Surface Flaw                                | 182  |
| 79     | Analytical Crack Growth Predictions, Hole-to-Hole Specimen                                       | 185  |
| 80     | Reduction of Cyclic Notch Stress by Friction Beneath the Head of a Torqued Fastener              | 188  |
| 81     | Side Sectional View of Precompressed Joint Prior to Tension Test                                 | 194  |
| 82     | Load-Displacement Curve for Faying Surface Slip Test, Double Lap Joint                           | 195  |
| 83     | Effect of Fastener Torque on Faying Surface Friction Force in the Double Lap Shear Joints        | 197  |
| 84     | Summary of Test Results on Precracked Double Lap Joints From Reference 71                        | 200  |
| 85     | Effect of Fastener Head Type in Constant Amplitude Tests of the Single Lap Joint Specimen        | 203  |
| 86     | Two Fretting Cracks at Each Hole in the Fracture Surface of the Doubler of Specimen 4.7-10       | 205  |
| 87     | Fretting Crack Origins in the Skin Near the Hole Periphery in Specimen 4.7-12 (Front) and 4.7-13 | 205  |
| 88     | Spectrum Test Lives and Life Predictions   | 207  |
| 89     | <b>Failed</b> Skin in Spectrum-Loaded Specimen 4.6A-10   | 208  |
| 90     | Bearing $k_t$ for a Fastener Hole with a Crack from Hole to Edge (by Ratio Method of Figure 14)  | 209  |
| 91     | Lateral Deflection of Points Across the Width of the Test Section, Specimen 4.8-1-2              | 215  |

# LIST OF FIGURES (Continued)

| Figure |  | Page |
|--------|--|------|
| 92     | Strain Gage Data for Tee-Reinforced Specimen 4.8-1-2                                       | 216  |
| 93     | Summary of Test Lives, Stringer-Reinforced Specimens                                       | 217  |
| 94     | Crack Growth Prediction and Test Results, Inside Crack in Tee                              | 219  |
| 95     | Crack Growth Prediction and Test Results, Inside Crack in Skin                             | 220  |
| 96     | Crack Growth Prediction and Test Results, Outside Crack in Tee                             | 221  |
| 97     | Crack Growth Prediction and Test Results, Outside Crack in Skin                            | 222  |
| 98     | Crack Reinitiation Times on the Undamaged Side of the Precracked Hole, Specimen Type 4.8-1 | 223  |
| 99     | Comparison of Crack Growth in Tee Stringer in Specimens 4.8-1-7, -8 and -10                | 224  |
| 100    | Crack Growth Results, Inside Crack in Skin, Spanwise Splice Specimens                      | 226  |
| 101    | Crack Growth Results, Inside Crack in Tee, Spanwise Splice Specimens                       | 227  |
| 102    | Crack Growth Results, Outside Crack in Skin, Spanwise Splice Specimens                     | 228  |
| 103    | Crack Growth Results, Outside Crack in Tee, Spanwise Splice Specimens                      | 229  |
| 104    | Empirical and Analytical Stress Intensity Factor, Inside Crack in Tee                      | 234  |
| 105    | Predicted and Test Lives of Spectrum Loaded Tee-Reinforced Split-Skin Specimens            | 235  |
| 106    | Fracture Surface of Specimen 4.8-3-2 Showing Failure Sequence                              | 236  |
| 107    | Close-Up of Fracture Surface Markings on Specimen 4.8-3-2                                  | 237  |
| 108    | Strain Gage Locations and Results on Edge Stringer Specimen 4.9-7                          | 241  |
| 109    | Summary of Crack Growth Lives for Edge-Stringer Reinforced Specimens                       | 243  |

## LIST OF FIGURES (Continued)

| Figure |   | Page |
|--------|---|------|
| 110    | Prediction Compared to Five Outside Angle Cracks from Four Different Specimens                      | 245  |
| 111    | Summary of Strain Gage Data from Specimen 4.10-1  | 248  |
| 112    | Summary of Strain Gage Data from Specimen 4.10-3  | 249  |
| 113    | Stress Level Effect, Two-Bay Specimen with Precracked Edge Stringer and Skin                        | 252  |
| 114    | The Nearly Identical Crack Paths of Specimens 4.10-3 and 4.10-4                                     | 253  |
| 115    | Stress Level Effect, Two-Bay Specimen with Precracked Tee and Skin                                  | 254  |
| 116    | Early Crack Growth in Comparable Two-Bay and Center-Stringer Specimens                              | 257  |
| 117    | Early Crack Growth in Comparable Two-Bay and Edge-Stringer Specimens                                | 258  |
| A.1    | Damage Tolerance Design Requirements  | 262  |
| A.2    | Requirements for Slow Crack Growth Structure  | 263  |
| A.3    | Requirements for Fail-Safe Structure  | 264  |
| B.1    | Drawing for Tee-Reinforced Panel  | 268  |
| B.2    | Drawing for Edge Stringer Specimens   | 271  |
| B.3    | Two-Bay Specimen, Type 4.10-X   | 273  |
| C.1    | Equivalence Between Manufactured Imperfections and 0.005-inch Fatigue Cracks                        | 275  |
| C.2    | Continuing Damage Flaw Tests Conducted  | 277  |
| C.3    | Set-up for Inducing 0.005-inch Cracks in Bending  | 278  |
| C.4    | Summary of Test Results for Continuing Damage Flaws   | 286  |
| C.5    | Fracture Surfaces Showing Equivalent Flaw Front Shapes for 0.005-inch Cracks and 0.020-inch Notches | 287  |

## LIST OF TABLES

| Table |   | Page |
|-------|---|------|
| 1     | Structural Test Specimen Summary  | 10   |
| 2     | Test Plan, Phase I Stringer-Reinforced Specimens  | 20   |
| 3     | Phase II Tests to Assess Spectrum Loading Effects   | 23   |
| 4     | Phase II Tests of Single Lap Joints and Two-Bay Stringer-Reinforced Panels                      | 26   |
| 5     | Baseline Test Summary   | 29   |
| 6     | Constants for Stress Severity Factor Analysis   | 46   |
| 7     | Averages of Measured Tensile Properties   | 79   |
| 8     | Coupon Fatigue Test Results   | 80   |
| 9     | Summary of Fastener Fatigue Data  | 81   |
| 10    | Summary of Baseline Fatigue Crack Growth Tests  | 93   |
| 11    | Baseline Constant Amplitude, $R = 0.1$ , S-N Curve Used in Computing Spectrum Fatigue Estimates | 111  |
| 12    | Damage Cases Analysed for Double Lap Joint Specimen   | 115  |
| 13    | Calculated Fastener Loads in Double Lap Joint   | 117  |
| 14    | Computed Fastener Loads ( $P/P_{avg}$ ) in Skin, Single Lap Joint                               | 123  |
| 15    | Spectrum Crack Growth Predictions for Structure by Equivalent $k_t$ Prediction Method           | 141  |
| 16    | Spectrum Crack Growth Predictions for Structure by Equivalent Stress Intensity Factor Method    | 141  |
| 17    | Modified Compact Tension Specimen Fatigue Tests   | 190  |
| 18    | Test Plan for Precracked Double Lap Joints from Reference 71                                    | 199  |
| 19    | Tests of Single Lap Joint Specimens for Effect of Fastener Head Type                            | 201  |

LIST OF TABLES (Continued)

| Table |   | Page |
|-------|---|------|
| B.1   | Dimensional Drawings for Structural Specimens                                   | 267  |
| C.1   | Summary of Data for Unflawed Fatigue Specimens                                  | 281  |
| C.2   | Summary of Data for Specimens with 0.005 inch<br>Fatigue-Induced Initial Cracks | 283  |
| C.3   | Summary of Data for Razor-Flawed Specimens                                      | 285  |

## SECTION I

### INTRODUCTION

#### 1. BACKGROUND

Experience with new high-strength materials has shown that higher strength does not imply better fracture toughness or fatigue resistance. Therefore, when the design ultimate stress allowables are increased for new high-performance aircraft structure, the desired levels of damage tolerance and safe life may become more difficult to maintain.

Following the F-111 incidents and the C-5 wing fatigue problems, the Air Force has undertaken a thorough revision of its damage tolerance and durability requirements. The new requirements for ensuring adequate damage tolerance in future Air Force aircraft are given in MIL-A-83444 (Reference 1).

A summary of Reference 1 is presented in Appendix A. Reference 1 defines initial damage sizes, specifies residual strength load requirements, and requires fatigue crack growth analyses to establish the life interval between the initial damage state and the state when the residual strength load can just be sustained. This program has been concerned with investigating the crack growth analyses required by Reference 1 with particular emphasis on complex multielement structure.

Such analyses were attempted in simulated design studies of damage tolerant aircraft structure (References 2 through 6). To perform the fatigue crack growth calculations, it was necessary to make a series of arbitrary assumptions about the initial flaw location and multiplicity and the sequence of cracking in various interacting structural elements leading up to the terminal catastrophic failure. Alarming, altering these assumptions was often found to have a major effect on predicted fatigue crack growth lives.

The nature of these assumptions can be clarified by reviewing a crack growth analysis performed in Reference 7. The analysis was for the upper forward spar cap area of the P-3 aircraft near the inboard nacelle. A cross-sectional view of the area analyzed is shown in Figure 1. Some questions that arose in the course of this analysis and their impact upon the analytically computed crack growth life were:

- 1) Where is the location of the most critical initial crack? Alternate locations selected were in the integrally-stiffened skin at point A, the spar cap at B, or the shear web at C. The choice had up to a factor of 2 impact on computed life.
- 2) What degree of multiple initial damage is reasonable to assume? (Reference 1 requires assumed initial cracks in both members joined by a common fastener, but only on one side of the hole.) Alternate assumptions in Reference 7 were an initial crack on one side of the hole or equal initial cracks on both sides. Impact on computed life was up to a factor of 2.
- 3) What analytical approach should be used for the continuing damage aspects of crack arrest and reinitiation at fastener holes in the path of the crack?

The concept of continuing damage needs some elaboration. The term continuing damage was introduced in Reference 1. It is used there as a name for a particular method of accounting for a crucial step in crack growth analysis of structure. The significance of this step in the analysis was first pointed out in Reference 2 where it was described as part of the analysis where "a sequence of events has to be assumed as the crack progresses through and across various structural elements."

The sequence of events assumed is dictated in Reference 1 by the assumed initial presence of 0.005-inch corner flaws at all fastener holes in the structure. This assumption has the advantage that it allows a fatigue-crack-initiation analysis to be performed within a fracture mechanics framework. Reference 8 presents results of the F-4 Independent Review Team which concluded that 0.005-inch cracks could be shown, by back calculation of larger observed fatigue cracks, to be representative of a 95 percent confidence level of hole quality in their tests.

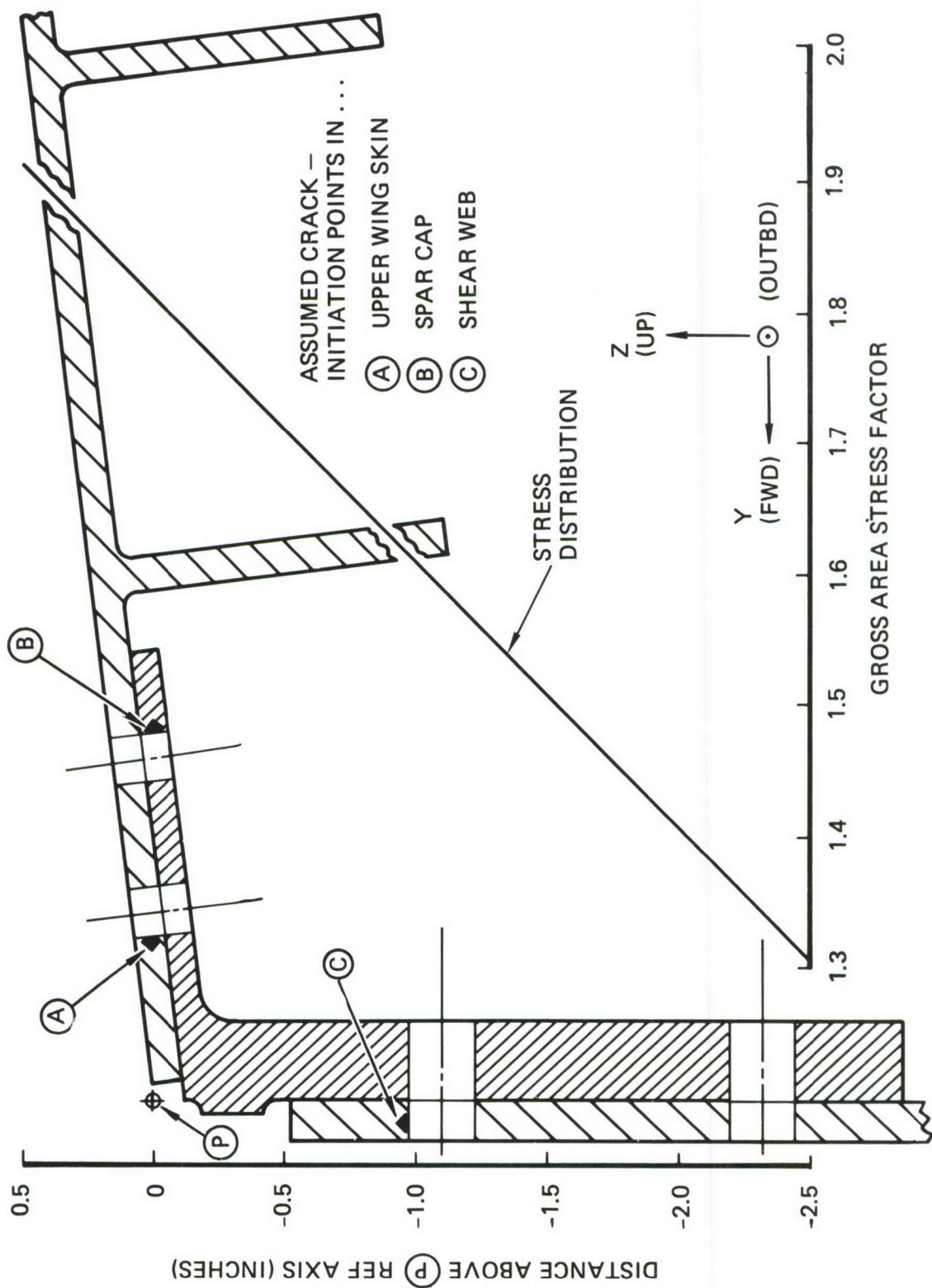


Figure 1. Section View (Looking Spanwise) of Upper Skin, Front Spar Cap, and Shear Web

Initial 0.005-inch flaws were not assumed in Reference 7. Instead, two alternative assumptions were made about crack sequence. In both, it was assumed for purposes of computing stress intensity that the arrested crack was extended by an incremental distance equal to the hole diameter, and the hole was otherwise neglected. This extension was assumed to be either instantaneous, with growth continuing immediately, or delayed for some time period prior to further growth. The delay period was computed from crack initiation data and theory using a stress concentration factor ( $k_t$ ) expression. Inclusion of the delay period increased the estimated life by up to a factor of 4.2. The variations in estimated lives for different assumed sequences of events can be significantly greater than a factor of 4 for other realistic design considerations and loadings.

The use of crack initiation data and  $k_t$  to compute crack reinitiation times of arrested cracks was further developed in Reference 9. This work is reviewed in some detail in Section III, Paragraph 1. By this analytical approach there is no requirement for either a crack growth sequencing assumption, or an initial continuing damage flaw size assumption. (A further development of this approach is utilized herein in the analysis of structural specimens without induced initial continuing damage flaws).

References 2 through 7 were purely analytical studies. The analytically-estimated effects of flaw location and multiplicity discussed above were not supported by any direct fatigue tests of precracked structure. Furthermore, the impact of the 0.005-inch continuing damage flaws on the sequence of events in the structural crack growth process and structural life had never been experimentally investigated.

Prior to the research reported herein, many fatigue crack growth tests of built-up mechanically-fastened metallic structure had been conducted (References 10-28). Often, however, the instrumentation, observations, or reporting was somewhat fragmentary, making a thorough crack growth rate analysis of the test results difficult. There were some exceptions, where successful analyses were reported (e.g., Reference 24), but in all these cases the initial cracks were more than an inch long.

A large proportion of the crack growth period of a 0.050-inch initial crack occurs before the crack is one inch long. Furthermore, even for such short cracks, there are potentially important interaction effects between the growing crack and the immediately adjacent structural members and fasteners.

Thus, the need existed for a systematically planned program, including supporting baseline data and analyses, of fully instrumented, observed, and reported fatigue crack growth tests of mechanically fastened structural specimens with 0.050-inch initial corner cracks at fastener holes.

## 2. PROGRAM OBJECTIVES

The primary objective of this program was to evaluate experimentally and analytically the effects of initial flaw location and multiplicity on fatigue crack growth life and element failure sequence in multiple element, mechanically-fastened metallic structure. The intent was to provide designers with experimental and analytical evidence of the impact of the initial flaw assumptions and the accuracy of analysis methodology used in applying the Damage Tolerance Design Requirements (Reference 1) to various types of complex aircraft structure.

The primary objective was accomplished via a sequence of tasks. These were:

- 1) Conduct baseline tests to determine basic tensile, fatigue, cyclic crack growth, and fracture properties of the selected material (7075-T6 Aluminum sheet, plate and extrusion); and to provide a basis for crack growth predictions.
- 2) Plan an experimental program wherein specimens, configured and sized to simulate typical primary aircraft structural arrangements, are fabricated, preflawed, and cycled under constant amplitude loading. Systematically vary the flaw location and number of flaws in each specimen. In particular, flaw sizes, locations, and multiplicity should be based on Reference 1. Consider multiple load path (MLP) fail safe, crack arrest fail safe, and slow crack growth structure. Include riveted (and mechanically attached) stiffened, planked, and chordwise splices. In addition, test a limited number of specimens under flight-by-flight spectrum loading to verify significant crack growth patterns and behavior.

- 3) Fabricate and preflaw the specimens in a manner consistent with expected manufacturing operations and the requirements of Reference 1.
- 4) Develop stress intensity factors for each specific case.
- 5) Perform a crack growth analysis for each growth condition tested in the experimental program to predict the growth behavior from initial flaw to complete specimen failure.
- 6) Conduct the cyclic tests of complex structural specimens and observe the complete growth pattern from initial flaw to complete specimen failure, but especially observe the following:
  - a. The early stage of growth of initial 0.050-inch corner flaws
  - b. The crack growth path and element failure sequence
  - c. Initiation of secondary fatigue cracks and crack reinitiation following arrest at a free edge or fastener hole.
- 7) Explain the differences between predictions and test results, with the aid of strain gage measurements and supplementary analyses.
- 8) Assess the significance of load shedding from cracked to intact members and the capability to predict flaw growth in complex structure.
- 9) Assess the reasonableness of the continuing damage and remaining structural damage assumptions required by Reference 1.
- 10) Prepare a set of guidelines (recommended assumptions) for the application of Reference 1 to various types of complex aircraft structure.

### 3. SUMMARY OF THE FINAL REPORT

This report consists of three volumes. Volume I is the detailed technical report. Volume II is a specimen-by-specimen tabulation and plot of the test data and crack growth predictions for the complex structural specimens. Volume III is a short summary, extracted from Volume I, emphasizing the major accomplishments, conclusions and recommendations.

There are eight major sections in Volume I including this introductory section. Section II describes the test plan, including specimen configurations, fastener types, precrack locations, instrumentation, and summary of baseline data. The general methods used to predict crack growth in the structural

specimens are presented in Section III, including numerous equations for estimating stress intensity factors for growing cracks and stress severity factors for cracks arrested at fasteners. The baseline data used for prediction, material characterization, etc., are described in Section IV. Section V gives the details of specific prediction calculations for each specimen type. The fabrication and testing procedures are described in Section VI. The last two sections discuss the test results for the pre-cracked mechanically fastened structural specimens. Section VII covers joints; Section VIII, stringer-reinforced panels.

The data in Volume II consist of annotated tables of crack lengths and cycles, and plots showing the data for each specimen and the corresponding crack growth prediction. Data are presented in order by specimen number. Sixty-eight structural specimens were tested, and because of their complexity an almost unlimited amount of time could be spent in reviewing the data. The purpose of Volume II is to provide an easy-to-read, concise, yet complete summary of each test result in the program, to facilitate future analytical review and use of the data by readers of the report.

To convey the message of this report to a larger audience, the technical summary has been extracted to form a short separate report, Volume III.

## SECTION II

### TEST PROGRAM

#### 1. INTRODUCTION

Sixty-eight precracked mechanically fastened structural specimens were fatigue tested to failure in controlled (Lockheed Rye Canyon) laboratory air environment ( $69^{\circ}$  -  $75^{\circ}$ F, 30 - 50% RH). A large number of supporting baseline tests were run as well. This section summarizes the test program.

The test program consisted of two phases. Each phase included baseline testing, tests of precracked joints, and tests of precracked stringer-reinforced structure. Joints representative of chordwise splices and stiffened skins representative of wing structure were sufficiently diverse to meet the overall program objectives. The baseline testing in each phase was performed to support the analysis and testing methodology for the structural tests. Phase I tests consisted of constant amplitude fatigue tests designed to investigate the effect of the primary variables of interest: initial flaw locations, initial flaw multiplicity, continuing damage assumptions, and structural arrangement. Phase II tests were used to answer questions raised by the Phase I tests and to check that conclusions derived from the Phase I tests were valid for spectrum loading and for configurations of increasing complexity. All tests were used to assess the crack growth prediction methodology that would be used to comply with Reference 1. A crack growth analysis was performed for each Phase I test prior to the test results being available to the analyst.

In the Phase I joint specimens, variations in structural arrangement included: single lap shear and double lap shear joints, variations in fastener diameter and element thickness, interference and clearance-fit fasteners, low and high fastener torque, and protruding and flush head fasteners. Initial flaw configurations included: single and multiple fatigue-induced cracks, continuing damage flaws and no continuing damage flaws.

In the Phase I stringer-reinforced specimens, variations in structural arrangement included: angle edge stringers and central tee stringers, continuous skin and spanwise splice, rivets and Hi-lok fasteners, interference and clearance-fit fasteners, high and low fastener torque, and variations in fastener diameter. Initial flaw configurations included: cracks going toward the inside and the outside of the panels, single and multiple fatigue-induced cracks, continuing damage flaws and no continuing damage flaws.

Cost considerations precluded a full matrix of tests with the above variables and therefore only a partially-filled test matrix was performed during Phase I. Each test, however, supplied much more than a single result (such as total life), since crack growth was observed throughout the test. This allowed the separation of the effects of certain variables within a single test. For example, observations of each crack at short crack lengths enables the effects of multiple and single cracks to be separated from fastener effects. Therefore, by making such detailed observations, and by comparing with analysis and Phase II test results, the impact of all the above variables were investigated while running a limited test program.

Additional constant amplitude fatigue tests of precracked joint specimens were included in the Phase II program. These tests helped to separate and clarify effects of flush-head versus protruding-head fasteners and differences in crack growth behavior of single versus double lap joints which were unresolved at the end of the Phase I tests. A simulated fighter spectrum was used in loading a series of single lap joints, double lap joints, and center tee stiffened structures during Phase II. Also included in the Phase II testing was a series of constant amplitude tests on two-bay panels which had both center tees and angle edge stiffeners. A summary of the Phase I and Phase II structural tests is given in Table 1.

All primary initial flaws in the structural test specimens in this program were fatigue-induced 0.050-inch quarter-circular cracks growing out of fastener holes. An alternative initial flaw consistent with Reference 1 would have been a 0.125-inch-deep semicircular surface flaw or, for sheet thicknesses less than 0.125 inch, a 0.25-inch through crack.

TABLE 1. STRUCTURAL TEST SPECIMEN SUMMARY

| Specimen Type<br>(Specimen Designation) | Number Of Tests |                    |          |
|---|-----------------|--------------------|----------|
|   | Phase I         | Phase II           |          |
|   |                 | Constant Amplitude | Spectrum |
| Double Lap Joint (Thick)<br>(4.6A - X)  | 8               |                    | 2        |
| Double Lap Joint (Thin)<br>(4.6B - X)   | 4               |                    |          |
| Single Lap Joint<br>(4.7 - X)           | 6               | 2                  | 4        |
| Continuous Skin Tee<br>(4.8-1 - X)      | 12              |                    |          |
| Split Skin Tee<br>(4.8-3 - X)           | 12              |                    | 2        |
| Edge Stiffened<br>(4.9 - X)             | 12              |                    |          |
| Two Bay<br>(4.10 - X)                   |                 | 4                  |          |

The stress intensity factors for a 0.25-inch through crack and a 0.125-inch-deep surface flaw under remote tensile loading are in the same range as the stress intensity due to remote tensile loading of a 0.050-inch corner crack emanating from the fastener hole for the hole sizes (0.25- to 0.375-inch diameter) used in this program. However, if the corner crack condition is selected, Reference 1 requires the assumption of multiple flaws (flaws in more than one adjacent element) at the critical hole. In mechanically-fastened structure this flaw multiplicity tends to make the corner crack condition the more critical. Furthermore, in those cases wherever the fastener in the hole transfers load, the 0.050-inch crack at that hole tends to have a significantly higher initial stress intensity factor. These considerations, combined with the fact

that fastener holes are found to be the most prevalent source of cracking in aircraft structure and a knowledge of the cost impact of including additional damage cases, led to the exclusive use of initial corner cracks at holes.

## 2. SPECIMENS AND INITIAL DAMAGE FOR PHASE I TESTS

### 2.1 Precracked Joints

Eighteen precracked chordwise splice specimens were tested in Phase I. The specimen configurations, shown in Figures 2 through 4, include two double lap shear joints of different thicknesses and a single lap shear joint. Steel Hi-lok fasteners with a large enough diameter to be bearing critical were used. Protruding-head fasteners were selected for the double lap shear joints shown in Figures 2 and 3 to simulate internal structure, whereas flush-head fasteners were selected for the single lap shear joints shown in Figure 4 to simulate external structure. The fastener spacing was 4 diameters, typifying standard design practice.

This series of tests was conducted to demonstrate the differences in crack growth life for four different initial damage conditions. These four conditions, shown in Figures 5 and 6, are:

- A. Multiple 0.050-inch quarter-circular corner cracks (one in each member) at one fastener hole, simulated 0.005-inch continuing damage flaws at other critical fastener holes, and all fasteners clearance fit (C1) with no beneficial clamp up (finger-tight). This simulates the requirements of Reference 1.
- B. Same as A except no continuing damage flaws.
- C. Same as B except for fastening method used in unflawed holes. Standard fastener interference (P1) and standard clamp-up are used in all unflawed holes. The fastener at the precracked hole is C1 fit and finger-tight.
- D. Same as C except initial flaw is in one member only.

Note in Figures 5 and 6 that all initial flaws were induced at the faying surfaces rather than at the external surfaces, since peak stresses associated with fastener load transfer tend to be highest at the faying surface.

All initial flaws in the double-lap shear joints (Figure 5) were in the second fastener row where the stresses in the two external doublers are

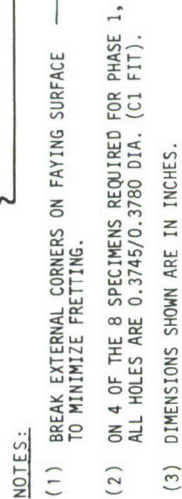
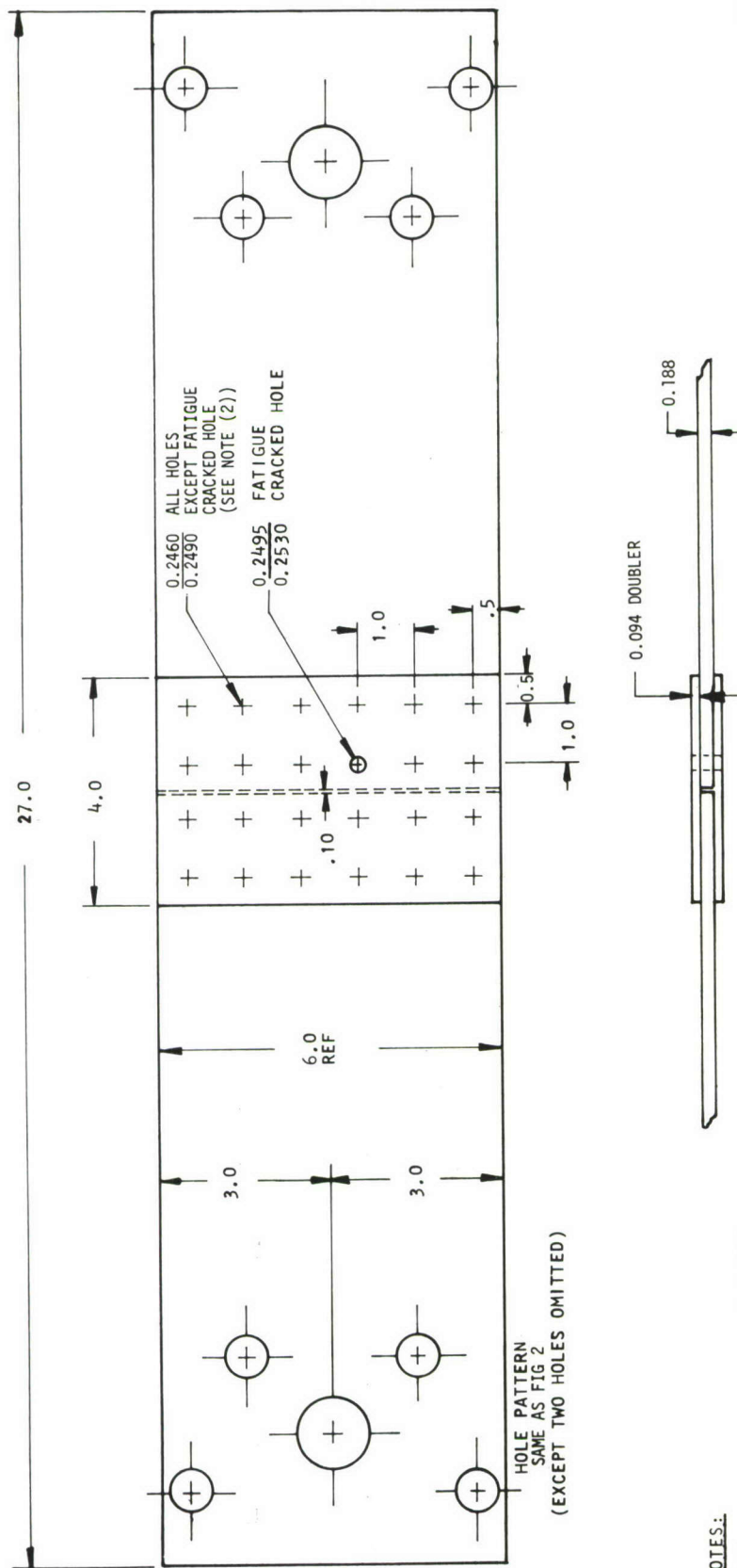


Figure 2. Double Lap Joint Specimen with 0.188-Inch Doublers



**NOTES:**

- (1) BREAK EXTERNAL CORNERS ON FAYING SURFACE TO MINIMIZE FRETTING.
- (2) ON 2 OF THE 4 SPECIMENS REQUIRED FOR PHASE I, ALL HOLES ARE 0.2495/0.2530 DIA. (C1 FIT).
- (3) DIMENSIONS SHOWN ARE IN INCHES.

Figure 3. Double Lap Joint Specimen with 0.094-Inch Doublers

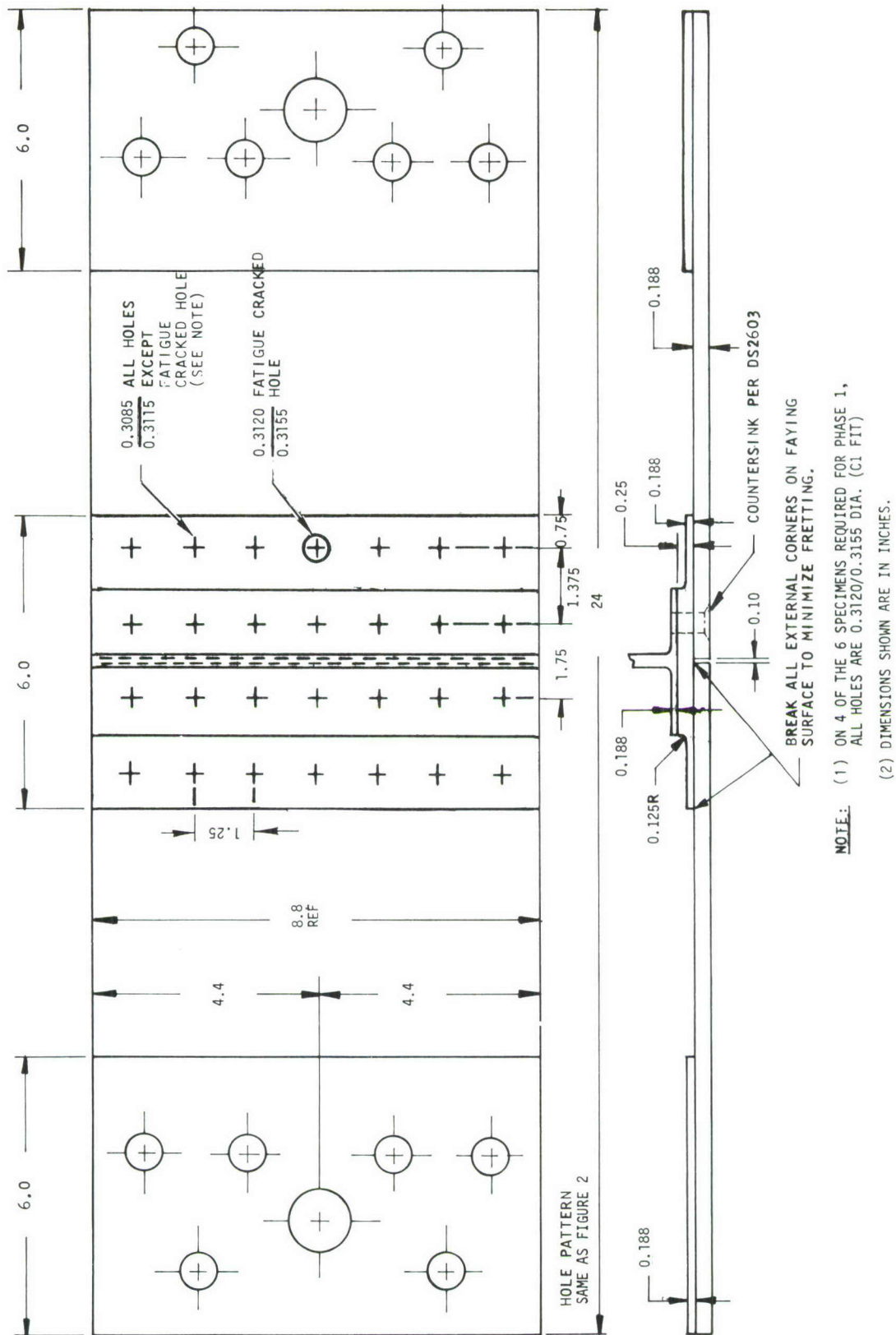


Figure 4. Single Lap Joint Specimen

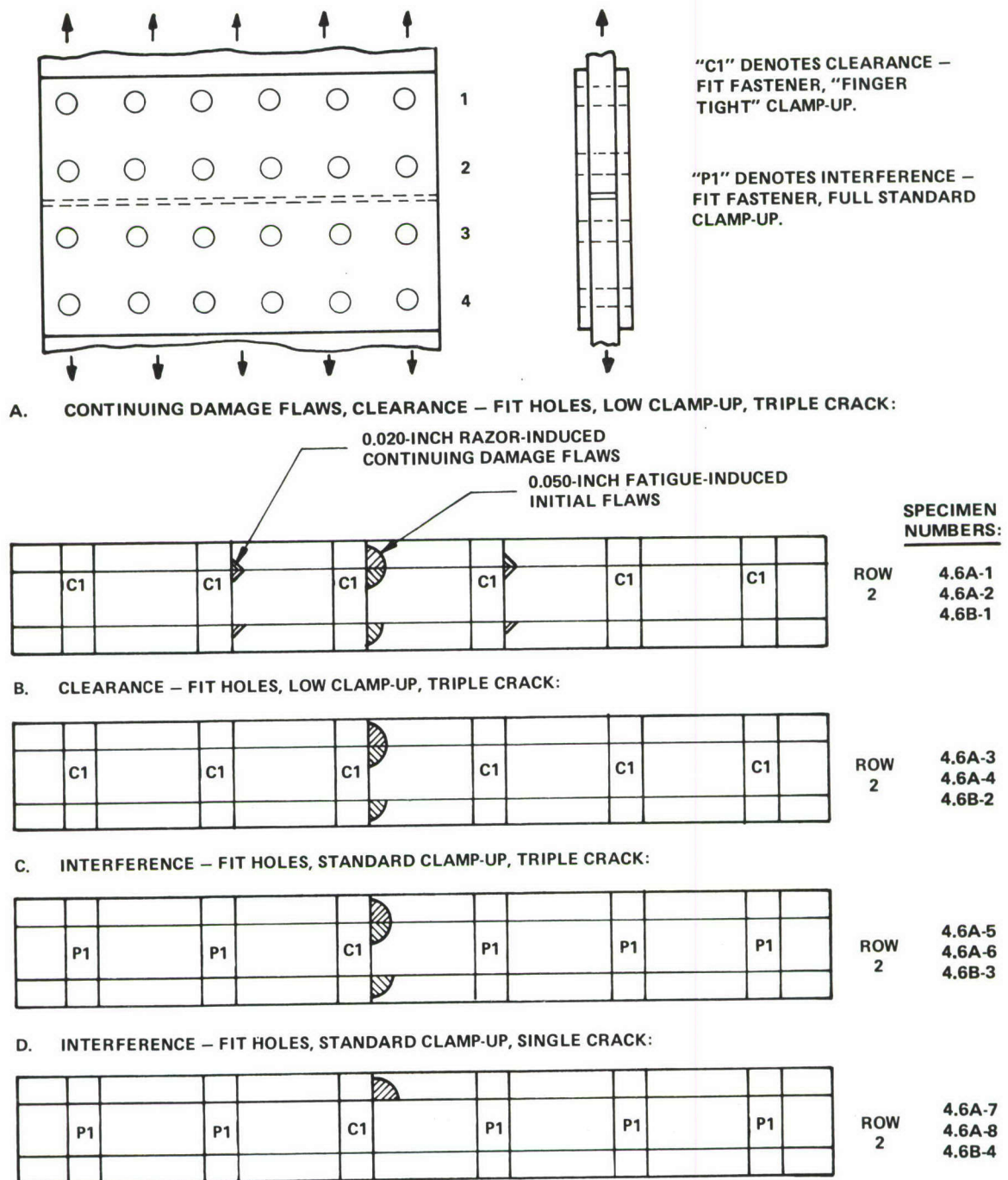
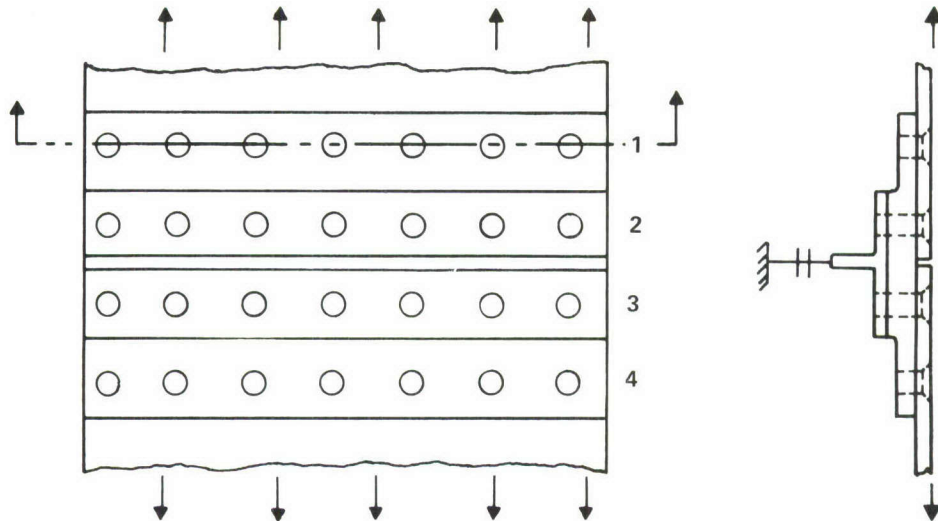


Figure 5. Summary of Initial Damage Conditions, Double Lap Joint Specimens



CROSS SECTIONAL VIEW OF ROW 1:

A. CONTINUING DAMAGE FLAWS, CLEARANCE – FIT HOLES, LOW CLAMP-UP, DOUBLE CRACK: SPECIMEN NUMBERS:



4.7-2  
4.7-3

B. CLEARANCE – FIT HOLES, LOW CLAMP-UP, DOUBLE CRACK:



4.7-1  
4.7-4

C. INTERFERENCE – FIT HOLES, STANDARD CLAMP-UP, DOUBLE CRACK:



4.7-5

D. INTERFERENCE – FIT HOLES, STANDARD CLAMP-UP, SINGLE CRACK:



4.7-6

Figure 6. Summary of Initial Damage Conditions, Single Lap Joint Specimens

approximately twice as great as the stresses in the thicker central member. Thus, the cracks in the doublers controlled the crack growth behavior; the growth of the hidden crack in the central member was slow and unimportant. Transverse bending was minimal during the crack growth life of the double-lap shear joint specimens with multiple initial cracks. Those with a pre-crack in only one doubler were unsymmetrical with respect to the specimen middle plane, so bending effects were present, especially later in the tests.

All initial flaws in the single-lap shear joints (Figure 6) were in the first fastener row where the stresses in the skin member are higher than the stresses in the doubler. Thus the skin crack controlled the crack growth behavior, while the growth of the doubler crack was slower and of secondary importance. A lateral support applied to the tee member reduced the severity of the transverse bending. Nevertheless, the bending effects in this specimen had an important bearing on the crack growth behavior.

The eighteen Phase I joint specimens are listed with their respective initial damage conditions in Figures 5 and 6. Eight double lap joints with 0.188-inch doublers (type 4.6A-X) were tested, including duplicate tests of all four of the damage conditions shown in Figure 5. The replication was considered to be necessary to distinguish real effects from test scatter. Four double lap joints with 0.094-inch doublers (type 4.6B-X) were also tested. Replication was considered unnecessary here due to the similarity to the thicker double lap joint specimen. Finally, six single lap joints (type 4.7-X) were tested, including duplicate tests for damage conditions A and B in Figure 6. Single tests seemed sufficient for conditions C and D, because they are similar to one another. Indeed, the initial doubler crack did not appreciably alter the crack growth life of Specimen 4.7-5 compared to that of Specimen 4.7-6.

Each Phase I specimen was cyclically loaded until complete failure occurred. A maximum stress of 17 ksi and a stress ratio of 0.1 were used in all cases. Intermittently, blocks of marking cycles were applied to the first few specimens at  $S_{\max} = 17$  ksi and  $R = 0.82$ . However, the marking cycles did not mark the fracture surface successfully, and the process was abandoned for the

remainder of the joint tests. The apparent reasons for their failure to mark are discussed in Section VII, Paragraph 2.3, page 196.

## 2.2 Stringer Reinforced Specimens

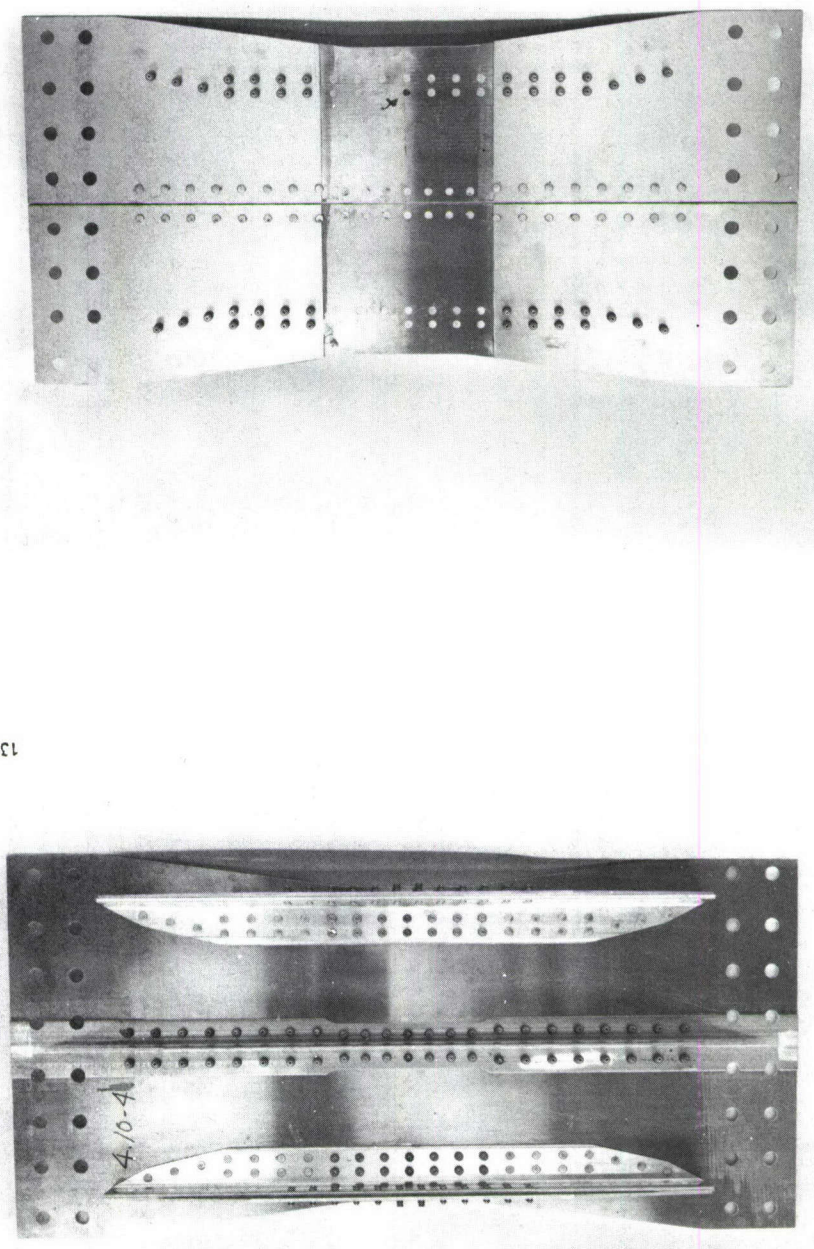
The test plan for Phase I included three configurations of stringer-reinforced test specimens. All the stringer-reinforced specimens tested are derived from the basic 18-inch-wide two-bay configuration which was tested in Phase II. Photographs of the two-bay specimen are shown in Figure 7. For the edge-stiffened specimen (Type 4.9), the center tee is not present. The tee-stiffened specimens (Types 4.8-1 and 4.8-3) had no angles at the edges and the grip areas tapered out to 24 inches. In specimen type 4.8-1, the skin under the tee was continuous, whereas in the two-bay panels and specimen type 4.8-3, the skin under the tee was split. Detailed drawings for specimen types 4.8-1 and 4.8-3 are presented in Figure B-1 of Appendix B. Detailed drawings for specimen type 4.9 are shown in Figure B-2 of Appendix B.

All stringer-reinforced test specimens had an overall nominal length of 44.5 or 47.5 inches and were 18 inches wide in the test section. Specimen type 4.8-1 consisted of 0.188-inch sheet with a central tee stringer. Specimen type 4.8-3 consisted of two 0.188-inch sheets spliced together longitudinally across the base of a 0.188-inch-thick tee stringer. Specimen type 4.9 consisted of a 0.188-inch sheet with a 0.25-inch-thick angle stringer on each edge to simulate a spar cap on a wing, and a 3.25-inch wide strip of 0.188-inch sheet attached to the protruding leg of the angle to simulate a portion of the shear web as shown in Figure 1.

Twelve each of specimen types 4.8-1, 4.8-3, and 4.9 were tested in Phase I for a total of 36 Phase I stringer-reinforced specimens. The Phase I test plan for these specimens is summarized in Table 2. There are two basic flaw locations identified for each specimen configuration. The inside crack faces the center of the panel; the outside crack faces the panel edge. There are three levels of flaw multiplicity: single crack, double crack, and double crack with continuing damage flaws. Note that there are two more single initial crack cases for the edge-stringer specimens than for the tee-reinforced specimens, and two fewer replications of double initial flaw

137 049H

137 046H



(a) Front View (b) Back View

Figure 7. Two-Bay Stringer-Reinforced Specimen

TABLE 2. TEST PLAN, PHASE I STRINGER-REINFORCED SPECIMENS

| Specimen Type   | INITIAL FLAWS | SPECIMEN NUMBERS                    |                            |                                    |                                |                                |  |
|---|---------------|-------------------------------------|----------------------------|------------------------------------|--------------------------------|--------------------------------|--|
|   |               | Fastener 2                          |                            | Fastener 2                         |                                |                                |  |
|   |               | Same as Fastener 1                  |                            | Same as Remote Fasteners           |                                |                                |  |
|   |               | Double Initial Flaws, $F_1$ , $F_2$ |                            | No Continuing Damage Flaws         |                                |                                |  |
|   |               | Continuing Damage Flaws 0.005 Inch  | No Continuing Damage Flaws | Double Initial Flaws $F_1$ , $F_2$ | Single Initial Flaw $F_1$ Only | Single Initial Flaw $F_2$ Only |  |
| Center Stringer Continuous Skin Type 4.8-1 - X (Fig. B-1, Appendix B) | INSIDE        | 4.8-1-1<br>4.8-1-2                  | 4.8-1-3<br>4.8-1-4         | 4.8-1-5                            | 4.8-1-6                        |                                |  |
|   | OUTSIDE       | 4.8-1-7<br>4.8-1-8                  | 4.8-1-9<br>4.8-1-10        | 4.8-1-11                           | 4.8-1-12                       |                                |  |
|   | INSIDE        | 4.8-3-13<br>4.8-3-14                | 4.8-3-3<br>4.8-3-4         | 4.8-3-5                            | 4.8-3-6                        |                                |  |
|   | OUTSIDE       | 4.8-3-9<br>4.8-3-10                 | 4.8-3-7<br>4.8-3-8         | 4.8-3-11                           | 4.8-3-12                       |                                |  |
| Edge Stringer Type 4.9 - X (Fig. B-1, Appendix B)                     | OUTSIDE       | 4.9-1<br>4.9-2                      | 4.9-3                      | 4.9-5                              | 4.9-6                          | 4.9-4                          |  |
|   | INSIDE        | 4.9-7<br>4.9-8                      | 4.9-9                      | 4.9-11                             | 4.9-12                         | 4.9-10                         |  |

Fastener 1 was flush head steel Hi-lok, clearance fit, low fastener torque.  
 $F_1$  and  $F_2$  were nominally 0.050 inch quarter-circular-shaped fatigue cracks.  
 Razor flaws of 0.020 inch were used to simulate fatigue-induced 0.005 inch continuing damage flaws.  
 All specimens constant-amplitude cycled at  $S_{MAX} = 17$  ksi,  $R = 0.1$ .

cases. This reflects a change made during the program because the single initial damage cases were found to have provided some of the more interesting test data for the center-stringer specimens. In addition, test scatter had been low for stringer-reinforced specimens, reducing the need for replication. Fastener 1, in the precracked hole, is always a clearance-fit, untorqued steel Hi-lok fastener, and the remote fasteners in all other rows are standard rivets or interference-fit Hi-loks. However, Fastener 2, in the hole adjacent to the initial crack, is either like Fastener 1 (for double initial crack cases with or without continuing damage flaws) or like the remote fasteners (for single or double initial crack cases without continuing damage flaws).

Clearance-fit steel Hi-lok fasteners were used in the flawed holes. Fasteners in the six rows nearest the center of the specimens were selected to be representative of standard design practice for each configuration. Thus, interference-fit steel flush-head fasteners were used where the specimen simulates a skin-to-skin splice (Specimen type 4.8-3) or skin-to-web splice (Specimen type 4.9), whereas flush-head aluminum rivets were used where there was no splice (4.8-1 type specimen). Protruding head fasteners were used at the remaining locations between grips because these fasteners have good fatigue characteristics, are easy to install and are sufficiently removed from the test section so as not to influence the crack growth results.

Doublers were bonded to each end of the specimens to provide a gradual transition from the test section to the end grips without introducing appreciable bending stresses. The specimens were also necked down so that the combined bending and axial stresses in the transition sections were less than in the test section. To further minimize the possibility of fatigue failures in the grip area, clamp-type end attachments were used. The tee stringer was tapered down in the grip area, so that only its base projected into the grip area. This resulted in induced bending stresses. The edge stringers, being of greater cross section, were directly picked up by the grips through pairs of aluminum channels clamped to the protruding legs of the angles and the simulated shear webs. Constant-amplitude cycling at  $S_{\max} = 17$  ksi,  $R = 0.1$  was used for all Phase I tests. Marking cycles were applied periodically at  $S_{\max} = 17$  ksi,  $R = 0.82$ . The marking cycles produced negligible

crack growth. Marking cycles were not used for the edge stiffened panels.

### 3. PHASE II TESTS

The purpose of the Phase II testing was to answer questions raised by the Phase I tests and/or to extend the Phase I test results to more complex structures and to spectrum loading. Fourteen Phase II tests were conducted, consisting of

- Two thick double lap joint specimens and two split-skin tee-reinforced panels to study spectrum loading effects,
- Six single lap joint specimens to study spectrum loading effects and the effect of fastener head (protruding or flush) on crack reinitiation time at a fully-torqued, interference-fit Hi-lok fastener,
- Four two-bay stringer-reinforced panels to study the effects of multiple stringers (more structural complexity) and a lower cyclic stress level.

#### 3.1 Flight-Simulation Spectrum Tests

The Phase II test program included eight flight-simulation spectrum tests. The purpose of spectrum testing was to establish the extent to which structural effects and load history effects can be considered independently in crack growth analysis of complex structure. The more independent these effects are, the more directly applicable will be the results of the Phase I testing, since aircraft structures experience variable-amplitude fatigue loads whereas Phase I consisted of constant-amplitude fatigue testing.

The test matrix summarized in Table 3 was specifically designed to examine the independence of structural effects and load-history effects. Both baseline and structural spectrum tests were conducted. There were duplicate spectrum tests for each of the structural configurations. For each test condition (including baseline tests), there was a corresponding set of identical specimens tested under constant-amplitude loading. The same loading sequence was used in all spectrum tests for direct comparability.

TABLE 3. PHASE II TESTS TO ASSESS SPECTRUM LOADING EFFECTS

| Specimen Configuration                        | Spec. No.                                      | Reference Load or Ref. Stress                | Corresponding Const. Amplitude Data |
|---|--|--|-------------------------------------|
| CT Specimen<br>(Baseline da/dN)               | CT5-1<br>CT5-2                                 | 1.6 kip<br>1.0 kip                           | Figure 37, Section 4                |
| Modified CT<br>(Baseline Crack Initiation)    | MCT-1<br>MCT-2<br>MCT-3<br>MCT-4               | 1.8 kip<br>1.8 kip<br>3.125 kip<br>3.125 kip | Figure 35, Section 4                |
| Split Skin Tee<br>(Figure B-1,<br>Appendix B) | 4.8-3-1<br>4.8-3-2                             | 30.0 ksi<br>30.0 ksi                         | Spec. No. 4.8-3-3<br>and 4.8-3-4    |
| Double Lap Joint<br>(Figure 2)                | 4.6A-9<br>4.6A-10                              | 30.0 ksi<br>30.0 ksi                         | Spec. No. 4.6A-3 and<br>4.6A-4      |
| Single Lap Joint<br>(Figure 4)                | 4.7-10 <sup>(1)</sup><br>4.7-11 <sup>(1)</sup> | 25 ksi<br>30 ksi                             | Spec. No. 4.7-6                     |
|   | 4.7-12 <sup>(1)</sup><br>4.7-13 <sup>(1)</sup> | 30 ksi<br>30 ksi                             | Spec. No. 4.7-7 and<br>4.7-8        |

(1) Also tested to assess effects of fastener types (See Table 4A).

With the data generated, predictions for the spectrum tests can be made by using the constant amplitude baseline data and retardation modeling, or by the direct use of the spectrum baseline data. The stress intensity expressions used can be the theoretical expressions used for the constant-amplitude structural specimens, or empirical K expressions obtained by the semi-inverse method from the observed crack growth rates in the constant-amplitude structural tests.

Figure 8 shows the 80-flight loading sequence that was used in all spectrum tests in this program. It was a randomized sequence that simulated the lower wing surface loads in the spanwise direction, excluding compression, for a typical fighter aircraft during a pilot training course. The training course consisted of a sequence of 80 flights and was given repeatedly, without significant variation, to successive groups of students. Thus the loading sequence, shown in Figure 8 was periodic and was identically repeated every 80 flights.

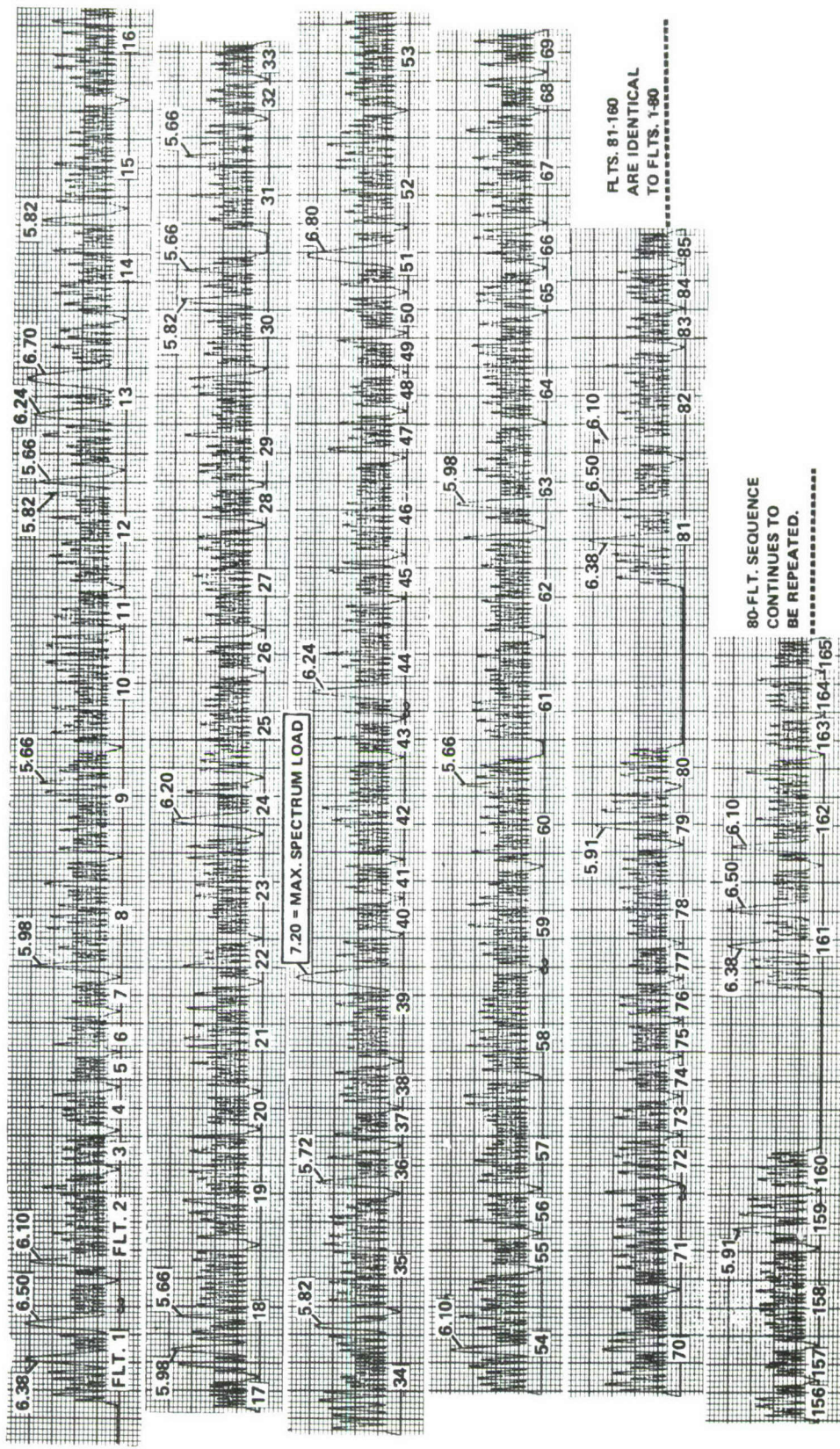


Figure 8. The 80-Flight Spectrum Loading Sequence

The largest 25 loads in the sequence are identified in Figure 8. The magnitudes noted are peak load factors. The largest load factor, 7.2, which occurs in flight number 39, is the reference load factor for the sequence. The magnitude of the reference load factor is close to a typical design limit load factor value ( $N_z$ ) for a fighter aircraft. For example,  $N_z = 7.33$  is used as typical in Reference 2.

Typical design stress at limit load for 7000 series aluminum for a fighter is 30 ksi. For example, fatigue design computations in Reference 2 led to a design ultimate stress of 44.5 ksi, where design limit stress is two-thirds of design ultimate. Therefore, for all but one of the structural tests, a spectrum reference stress of  $S_{Ref} = 30$  ksi was selected.  $S_{Ref}$ , of course, is the gross area stress value corresponding to the reference load factor.

An important advantage of this loading sequence is that the occurrence of the reference load in Flight Number 39 of each 80-flight sequence tends to visibly mark the fracture surface. This provides a history of the crack front shape and (by the spacing of the marks) crack growth rate for cracks hidden within the structure.

### 3.2 Joint Tests for Fastener Head Effects and Two-Bay Panel Tests

To clarify the role of fastener head type on the reinitiation time of a crack arrested at a fully-torqued, interference-fit Hi-lok fastener, two of the single lap joint specimens (4.7-7 and 4.7-8) were fabricated and tested identically to Specimen 4.7-6, except that protruding head rather than flush head Hi-lok fasteners were used. For similar reasons two of the remaining four single lap shear specimens had flush head and two had protruding head fasteners. These last four single lap joint specimens were spectrum tested using the 80-flight loading sequence. Table 4A shows these test conditions and the corresponding test specimen numbers.

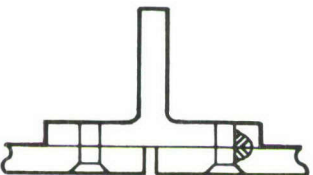
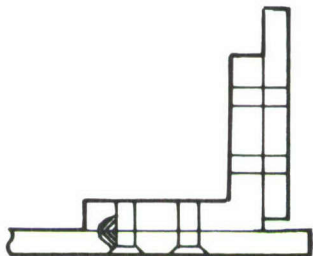
Table 4B summarizes the two-bay test group. Specimens 4.10-1 and -2 had the identical specimen geometry and precrack condition to two of the split-skin tee specimens tested except for the addition of edge stiffeners and simulated shear web strips. Likewise, Specimens 4.10-3 and -4 had the identical geometry and precrack condition to two of the edge-stringer specimens except

TABLE 4. PHASE II TESTS OF SINGLE LAP JOINTS AND TWO-BAY STRINGER-REINFORCED PANELS

A. SINGLE LAP JOINT SPECIMENS

| Specimen No.  | Fastener Type                        | Loading  |
|---|--------------------------------------|--|
| 4.7-7<br>4.7-8  | HL50-10<br>Protruding Head<br>Hi-lok | Constant Amplitude<br><br>$S_{\max} = 17 \text{ ksi}, R = 0.1$   |
| 4.7-10<br>4.7-11  | HL51-10<br>Flush Head<br>Hi-lok      | 80 FLIGHT<br>SPECTRUM<br>(SEE TABLE 3)<br>$S_{\text{Ref}} = 25$<br>$S_{\text{Ref}} = 30$<br>$S_{\text{Ref}} = 30$<br>$S_{\text{Ref}} = 30$ |
| 4.7-12<br>4.7-13  | HL50-10<br>Protruding Head<br>Hi-lok |  |
| <u>Specimen Type:</u> Figure 4. <u>Initial Damage:</u> D, Figure 6. |                                      |  |

B. TWO BAY SPECIMENS

| <div style="text-align: center;">  </div>  | <div style="text-align: center;">  </div> |
|---|--|
| STRESS LEVEL \ DAMAGE   |  |
| $S_{\max} = 12 \text{ ksi}$   | 4.10-1   |
| $S_{\max} = 17 \text{ ksi}$   | 4.10-2   |
|   | 4.10-3<br>4.10-4   |
| <p>Fasteners: P-1 fit, full torque except the following, which are C-1 fit, low torque:</p> <ul style="list-style-type: none"> <li>• The six skin-stringer fasteners in the initial crack plane</li> <li>• The eight web-stringer fasteners adjacent to the initial crack plane.</li> </ul> |  |

for the addition of a central tee stiffener and the split in the skin. As such, they were excellent tests for evaluating the effects of increased complexity. In addition, a lower stress level (12 ksi as opposed to 17 ksi) was used on half of the two-bay tests to investigate the effect of stress level on the crack growth behavior and to insure that multistringer interaction effects would be present.

Photographs of the two-bay specimen are shown in Figure 7, and a dimensioned drawing is given in Figure B-3, Appendix B.

#### 4. STRAIN GAGING

Strain gage surveys of each type of specimen<sup>\*</sup> were made. Included in the strain gaging were specimens 4.6A-8, 4.7-3, 4.7-7, 4.8-1-2, 4.9-7, 4.10-1, and 4.10-3. The purpose of the strain measurement was to:

- Check that the gripping and loading configuration used produced uniform loading across the width for the initial test conditions
- Evaluate the bending in the specimen
- Monitor the changes in the strains as the cracks grew
- Use the results of the strain survey (bending and variations with crack length) to understand any discrepancies between the before-test predictive analysis and the fatigue test results.

#### 5. BASELINE TEST SUMMARY

In support of the structural test program described in the previous sections, a series of baseline tests was conducted which evaluated more fundamental material properties. Other tests which are not yet available in the open literature but contribute to an understanding of the overall program are also discussed in this section as baseline tests.

---

\* No strain gages were necessary on the thin double lap joints (type 4.6B) or split-skin tee-reinforced panels (type 4.8-3) because of their similarity to specimen types 4.6A and 4.8-1, respectively, which were strain gaged.

The objectives of the baseline tests were to:

- Establish that the material was typical of the alloy used
- Generate data for use in the predictive analysis
- Develop methodology for producing specific effects during the structural testing
- Investigate and check phenomena observed in the structural test data of Phase I.

These objectives were met by performing the following corresponding tests, summarized in Table 5:

- 1) Tensile tests on coupons from 0.094- and 0.188-inch sheet, 0.250- and 0.375-inch plate, and angle and tee extrusions (6 specimens each).
- 2) Fatigue crack initiation, fatigue crack growth, and fracture tests as follows:
  - Constant-amplitude fatigue crack initiation tests of open-hole coupons (for sheet, plate and extrusion) and small specimens with fasteners (0.188-inch sheet only) for predicting the initiation of secondary cracks ("crack reinitiation") at initially undamaged locations in the structural specimens.
  - Constant amplitude fatigue crack growth rate tests (sheet, plate and extrusion).
  - Crack growth resistance curve tests (sheet and plate) and fracture tests (extrusion).
  - Spectrum fatigue crack initiation tests of open-hole coupons and fatigue crack growth tests (0.188-inch sheet) using the 80-flight flight-simulation loading sequence used in the Phase II structural tests.
- 3) Tests to develop a technique for marking the fracture surface using variations in cyclic loading that did not appreciably affect the crack growth rates.

A series of tests to establish the size of razorblade-induced corner flaw that would best simulate a 0.005-inch fatigue-induced initial flaw. See Appendix C.

TABLE 5. BASELINE TEST SUMMARY

| Test     | Product Form  |                      |            |             |                 |               |
|----------|---|----------------------|------------|-------------|-----------------|---------------|
|          | 0.188 Sheet   | 0.094 Sheet          | 0.25 Plate | 0.375 Plate | Angle Extrusion | Tee Extrusion |
| Phase I  | Tensile   | 6                    | 6          | 6           | 6               | 6             |
|          | Fatigue initiation<br>Open-Hole Coupon<br>Fasteners | 8 + (5*)<br>7 + (6*) | 3          | 3           | 3               | 3             |
|          | Fatigue crack<br>Growth                             | 7                    | 2          | 2           | 3               | 6             |
|          | Fracture  | 2                    | 1          | 1           | 1               | 2             |
|          | Marking Cycle                                       | 3                    |            |             |                 |               |
|          | Razor   | 35*                  |            |             |                 |               |
|          | Precracking shapes                                  | 1                    | 1          |             |                 |               |
|          | Fatigue initiation                                  |                      |            |             |                 |               |
| Phase II | Fastener crack<br>Arrestment<br>Spectrum            | 6<br>4               |            |             |                 |               |
|          | Fatigue crack<br>Growth<br>Spectrum                 | 2                    |            |             |                 |               |
|          |   |                      |            |             |                 |               |

\*Conducted under other funding. See Appendix C

Tests to check the shape of the nominal 0.050-inch cracks generated by precracking.

- 4) Fatigue initiation tests evaluating the effectiveness of fully-torqued flush head and protruding head Hi-lok fasteners for crack arrestment.

## SECTION III

### ANALYSIS METHODS

#### 1. BACKGROUND

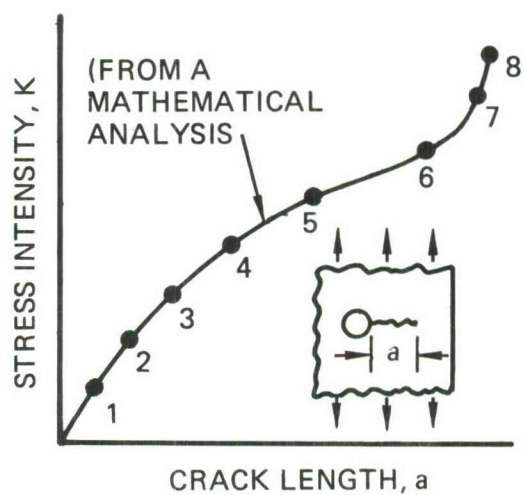
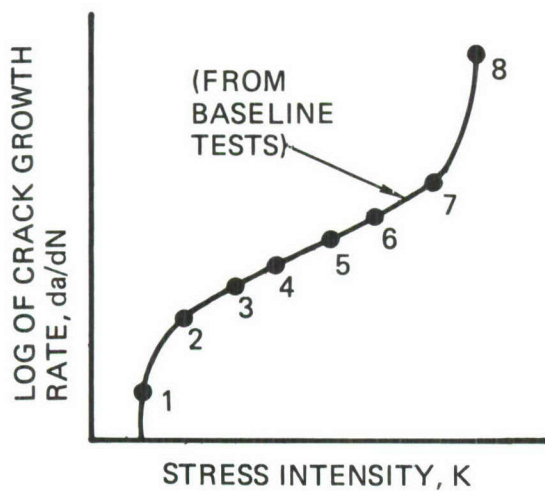
##### 1.1 Summary of Analysis Approach

The approach to predicting constant-amplitude fatigue crack propagation in simple monolithic structural members consists of the steps shown in Figure 9. Baseline crack growth rate data ( $da/dN$  vs  $K$ ) are obtained by test for the appropriate material, loading, and environment. The stress intensity factor vs crack length ( $K$  vs  $a$ ) curve for the geometry of the cracked structural member is obtained from a mathematical analysis. By combining these two and integrating  $dN/da$ , predictions can be obtained of the number of cycles required to reach any desired crack length "a." The primary limitation to this approach is that inelastic deformations must be limited to the immediate crack tip neighborhood (small-scale yielding).

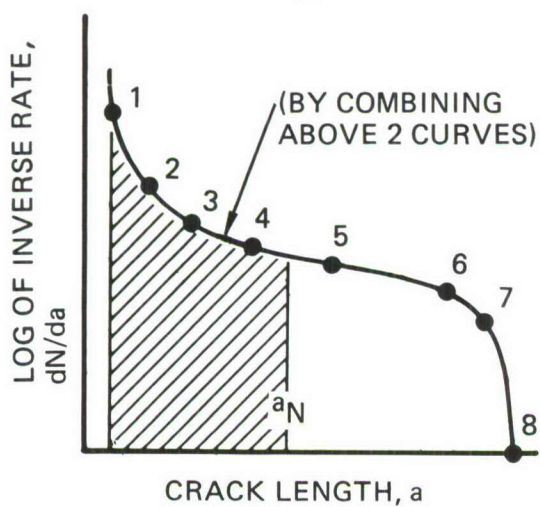
In mechanically fastened structure the problem of crack growth prediction requires additional considerations. As the crack grows, the fastener loads will, in general, change. This change could be important since the fastener load distribution affects the magnitude of the stress intensity factor. Furthermore, the propagating crack may be arrested at a fastener hole or free edge. If no flaw is present at the opposite side of the arresting hole, then crack reinitiation time must be predicted.

The phenomenon of crack arrest and reinitiation was studied in Reference 9. It was found that the reinitiation time of a crack arrested at an unflawed empty hole can be estimated using fatigue data from center-notched (unflawed) coupons. It is necessary to estimate the stress concentration factor  $k_t$  for the long notch created by the arrested crack. Then by matching both the peak elastic stress ( $k_t S$ ) and the notch radius with those of the

1



2



3

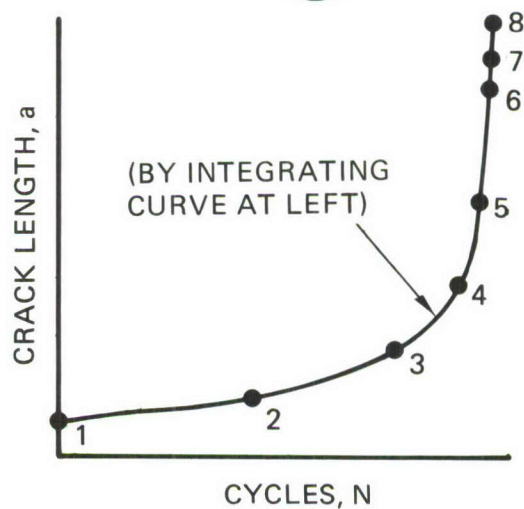


Figure 9. Crack Growth Prediction Method

baseline fatigue coupon, the crack initiation times also match. This background work is summarized in Section III, Paragraph 1.3.

Estimation of the crack arrest time at a fastener hole in mechanically fastened structure requires an extension of the approach used in Reference 9, wherein the stress concentration factor  $k_t$  is replaced by the stress severity factor ( $\lambda$ ). The stress severity factor concept was first introduced by Jarfahl (Reference 29) to account for the effects of fastener variables and fastener load transfer on the fatigue life of mechanical joints. The extended stress severity factor approach for predicting crack reinitiation times at fastener holes is presented in Section III, Paragraph 2.

Of course, Reference 1 requires the assumption of initial continuing damage flaws equivalent to quarter circular-shaped corner fatigue cracks with a 0.005 inch radius. For specimens containing these flaws, the entire analysis can be done by fracture mechanics using a baseline crack growth rate curve and estimates of the stress intensity factor.

There are several sophisticated methods for computing stress intensity factors for complex configurations. Examples are:

- Special purpose computer programs for calculating stress intensity factors for stringer-reinforced sheets containing long cracks (References 19(a), 24, 30-32) or for cracks from cold-worked or pin-loaded holes (Reference 33). The applicability of each such program is limited to a certain class of configurations.
- Finite element analysis, especially using a special crack-tip finite element containing the correct stress singularity (References 34-38). The man-hours required to set up the modeling for a proper finite element analysis of structure at a sequence of anticipated crack lengths appears to make this approach too costly for routine damage tolerance design analysis.

An engineering approach to the estimation of stress intensity factors is by the use of multiplicative correction factors based on existing K solutions. This approach has been used in References 2, 7, 9, and 39 and is used in this report. Rooke and Cartwright (References 40 and 41) use a similar approach and call it the "compounding from known solutions." References 42 and 43 provide stress intensity solutions for a large number of configurations and loading conditions for use in this method. Section III, Paragraph 3. contains

all the stress intensity formulas and correction factors used in predicting crack growth for the structural specimens tested in this research program.

A crack growing in a mechanically-fastened joint will cause a redistribution of the fastener loads. Finite element analyses can be used to compute the array of fastener loads in the joint test specimens as a function of crack size. The load transferred by the fastener in the cracked hole decreases, while the loads of the other fasteners in general increase. This redistribution of fastener loads will affect the crack growth rate. The importance of this effect was not known prior to this research program. The finite element analysis used to calculate the redistributed fastener loads as a function of crack length is presented in Section III, Paragraph 4.

#### 1.2 Continuing Damage for a Crack Growing Along a Row of Holes

One of the central questions considered in this research program was how to handle continuing damage. That is, when the crack arrests at a free edge or fastener hole, how does the analysis deal with the reinitiation of the arrested crack?

An experimental and analytical study was completed (Reference 9) of the continuing damage aspects of crack growth along a row of collinear fastener-sized holes. Four flat-sheet 7075-T6 Aluminum specimens (Figure 10) containing 11 fastener-sized holes and an E.D.M. notch at the edge of the centermost hole were tested under constant-amplitude cyclic loading at two stress levels and  $R = 0.1$  in laboratory air environment.

For purposes of analysis, the crack growth life of each specimen can be separated into a succession of crack propagation periods and crack reinitiation periods. A surface crack length of 0.050 inch, measured from the edge of the nearest hole, is selected here as the criterion for initiation or reinitiation. The time increment for a 0.050-inch crack to grow until arrest at the next hole is designated as a crack growth period; the time increment between crack arrest at the hole and the development of a 0.050-inch crack on the other side of that hole is a crack reinitiation period.

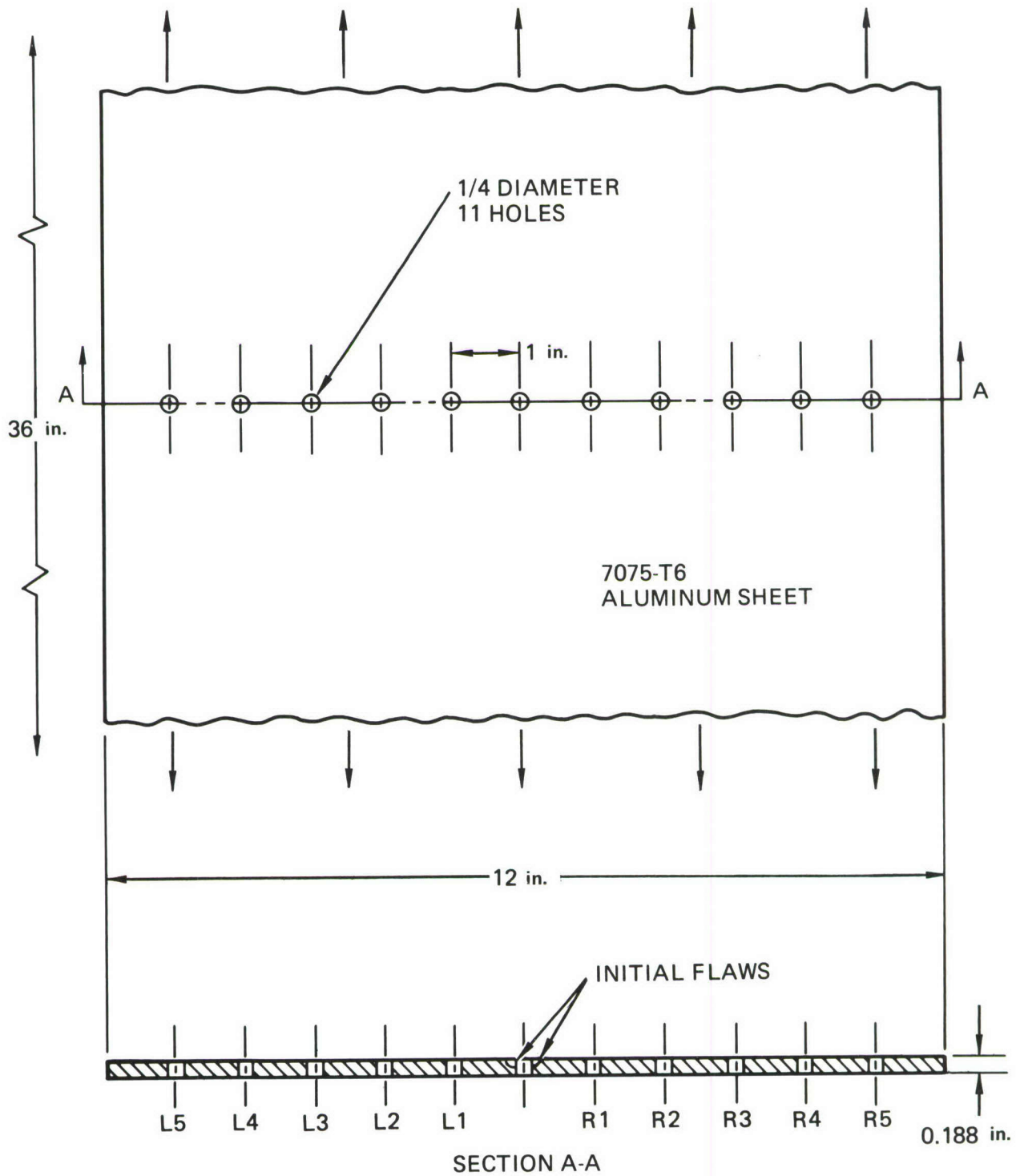


Figure 10. Test Specimen Configuration from Reference 9

A typical test result is shown in Figure 11. The loci of the right- and left-hand crack tips are plotted against time. The distance between these loci is the crack length. The horizontal segments (parallel to the time axis) correspond to crack reinitiation periods. Note that after the first crack arrest, it was predominately the crack reinitiation periods that determined the remaining test life. Clearly, a reliable method to estimate crack reinitiation periods is needed if the crack growth lives are to be accurately estimated for configurations such as a crack growing along a row of holes.

Crack reinitiation times can be estimated by at least two different procedures. One is to assume that a microcrack of a designated size is present at the reinitiation site at some designated time, estimate its stress intensity factor, and use linear elastic fracture mechanics to compute the time required for that crack to grow to a length of 0.050 inch. (Reference 1 requires the assumption of initial 0.005 microcracks at potential reinitiation sites.) The second is to use crack initiation data and an estimate of  $k_t$ , the stress concentration factor at the crack reinitiation site. Figure 12 compares the observed crack reinitiation periods for the four row-of-holes specimens with the reinitiation periods computed by using fracture mechanics and using crack nucleation data.

Paragraph 3.1.1.2c of Reference 1 states the following:

"When the crack growth from the assumed initial flaw enters into and terminates at a fastener hole, continuing damage shall be an 0.005-inch radius corner flaw  $+\Delta a$  (the amount of prior growth) emanating from the diametrically opposite side of the fastener hole at which the primary damage terminated."

This continuing damage criterion was directly applied in Reference 9 by assuming the pre-existence\* of a 0.005-inch corner crack at each eventual crack reinitiation site. However, when its accumulated length at the time of arrest of the main crack was calculated, it was found in every case to already exceed 0.050 inch. The computed reinitiation periods did not exist. (Recall that a reinitiation period is defined as the time from the instant

---

\*i.e., existence at the time that the original 0.030-inch EDM flaw at the centermost hole had developed into a 0.050-inch crack.

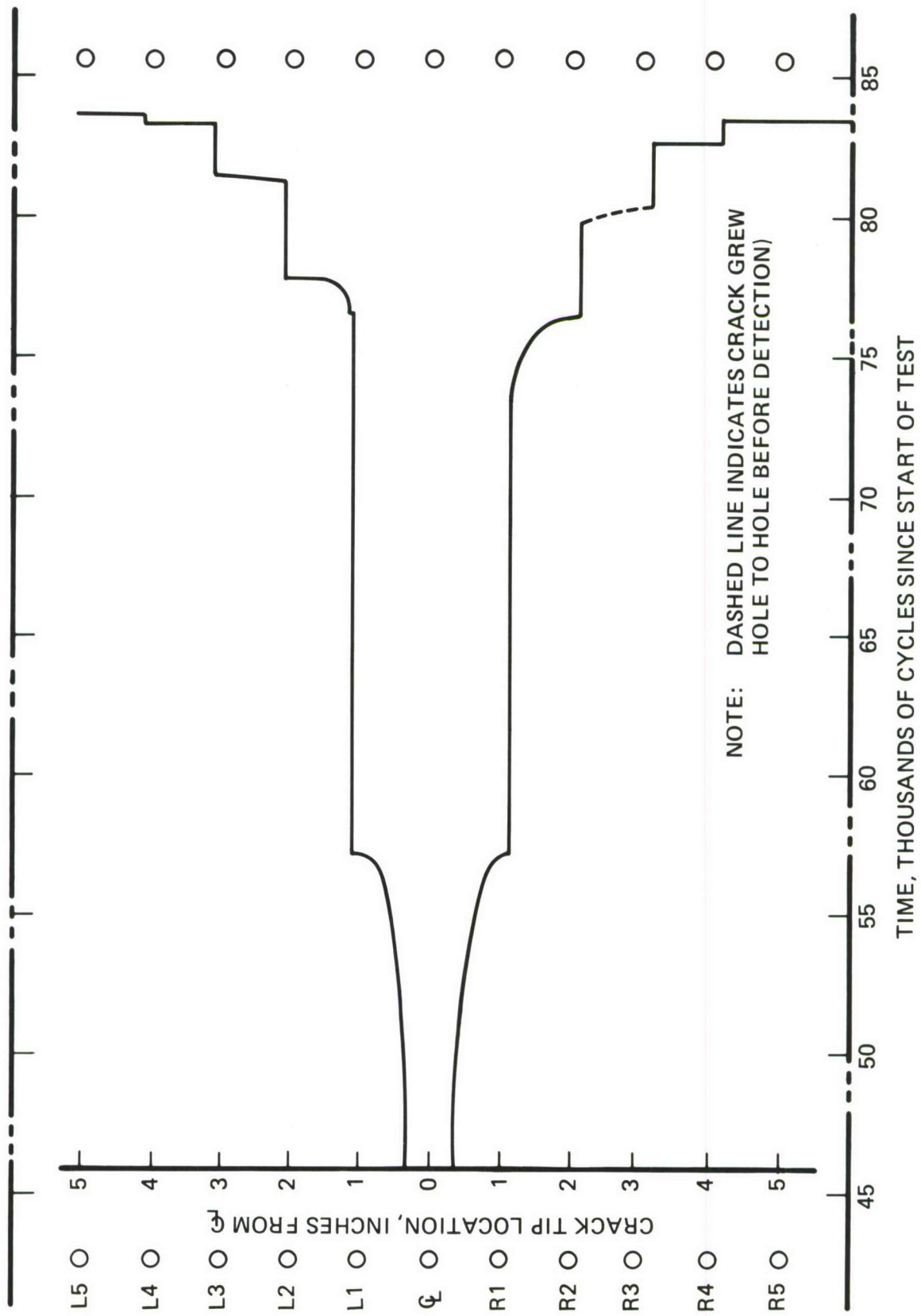


Figure 11. Test Data from Reference 9

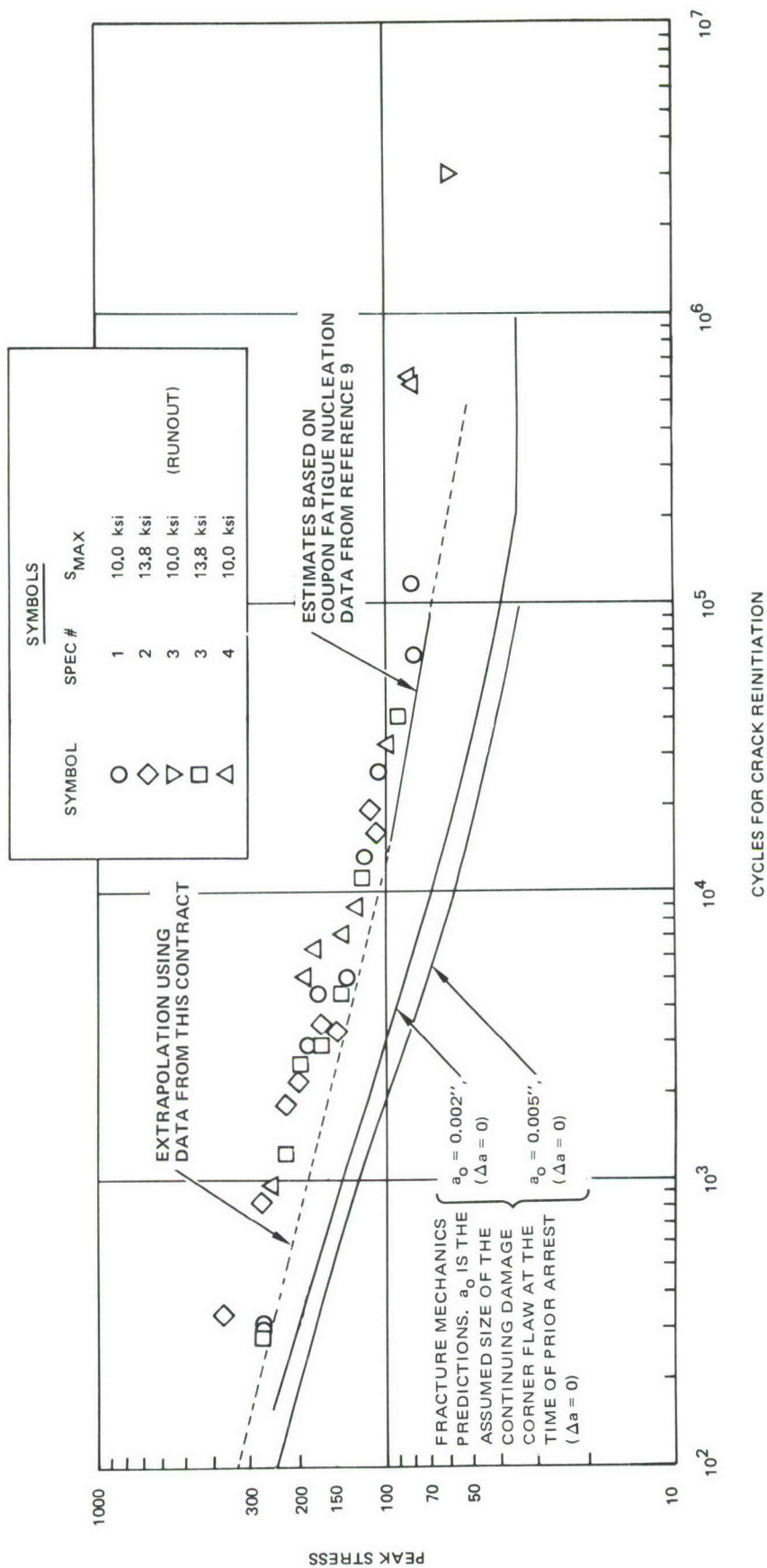


Figure 12. Actual and Estimated Crack Reinitiation Periods

of crack arrest at a hole to the development of a crack of 0.050-inch surface length on the opposite side of that hole.) For the cases tested, the existing continuing damage criterion from Reference 1 would have led to estimates so conservative that they are impossible to plot in Figure 12.

It should be noted, however, that for structural configurations where the stress intensity factor is due primarily to local fastener loads as opposed to remote tensile loads, the assumption of 0.005-inch cracks may be more accurate. This assumption also may be more accurate when the remote stresses are higher, so that crack initiation times at unflawed fastener holes are relatively short.

The lines in Figure 12 labeled Fracture Mechanics Predictions were calculated with the assumption that there was no accumulated prior growth ( $\Delta a = 0$ ). Even at that, the assumption of a continuing damage crack of  $a_o = 0.005$  inch at the moment of prior crack arrest is conservative by a factor of roughly 6 to 12 in its prediction of crack reinitiation times. Even with the assumption of a smaller initial crack size ( $a_o = 0.002$  inch as was successful in Reference 44), the predicted reinitiation periods are shorter than the actual reinitiation periods by a factor of about 4 to 8.

The use of crack nucleation data for prediction of reinitiation periods led to better agreement in the range of interpolation of the data (solid line in Figure 12), where the error amounted to about a factor of 2. It should be borne in mind that this study dealt with empty holes, not holes containing fasteners.

Note that the data and analytical results are plotted in Figure 12 in terms of the peak elastic stress at the notch tip (crack initiation site). The discussion in Reference 9 develops the theoretical basis for using this variable by itself to characterize the rate of damage accumulation and microcrack growth in the notch root neighborhood. The arguments in this discussion are fundamental to the way continuing damage analyses are conducted in this program. Therefore this discussion, taken from Reference 9, is included in the following subsection.

### 1.3 Some Observations on the Notch Root Neighborhood

In this section the elastic stress field in the neighborhood of an internal notch in a plate is considered. Figure 13 shows an isolated elliptical hole of major diameter  $2A_o$  and minimum radius of curvature  $R_o$  in an infinite plate subjected to a uniform tension field  $S$  normal to the direction of the major diameter.

For this case the peak elastic tensile stress at the edge of the notch is given by

$$\sigma_{22}(0) = (1 + 2\sqrt{A_o/R_o})S = k_t S \quad (1)$$

The expansion

$$\sigma_{ij}(x_1) = \sigma_{ij}(0) + x_1 \sigma'_{ij}(0) + \dots \quad (2)$$

is a valid representation of the elastic stresses for small values of  $x_1/R_o$ , where  $x_1$  is measured from the notch root and prime denotes differentiation with respect to  $x_1$ . The solution, expressed in the form of Equation (2), is given by

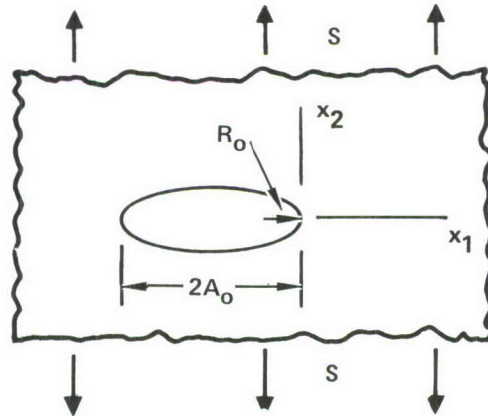


Figure 13. Elliptical Hole in a Plate

$$\frac{\sigma_{22}(x_1)}{\sigma_{22}(0)} = 1 - \left(1 + \frac{1}{2k_t}\right) \frac{2x_1}{R_o} + \dots$$

$$\frac{\sigma_{11}(x_1)}{\sigma_{22}(0)} = \frac{2x_1}{R_o} + \dots \quad (3)$$

a,b,c

$$\frac{\sigma_{12}(x_1)}{\sigma_{22}(0)} = 0$$

Note that the term  $1 + 1/(2k_t)$  is approximately constant and equal to unity when  $k_t \geq 3.0$ . There is no other dependence on  $k_t$  in Equations (3).

Thus, in a manner similar to the way the crack tip stress intensity factor governs the elastic stress field at a crack tip, the peak elastic notch stress  $\sigma_{22}(0)$  governs the elastic stress field for all  $k_t \geq 3.0$  notches of equal notch root radius  $R_o$ .

Stated another way, the elastic stress distribution near any long elliptical hole of minimum radius  $R_o$  and peak elastic notch stress  $\sigma_{22}(0)$  is approximately identical to the elastic stress distribution near a circular hole having the same minimum notch radius and peak elastic stress. This local equivalence of notch root stresses occurs despite the fact that the  $k_t$  values for the circular and elliptical holes may be vastly different. The elastic notch-root stress field for a long slot formed by collinear circular holes connected by a crack, is likewise expected to be equivalent to that of one circular hole, provided notch radius and peak stress match. This is expected because of the geometric similarity between such a slot and a long ellipse, although exact stress gradient expressions for a long slot are not available.

The equivalence among notch stresses for equal-radius internal notches with different geometries and  $k_t$  values has important implications for analysis methods for fatigue crack nucleation and the fatigue propagation of tiny cracks at notch roots.

Referring to Figure 14, let  $\rho$  denote the region in the notch-root neighborhood of an arbitrary elliptic notch within which the exact elastic stress field  $\sigma_{ij}$  is essentially equal to  $\sigma_{ij}^{(App)}$ , the notch stress field for a circular hole of the same radius. Suppose that some inelastic behavior, such as plasticity, fatigue damage, or microcracking occurs within the subregion  $\delta$ , embedded within  $\rho$ . If  $\delta$  is small enough, this inelastic behavior will have no effect outside the region  $\rho$ .

Under this condition of small-scale inelasticity, the mechanical response of the material (i.e., true plastic strain, rate of fatigue damage, or propagation rate and stress intensity factor of a microcrack) near the root of an arbitrary elliptic notch will be totally governed by  $\sigma_{ij}^{(App)}$ ; in other words, it will be the same as that for a circular notch of the same material and notch radius, similarly fabricated and subjected to the same environment and peak elastic notch stress history.

This statement and its supporting argument are analogous to the classical Irwin-Rice arguments (References 45-46) for why the elastic stress intensity factor history governs the propagation behavior of a crack for cases of small-scale yielding.

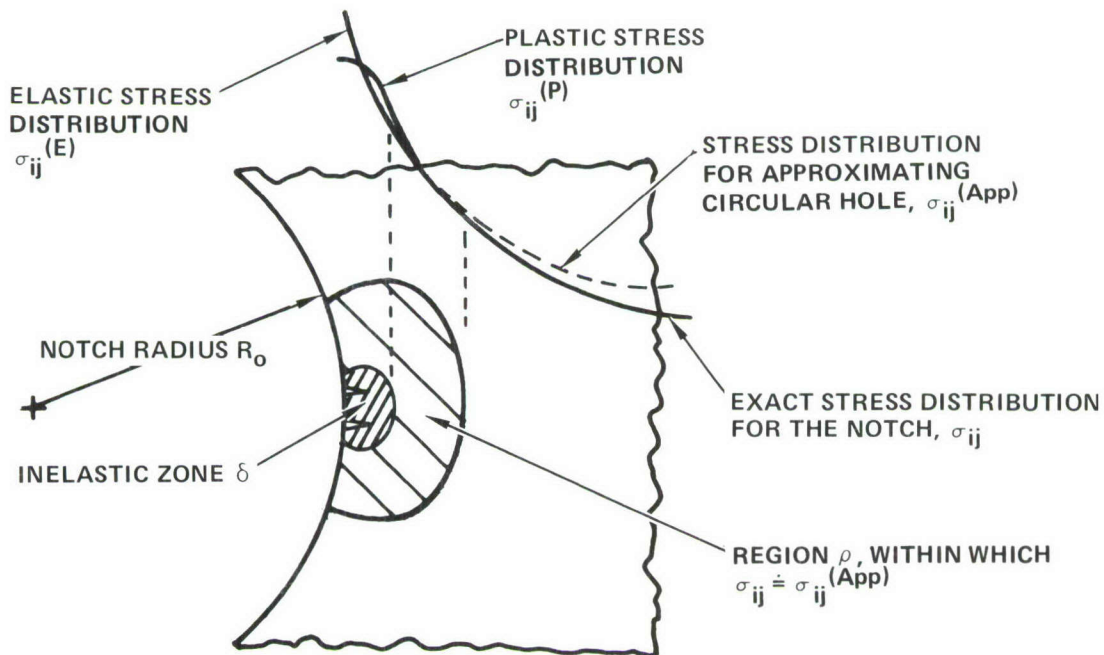


Figure 14. Notch Root Neighborhood, Long Elliptical Notch

For cases of small-scale inelasticity near a notch root several important analysis simplifications are possible. Among them are the following:

- a. Results of inelastic analyses for a circular hole (such as true plastic strain at the notch edge, plastic zone size, etc.) are accurate approximations (in the case of small-scale inelasticity) for long elliptic holes and slots with the same minimum notch radius and peak elastic stress at the edge of the notch.
- b. Standard fatigue coupons with a central circular hole of (for example) radius  $R_0 = 0.125$  inch can be fatigue tested to obtain a plot of peak notch stress against fatigue crack nucleation life. This plot should predict the life for any elliptical notch or slot with  $k_t > 3$  having a minimum notch radius  $R_0 \doteq 0.125$  inch.
- c. The stress intensity factor for a tiny through-the-thickness crack of length "a" emanating from the root of a long elliptical notch or slot of minimum radius  $R_0$  should be essentially proportional to the stress intensity factor for a crack of the same length emanating from a circular hole of the same radius. Thus, for the through-thickness microcrack emanating from a long notch,

$$K_I^{(0)} = \frac{k_t}{3} S \sqrt{\pi a} F\left(\frac{a}{a + R_0}\right), \quad \frac{a}{a + R_0} \ll 1 \quad (4)$$

where  $F(a/(a + R_0))$  is taken from Reference 47 (See Equation (18)).

- d. The propagation rate of a small crack near the root of a long notch should be the same as the propagation rate of an identical crack near the root of a circular notch of like radius subjected to an identical peak elastic notch stress history. (This would not necessarily follow from paragraph b since the plastic zone, while small compared with the notch neighborhood  $\rho$  of Figure 14, may be large when compared with the crack length, so that  $K$  will not fully govern crack propagation rate.)

The above hypotheses are the keys that permit the analyses of the crack reinitiation periods for cracks arresting at holes.

## 2. PREDICTING THE REINITIATION OF AN ARRESTED CRACK

In Reference 9 the reinitiation time of a fatigue crack that had arrested at an open hole is estimated from baseline coupon fatigue (crack initiation) data and a computed value of the stress concentration factor  $k_t$ . The presence of the arrested crack is accounted for in the  $k_t$  value.

In the following, the theory is developed to extend the prediction approach of Reference 9 to estimate the reinitiation of an arrested fatigue crack at a fastener hole where some fastener load transfer may occur. Here it is assumed that the stress severity factor  $\lambda$  (Reference 29) can be used to replace  $k_t$  as the parameter characterizing the severity of the stresses at the crack nucleation site. The factor  $\lambda$  includes a term intended to account for fastener-load transfer and factors to account for the nature of the fastener and differences in hole radius.

## 2.1 Modified Stress Severity Factor Equation

As used here, the stress severity factor  $\lambda$  is a factor which can be multiplied by the gross area stress in a joint to compute an effective value of the peak tensile stress at the potential crack initiation site at the edge of the fastener hole.

The equation to be used here is nearly identical to that of Jarfahl in Reference 29. Let  $S$  be the reference gross area stress for any mechanically-fastened structure. Consider a member of width  $W$  and thickness  $t$ . For a selected fastener of radius  $R_o$  in a given fastener row, let  $\Delta P$  be the load transferred by the fastener; let  $\Sigma \Delta P$  be the load transferred in that row of fasteners; and let  $P_{bp}$  be the load bypassing that row in that member. Then the stress severity factor is

$$\lambda = \alpha \beta \left[ \frac{\Delta P}{2R_o t S} k_{tb}^\theta + \frac{P_{bp} + \frac{1}{2} \Sigma \Delta P}{W t S} k_{tg} \right] \quad (5)$$

In this equation  $\alpha$ ,  $\beta$ ,  $\theta$ ,  $k_{tb}$  and  $k_{tg}$  are constants with the following meanings:

$\alpha$  = An empirical factor to account for hole quality and hole size.

$\beta$  = An empirical factor to account for fastener and fastener fit.

$\theta$  = A theoretical "tilt factor" to account for the fastener rotation and deflection. Defined as the peak bearing stress divided by the average bearing stress at the hole.

$k_{tb}$  = Stress concentration factor for a plate with a hole subjected to a bearing load; equal to the peak tensile stress (due to  $\Delta P$ ) divided by the average bearing stress.

$k_{tg}$  = Gross area stress concentration factor for a hole in a finite-width plate under uniform tension; peak tensile stress due to the remote loading divided by the average remote stress.

The factors  $\alpha$  and  $\beta$  were determined empirically using the baseline fastener fatigue specimens; see Section 4.2.3. Theoretical values of the tilt factor  $\theta$ , calculated as background to Reference 48, were supplied for use in this research program by Lockheed-Georgia Company personnel and, in some cases, computed by a finite element analysis. Some values of  $\alpha$ ,  $\beta$  and  $\theta$  used in this program are presented in Table 6. The stress concentration factors  $k_{tb}$  and  $k_{tg}$  are discussed in the following two sections.

## 2.2 Stress concentration Factor $k_{tb}$ for Fastener Load

The factor  $k_{tb}$  in Equation (5) is 1.0 for a pin-loaded hole in a plate of infinite width. For a plate of finite width, Figure 147 of Reference 49 shows  $k_{tb}$  to increase with decreasing plate width. However, for  $2R_o/W < 0.3$ , this increase in peak stress above 1.0 times the bearing stress is not caused by the pin load itself. Rather, it is due entirely to the stress concentration caused by the remote load needed to equilibrate the pin load. Therefore the increase in  $\lambda$  more properly enters Equation (5) through the remote-load term (second parenthesized term), not through the constant  $k_{tb}$ . This is the reason for the  $\Sigma\Delta P$  quantity in the second term of Equation (5). Thus,  $k_{tb} = 1.0$  is used for circular holes when  $2R_o/W < 0.3$ .

This research program is concerned with crack reinitiation after a crack is arrested at a fastener hole. An appropriate expression for  $k_{tb}$  is obtained by use of the similarities in the four problems shown in Figure 15. Problem A in the figure, which has an arbitrary number (shown as  $J = 3$ ) of fastener loads, is the one for which a solution must be estimated for bearing stress concentration factor  $k_{tb}$  on the right-hand side of the notch. The

TABLE 6 . CONSTANTS FOR STRESS SEVERITY FACTOR ANALYSIS

$\alpha$  value for drilled holes (from baseline data, Section IV):

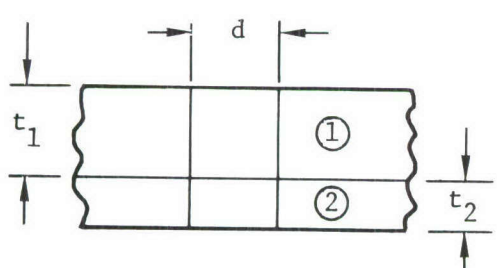
|                 |                           |
|-----------------|---------------------------|
| 0.25 dia. hole  | $\alpha = 1.00$ (assumed) |
| 0.312 dia. hole | $\alpha = 1.03$           |
| 0.375 dia. hole | $\alpha = 1.06$           |

$\beta$  values for Steel Hi-lok Fastener (from baseline data, Section IV):

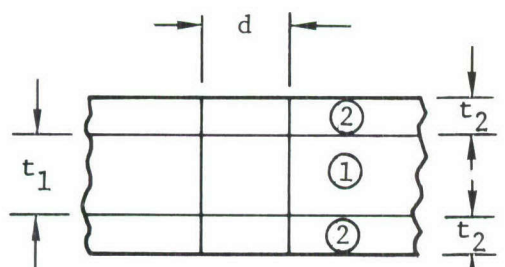
|                                       |                 |
|---------------------------------------|-----------------|
| Open Hole (assumed)                   | $\beta = 1.00$  |
| Clearance fit, finger-tight only      | $\beta = 1.00$  |
| 0.001 in. Interference, full clamp-up | $\beta = 0.635$ |

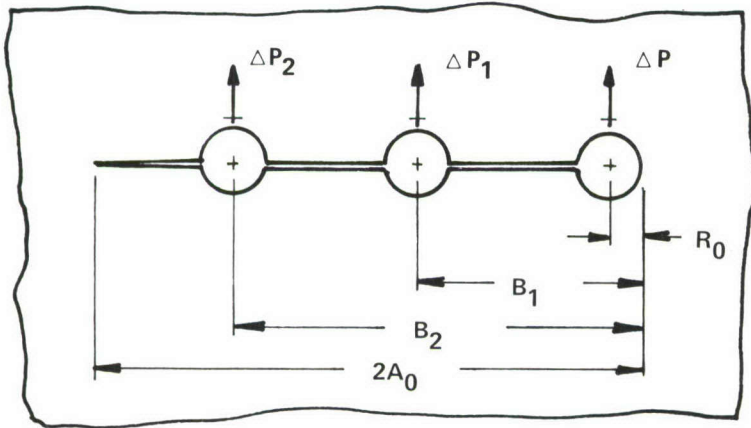
$\theta$  values for steel fasteners in aluminum sheet (theoretical results for Reference 48):

#### Single Shear Joints

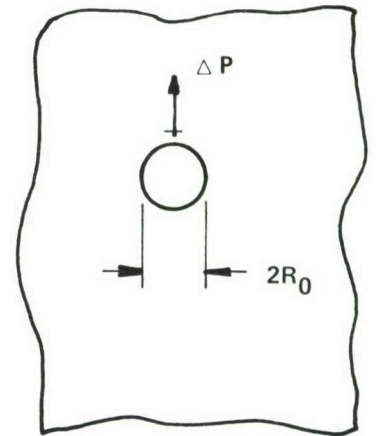
|  |  | $\frac{t_2}{t_1}$ | $\frac{t_1}{d}$ | $\theta_1$ | $\theta_2$ |
|---|--|-------------------|-----------------|------------|------------|
|   |  | 1.0               | 0.50            | 1.05       | 1.05       |
|   |  | 1.0               | 0.60            | 1.09       | 1.09       |
|   |  | 1.0               | 0.75            | 1.21       | 1.21       |
|   |  | 1.0               | 1.00            | 1.50       | 1.50       |
|   |  | 0.75              | 1.00            | 1.43       | 1.23       |
|   |  | 0.53              | 1.00            | 1.35       | 1.08       |

#### Double Shear Joints

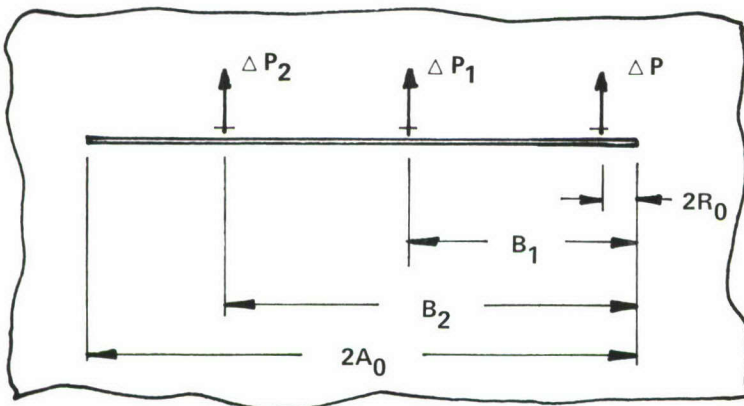
|  |  | $\frac{2t_2}{t_1}$ | $\frac{t_1}{d}$ | $\theta_1$ | $\theta_2$ |
|---|--|--------------------|-----------------|------------|------------|
|   |  | 1.0                | 0.75            | 1.04       | 1.04       |
|   |  | 1.0                | 1.00            | 1.07       | 1.07       |



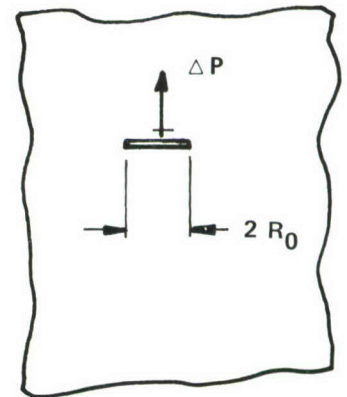
PROBLEM A



PROBLEM B



PROBLEM C



PROBLEM D

Figure 15. Equivalent Crack and Notch Problems

solution for  $k_{tb}$  for problem B is 1.0. The stress intensity factors for Problems C and D are also known. For problem C at the right-hand crack tip, from Reference 43,

$$K_I^{(C)} = \frac{\Delta P}{2t\sqrt{\pi R_o}} \phi \quad (6)$$

where

$$\phi = \sqrt{\frac{R_o}{A_o}} \left[ \sqrt{\frac{2A_o}{R_o} - 1} + \sum_{j=1}^{J-1} \left( \frac{\Delta P_j}{\Delta P} \sqrt{\frac{2A_o}{B_j} - 1} \right) \right] \quad (7)$$

For problem D, from Reference 43,

$$K_I^{(D)} = \frac{\Delta P}{2t\sqrt{\pi R_o}} \quad (8)$$

By the similarity of these configurations it is assumed that the solutions to problems A, B, C and D in Figure 15 are related by

$$\frac{k_{tb}^{(A)}}{k_{tb}^{(B)}} = \frac{K_I^{(C)}}{K_I^{(D)}} \quad (9)$$

Combining Equations (6) through (9) gives

$$k_{tb}^{(A)} = \phi = \sqrt{\frac{R_o}{A_o}} \left[ \sqrt{\frac{2A_o}{R_o} - 1} + \sum_{j=1}^{J-1} \left( \frac{\Delta P_j}{\Delta P} \sqrt{\frac{2A_o}{B_j} - 1} \right) \right] \quad (10)$$

### 2.3 Stress Concentration Factor $k_{tg}$ for Remote Loading

Approximate expressions can be developed for  $k_{tg}$  on the uncracked side of a cracked hole in a strip subjected to uniform tension. The approach used here is the compounding of known solutions. A set of multiplicative correction factors are applied to modify a fundamental solution so as to account for secondary structural details such as strip width.

The fundamental solution, from Equation (1) is for the elliptical hole problem shown in Figure 13.

$$k_t^{(1)} = 1 + 2\sqrt{A_o/R_o} \quad (11)$$

A shape factor is used to adjust for the difference in notch shape between an elliptical hole and a crack arrested at a circular hole, Figure 16. The solution for this problem, plotted in Reference 43, is approximated by

$$k_t = k_t^{(1)} \gamma_{o-o} \quad (12)$$

where the shape correction factor is

$$\gamma_{o-o} = 1 + \left[ \frac{2}{\pi} \sin^{-1} \left( 1 - \frac{R_o}{A_o} \right) \right]^3 \bigg/ 6 \quad (13)$$

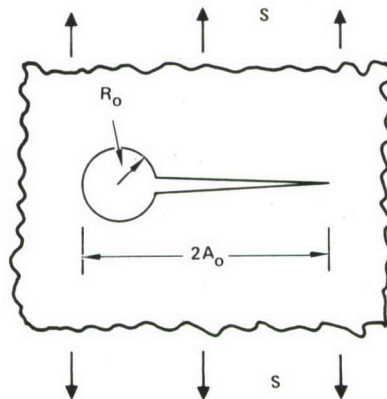


Figure 16. Crack Arrested at a Circular Hole

Isida (Reference 50) solved the problem of remote tension on a finite-width strip of width  $W$  with a central elliptical hole. The following approximate width correction was worked out in Reference 9.

$$k_t = \gamma_W k_t^{(1)} \quad (14)$$

$$\gamma_W = \left[ \sec \frac{\pi A_o}{W} \right] \left[ (1 + \sqrt{R_o/A_o})/2 \right] \quad (15)$$

It is convenient to factor  $\gamma_W$  into parts as follows

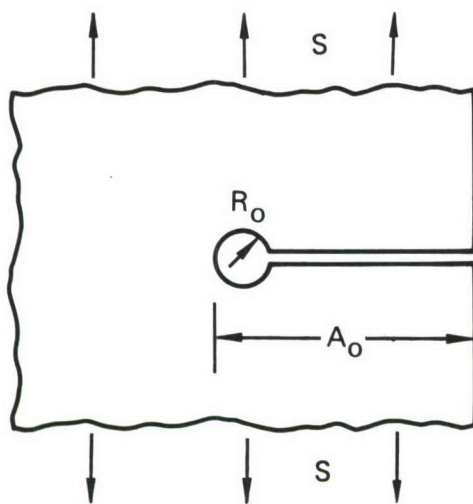
$$\gamma_W = \gamma_{FW} \gamma_{RW} \quad (16a)$$

$$\gamma_{FW} = \sqrt{\sec \frac{\pi A_o}{W}} \quad (16b)$$

$$\gamma_{RW} = \left( \sec \frac{\pi A_o}{W} \right)^{\sqrt{R_o/4A_o}} \quad (16c)$$

Note that  $\gamma_{FW}$  is the width correction associated with a crack in a finite strip. Thus  $\gamma_{RW}$  accounts for the difference between finite width effects for  $k_t$  of an elliptical hole and for  $K_I$  of a crack. For several other cases, correction factors for  $k_t$  are assumed to be identical to those for  $K_I$ , the stress intensity factor. Equations for these are described in Section III, Paragraph 4. The configurations for these cases are shown in Figure 17, along with the applicable  $k_t$  expressions for each case.

Note in Figure 17 that Equation (16) can be extended and used for a mildly eccentric notch in a finite-width strip. The stress intensity solution for an eccentrically-cracked strip, discussed in Section III, Paragraph 3.2.2 and approximated in Equations (27a) and (27b), is recommended for this purpose.

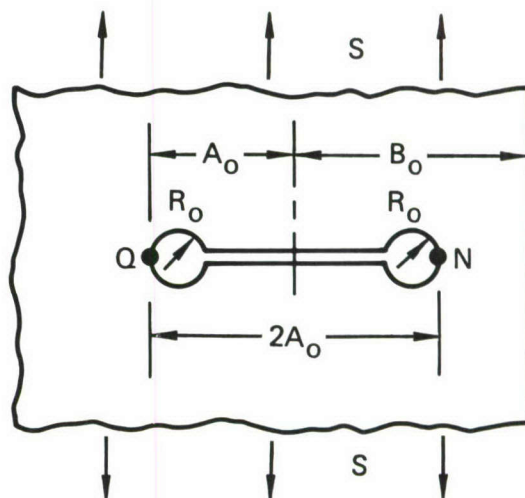


#### SEMI-INFINITE PLATE

$$k_t = k_t^{(1)} \gamma_{EC} \gamma_{o-o}$$

$$\gamma_{EC} = 1.1215$$

from Eq (22)



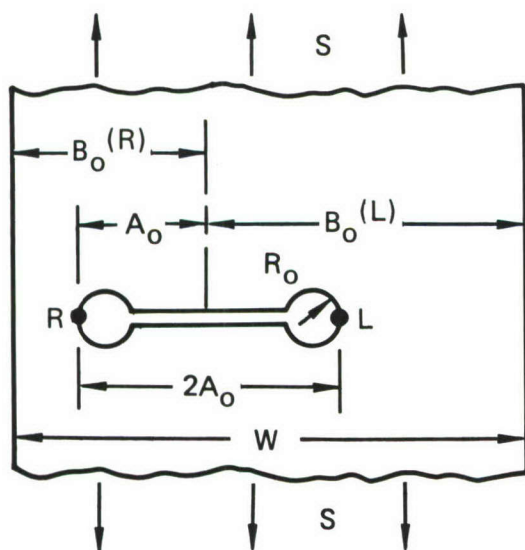
#### SEMI-INFINITE PLATE

$$k_t^{(Q)} = k_t^{(1)} \gamma_{QE} \gamma_{o-o}$$

$$k_t^{(N)} = k_t^{(1)} \gamma_{NE} \gamma_{o-o}$$

$\gamma_{QE}$  from Eq (26)

$\gamma_{NE}$  from Eq (24)



#### FINITE-WIDTH STRIP

$$k_t^{(L)} = k_t^{(1)} \gamma_{o-o} \gamma_{RW} \gamma_{FW}^{(L)}$$

$\gamma_{FW}^{(R)}$  from Eq (27a)

$\gamma_{FW}^{(L)}$  From Eq (27b)

Figure 17. Stress Concentration Factors for Common Notch Configurations

## 2.4 Baseline Fatigue Data Required

Equation (5) is the general equation for stress severity factor used in this research study. If the fastener loads are known,  $\lambda$  can be computed. What is then needed is a relationship between  $\lambda$  and fatigue life for the material, environment, and loading history of interest.

The material is 7075-T6 aluminum in several product forms, most commonly 0.182-inch sheet. The loading history for Phase I testing is constant cyclic amplitude,  $R = 0.1$ . Phase II has some testing with a specific flight-by-flight loading sequence. The environment is laboratory air ( $69-75^{\circ}\text{F}$ , 30-50% RH).

Thus, coupons with known values of  $\lambda$  were fatigue tested at various stress levels to determine the time until crack initiation. Open-hole coupons (for which  $\lambda = \alpha\beta k_t$ ) were used with 0.250-inch diameter holes.  $\alpha$  was set equal to 1.0 for this hole diameter and  $\beta$  was set equal to 1.0 for the empty hole or clearance-fit fastener case.

Specimens were also tested with 0.25 and 0.375-inch diameter fasteners and different levels of fastener interference, torque and load transfer to empirically estimate  $\alpha$  as a function of hole diameter and  $\beta$  as a function of the fastener characteristics.

The results of all baseline fatigue tests are presented in Section IV.

## 2.5 Cumulative Damage Computation of Crack Initiation Times

Consider the crack initiation phenomenon that occurs on the left-hand side of the hole in Figure 16. Simultaneously the crack is growing on the right-hand side of the hole, imposing a continuous change upon the stress severity factor for the initiating crack. Therefore the damage rate at the hole changes, and it is necessary to do a linear cumulative damage analysis.

The baseline fatigue data presented in Section 4 provide a relationship between damage rate  $dD/dt$  (equal to inverse fatigue life,  $1/N$ ), and the stress severity factor. Equations (5) through (16) give stress severity factors as a function of crack length. The results of the crack growth

computation for the right-hand crack in Figure 16 provide crack length as a function of time. Combining these three, the damage rate can be expressed as a function of time. Integration then results in the required estimate of the number of load cycles  $N_1$  required to accumulate sufficient damage  $D_1$  on the uncracked side of the hole in Figure 16 to form a "fracture mechanics crack;" viz.,

$$\int_0^{N_1} \frac{dD}{dt} dt = D_1 \quad (17)$$

A crack of about 0.050 inch is assumed to be a fracture mechanics crack (i.e., one whose growth can be estimated using linear elastic fracture mechanics methods). The baseline data that form a basis for estimating damage rate are from coupons which cracked beyond 0.050-inch and failed completely when the damage was 1.0. Back-calculating crack growth in some of these coupons shows that typically a 0.050-inch crack is formed at about 85 percent of the observed specimen failure life. Therefore a 0.050-inch crack is assumed to be initiated when  $D_1 = 0.85$ . Thereafter a  $da/dN$  analysis is applied to the initiated crack, using baseline  $da/dN$  data from Section 4 and stress intensity equations constructed using the equations of the following section.

### 3. STRESS INTENSITY FACTOR ANALYSIS

Stress intensity factor ( $K_I$ ) expressions are available in References 42 and 43 for a large variety of simple crack configurations, element geometries and loading conditions. Estimates of  $K_I$  for complex geometries can be obtained by combining an appropriate set of available simple solutions. Reference 40 calls this type of approach "compounding from known solutions."

In this section, approximate expressions for  $K_I$  are developed for various complex crack configurations which occur in the structural test specimens, by

compounding from known stress intensity solutions. In this method each  $K_I$  expression is constructed using a "fundamental" solution multiplied by an appropriate set of nondimensional correction factors.

### 3.1 The Fundamental $K_I$ Solutions

Three fundamental stress intensity factor solutions are used alternatively in this report.

All of the cases of interest here involve cracks emanating from fastener holes. Thus the known stress intensity factor solution for the crack problem shown in Figure 18 is the first fundamental solution to be used. Tweed and Rooke (Reference 47) have improved upon the accuracy of Bowie's original solution (Reference 51) to this problem, and the following expression (Reference 9) fits their numerical results to within one percent for any value of  $a/R_o$ :

$$K_I^{(1)} = S \sqrt{\pi a} F \left( \frac{a}{a + R_o} \right) \quad (18a)$$

where

$$F \left( \frac{a}{a + R_o} \right) = \text{EXP} \left[ 1.2133 - 2.205 \left( \frac{a}{a + R_o} \right) + 0.6451 \left( \frac{a}{a + R_o} \right)^2 \right] \quad (18b)$$

When the crack is long and its tip is remote from the edge of the fastener hole, as shown for example in Figure 19 (a),  $K_I$  is approximately equal to the  $K_I$  value for the equivalent line crack, Figure 19 (b). This means that the effect of the hole is negligible if the hole is not nearby, except that the hole diameter is added to the crack length. Thus, the solution to the line-crack problem in Figure 19 (b) is the second fundamental solution used here. This solution is simply

$$K_I^{(2)} = S \sqrt{\pi A_o} \quad (19)$$

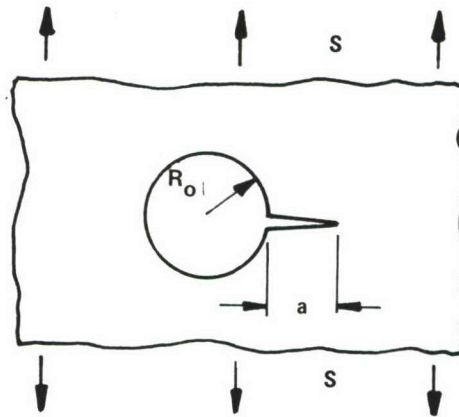
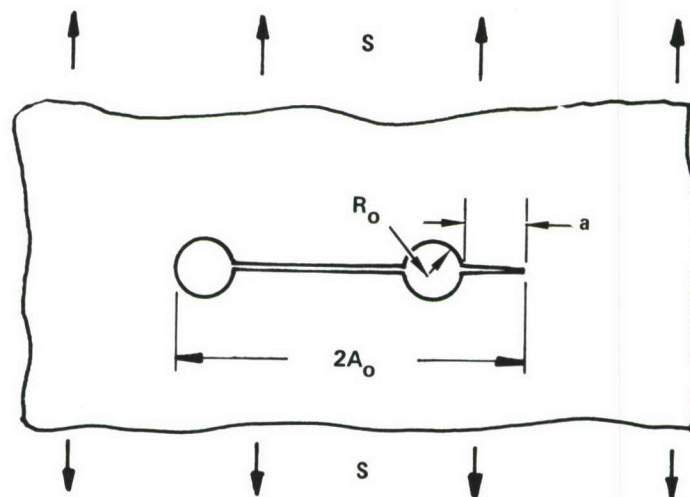
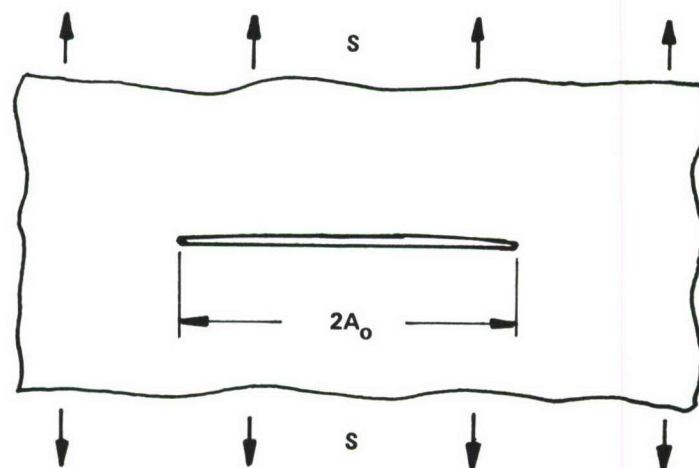


Figure 18. Uniform Tension Applied to a Through-Thickness Crack at a Circular Hole



(a) Crack Across Fastener Holes



(b) Through-Thickness Line Crack in a Sheet

Figure 19. Two Approximately Equivalent Cases (if  $a \gg R_o$ )

If the crack tip in Figure 19 (a) is very close to the edge of the hole (that is, if  $a \ll R_o$ ) then the appropriate fundamental solution is the short crack solution introduced in Section III, Paragraph 1.3., Equation (4):

$$K_I^{(0)} = \frac{k_t}{3} K_I^{(1)} \quad (20)$$

Although all the configurations of interest in this research resemble one of the fundamental configurations shown in Figures 18 and 19, all are slightly different. For example, the crack from a hole may be a corner crack rather than a through-thickness crack; the finite width of the specimen may have an influence; the loads may be applied at nearby fastener locations rather than uniformly at infinity; etc. A set of multiplicative correction factors account for these deviations from the fundamental cases.

### 3.2 Correction Factors for Adjacent Holes and Edges

3.2.1 Crack at or Near a Free Edge. - The stress intensity factor for an edge crack in a semi-infinite plate, Figure 20 (a), is

$$K_I = Y_{EC} K_I^{(2)} \quad (21)$$

where  $Y_{EC} = 1.1215 \quad (22)$

is the edge crack correction factor for stress intensity.

Figure 20 (b) shows a crack of length  $2A_o$  located a distance  $B_o$  from the edge of a semi-infinite plate loaded in uniform tension. The stress intensity factors at crack tip Q and crack tip N are different. At the near edge, point N,

$$K_I = K_I^{(2)} Y_{NE} \quad (23)$$

The near-edge correction  $\gamma_{NE}$  is from Isida's (Reference 52) solution and is accurately fitted (as described in Reference 7) as follows:

$$\gamma_{NE}(x) = 1 + (0.6 + 0.39x - 0.33x^2) \left( \sqrt{\frac{2}{\pi x} \tan\left(\frac{\pi x}{2}\right)} - 1 \right) \quad (24)$$

where  $x = A_o/B_o$ .

At the crack tip remote from the free edge, point Q,

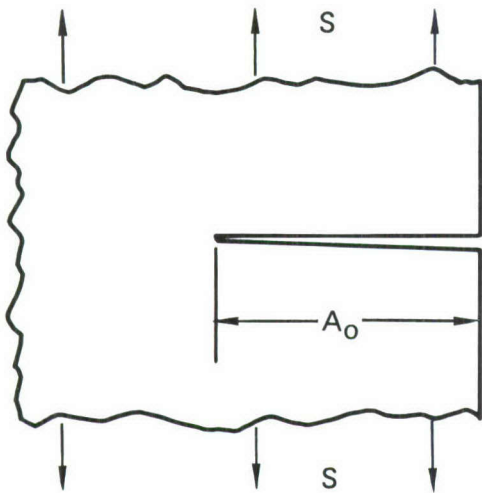
$$K_I = K_I^{(2)} \gamma_{QE} \quad (25)$$

The remote-tip factor  $\gamma_{QE}$  was also derived numerically by Isida (Reference 52) and is accurately represented by the following formula from Reference 7:

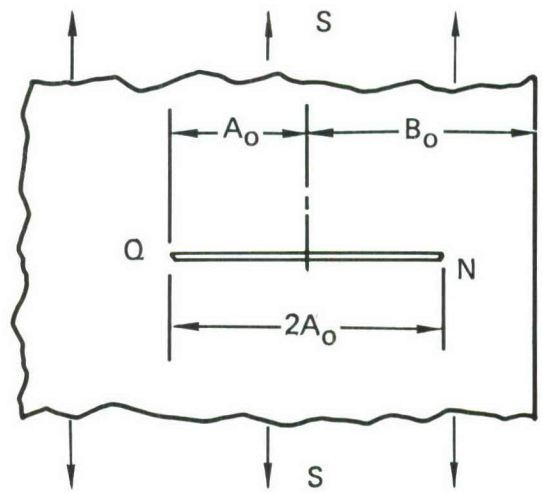
$$\gamma_{QE}(x) = 1 + \frac{x \ln(x+1)}{4} + \frac{x^4}{20(1+x)} + \frac{0.0344x^5}{1-0.8x^2} + \frac{0.0021x^6}{1-0.99x} \quad (26)$$

where  $x = A_o/B_o$ .

**3.2.2 Crack in a Finite Width Strip.** - Figure 21 shows a cracked strip subjected to uniform tension. This problem has been solved numerically by Isida (Reference 52). The finite-width factor at the tip (R) in Figure 21 can be approximated by extending the range of application of the simple secant formula suggested for the symmetric crack by Feddersen (Reference 53), as follows:



(a) EDGE CRACK



(b) CRACK NEAR AN EDGE

Figure 20. Cracked Semi-Infinite Plate

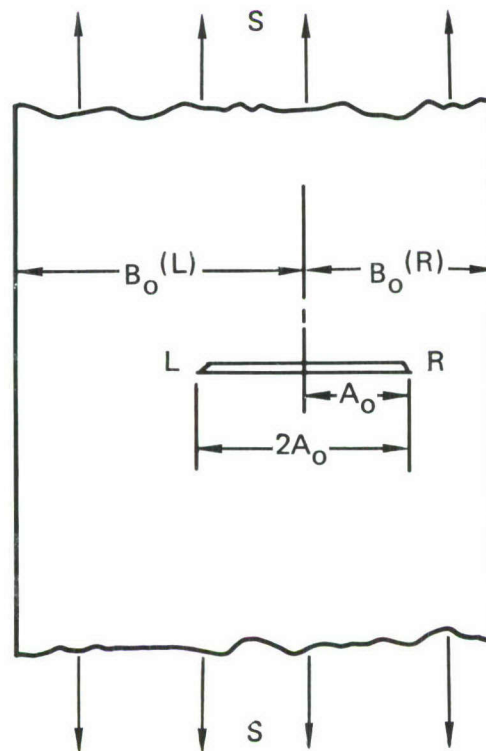


Figure 21. Eccentrically Cracked Strip in Uniform Tension

$$\gamma_{FW}^{(R)} = \sqrt{\sec\left(\frac{\pi A_o}{2B_o^{(R)}}\right)} \quad (27a)$$

$$1 \leq \frac{B_o^{(L)}}{B_o^{(R)}} \leq 3$$

A similar approximation can be used for the other tip of the crack, tip L, as follows:

$$\gamma_{FW}^{(L)} = \sqrt{\sec\left[\frac{\pi}{6}\left(\frac{2A_o}{B_o^{(R)}} + \frac{A_o}{B_o^{(L)}}\right)\right]} \quad (27b)$$

$$1 \leq \frac{B_o^{(L)}}{B_o^{(R)}} \leq 3$$

Note that Equations (27a) and (27b) are identical when  $B_o^{(R)} = B_o^{(L)}$ .

**3.2.3 Crack Approaching a Hole.** - In the chordwise splice specimens the crack is expected to grow from fastener hole to fastener hole. Therefore the stress intensity factor expression should account for the growth of a crack toward a hole. Figure 22 shows this configuration. The stress intensity factor originally calculated by Isida (Reference 54) is summarized in References 42 and 43. The correction factor  $\gamma_{AH}$  is defined as the ratio of the stress intensity for the problem in Figure 21 to  $K_I^{(2)}$  from Equation (19). The following approximation of Isida's solution can be used:

$$\gamma_{AH} = \left( \frac{C_o - A_o}{R_o + C_o - A_o} + \frac{0.1A_o}{R_o + A_o} \right)^{-0.3} \quad (28)$$

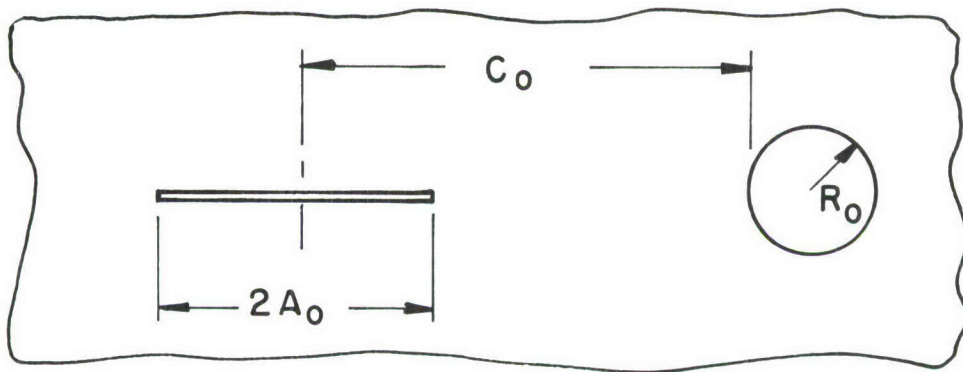


Figure 22. Crack Approaching a Hole

### 3.3 Corner Flaw at a Hole

From Reference 39 the stress intensity factor for a nearly quarter-circular corner flaw at a hole in a plate (Figure 23) is given by \*

$$K_I^{(co)} = S \sqrt{2a} \frac{F\left(\frac{a}{a + R_o}\right)}{1.1215} \quad (29)$$

By definition the corner flaw correction factor  $\gamma_{co}$  times  $K_I^{(1)}$  (from Equation (18)) equals  $K_I^{(co)}$ . Thus,

$$\gamma_{co} = \frac{K_I^{(co)}}{K_I^{(1)}} = 0.7114 \quad (30)$$

The corner flaw should be nearly quarter circular (a and c in Figure 23 approximately equal) for Equation (30) to apply.

**3.3.1 Transition Criterion.** - During the transition from a corner crack to a through-thickness crack the stress intensity factor at the crack tip on the front face would be expected to increase gradually and continuously. For small flaws ( $c \ll t$  in Figure 23) the stress intensity factor is given by Equation (29). For large flaws ( $a \gg t$ ) the through-thickness formula, Equation (18), applies. For intermediate crack lengths Reference 9 suggests a weighted average. The weighting factor is selected based on engineering judgement, and the stress intensity is given by

$$K_I^{(TR)} = \frac{1}{1 + 2(c/t)^2} K_I^{(co)} + \frac{2(c/t)^2}{1 + 2(c/t)^2} K_I^{(1)} \quad (31)$$

---

\*Reference 39 actually uses  $F\left(\frac{a}{a + \sqrt{2} R_o}\right)$  in place of  $F\left(\frac{a}{a + R_o}\right)$ , but

Equation (29) was used here to simplify succeeding equations such as Equation (32).

Thus when  $c = t$  and the crack is tangent to the back surface (Figure 24) the stress intensity according to Equation (31) is

$$(1/3)K_I^{co} + (2/3)K_I^{(1)} .$$

By definition the product of the correction factor  $Y_{TR}$  for a transitioning corner crack times  $K_I^{(1)}$  (from Equation (18)) equals  $K^{(TR)}$  (from Equation (31)). Using this definition and substituting from Equation (30) leads to

$$Y_{TR} = \frac{K_I^{(TR)}}{K_I^{(1)}} = 1.0 - \frac{0.2886}{1 + 2(c/t)^2} \quad (32)$$

**3.3.2 Experimental Verification.** - Because Equation (30) deviates slightly from the expression given in Reference 39 and Equation (31) is a product of engineering judgment rather than mathematics, an experimental check of Equation (32) was conducted. Data from Reference 55 were used so no new testing was necessary.

In Reference 55, 0.005-inch corner cracks were fatigue-induced into six  $k_t = 3.1$  coupons (see Figure 31, Section IV). Constant amplitude fatigue crack growth tests were conducted at  $R = 0.1$  and at either  $S_{max} = 22.8$  ksi or 36.45 ksi. The crack growth rate was observed as a function of crack length as each initial corner crack grew through a transition and became a through-thickness crack. (A summary is contained in Appendix C.)

These specimens were 0.188 inch 7075-T6 sheet from the material lot used in the current program. Figure 43 in Section IV provides an empirical relationship between the stress intensity factor and the crack growth rate for this lot of material based on test results from compact tension and center-cracked specimens. By matching the observed crack growth rate in the corner-flawed coupon with a point on the  $da/dN$  curve, experimental values of apparent stress intensity were plotted against crack size for six transitioning corner cracks in the  $k_t = 3.1$  coupons from Reference 55. These points are shown in Figure 25. Note the apparent stress level effect. For a nominal stress of

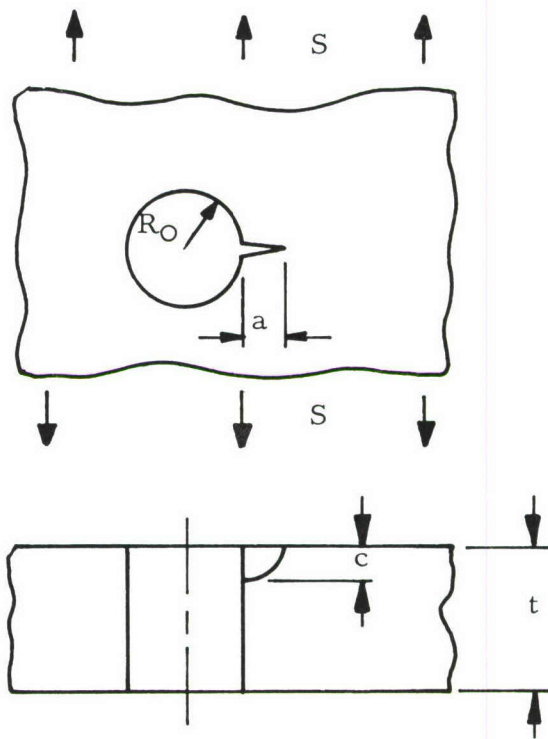


Figure 23. Corner Flaw at a Hole in a Plate

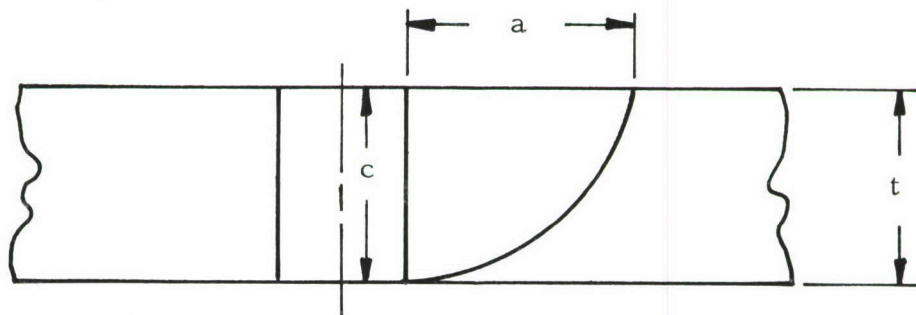


Figure 24. Corner Crack Tangent to Back Surface

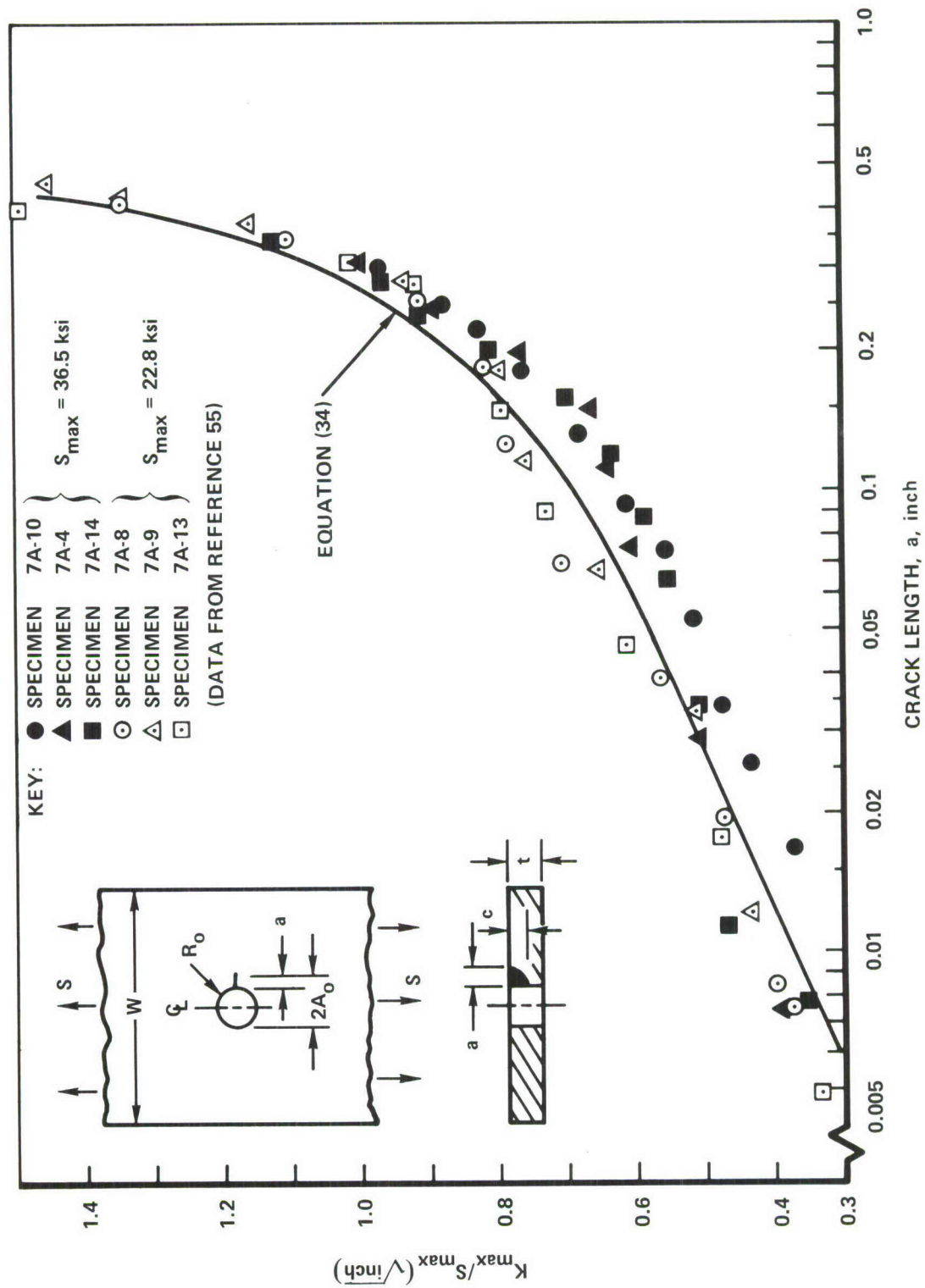


Figure 25. Comparison of Experimental and Theoretical Stress Intensity Factors for a Transitioning Corner Crack

36.45 ksi the computed peak elastic notch stress is far in excess of material yield strength. Therefore the presence of a stress effect is not surprising.

The analytical estimate of the stress intensity for this specimen, based on the fundamental solutions and correction factors discussed above, would be

$$K_I = K_I^{(1)} \gamma_{FW} \gamma_{TR} \quad (33)$$

Substitution into Equation (33) from Equations (18), (27a), and (32) gives

$$K_I = S\sqrt{\pi a} \sqrt{\sec \left[ \pi(a + 2R_o)/2(W - a) \right]} \left[ 1 - \frac{0.2886}{1 + 2(c/t)^2} \right] F\left( \frac{a}{a + R_o} \right) \quad (34)$$

Fracture surface markings on spectrum fatigue tests of other  $k_t = 3.1$  specimens with initial corner flaws tested for Reference 55 show clearly that the crack remains quarter circular, so that  $c = a$ . See Figure C-5, Appendix C. The specimen dimensions are  $R_o = 0.125$  inch,  $W = 1.5$  inch and  $t = 0.182$  inch. Using these values in Equation (34), a theoretical curve of stress intensity versus crack size was calculated and plotted in Figure 25. The close agreement, especially for the lower stress level, provides strong support for using  $\gamma_{TR}$  as given in Equation (32) as the correction factor for the corner crack to through-thickness crack transition.

### 3.4 Fastener Load Effects on $K_I$

3.4.1 Fastener Loads Near the Crack. - In the chordwise splice specimens the loads are transferred between members at the fasteners, some of which are near the crack. Thus a correction factor expression must be found for cases in which the load is applied at finite points, rather than uniformly at infinity.

Tada (Reference 43) provides the following  $K_I$  solution for the right-hand crack tip in Figure 26:

$$K_{Ij}^{(RE)} = \frac{1 + \nu}{8\sqrt{\pi A_o}} \operatorname{Im} \left[ \frac{-A_o - z_j}{\phi(z_j)} + \frac{3 - \nu}{1 + \nu} \frac{A_o + \bar{z}_j}{\phi(z_j)} + \frac{(\bar{z}_j - z_j) A_o}{(\bar{z}_j - A_o)\phi(z_j)} \right] \frac{P_j}{t} \quad (35)$$

In this equation  $\nu$  is Poisson's ratio;  $\text{Im}()$  indicates the imaginary part of the complex argument;  $z_j$  is the complex variable  $x_j + iy_j$ ;  $\bar{z}_j$  is its complex conjugate;  $\phi(z_j)$  is given by

$$\phi(z_j) = \sqrt{|z_j^2 - A_0^2|} \exp\left(\frac{i\theta_{1j} + i\theta_{2j}}{2}\right) \quad (36)$$

and  $\overline{\phi(z_j)}$  is its complex conjugate. The angles  $\theta_{1j}$  and  $\theta_{2j}$ , defined in Figure 26, are restricted to values between 0 and  $2\pi$ .

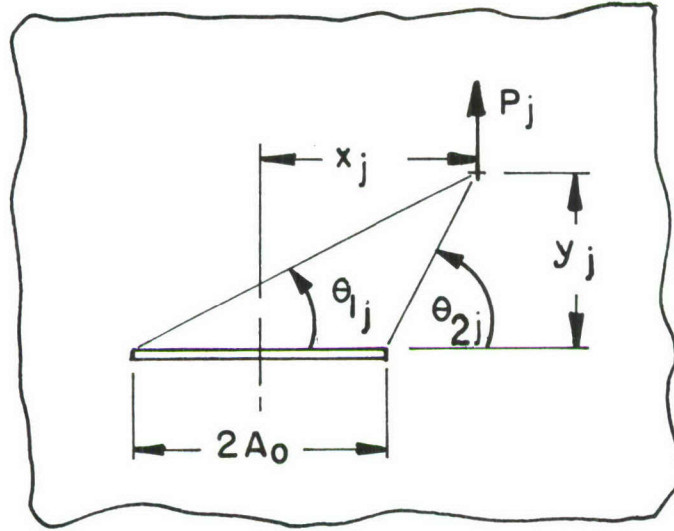


Figure 26. Point Force in the Cracked Plane of Thickness  $t$

Superposition applies if there are point loads at several points in the plane. Let  $J$  denote the total number of applied point loads directed normal to the crack. Then the total stress intensity is

$$K_I^{(RE)} = \sum_{j=1}^J \left[ K_{Ij}^{(RE)} \right] \quad (37)$$

The correction factor  $\gamma_{RE}$ , which accounts for the load being applied at fastener locations rather than uniformly at infinity, is by definition

$$\gamma_{RE} = \frac{K_I^{(RE)}}{K_I^{(2)}} = \sum_{j=1}^J \left( \frac{K_{Ij}^{(RE)}}{K_I^{(2)}} \right) \quad (38)$$

where  $K_{Ij}^{(RE)}$  is obtained for each fastener load using Equation (35) and  $K_I^{(2)}$  is as given in Equation (19).

3.4.2 Fastener Load at the Crack Origin. - The most important fastener load in the growth of small cracks in joints is the load transferred by the fastener located at the crack origin.

According to Reference 56 the stress intensity factor due to a fastener load  $P_o$  at the flaw origin is given by

$$K_I^{(FO)} = \frac{P_o}{2R_o t} F_{pl} \left( \frac{a}{a + R_o} \right) \sqrt{\pi a} \quad (39)$$

The solution for the function  $F_{pl}$  from Reference 56 is plotted as a dashed line in Figure 27.

An independent estimate of  $F_{pl}$  can be obtained. Figure 28 shows four related problems; Problem A is the one for which a solution must be estimated. By their similarity in loading, Problem A is related to Problem B, and C is related to D. By their similarity in geometry, problem A is related to C and B is related to D. All four have the same total notch length,  $2A_o$ . Thus, if  $K_I(A)$ ,  $K_I(B)$ ,  $K_I(C)$  and  $K_I(D)$  are their respective stress intensity factors, then approximately

$$\frac{K_I(A)}{K_I(B)} = \frac{K_I(C)}{K_I(D)} \quad (40)$$

The solution for  $K_I(B)$  is well known (Reference 43, page 5.4), and  $K_I(C)$  and  $K_I(D)$  have already been presented here (Equations (18) and (19) respectively). Substitution into Equation (40) leads to the following approximate expression for  $F_{pl}$ :

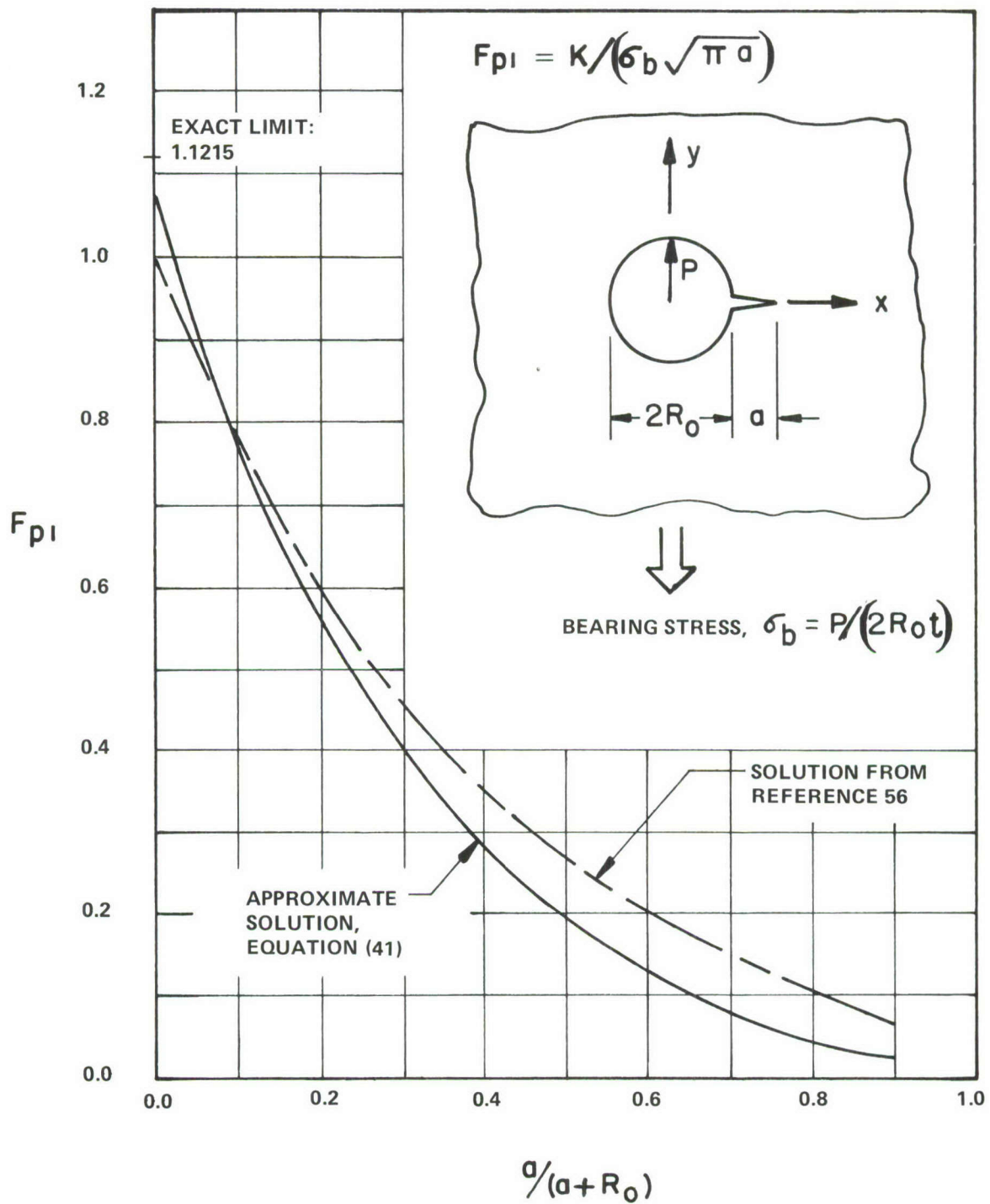
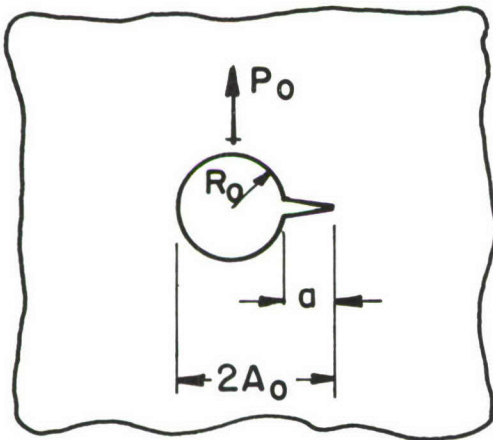
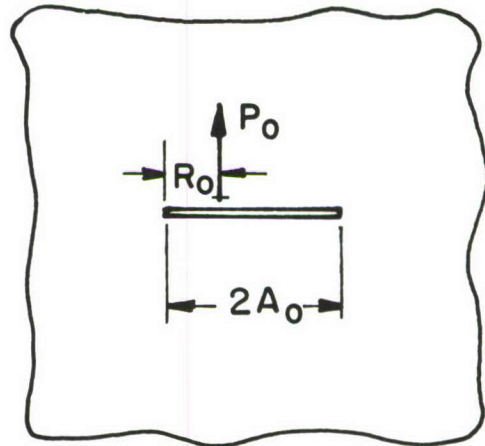


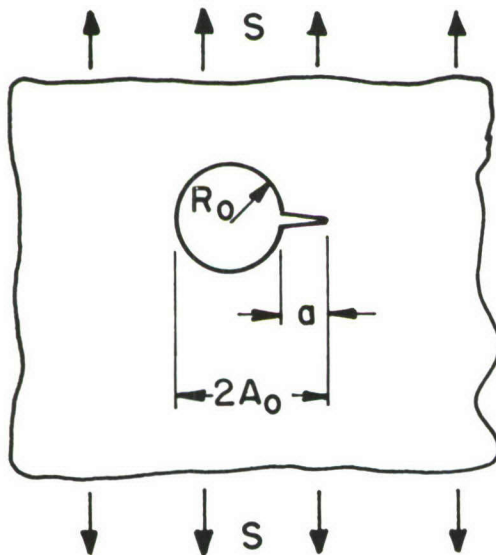
Figure 27. Stress Intensity Factor for a Crack at a Loaded Hole



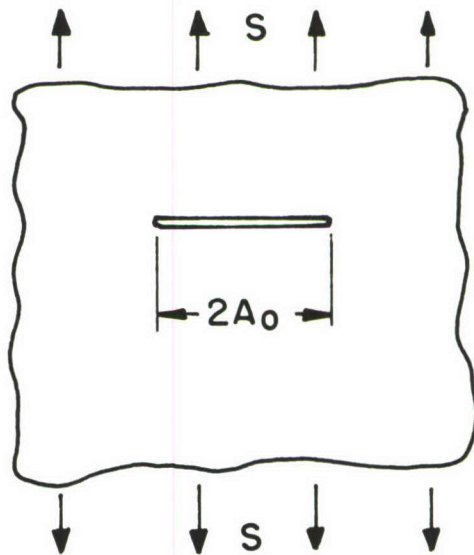
PROBLEM A



PROBLEM B



PROBLEM C



PROBLEM D

Figure 28. Four Similar Problems. (Unknown Solution to Problem A is Estimated from Known Solutions to the Others.)

$$F_{p1} \left( \frac{a}{a + R_o} \right) = \frac{R_o}{\pi A_o} \sqrt{\frac{2A_o}{R_o + a} - 1} F \left( \frac{a}{a + R_o} \right) \quad (41)$$

Note that in the limit as  $a/(a + R_o)$  approaches 1.0,  $K_I(A)$  and  $K_I(B)$  become identical, because the hole becomes small and remote from the crack tip. Thus (41) is asymptotically correct as  $a/(a + R_o)$  approaches 1.0.

Equation (41) is plotted as a solid line in Figure 27. The solution from Reference 56 appears to over-estimate  $F_{p1}$  for values of  $a/(a + R_o)$  between 0.5 and 1.0. That solution and Equation (41) agree reasonably well for low values of  $a/(a + R_o)$ . Equation (41) comes closer to approaching the correct limiting solution of 1.1215 as  $a/(a + R_o)$  approaches zero.

On this basis, Equation (41) was used as a basis for the correction factor  $\gamma_{FO}$  due to the fastener force at the crack origin. By definition

$$\gamma_{FO} = \frac{K_I^{(FO)}}{K_I^{(1)}} \quad (42)$$

Substituting from Equations (17), (39) and (41) leads to

$$\gamma_{FO} = \frac{P_o}{2\pi A_o tS} \sqrt{\frac{2A_o}{R_o + a} - 1} \quad (43)$$

**3.4.3 Correction for Fastener Tilting.** - It is assumed in all of the preceding that all loads are in-plane tensile loads. Generally in complex structure, the fasteners transfer load from the plane of one member to the plane of another member. This cannot be done without some tilting of the fastener, accompanied by induced transverse bending stresses in the members.

When a faying-surface corner crack is growing from a fastener hole and the fastener tilts, local transverse bending stresses are induced which affect the crack in two ways. First, the crack grows faster because near the faying

surface the bending stresses add to the in-plane tensile stresses, raising the stress intensity value. Secondly, the crack shape changes ( $a/c$  in Figure 23 increases).

Fastener tilting is considered in the stress severity factor analysis of undamaged joints, discussed in Section III, Paragraph 2.1. A tilt factor  $\theta$ , defined as the ratio of the peak induced stress (bending plus tension) to the average tensile stress, is used as an amplification factor on the bearing stress of the fastener.

The tilt factor  $\theta$  can be used in a similar manner in the crack growth analysis. Thus Equation (43) for the correction factor for the fastener load at the crack origin becomes

$$Y_{FO} = \frac{\theta P_o}{2\pi A_o t S} \sqrt{\frac{2A_o}{R_o + a} - 1} \quad (44)$$

The flaw shape is not considered directly except in Equation (32), relating to the transition between a corner crack and a through-thickness crack, where the flaw depth  $c$  appears explicitly. In the absence of fastener-induced bending, fracture surface markings in spectrum tests of 7075-T6 sheet have shown a quarter-circular shape (Reference 55); thus it may be assumed that  $c = a$ . When fastener bending is present, the nominal stresses on the two opposite surfaces differ by a factor of  $\theta / (2 - \theta)$ . It is assumed that the flaw shape ratio  $a/c$  is inversely proportional to the square of the local stresses on the two major axes of the flaw. Thus, when the corner flaw is tangent to the back surface as shown in Figure 24, the shape ratio can be approximated as follows:

$$\frac{a}{c} = \left( \frac{\theta}{2 - \theta} \right)^2 \quad (45)$$

#### 4. FASTENER LOAD ANALYSIS IN STRUCTURAL JOINT SPECIMENS

The stress severity factor and stress intensity factor expressions of the preceding sections cannot be used unless all the loads applied to the cracked member are known. The fastener load at the flaw origin is of particular interest because it most strongly affects the early growth of the crack. Regardless of crack length this load is zero in the stringer-reinforced panels, because the crack plane is a plane of symmetry. However, it is non-zero in the structural joint specimens, and can vary with crack size.

The following sections describe in detail the finite element analysis approach used on the structural joint specimens to determine fastener loads. No finite element analyses of the stringer-reinforced panels were conducted.

##### 4.1 Approach

The distribution of fastener loads in a damaged joint is influenced by the extent of damage and by transverse bending deformations of both the fasteners and the joint. Since the cracking and the bending occur in different planes, the structural analysis of such joints is a three-dimensional problem.

By the approach employed here, approximate solutions for the fastener load distribution were obtained for various assumed damage conditions. Two different types of two-dimensional finite element analysis were conducted.

In the first type of analysis the two-dimensional model corresponds to a profile view of the joint, where the stretching and transverse bending of the joint and all the deformations of the fasteners can be viewed. From this profile view the widthwise details of the specimen, including the crack length itself, cannot be modeled.

However, the two-dimensional finite element model corresponding to this view can be used to obtain effective fastener stiffnesses for the second analysis model. Those effective stiffness values are intended to account for the transverse deformations of the fastener and the joint itself.

In the second type of analysis the two-dimensional model corresponds to a top view of the joint. From this view the (through-the-thickness) crack is

visible and all of the fasteners can be modeled separately. Each fastener is assigned an effective stiffness value as obtained from the first analysis. The crack length is selected and the fastener loads are calculated.

The profile model analyses were conducted using the "2-D Analysis Program" in conjunction with existing test data from Reference 57 on fastener stiffness. The top view model analyses were conducted using the NASTRAN system.

#### 4.2 Computation of Effective Fastener Stiffness

A typical 2-D profile model of the double lap shear joint specimen is shown in Figure 29. In this type of model the axial, shear and bending stiffnesses of the splice plates and fasteners are represented by two axial elements tied together by a shear panel. The axial elements are separated in order to obtain the correct plate bending stiffness. The fastener head is represented by a beam element which transmits only bending forces to the plate (i.e., axial stiffness is approximately zero). The plate-fastener interface which accounts for the local deformation at the fastener hole is represented by axial elements connecting the plate to the fastener. Based on results from Reference 57 this interface stiffness for steel fasteners and aluminum plates is taken to be approximately  $4.6 \times 10^6$  lb/in/in. This value is used for the analyses of all the structural joint test specimens, since their fastener spacing (4D) and edge distances (2D) are all similar.

Let  $n_e$  be the number of axial elements of length  $\ell_e$  at the plate-fastener interface. If  $t$  and  $E$  are the thickness and Young's modulus of the plate, then the area of each axial element at the interface is calculated as follows:

$$\text{Element area} = \frac{4.6 \times 10^6 t \ell_e}{E n_e} \quad (46)$$

The values of the effective stiffnesses of the fasteners, used later in constructing finite element models of a joint, are calculated using the deflections and the transferred load at each fastener location. When the

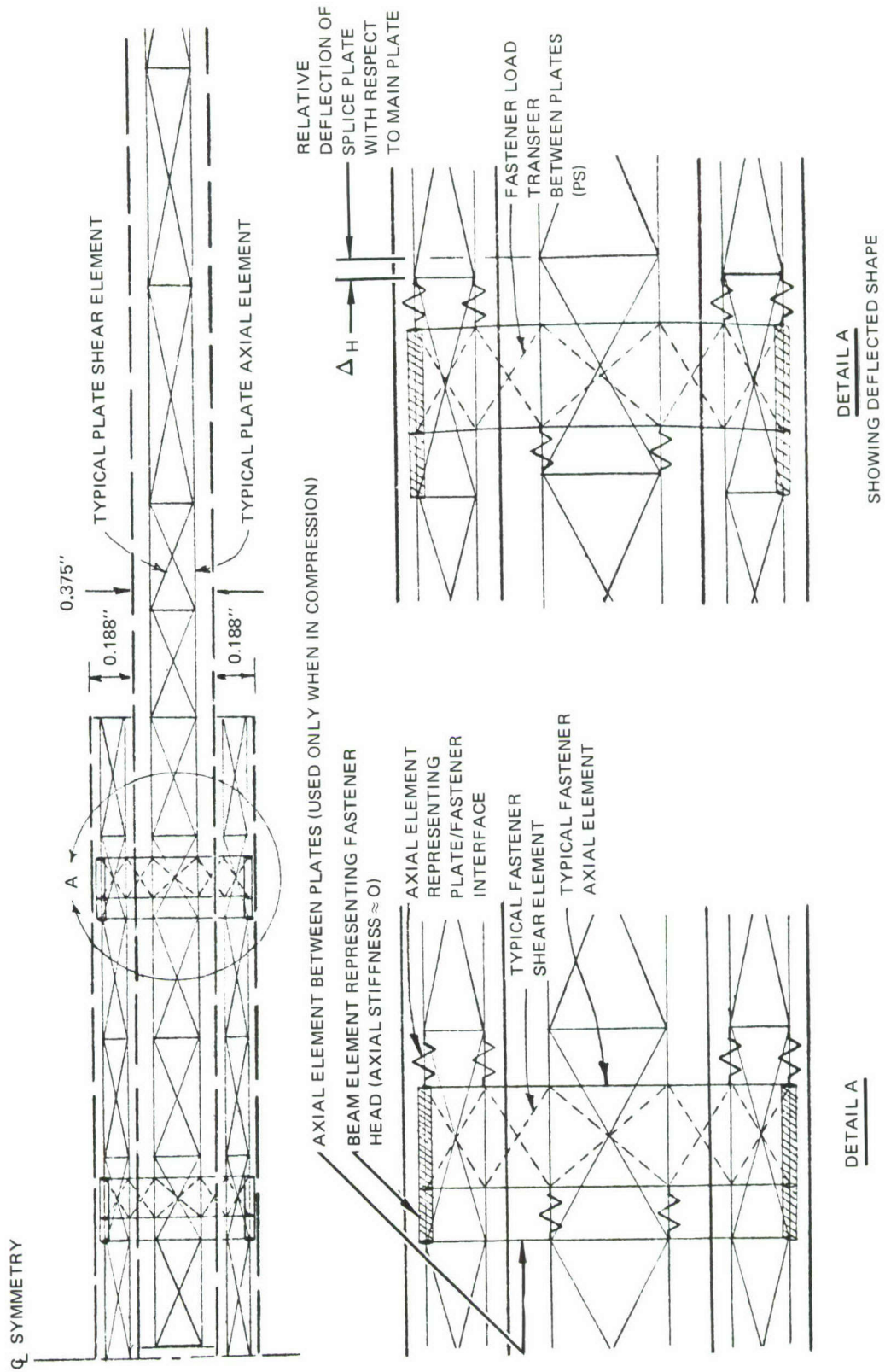


Figure 29. Profile Model of the Double Lap Shear Joint Specimen

double lap joint specimen is subjected to an applied load of  $P$  pounds, an average deflection of  $\Delta_H$  inches is calculated at the location shown in Figure 30 and the load transferred is  $P_s$  pounds. Hence the effective fastener stiffness is  $P_s / \Delta_H$  pounds per inch.

#### 4.3 Computation of Fastener Loads Using NASTRAN

4.3.1 Modeling Techniques. - For the NASTRAN models, two techniques of simulating the fastener and its interaction with the fastened plates are considered. A simple model of linear spring connections is used to simulate fasteners remote from the crack path. For the fastener hole with initial damage and the fastener hole where the first crack arrestment occurs, a more detailed finite element model is used. The more detailed model (Figure 30) is needed for a better simulation of the loss of bearing stiffness due to the existence of a crack.

There are two basic reasons for introducing the cutout. First the proper load bypass condition around the fastener hole is simulated. Secondly, the loss of bearing stiffness of the fastener system due to cracking is accounted for without artificially reducing the fastener stiffness value originally calculated for the undamaged joint. As the figure shows, a more detailed finite element grid is used to model the region adjacent to the fastener. A square cutout one fastener diameter wide is used to simulate the fastener hole.

The connection point between fastened members is through an axial spring element connecting the grid point A in one member to A' in the adjacent member. The point A is then rigidly connected to points B, C, and D located on the compressive side of the fastener. The total stiffness of the spring element is greater than the stiffness of elements used to simulate remote fasteners. This increase is necessary to compensate for the decrease in local stiffness due to the square hole. The amount of increase in stiffness depends on the specimen configuration, and some trial runs are required. The final value of the spring stiffness is selected to provide approximately equal fastener loads for all fasteners across the width of the undamaged chordwise joint. The NASTRAN models were constructed utilizing elements available in the Lockheed-California Company version of NASTRAN. These elements are linear springs,

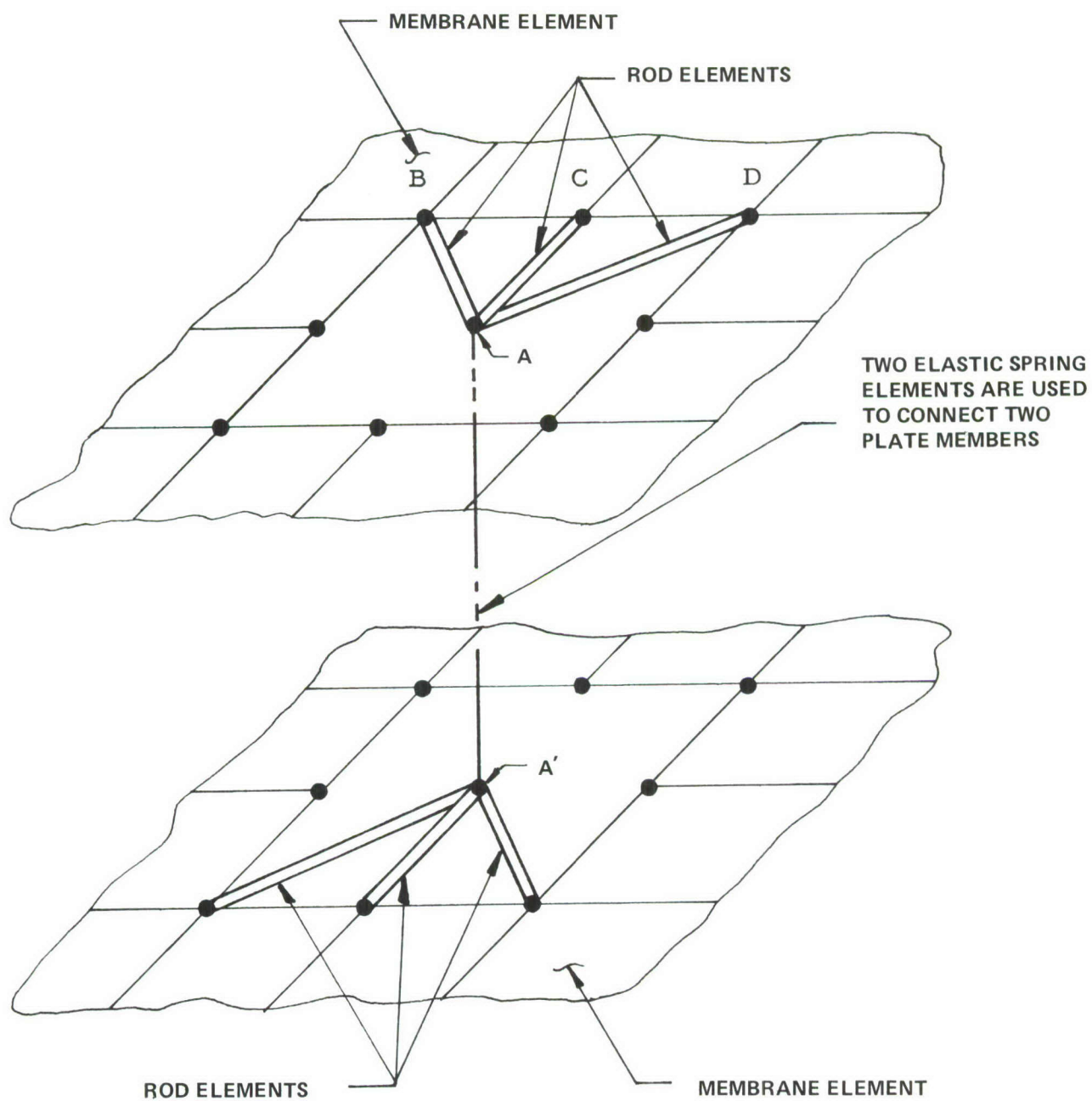


Figure 30. Details of Fastener System Model with a Square Cut-Out

rod elements, triangular elements, and Lockheed's membrane elements. Only two-dimensional models are considered. Bending effects, when considered significant for a particular fastener, are taken into account by reducing the fastener stiffness value used in the spring element connecting A and A' in Figure 30. In this way the redistribution of in-plane load for each individual element of the joint is included in an average sense.

The simulation of crack growth is accomplished in the following manner. Double nodes are assigned to grid point locations along the crack path. Constraints are imposed initially for the two nodes within a pair to have the same displacements. Subsequent models simulating longer cracks are generated simply by releasing these constraints in progression.

## SECTION IV

### BASELINE TEST RESULTS

Baseline material tests were performed on each product form to be used in the test program, to verify material acceptance and to provide reference data for use in the crack growth predictions. These baseline tests included tensile tests, fatigue crack initiation tests, fatigue crack propagation tests, and fracture or R-curve tests.

Additional baseline tests were conducted to verify the key fabrication and testing procedures used for the complex structure specimens, including

- Tests to develop and verify the marking cycle procedure used to mark the fracture surfaces.
- Tests to measure flaw size and shape to verify the procedure used to initiate the 0.050-inch quarter-circular fatigue cracks in the complex structure specimen; See Section VI, Paragraph 1.

In addition to data obtained in this program, applicable data are available from Reference 55. An extensive test program reported in Reference 55 and summarized in Appendix C verifies that 0.020-inch razor-induced flaws can be used to simulate 0.005-inch fatigue-induced cracks in 7075-T6 Aluminum. Razor flaws were induced into some of the structural test specimens in the manner described in Appendix C.

#### 1. TENSILE TESTS

Thirty-six tensile tests have been conducted to measure tensile yield strength, tensile ultimate strength, and percent elongation for the six different thicknesses and product forms tested in the program. Three specimens each were tested in both the longitudinal and transverse grain directions. The average measured tensile properties are summarized in Table 7.

TABLE 7. AVERAGES OF MEASURED TENSILE PROPERTIES

| Product Form     | $F_{tu}$ , ksi |        | $F_{ty}$ , ksi |        | % Elong. |        |
|------------------|----------------|--------|----------------|--------|----------|--------|
|                  | Long.          | Trans. | Long.          | Trans. | Long.    | Trans. |
| 0.188 sheet      | 85.2           | 87.2   | 78.6           | 76.5   | 14.2     | 13.2   |
| 0.094 sheet      | 83.6           | 85.3   | 77.4           | 74.3   | 12.8     | 12.8   |
| 0.25 plate       | 83.2           | 84.1   | 78.0           | 72.9   | 13.0     | 12.8   |
| 0.375 plate      | 84.3           | 85.6   | 78.8           | 74.9   | 13.8     | 11.5   |
| 0.25 angle extr. | 89.2           | 80.2   | 80.8           | 72.4   | 11.7     | 12.3   |
| 0.188 tee extr.  | 88.0           | 80.6   | 80.6           | 71.9   | 10.5     | 13.3   |

## 2. FATIGUE CRACK INITIATION TESTS

Fatigue crack initiation tests were conducted to provide data for estimation of reinitiation periods for cracks arrested at fastener holes in the complex structure test specimens. Constant amplitude cycling at a stress range ratio of 0.1 was used in all tests. The following three groups of tests were conducted.

- Coupon tests of the 0.188-inch sheet material at different stress levels to develop an S-N curve.
- Coupon tests of the 0.094-inch sheet, 0.375-inch plate, 0.188-inch tee extrusion, and 0.25-inch angle extrusion to measure the corresponding changes in fatigue strength from that of the 0.188-inch sheet.
- Fastener fatigue tests of clearance and interference-fit steel Hi-Lok fasteners to empirically estimate the constants  $\alpha$  and  $\beta$  in the stress severity factor expression, Equation (5).

Results from 25 coupon fatigue tests are summarized in Table 8. Five of these specimens (specimens 7B-X) were tested as part of a separate research program (Reference 55). Results from 13 fastener fatigue tests are summarized in Table 9. Six of these specimens were tested under the program reported in Reference 55. The specimen geometries are shown in Figures 31 through 34. Material for all 0.188-inch thick specimens (including specimens from Reference 55) was from one lot of material.

TABLE 8. COUPON FATIGUE TEST RESULTS

| Material              | Specimen Number | Geometry See Figure | Thickness t (inch) | Width W (inch) | Hole Diameter D (inch) | Maximum Load P (kip) | Maximum Stress P/tW (ksi) | Notch Stress $k_t P/tW$ (ksi) | Life To Failure (Actual) (Cycles) | Life Estimate Eqn (48) (Cycles) |
|-----------------------|-----------------|---------------------|--------------------|----------------|------------------------|----------------------|---------------------------|-------------------------------|-----------------------------------|---------------------------------|
| 0.188 Sheet           | N-1             | 32                  | 0.182              | 5.009          | 0.25                   | 1.577                | 1.73                      | 113.4                         | 7,570                             | 8,211                           |
|                       | N-2             | 32                  | 0.182              | 5.004          | 0.25                   | 1.577                | 1.73                      | 113.4                         | 8,671                             | 8,211                           |
|                       | N-3             | 32                  | 0.182              | 5.005          | 0.25                   | 2.453                | 2.69                      | 176.3                         | 1,344                             | 1,231                           |
|                       | N-4             | 32                  | 0.182              | 5.007          | 0.25                   | 2.453                | 2.69                      | 176.3                         | 1,236                             | 1,321                           |
|                       | N-5             | 32                  | 0.182              | 5.005          | 0.25                   | 6.250                | 6.86                      | 449.3                         | 1                                 | 22                              |
| 0.188 Sheet (Ref. 55) | 7B-3            | 31                  | 0.1817             | 1.504          | 0.25                   | 6.231                | 22.8                      | 70.7                          | 64,957                            | 62,620                          |
|                       | 7B-4            | 31                  | 0.1805             | 1.505          | 0.25                   | 6.192                | 22.8                      | 70.7                          | 64,501                            | 62,620                          |
|                       | 7B-1            | 31                  | 0.182              | 1.502          | 0.25                   | 9.692                | 35.45                     | 109.9                         | 11,301                            | 9,396                           |
|                       | 7B-5            | 31                  | 0.1811             | 1.503          | 0.25                   | 9.922                | 36.45                     | 113.4                         | 7,155                             | 8,211                           |
|                       | 7B-11           | 31                  | 0.18               | 1.50           | 0.25                   | 9.9                  | 36.45                     | 113.4                         | 6,798                             | 8,211                           |
| 0.188 Sheet           | BF-1            | 31                  | 0.1816             | 1.510          | 0.25                   | 8.665                | 31.6                      | 98.0                          | 14,792                            | 15,407                          |
|                       | BF-2            | 31                  | 0.1820             | 1.507          | 0.25                   | 8.668                | 31.6                      | 98.0                          | 14,470                            | 15,407                          |
|                       | BF-3            | 31                  | 0.1814             | 1.509          | 0.25                   | 8.649                | 31.6                      | 98.0                          | 16,807                            | 15,407                          |
| 0.094 Sheet           | AF-1            | 31                  | 0.0945             | 1.508          | 0.25                   | 4.503                | 31.6                      | 98.0                          | 19,125                            | 21,176                          |
|                       | AF-2            | 31                  | 0.946              | 1.507          | 0.25                   | 4.506                | 31.6                      | 98.0                          | 24,065                            | 21,176                          |
|                       | AF-3            | 31                  | 0.0943             | 1.508          | 0.25                   | 4.494                | 31.6                      | 98.0                          | 20,519                            | 21,176                          |
| 0.375 Plate           | CF-1            | 31                  | 0.3850             | 1.513          | 0.25                   | 18.423               | 31.6                      | 98.0                          | 10,160                            | 10,315                          |
|                       | CF-2            | 31                  | 0.3855             | 1.512          | 0.25                   | 18.423               | 31.6                      | 98.0                          | 10,039                            | 10,315                          |
|                       | CF-3            | 31                  | 0.3852             | 1.512          | 0.25                   | 18.391               | 31.6                      | 98.0                          | 10,705                            | 10,315                          |
| 0.25 Angle            | LF-1            | 31                  | 0.25               | 1.50           | 0.25                   | 11.85                | 31.6                      | 98.0                          | 16,276                            | 15,407                          |
|                       | LF-2            | 31                  | 0.25               | 1.50           | 0.25                   | 11.85                | 31.6                      | 98.0                          | 15,781                            | 15,407                          |
|                       | LF-3            | 31                  | 0.25               | 1.50           | 0.25                   | 11.85                | 31.6                      | 98.0                          | 16,387                            | 15,407                          |
| 0.188 Tee             | TF-1            | 31                  | 0.1888             | 1.511          | 0.25                   | 9.015                | 31.6                      | 98.0                          | 17,160                            | 15,407                          |
|                       | TF-2            | 31                  | 0.1891             | 1.511          | 0.25                   | 9.028                | 31.6                      | 98.0                          | 18,640                            | 15,407                          |
|                       | TF-3            | 31                  | 0.1891             | 1.511          | 0.25                   | 9.028                | 31.6                      | 98.0                          | 14,438                            | 15,407                          |

TABLE 9. SUMMARY OF FASTENER FATIGUE DATA

|   | Specimen Number | Geometry See Figure | Stress Severity Factor Eqn (5) | Thickness t (inch) | Width W (inch) | Hole Diameter (inch) | Fastener Diameter (inch) | Maximum Load P (kip) | Maximum Stress P/Wt (ksi) | Life Estimate Eqn (49) (Cycles) | Life to Failure (Actual) (Cycles) |
|---|-----------------|---------------------|--------------------------------|--------------------|----------------|----------------------|--------------------------|----------------------|---------------------------|---------------------------------|-----------------------------------|
| Clearance Fit Steel Hi-Lok Fasteners    | 2A-1            | 34                  | 3.286                          | 0.362              | 2.251          | 0.3765               | 0.3740                   | 18.580               | 22.8                      | 48,801                          | 45,800                            |
|   | 2A              | 34                  | 3.286                          | 0.361              | 2.251          | 0.3765               | 0.3740                   | 18.527               | 22.8                      | 48,801                          | 46,290                            |
|   | 3A-1            | 33                  | 9.354                          | 0.1803             | 4.50           |                      |                          | 18.491               | 22.8                      | 543                             | 550                               |
|   | 3A-2            | 33                  | 9.354                          | 0.1806             | 4.50           | 0.3750               | 0.3739                   | 9.756                | 12.0                      | 8,580                           | 7,000                             |
|   | 3A-3            | 33                  | 9.354                          | 0.1807             | 4.50           | 0.3753               | 0.3742                   | 9.756                | 12.0                      | 8,580                           | 8,320                             |
|   | 3A-4            | 33                  | 9.354                          | 0.1806             | 4.50           | 0.3754               | 0.3750                   | 9.756                | 12.0                      | 8,580                           | 8,110                             |
|   | (Ref. 55)       |                     |                                |                    |                |                      |                          |                      |                           |                                 |                                   |
|   | 4B              | 34                  | 4.368                          | 0.1803             | 2.250          | 0.3753               | 0.3738                   | 9.257                | 22.8                      | 14,351                          | 16,460                            |
|   | 3A              | 34                  | 4.368                          | 0.1801             | 2.250          | 0.3764               | 0.3742                   | 9.234                | 22.8                      | 14,351                          | 18,280                            |
|   | 2B-3            | 34                  | 4.368                          | 0.1804             | 2.556          |                      |                          | 9.277                | 22.8                      | 14,351                          | 16,550                            |
| Interference Fit Steel Hi-Lok Fasteners | 2B-2-4          | 34                  | 2.778                          | 0.1804             | 2.255          | 0.3728               | 0.3738                   | 9.300                | 22.8                      | 100,500                         | 94,407                            |
|   | 2B-1-3          | 34                  | 2.778                          | 0.1804             | 2.255          | 0.3727               | 0.3736                   | 9.275                | 22.8                      | 100,500                         | 107,105                           |
|   | 7B-F-1          | 31                  | 1.972                          | 0.1820             | 1.502          | 0.2486               | 0.24                     | 8.639                | 31.6                      | 107,900                         | >50,470                           |
|   | 7B-F-2          | 31                  | 1.972                          | 0.1826             | 1.503          | 0.2486               | 0.24                     | 8.671                | 31.6                      | 107,900                         | >80,620                           |

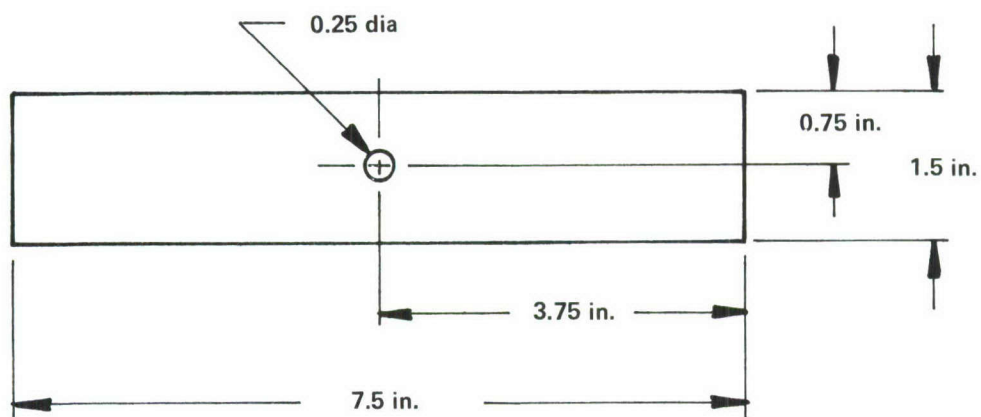


Figure 31.  $k_t = 3.1$  Coupon

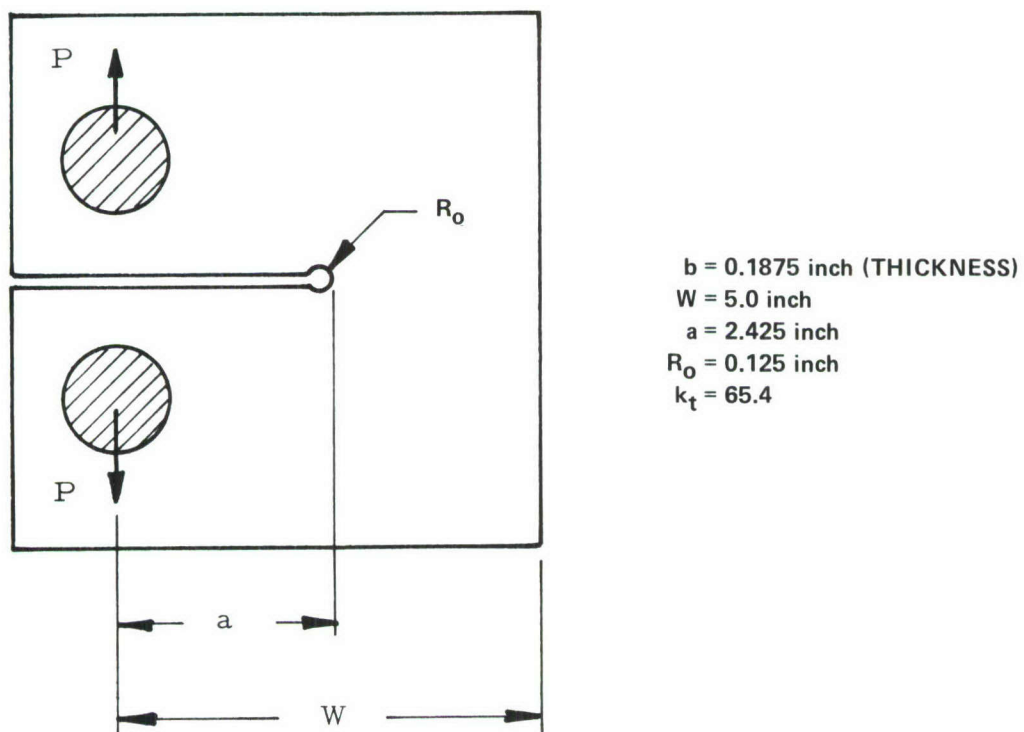


Figure 32. Modified CT Specimen





## 2.1 The S-N Curve for the 3/16 Inch Sheet

Data from the first 13 fatigue coupon tests listed in Table 8 were used to generate a curve of maximum stress versus cycles to failure for the 0.188-inch sheet material used in the program. Notched specimens with 0.25 inch diameter holes were subjected to constant amplitude cycling at a stress ratio of 0.1. The data cover the low cycle fatigue range, less than 65,000 cycles to failure.

The elastic notch stress listed in Table 8 is used as a measure of the stress severity at the fatigue origin. In all but two specimens this number exceeds the material yield strength of 78.6 ksi; therefore it is not equal to the true notch stress. However, it follows from Neuber's Rule (Reference 58) that the true notch stress and strain magnitudes are determined by  $k_t S_{t \max}$ .

Note that the highest value of  $k_t S_{t \max}$  fatigue tested was 176.3 ksi. If the  $k_t = 3.1$  fatigue coupon (Figure 31) had been used for that test, the specimen would nearly have undergone net section yielding because of its small size. Yielding was limited to the notch tip vicinity (small-scale yielding) by using the modified W=5 compact tension specimen shown in Figure 32 for testing at the highest notch stress levels. The following formula, from Reference 59, expresses  $k_t$  in terms of stress intensity factor  $K_I$  for "blunt cracks":

$$k_t S = \frac{K_I}{\sqrt{\pi R_o}} \quad (47)$$

If  $S=P/Wb$ , then  $k_t$  for the modified compact specimen is 65.4, according to Equation (47).

It is assumed (Reference 60) that the magnitude of true strain in the notch-tip neighborhood determined the low-cycle fatigue life. It was noted in Section III, Paragraph 1., that for small-scale yielding the peak elastic stress at the notch root ( $k_t S$ ) and the notch radius determine the true strains in the notch-tip neighborhood. As discussed in Section III, Paragraph 1.3, it should follow that the fatigue life, plotted against the elasticity parameter  $k_t S_{t \max}$ , should form a single curve for the two coupon configurations tested.

Figure 35 shows the fatigue data from the 13 coupon tests with the 3/16-inch sheet material. A linear relationship was hypothesized between the logarithm of fatigue life and the logarithm of peak elastic notch stress. The assumed relationship can be written as

$$N = c_o \left( \frac{\alpha \beta k_t S_{\max}}{100 \text{ ksi}} \right)^{c_1} \quad (48)$$

where  $\alpha = \beta = 1$  for an open, 0.25-inch diameter hole.

The solid line in Figure 35 is a plot of Equation (48) using the following values of the constants  $c_o$  and  $c_1$ :

$$c_1 = -4.3$$

$$c_o = 14,100 \text{ cycles to failure}$$

It is clear in the Figure that this provides an excellent data fit over the full range tested. Life estimates using Equation (48) are listed in Table 8 for each of the 0.188-inch sheet coupons tested.

## 2.2 Material Comparisons

Data from the last 15 coupons listed in Table 8 were used to compare fatigue lives at a common stress level for the heats of sheet, plate and extrusion material to be used in the complex structure specimens. The purpose of these tests was to expose and measure any major differences in material fatigue strength. There were three replications of each test.

The results of this comparison are clearly shown in the bar chart, Figure 36, where the following can be observed:

- The scatter among replicate specimens is extremely low.
- The geometric mean test lives for the 0.188-inch sheet, 0.188-inch tee extrusion, and 0.25-inch angle extrusion are within 9 percent of one-another.
- There is an apparent thickness effect in the sheet and plate materials.

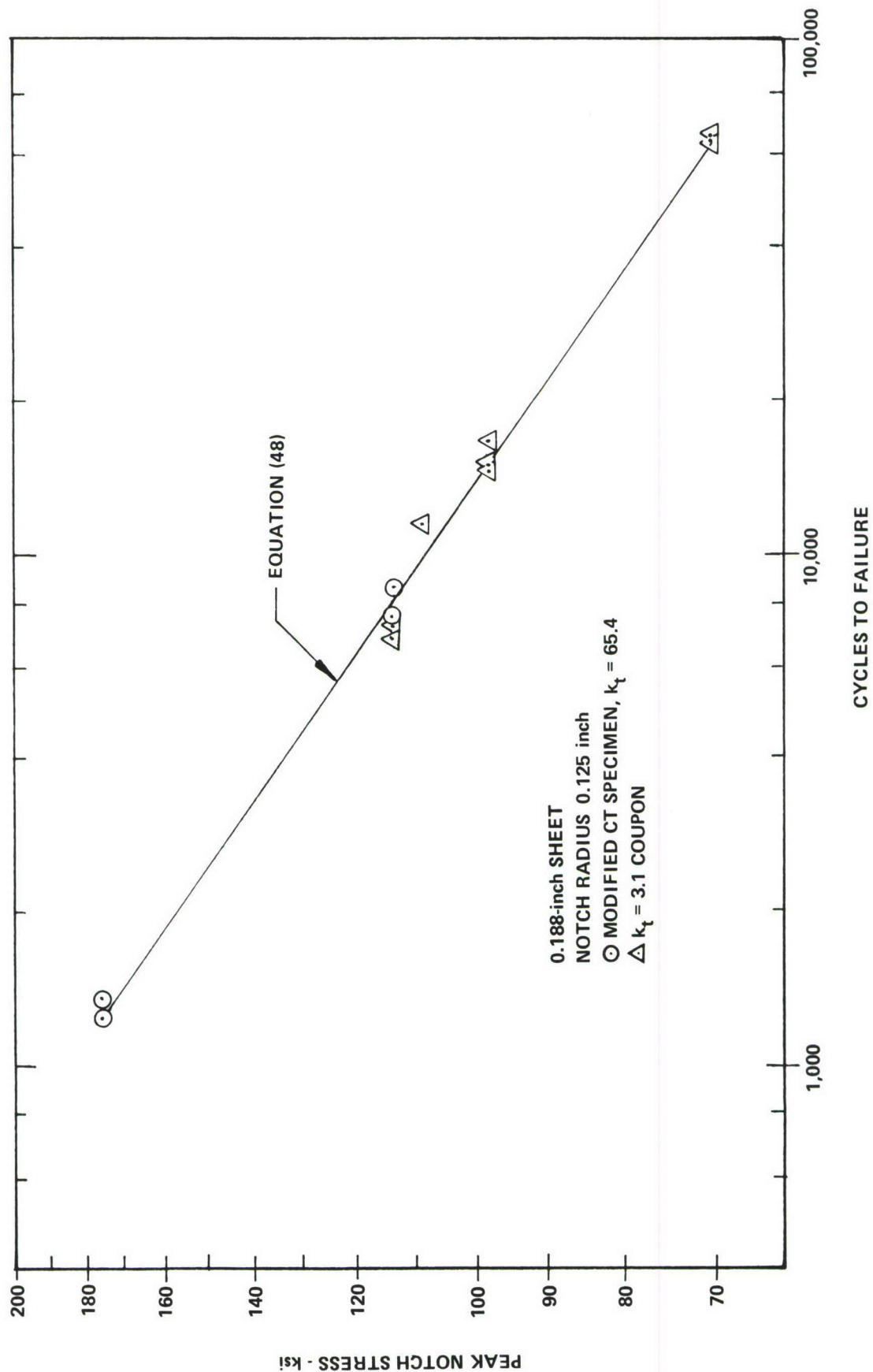


Figure 35. S-N Curve for 3/16 Inch 7075-T6 Aluminum Sheet,  $R = 0.1$

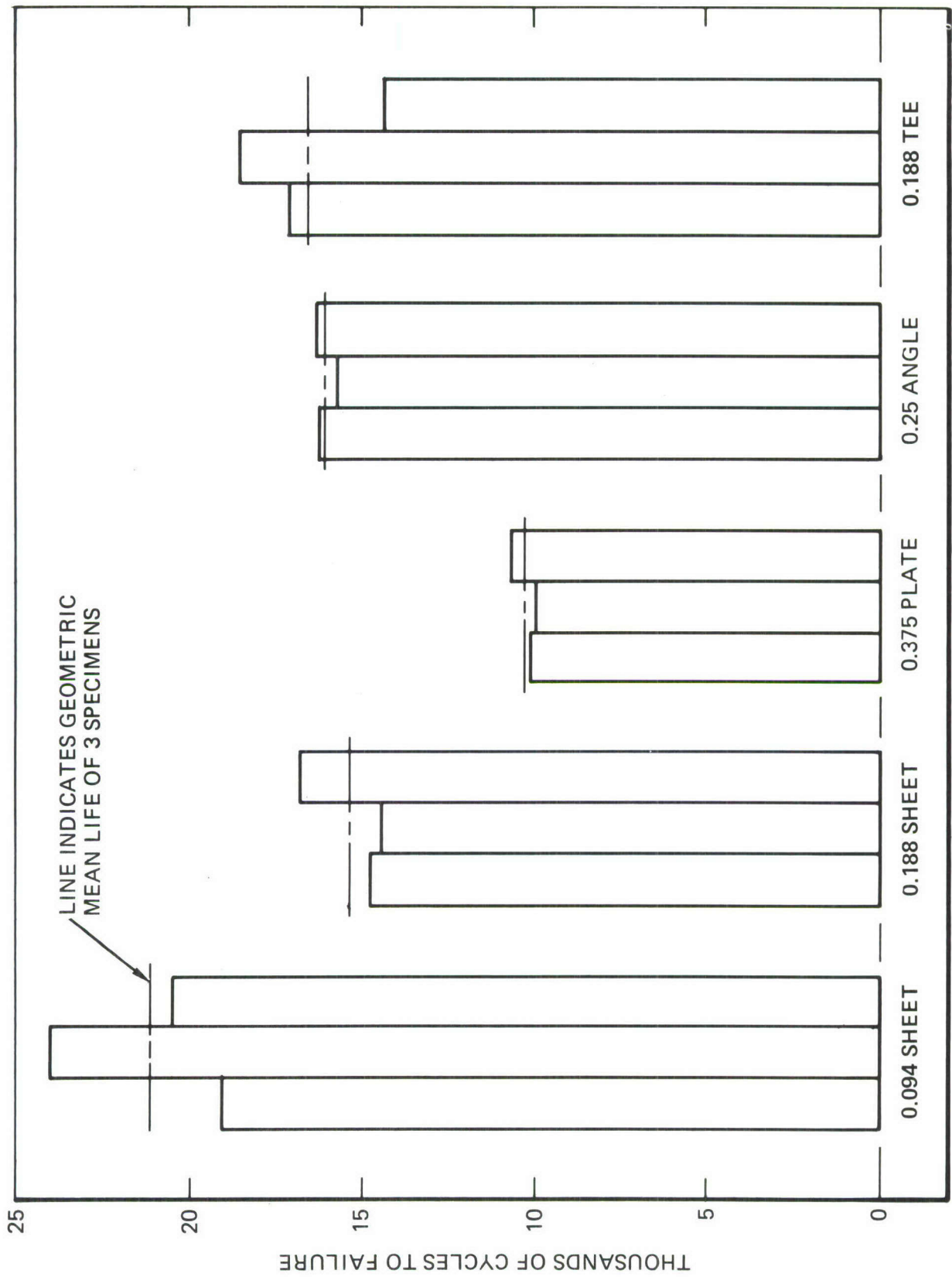


Figure 36. Comparison of Fatigue Lives for Various Thicknesses and Product Forms

It was assumed that the logarithmically plotted S-N curves for all five material product forms are parallel, with a slope  $c_1$  equal to -4.3 as measured for the 0.188-inch sheet. For the tee and angle extrusions, the coefficient  $c_0$  in Equation (48) retains about the same value as for the 0.188-inch sheet. Thus the following values of  $c_0$  will be used:

- For the 0.188 sheet and the tee and angle extrusion  
 $c_0 = 14,100$  cycles to failure
- For the 0.094 inch sheet  
 $c_0 = 19,380$  cycles to failure
- For the 0.375 inch plate,  
 $c_0 = 9440$  cycles to failure

Life estimates obtained using Equation (48) with the appropriate values of  $c_0$  are given in Table 8 for all coupons tested.

### 2.3 Fatigue Tests of Fastener Specimens

There were two fundamentally different fastening methods used in the structural tests. Clearance-fit steel Hi-lok fasteners with very low torque were used at all initial flaw locations of all specimens, and at unflawed holes of many of the specimens. Alternatively, standard fastening methods were used. Those standard fasteners were interference-fit, fully-torqued Hi-loks, except for the aluminum rivets used in the tee-reinforced continuous-skin specimens.

The fastener fatigue tests summarized in Table 9 were conducted to examine the fatigue properties of these two fastening methods. The 0.188-inch 7075-T6 Aluminum sheet was used exclusively. The hole diameters and fastener diameters were measured to within  $\pm 0.0002$  inch, so that the amount of clearance or interference was known.

Three different specimen geometries, covering three different levels of load transfer, were tested using clearance-fit fasteners with near-zero clamp-up. With this fastening method the fastener loads in the reversed dogbone specimen (Figure 34(b)) are estimated to be zero. The reason for this is simple: When loaded, the stiffness mismatch between the two reversed dogbone pieces comprising this specimen gives rise to a mismatch in the

displacement of the fastener hole centerlines; however, with clearance fit fasteners the fastener hole clearance exceeds the mismatch and there is no load transfer through the fasteners.

The one and one-half dogbone specimen (Figure 34(c)) is made by cutting one end off a reversed dogbone piece (piece shown in Figure 34(a)) and using one fastener to attach it to an uncut piece. Assuming a fastener stiffness of 280,000 pounds per inch it is estimated that 21.5 percent of the load is carried across the fastener.

A slotted single lap shear joint (Figure 33) simulates a crack arrested between two fasteners. A fastener loads computation led to fastener loads of 17.6 percent of the total load for each of the two fasteners adjacent to the slot. This value was used in establishing the stress severity factor for this specimen.

Two specimen geometries covering two levels of fastener load transfer were tested using interference-fit fasteners with full clamp-up torque. In the one and one-half dogbone specimen the interference and clamp-up increased the life by a factor of six compared to the clearance-fit, near-zero clamp-up case tested at the same stress level. The lower (zero) level of load transfer was investigated using interference-fit fasteners installed in the holes of two  $k_t = 3.1$  specimens (Figure 31). Since these specimens were not narrowed at the test section they failed in the grips. The lives exceeded, by factors of 3.3 and 5, the life of the open-hole  $k_t = 3.1$  specimen tested at the same stress level. Furthermore, no cracking was visible at the hole when the grips finally failed. This confirmed that substantial life extension is obtained due to the interference-fit, full clamp-up fastener.

The fatigue lives of all fastener-fatigue specimens were correlated in terms of the stress severity factor ( $\lambda$ ) using the following equation.

$$N = c_o \left( \frac{\lambda S_{\max}}{100} \right)^{-4.3} \quad (49)$$

The stress severity factor  $\lambda$  in Equation (49) replaces  $\alpha\beta k_t$  in Equation (48), and the product  $\lambda S_{\max}$  may be regarded as an effective value of the peak elastic notch stress for a fastener hole, as discussed in Section III, Paragraph 2.

Life estimates for all the fastener-fatigue specimens obtained using Equation (49) are listed in Table 9. The stress severity factors, also listed in Table 9, were calculated for these specimens using Equation (5), Section III, Paragraph 2. Values of  $\alpha$  and  $\beta$  in Equation (5) were selected from the fastener fatigue data themselves such that the test lives would be closely estimated by Equation (49).

The selection of  $\alpha$  and  $\beta$  values was carried out as follows. The assumption was made a priori that the fastener quality index  $\beta$  is 1.0 for both empty holes and clearance-fit fasteners with near-zero clamp-up torque. Then, to assure that Equation (49) is applicable to all the fatigue coupon data summarized in Table 8, the hole quality index  $\alpha$  must be 1.0 for 0.25-inch diameter drilled holes. With  $\alpha$  and  $\beta$  both equal to 1.0,  $\lambda$  is simply equal to  $k_t$  for these coupons. Thirdly, a good fit of the fatigue data for the three types of fastener fatigue specimens with 0.375-inch diameter clearance-fit fastener is obtained when an  $\alpha$  value of 1.06 is used for 0.375 inch diameter drilled holes. Finally, the geometric mean test life for the one and one-half dogbone specimens with interference fit fasteners is fitted exactly using a  $\beta$  value of 0.635. This completes the determination of the constants  $\alpha$  and  $\beta$ .

Note that, for the  $k_t = 3.1$  coupons with interference-fit 0.25-inch diameter fasteners, the predictions obtained using the designated  $\alpha$  and  $\beta$  values (1.00 and 0.635, respectively) are consistent with the test results: The predicted life (107,900 cycles) in the test section exceeds the observed lives (50,470 cycles and 80,620 cycles) in the grip areas.

### 3. FATIGUE CRACK PROPAGATION TESTS

Fatigue crack propagation specimens were tested to failure to provide baseline data for estimating stable crack growth rates and final crack instability for the complex structure test specimens. The baseline fatigue

crack growth tests are summarized in Table 10. Either compact tension specimens (specimen numbers ending with "-CT") or center-cracked panels (specimen numbers ending with "-CCT") were tested. Both specimen types were used in testing the 0.188-inch sheet. For the 0.188-inch sheet and the 0.188 inch tee extrusion, both grain directions were tested. A stress range ratio of 0.1 was used exclusively.

Figures 37 and 38 show the plotted crack growth rate data for the 0.188-inch sheet. Note in Figure 37 that all the data for the longitudinal grain direction follow the same crack growth rate curve, although specimen geometries, stress levels, and cyclic frequencies (0.5 to 20 Hz) were varied. A curve consisting of a series of straight-line segments of  $K_{\max}$  versus  $\log (da/dN)$  is fitted to the data and shown as a solid line. The same line is shown as a dashed line in Figure 38. The solid line in Figure 38 consists of straight line segments which fit the transverse-grain-direction data. Note that for stress intensity values below  $k_{\max} = 20 \text{ ksi} \sqrt{\text{inch}}$  there appears to be no effect of grain direction. Above this value, the crack growth rate is faster in the transverse grain direction.

Figure 39 shows the plotted crack growth rate data for the 0.375-inch plate material. The solid line is the fit of the data for the 0.188-inch sheet; clearly it is applicable to the 0.375-inch plate as well.

Figure 40 shows the plotted crack growth rate data for the 0.094-inch sheet material. The curve that fits the 0.188-inch sheet data (dashed line) overestimates crack growth rates for the 0.094-inch sheet at high stress intensity values. An improved fit is shown as a solid line.

Figure 41 shows the crack growth data for the 0.188-inch tee extrusion. The crack growth rate appears to be independent of grain direction. For low stress intensity values these data agree closely with the crack growth rate curve (dashed line) for the 0.188-inch sheet. However at stress intensity values above about  $20 \text{ ksi} \sqrt{\text{inch}}$  the crack grows faster in this extrusion than in the sheet. Perhaps the explanation for the faster rate of growth is somehow related to specimen size, since CT specimens with  $W = 1.5 \text{ inch}$  were used to test the extrusions whereas larger specimens were used to test the

TABLE 10. SUMMARY OF BASELINE FATIGUE CRACK GROWTH TESTS

| Specimen Number | Material    | Grain Direction | Width W (inch) | Thickness t (inch) | Maximum Load P (kip) | $S_{Max}$ P/Wt (ksi) |
|-----------------|-------------|-----------------|----------------|--------------------|----------------------|----------------------|
| B-1-CCT         | 0.188 Sheet | Long.           | 12             | 0.1816             | 26.00                | 11.93                |
| B-2-CCT         | 0.188 Sheet | Long.           | 12             | 0.1829             | 39.51                | 18.00                |
| CT50-CT         | 0.188 Sheet | Long.           | 4.989          | 0.1802             | 0.900                | 1.001                |
| CT51-3-CT       | 0.188 Sheet | Long.           | 4.999          | 0.1804             | 1.250                | 1.386                |
| NCT1-CT         | 0.188 Sheet | Trans.          | 5.007          | 0.182              | 0.37                 | 0.406                |
|                 |             |                 |                |                    | 0.41                 | 0.450                |
|                 |             |                 |                |                    | 0.46                 | 0.505                |
| NCT2-CT         | 0.188 Sheet | Trans.          | 5.005          | 0.182              | 1.20                 | 1.317                |
| NCT3-CT         | 0.188 Sheet | Trans.          | 5.003          | 0.182              | 0.80                 | 0.879                |
| C-1-CCT         | 0.375 Plate | Long.           | 12             | 0.3866             | 55.58                | 11.98                |
| C-2-CCT         | 0.375 Plate | Long.           | 12             | 0.3845             | 82.94                | 17.98                |
| C-3-CCT         | 0.375 Plate | Long.           | 12             | 0.386              | 56;37;28             | 12;8;6               |
| A-1-CCT         | 0.094 Sheet | Long.           | 12             | 0.0900             | 19.44                | 18.00                |
| A-2-CCT         | 0.094 Sheet | Long.           | 12             | 0.0903             | 13.01                | 12.01                |
| A-3-CCT         | 0.094 Sheet | Long.           | 12             | 0.0905             | 11.4;6.84            | 10.5;6.3             |
| L-1-CT          | 0.25 Angle  | Long.           | 1.594          | 0.246              | 0.450                | 1.148                |
| L-2-CT          | 0.25 Angle  | Long.           | 1.499          | 0.242              | 0.720                | 1.985                |
| L-3-CT          | 0.25 Angle  | Long.           | 1.500          | 0.245              | 0.850                | 2.313                |
| T1-1-CT         | 0.188 Tee   | Long.           | 1.499          | 0.178              | 0.350                | 1.312                |
| T1-2-CT         | 0.188 Tee   | Long.           | 1.500          | 0.176              | 0.520                | 1.970                |
| T1-3-CT         | 0.188 Tee   | Long.           | 1.496          | 0.178              | 0.850                | 3.192                |
| T-1-CT          | 0.188 Tee   | Trans.          | 1.598          | 0.185              | 0.520                | 1.759                |
| T-2-CT          | 0.188 Tee   | Trans.          | 1.497          | 0.185              | 0.400                | 1.444                |
| T-3-CT          | 0.188 Tee   | Trans.          | 1.495          | 0.1843             | 0.620                | 2.250                |

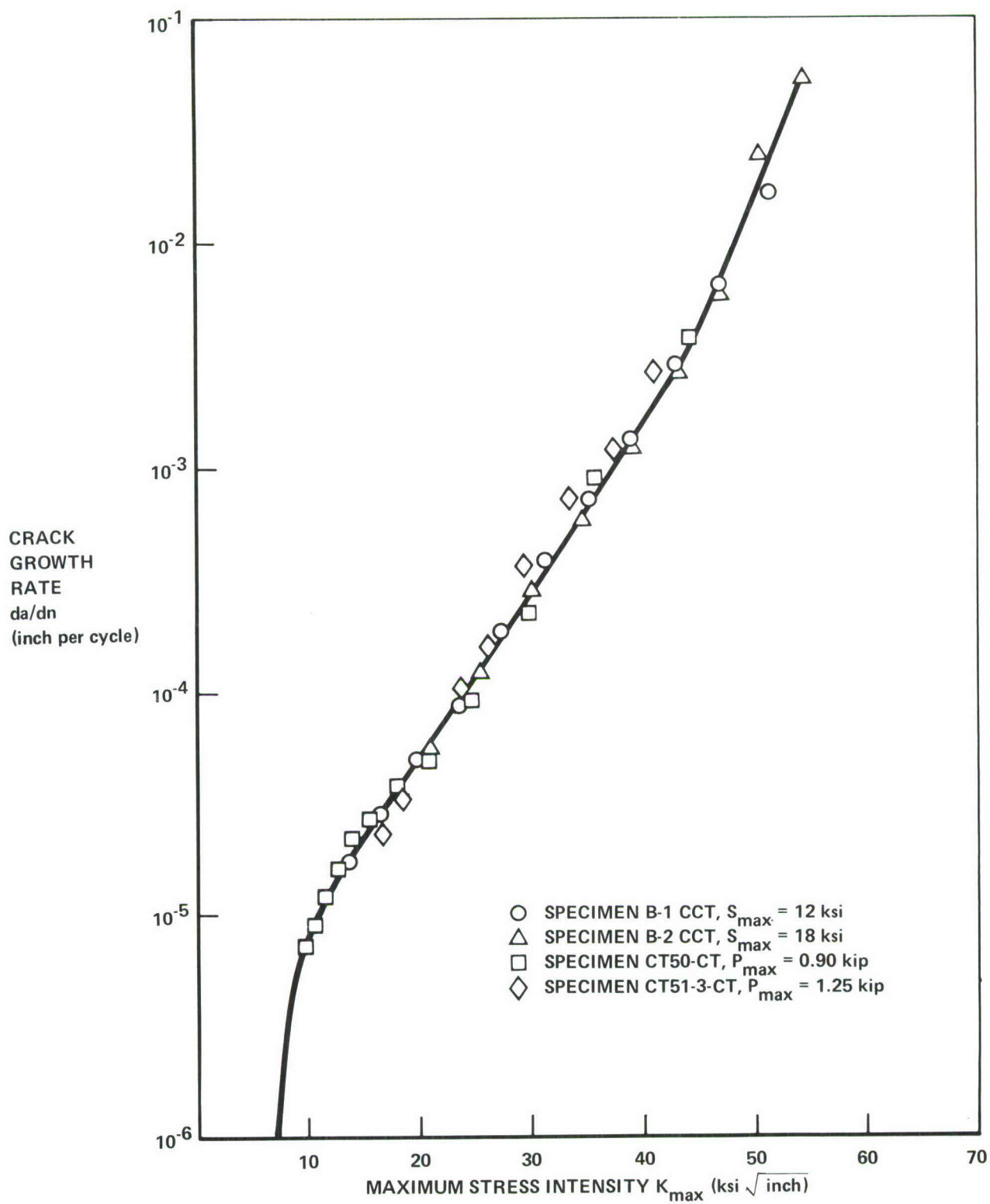


Figure 37. Fatigue Crack Growth Data, 0.188 Inch 7075-T6 Aluminum Sheet, Longitudinal Grain Direction,  $R = 0.1$

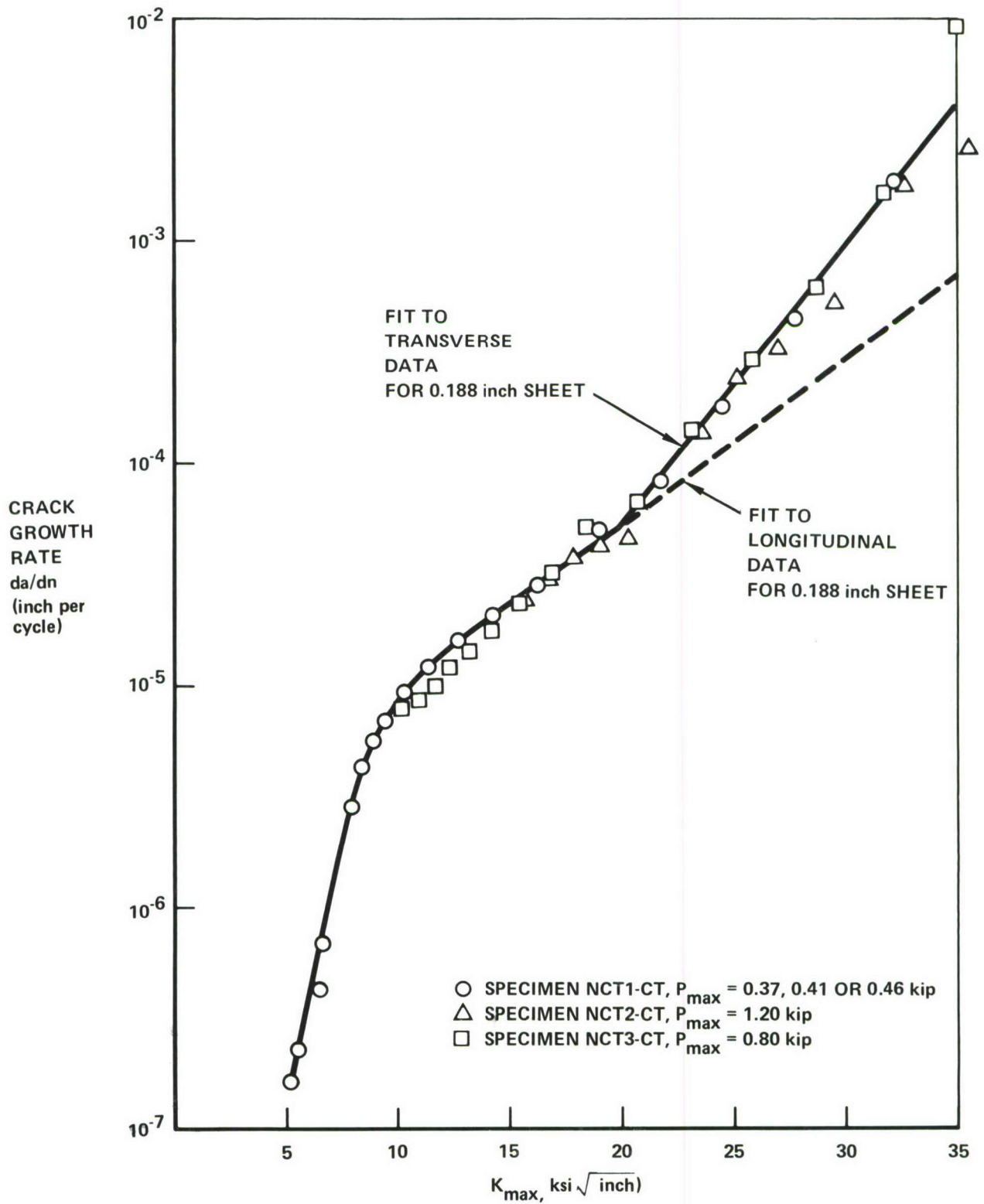


Figure 38. Fatigue Crack Growth Data, 0.188 Inch 7075-T6 Aluminum Sheet, Transverse Grain Direction,  $R = 0.1$

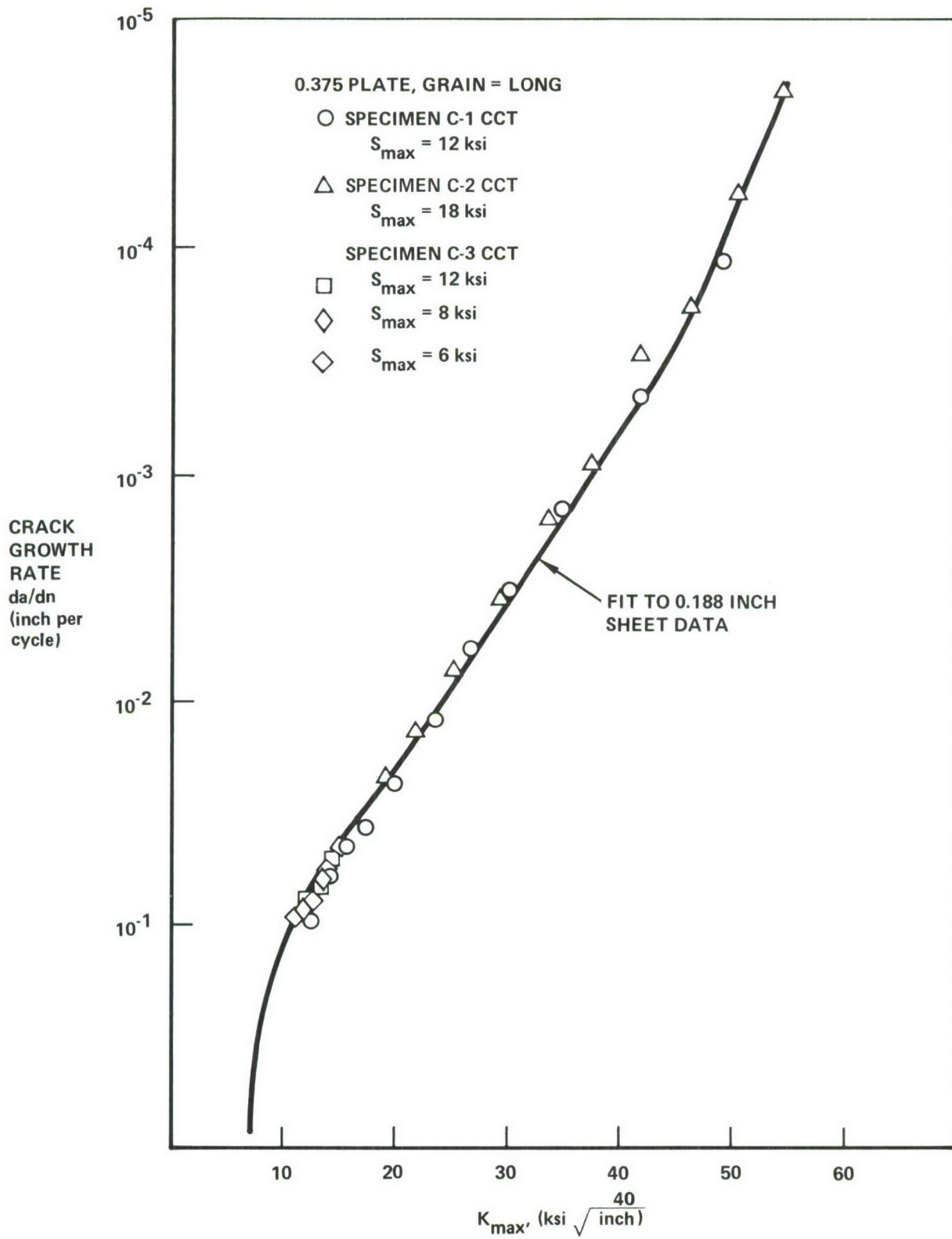


Figure 39. Fatigue Crack Growth Data, 0.375 Inch 7075-T6 Aluminum Plate, Longitudinal Grain Direction,  $R = 0.1$

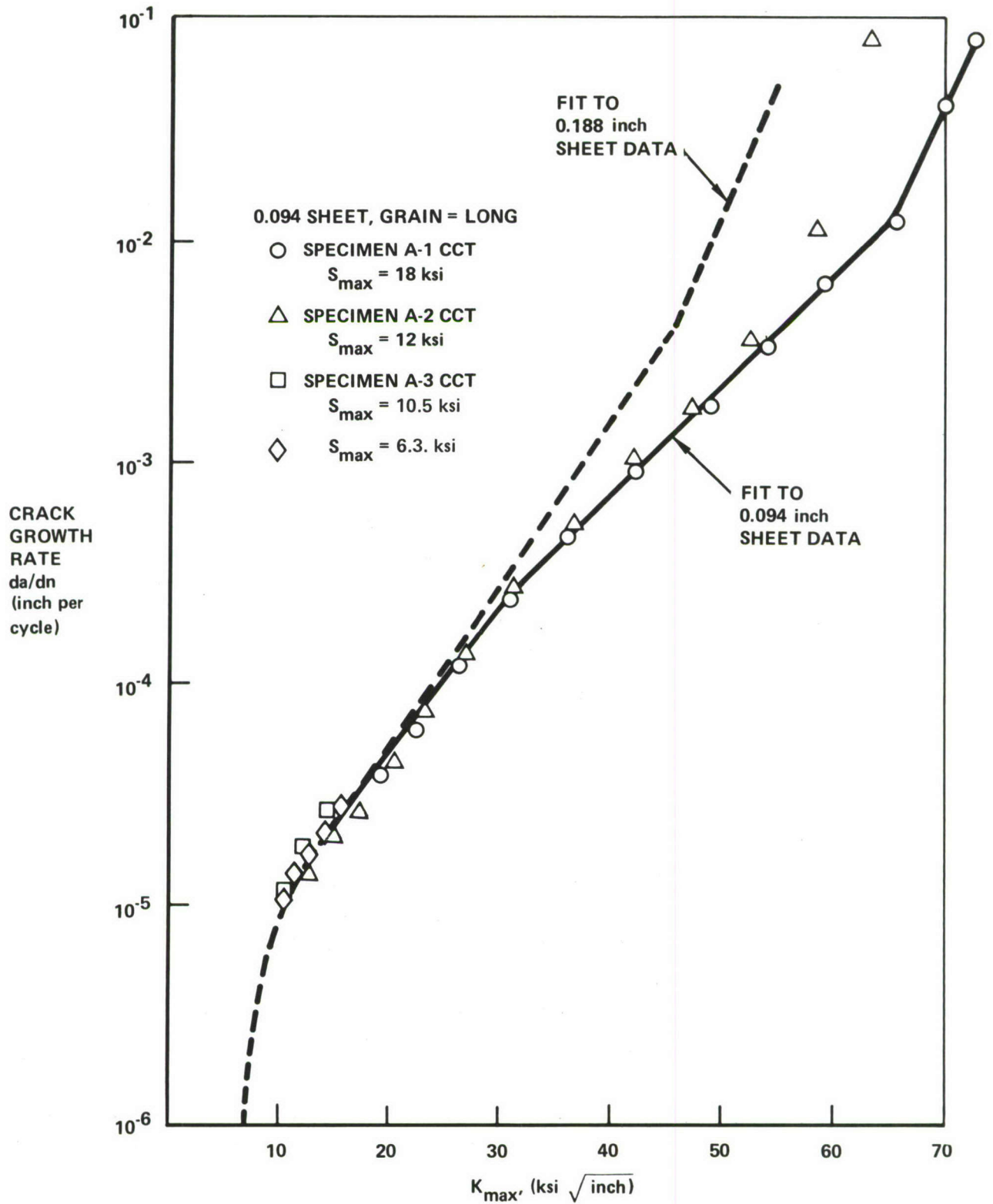


Figure 40. Fatigue Crack Growth Data, 0.094 Inch 7075-T6 Aluminum Sheet, Longitudinal Grain Direction,  $R = 0.1$

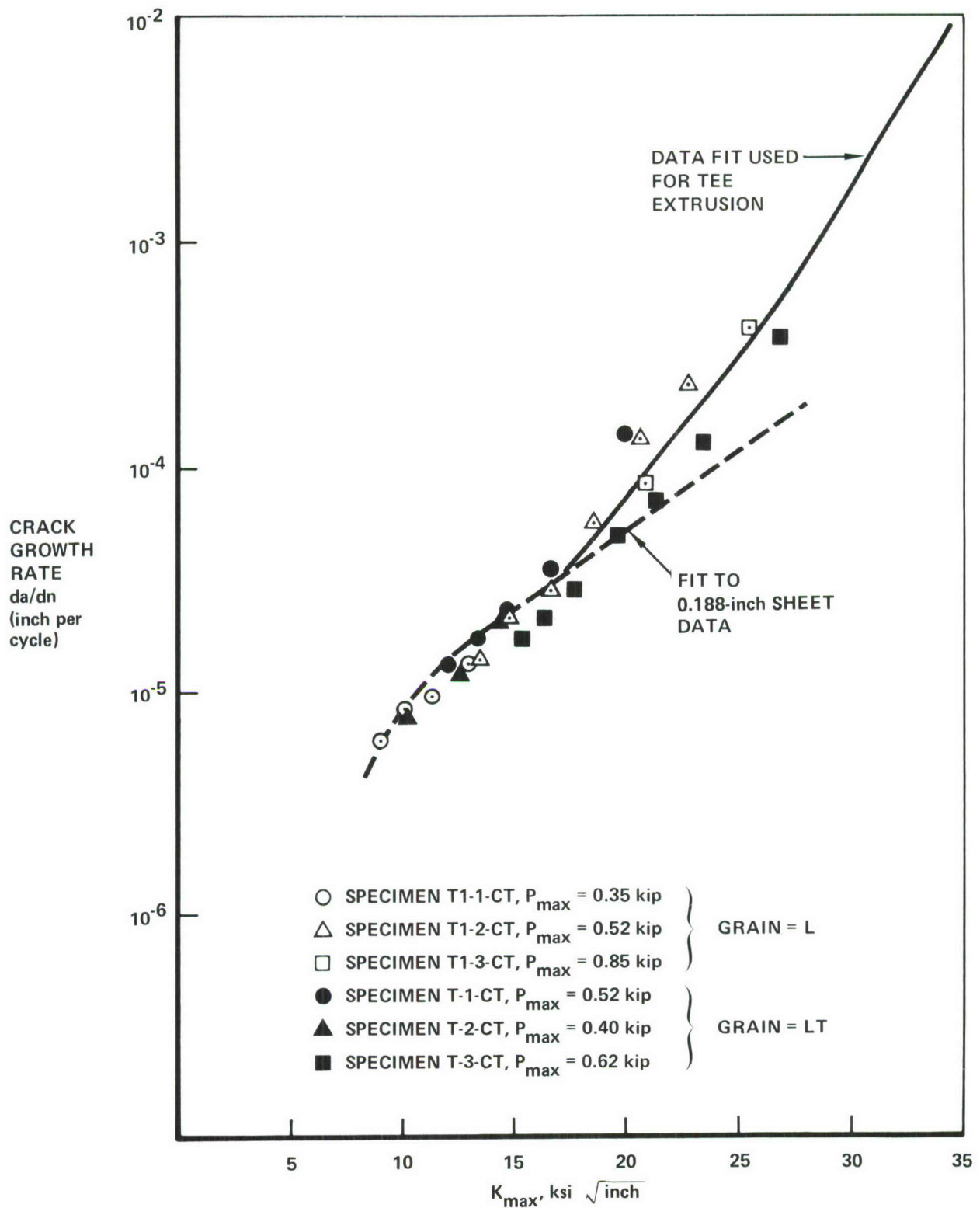


Figure 41. Fatigue Crack Growth Data, 0.188 Inch 7075-T651 Aluminum Tee Extrusion, Two Grain Directions,  $R = 0.1$

sheet material. However, it is assumed that the faster crack growth rate in the extrusion is a real effect.

Figure 42 shows the crack growth data for the 0.25-inch angle extrusion. These data agree well with the data for the 0.188-inch sheet (dashed line).

Segmented straight line plots of  $K_{\max}$  versus  $\log (da/dN)$ , taken from Figure 37 through 42, are summarized in Figure 43. This Figure was used in the crack growth predictions.

#### 4. FRACTURE TESTS

Four R-curve tests were conducted using 12-inch wide center-cracked tension panels. Two 0.188-inch specimens and one specimen each of the 0.094-inch sheet and 0.375-inch plate were tested.

Fracture toughness tests were attempted on three  $W=1.5$  inch CT specimens. These included one angle extrusion specimen (longitudinal grain direction) and two tee extrusion specimens (both grain directions). As anticipated, none of these three specimens meet the validity criterion of ASTM.

##### 4.1 R-Curve Test Procedure

Basic fracture behavior was evaluated for the 7075-T6 0.094-, 0.188-, and 0.375-inch thick sheet and plate materials used in the study by developing a crack growth resistance curve (R-curve) for each using center-cracked tension specimens 12 inches wide by 36 inches long.

In the past, measurement of material R-curves was made using the physically-measured crack length. More recently the use of compliance or crack-opening-displacement (COD) methods have become common. This method employs a plot of the crack surface displacement vs load, the slope of which can be correlated to the effective crack size by use of a calibration curve. This method is shown schematically in Figure 44. The crack length determined

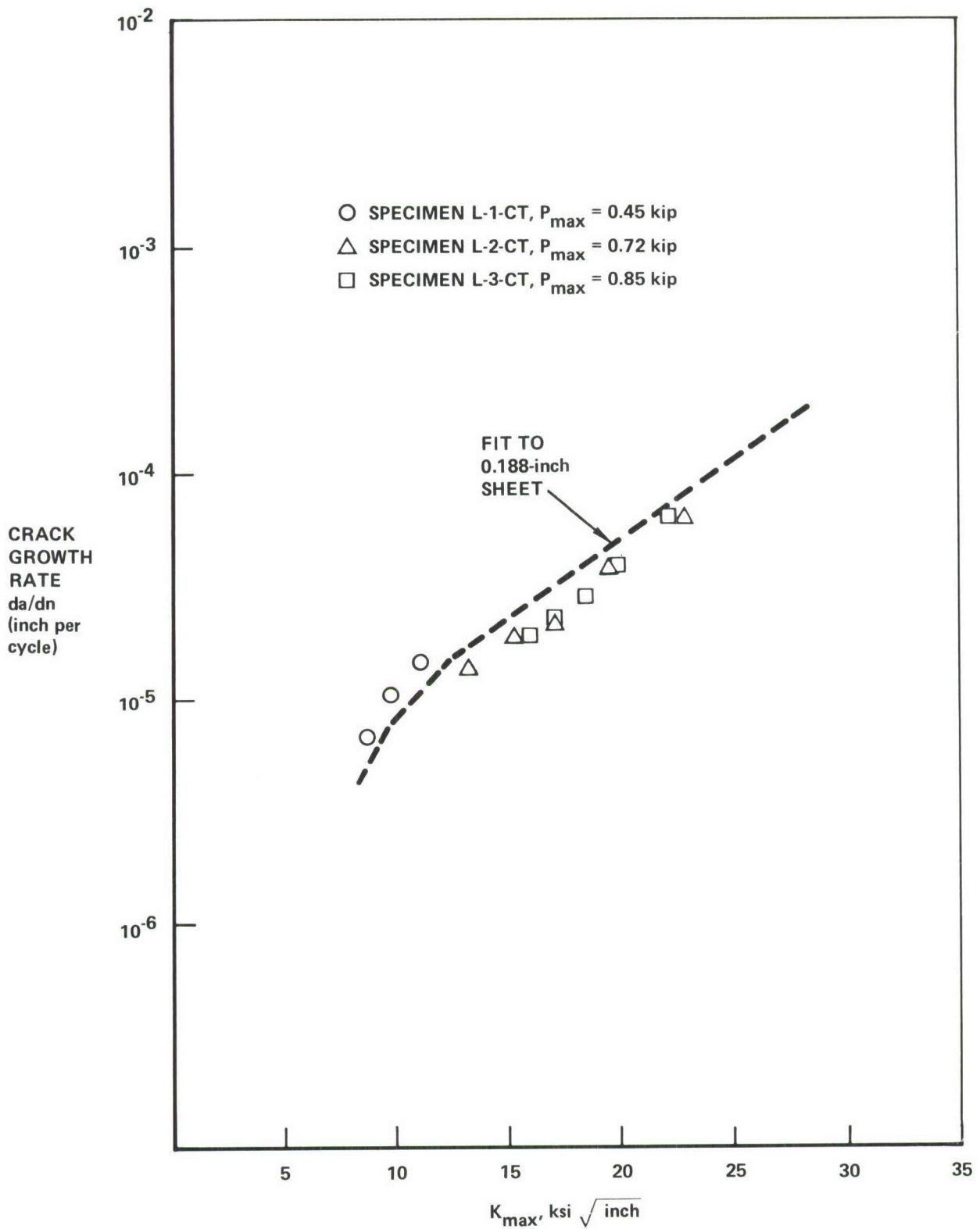


Figure 42. Fatigue Crack Growth Data, 0.25 Inch 7075-T651 Aluminum Angle Extrusion, Longitudinal Grain Direction,  $R = 0.1$

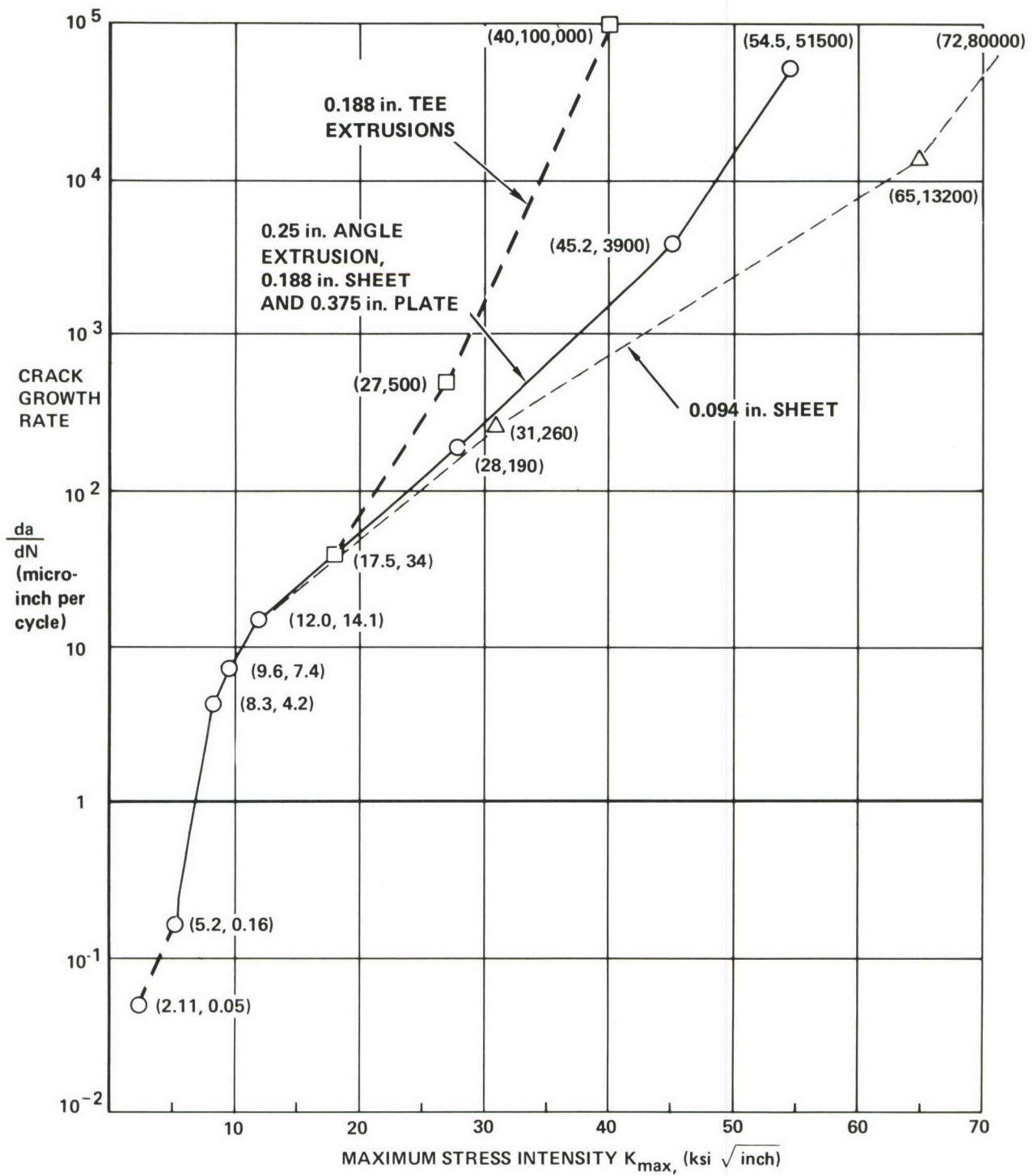


Figure 43. Summary of Fatigue Crack Growth Data, 7075-T6 Aluminum,  $R = 0.1$

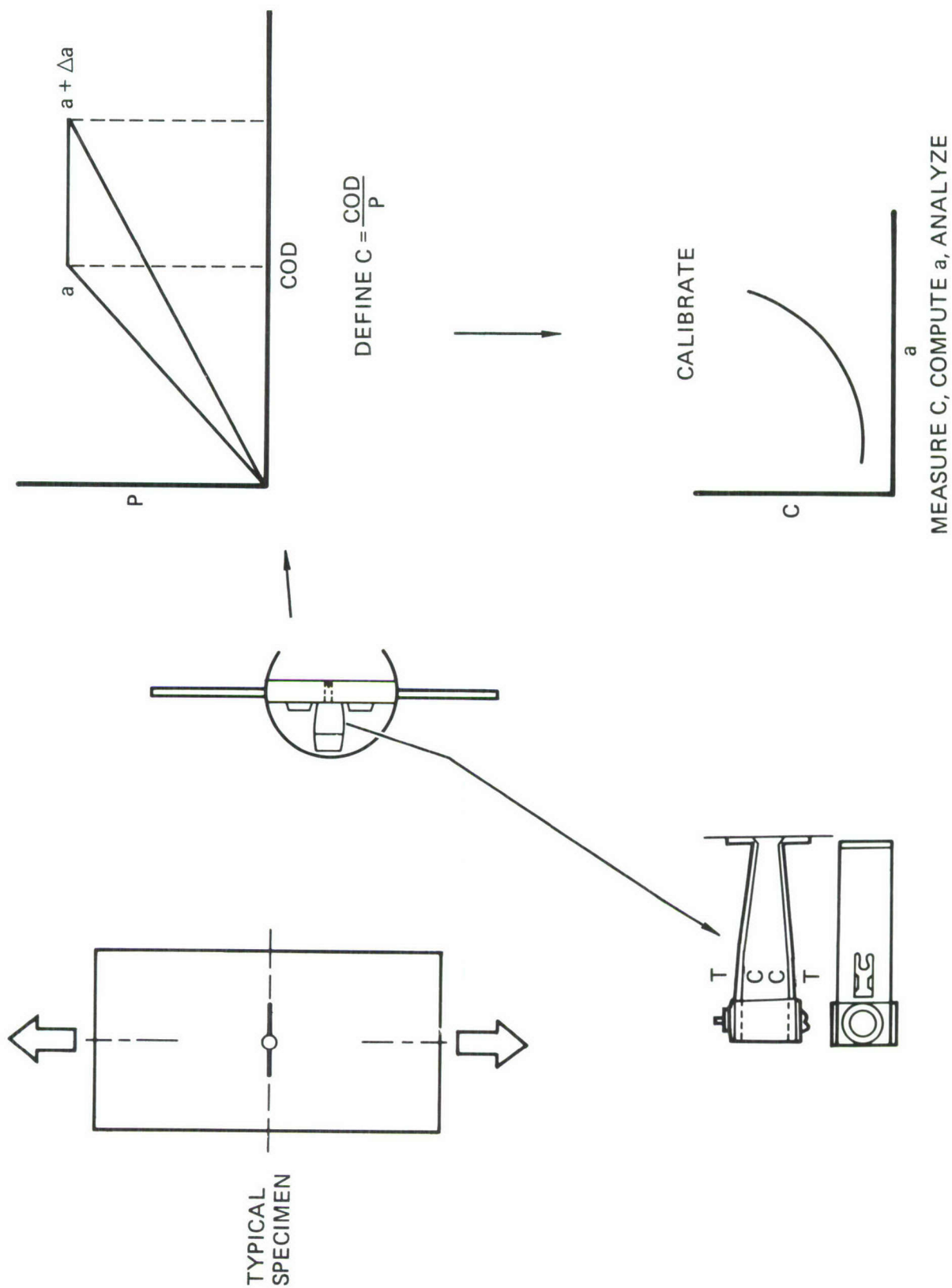


Figure 44. Compliance Method for R-Curve Testing

from the compliance method is the length of a known through-the-thickness crack in a calibration specimen of equal compliance. The calibration curve may be based on theory only, or on data from a similar panel containing either a saw cut slot or a fatigue crack induced at a low cyclic stress (small crack tip plastic zone).

Each specimen was precracked from a machined slot 0.5-inch long by fatigue cycling in laboratory air at a stress ratio of  $R = 0.1$  in a 200-kip MTS electrohydraulic test machine. Maximum loads were selected such that the final precrack maximum stress intensity,  $K_{\max}$ , was less than or equal to  $15 \text{ ksi} \sqrt{\text{inch}}$  to assure a sharp, flat crack front. Final total crack length,  $2c$ , was 4.0 inches for all tests, i.e.,  $c/W = 0.17$ .

Panel buckling can be a major problem in R-curve testing of center-crack tension (CCT) panels. Previous work (References 61, 62) has shown that the use of angle braces located parallel to and 0.5-inch above and below the crack path provides an effective constraint against buckling. Crack-opening-displacement (COD) was measured using a model 632.01 clip gage with a gage length of 0.20 inch between knife edges. Note that this gage differs from the hole gage in Reference 63 which fits into a hole at the crack center. However, comparison of the two gage types in Reference 61 has shown the hole gage to be mechanically unstable in the hole, thus increasing the possibility of errors in the COD output. The clip gage attachment is mechanically stable and provides excellent reproducibility. Using this configuration, it has been shown in References 61 and 62 that reproducible compliance calibration data are obtained for a range of aluminum alloys which correspond to the Irwin-Westergaard theoretical solution (Reference 64) when modified with the Eftis-Liebowitz width correction (Reference 65). The resulting expression is then

$$\begin{aligned} \frac{(\text{COD})_{\text{BE}}}{P} = & \sqrt{\frac{\pi a}{W} / \sin\left(\frac{\pi a}{W}\right)} \left\{ \frac{2W}{\pi Y} \cosh^{-1} \left[ \frac{\cosh(\pi Y/W)}{\cos(\pi a/W)} \right] \right. \\ & \left. - \frac{1+\mu}{\sqrt{1 + \left[ \frac{\sin(\pi a/W)}{\sinh(\pi Y/W)} \right]^2}} + \mu \right\} \frac{2Y}{W} \end{aligned} \quad (50)$$

where

B = thickness

E = Young's modulus

COD = crack opening displacement

a = c = half crack length

W = specimen width

Y = distance from crack plane to COD measurement point

$\mu$  = Poisson ratio

It should be noted that while this equation differs from the basic Irwin-Westergaard equation used in the ASTM Proposed Recommended Practice for R-curve Determination (Reference 63), the width corrected form is now being incorporated into the recommended practice and has been verified by both experimental and theoretical work as discussed in References 61 and 66. With this exception, all other test procedures corresponded to those in Reference 63.

All tests were conducted in laboratory air using the 200-kip MTS test machine. A typical test setup is shown in Figure 45. Load and COD were continuously monitored throughout the test by recording the load cell and clip gage outputs on a Mosely x-y recorder to provide visual real-time monitoring. In addition the load and COD were monitored by the Rye-Canyon Control Data computer. Periodically each specimen was partially unloaded and reloaded as a check to verify that no buckling was occurring as per the recommendations in Reference 64. No significant buckling was observed for any specimen.

#### 4.2 Test Results

The load vs COD data from each test were reduced using Equation (50) to compute the effective crack length at selected values of load or COD. The corresponding stress intensity was then computed using Equation (27a). The resulting R-curves are presented in Figure 46.

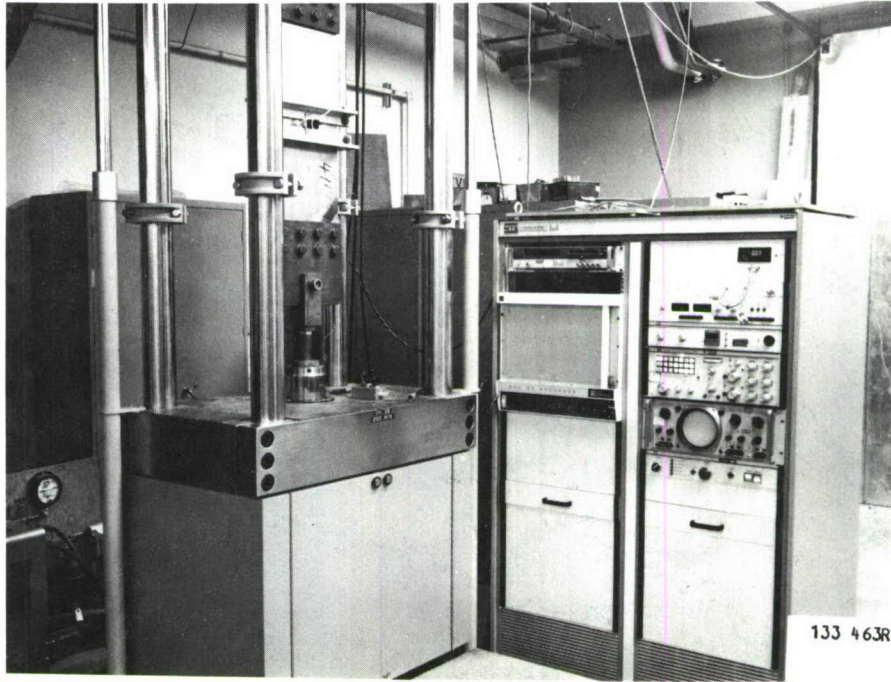


Figure 45. Typical R-Curve Test Set-Up

##### 5. MARKING CYCLE TESTS

Three  $k_t = 3.1$  coupons (Figure 31) were preflawed with a 0.020 inch razor cut on one edge of the hole and tested to attempt to develop a procedure for marking the fracture surface. In the third of these coupons the fracture surface was successfully marked. The procedure for marking was to change the stress ratio from the operating value of 0.1 to 0.82 while holding the same maximum stress and cycling at 0.82 until about 0.008 inches of crack growth could be seen on the specimen surface.

Since the structural tests involve cracks hidden in the faying surface, two additional tests were conducted on the one and one-half dogbone specimen (Figure 33). A 0.050-inch fatigue crack was induced in the faying surface at the corner of the fastener hole, and an attempt was made to mark the surface by the procedure developed in the coupon tests. To do so, an

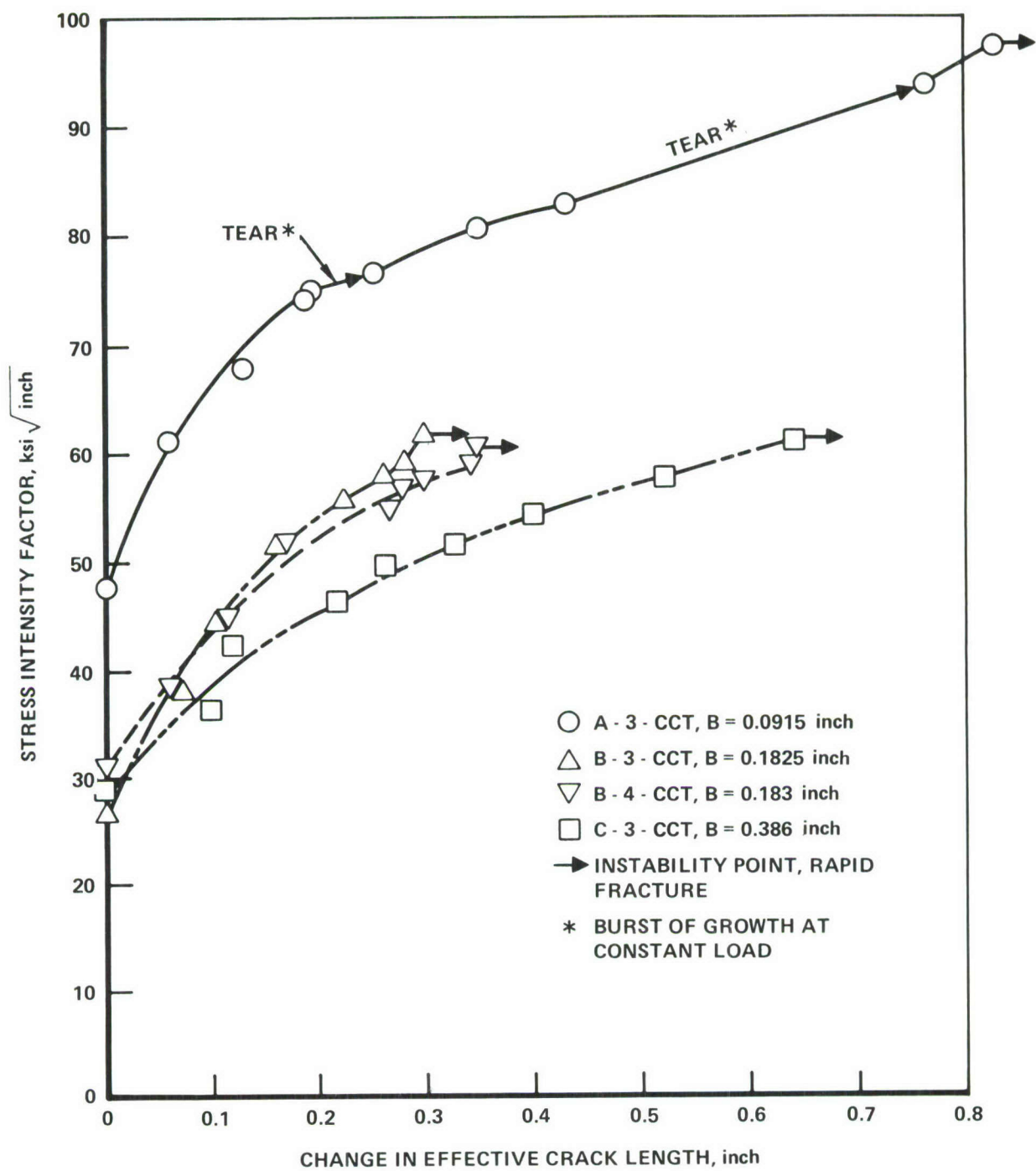


Figure 46. R-Curves for 7075-T6 Sheet Material

estimate had to be made of the number of marking cycles necessary to produce about 0.008 inches of growth. Only one or two markings were visible on the fracture surface of the first specimen. Changes were made in the number of marking cycles used, and consequently five of the six marks were visible on the fracture surface of the second specimen. The marks were not clear enough to be photographed, but they did show unmistakably the developing shape of the crack.

## 6. PREDICTED AND ACTUAL BASELINE SPECTRUM DATA

Baseline spectrum fatigue and crack growth tests were conducted using the 80-flight loading sequence shown in Figure 8, Section II. Two CT specimens were fatigue crack growth tested and four modified CT specimens were fatigue crack initiation tested. The test results are plotted as open symbols in Figures 47 and 48, respectively. The X-symbols in these two figures denote earlier data for this same spectrum loading sequence, obtained on a different batch of 0.188-inch-thick 7075-T6 sheet material. These earlier data were obtained on 6-inch-wide center-hole specimens, and are reported in Reference 55. In plotting these earlier data, a neat-fit aluminum pin in the center hole was assumed not to affect the  $k_t$  or stress intensity factor.

Predictions were made by using the baseline constant-amplitude data and first assuming no load-interaction effects; then assuming a modified Willenborg-type retardation model. Because of the short periodicity of the loading sequence, the estimated size of the overload-affected zone increases linearly with the square of reference stress intensity  $K_{Ref}$ . As a consequence, for each stress cycle in the spectrum, the corresponding values of the Willenborg effective peak stresses  $S_{eff}^{(max)}$  and  $S_{eff}^{(min)}$  are the same throughout the life and are closely approximated by

$$S_{eff}^{(max)} = \text{MAX} [0, 2S_{max} - S_{Ref}] \quad (51a)$$

$$S_{eff}^{(min)} = \text{MAX} [R_c S_{eff}^{(max)}, S_{max} - S_{Ref}] \quad (51b)$$

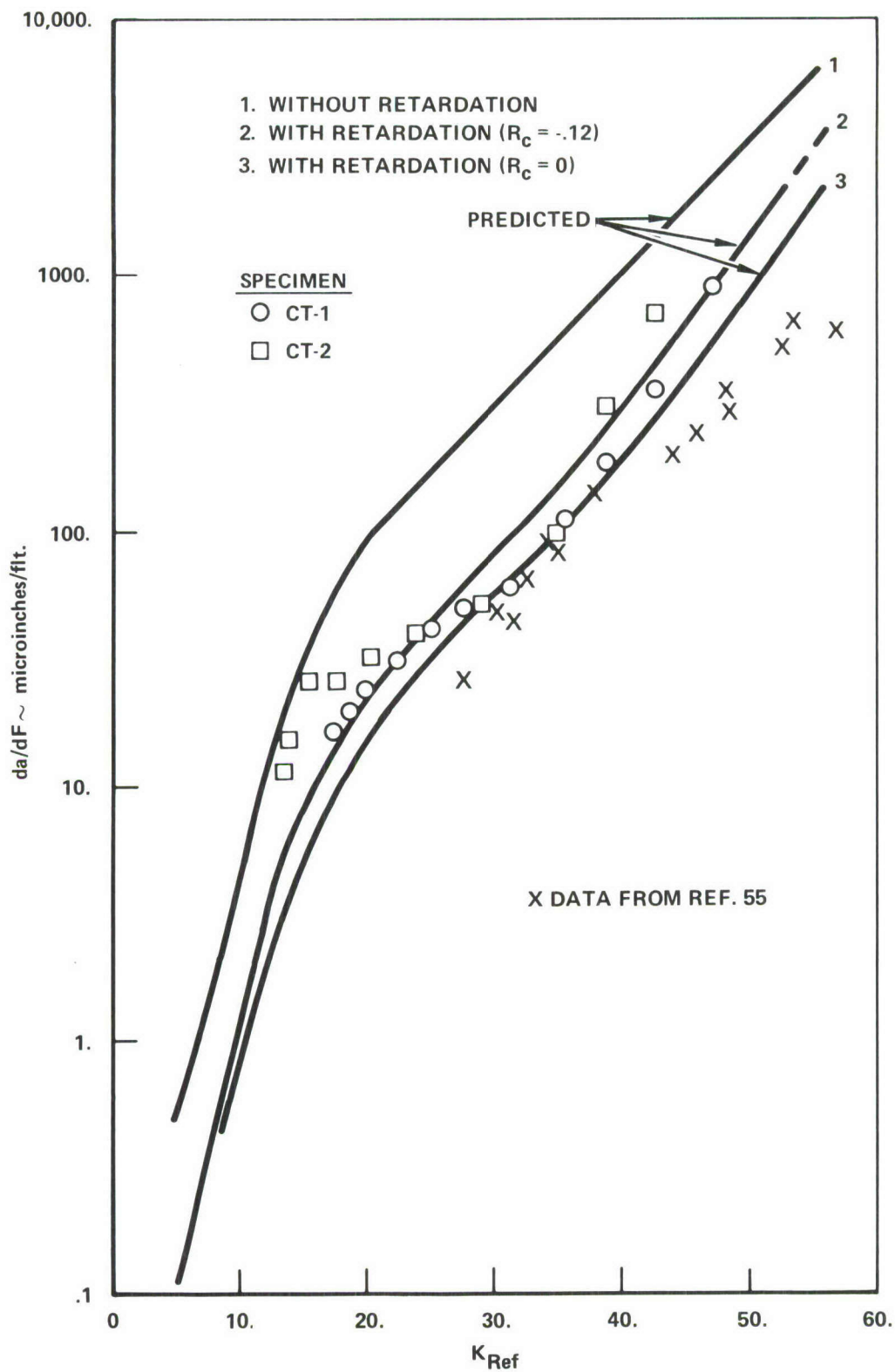


Figure 47. Baseline Spectrum Crack Growth Rates for 80-Flight Loading Sequence

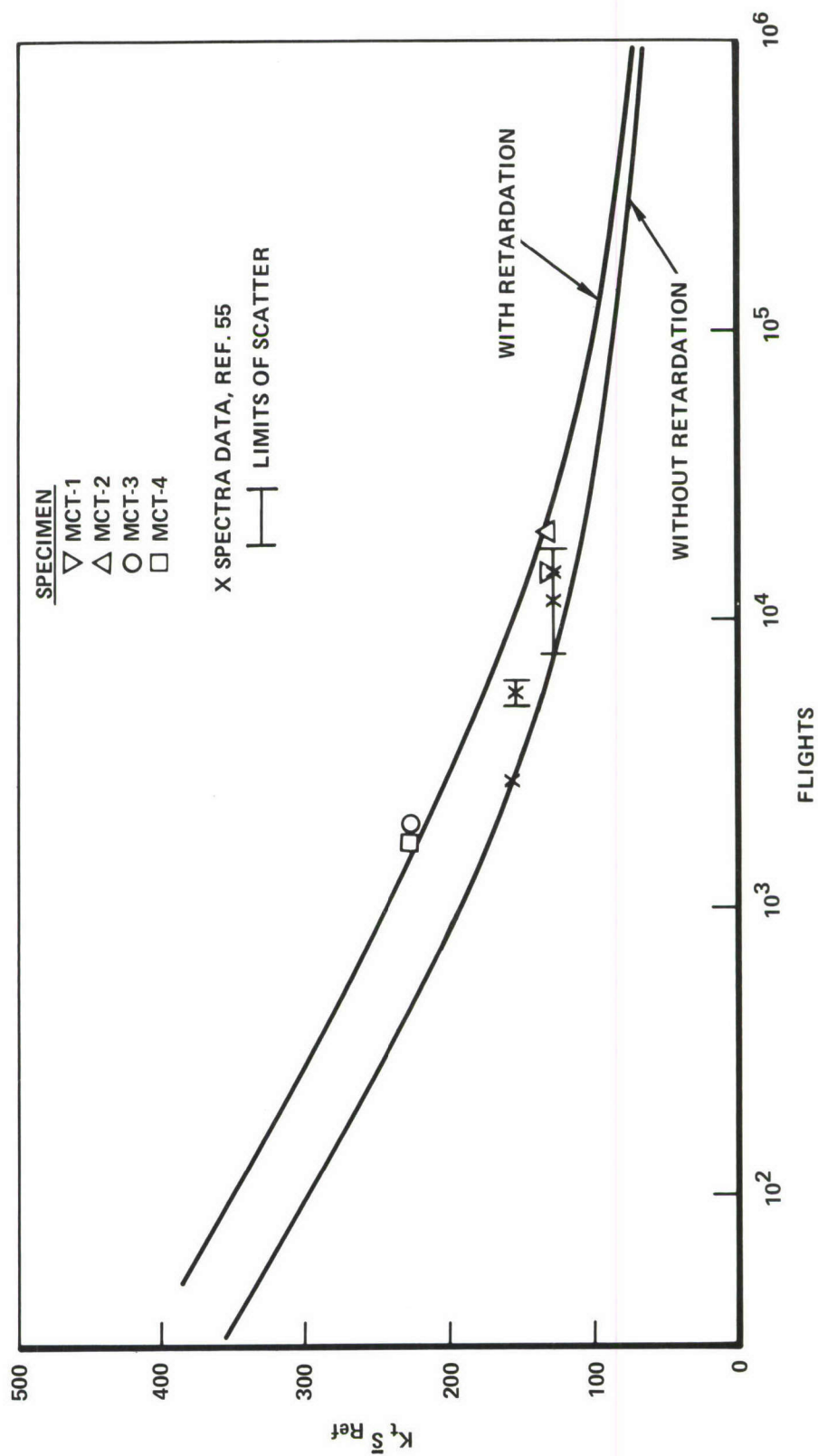


Figure 48. Baseline Spectrum Crack Initiation Lives for 80-Flight Loading Sequence

$R_c$  in Equation (51b) is the cutoff value of  $S_{eff}(min)/S_{eff}(max)$ , the effective stress ratio. Compressive stressing beyond  $R_c$  is assumed not to affect crack growth. The value  $R_c = 0$  is used in the standard Willenborg model. However, Reference 67 shows that constant-amplitude compression-tension data for 7075-T6 aluminum correlates if  $R_c = -0.12$  is used. If the retardation model is to be correct for the limiting case of constant-amplitude loading,  $R_c = -0.12$  should be used in Equation (51b).

The spectrum computations require that the baseline constant-amplitude data, all obtained at  $R = 0.1$ , be generalized for all range ratios. To accomplish this, Walker (Reference 68) uses the single parameter  $\overline{\Delta S}_{eff}$ , where

$$\overline{\Delta S}_{eff} = S_{eff}(max) [1 - S_{eff}(min)/S_{eff}(max)]^m \quad (52)$$

For aluminum,  $m = 0.5$ . Data have shown that equal values of  $\overline{\Delta S}_{eff}$  cause equal constant-amplitude crack growth rates regardless of stress ratio.

All three spectrum crack growth rate predictions shown in Figure 47 use the  $da/dN$  curve for the 3/16-inch-thick sheet material given in Figure 43, extrapolated to a threshold stress intensity point of  $k_{max} = 2.11 \text{ ksi} \sqrt{\text{inch}}$ ,  $da/dN = 0.05$  microinch per cycle. Stress ratio effects are handled by use of Equation (52).

Prediction Number 1 in Figure 47 is obtained by assuming no retardation effects. The effective maximum and minimum stresses in Equation (52) are set equal to the actual applied stresses for all cycles in the spectrum. Predictions 2 and 3 in Figure 47 are obtained by assuming retardation effects and employing Equations (51) to compute the effective maximum and minimum stresses, using  $R_c = -0.12$  and 0, respectively.

Since Equations (51) and (52) deal strictly with stresses and contain no crack length parameter, it is possible to use these equations in the estimation of crack initiation lives due to spectrum loading. The computation method is identical to Miner's Rule. The baseline constant-amplitude curve used in the computation is tabulated in Table 11. Recall that the baseline

TABLE 11. BASELINE CONSTANT AMPLITUDE,  $R = 0.1$ , S-N CURVE  
USED IN COMPUTING SPECTRUM FATIGUE ESTIMATES

| $k_t S_{\max}$<br>for $R = 0.1$<br>(ksi)  | $k_t \overline{\Delta S}_{\text{eff}}$<br>(ksi) | Crack Initiation<br>Life, N<br>(Cycles) | Source of Data |
|---|---|---|----------------|
| 48.3  | 45.8  | $10^7$                                  | Reference 69   |
| 53.8  | 51.1  | $10^6$                                  | Reference 69   |
| 70.0  | 66.4  | 65360                                   | Equation (49)  |
| 180   | 170.8   | 1126                                    | Equation (49)  |
| --  | 475.0   | 1                                       | Table 9        |
| Use linear interpolation of $\log(k_t \overline{\Delta S}_{\text{eff}})$ vs $\log(N)$ for intermediate points. Assume infinite life for $k_t \overline{\Delta S}_{\text{eff}} < 45.8$ . |   |   |                |

constant-amplitude,  $R = 0.1$  data are fitted closely over a broad range by Equation (49) with  $C_0 = 14,100$  cycles. By using other data from Reference 69 and employing Equation (52), the fatigue curve is extended to cover the full range of life and  $R$  ratio.

The computation of crack initiation time was done both without retardation (assuming that the effective maximum and minimum stresses are equal to their actual applied values), which is Miner's Rule, and with retardation (using Equations (51) with  $R_c = -0.12$ ). The results are plotted in Figure 48.

This is probably the first time that the Willenborg retardation model has been applied to predict spectrum fatigue crack initiation. No theoretical basis for using it is offered here, except that it has been empirically observed that the occurrence of an overload will delay crack initiation, just as it will slow the growth of a crack. Comparison in Figure 48 between the crack initiation data on Specimens MCT-1 through MCT-4 and the corresponding retardation prediction is interesting.

## SECTION V

### CRACK GROWTH PREDICTIONS

The analytical approach and equations presented in Section III and the baseline data presented in Section IV were used to obtain crack growth predictions for the 54 Phase I structural tests described in Section II. Volume II of this report contains a specimen-by-specimen summary of the actual predictions and the corresponding test results. The specific formulation of these predictions is presented in this section. All of these formulations preceded the corresponding test results.

#### 1. DOUBLE LAP JOINT SPECIMENS

##### 1.1 Modeling for the Double Lap Shear Joint Specimen

A typical NASTRAN finite element model of the double lap shear joint specimen is shown in Figure 49. The basic model is constructed specifically for the thicker specimens shown in Figure 2 of Section II. However, the results obtained using the basic model can be applied to the geometrically similar but thinner specimens, Figure 3.

Recall that in some of these specimens there was an initial crack in only one doubler plate, while in other specimens all three members were precracked. Thus two basically different cracking sequences were expected. In the former case, the cracking was limited to the one doubler plate until late in the test. In the other case, cracking occurred at approximately equal rates in both doubler plates.

Correspondingly, two different series of finite element analyses were needed, one with the assumed crack in one doubler only and the other with equal cracks in both doublers. Since the stresses in the crack plane were lower in the central skin member, its crack growth rate was assumed to be



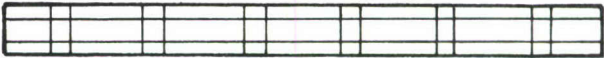
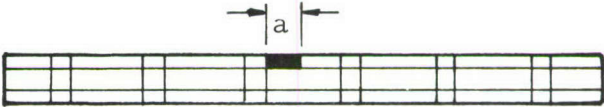
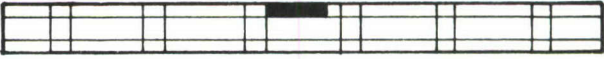

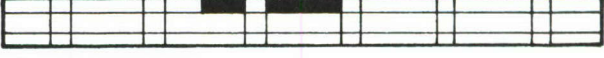

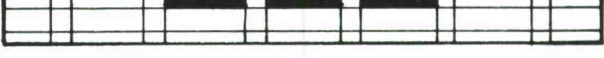

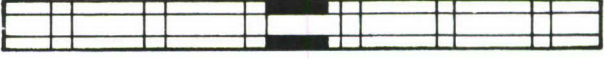
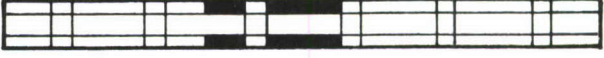


negligible, and was assumed to remain intact throughout the crack growth life. The analysis was repeated for different crack sizes. The number of analyses was selected to provide sufficient information on the redistribution of fastener loads to conduct the crack growth analysis. Some interpolations and extrapolations of results were necessary to complete the calculated data base for various damage conditions. A summary of the finite element models analyzed is presented in Table 12.

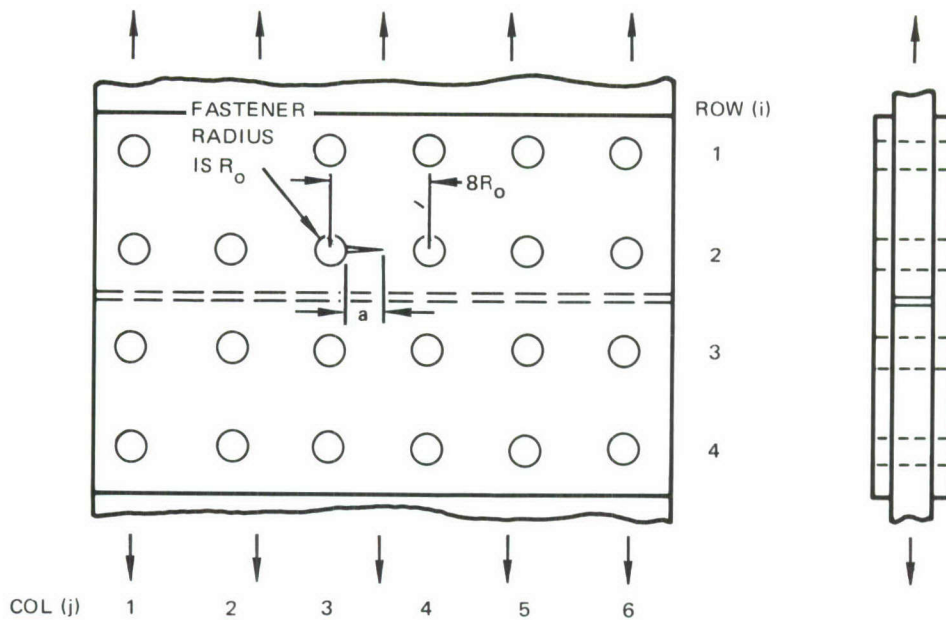
The fastener load distribution is presented in Figure 50 for the undamaged condition and one damage condition. The fastener loads are presented in normalized form,  $P/P_{ave}$ , where  $P_{ave}$  is the average fastener load. The damage condition is the case of one doubler damaged with crack length  $a = 3R_o$  (half the first ligament between fastener holes cracked). This particular damage condition is selected for presentation to show the fastener load redistribution as a result of the assumed damage. Fastener load distributions for all the damage conditions shown in Table 12 were obtained in similar form.

Compare the individual fastener loads calculated for the damaged case to the corresponding fastener loads for the undamaged case. The damage has very little effect on the magnitude of the remote fastener loads. Furthermore the remote fastener loads have a relatively small effect on the stress intensity factor.  $K_I$  due to a point force is, approximately, inversely proportional to the distance from the crack tip to the point of application of the load. Thus attention is focused on the fastener loads along the crack itself, in the crack path, and immediately above and below the crack. Table 13 summarizes these computed fastener load values for cracking across the first ligament.

The most important load is the load in the crack-origin fastener, Fastener 3 in Row 2. Let  $a_{34}$  be the length of the longer crack (growing from Hole 3 toward Hole 4), and let  $a_{32}$  be the length of the shorter crack (growing from Hole 3 toward Hole 2). Using the finite element results, the load at Fastener 3 of Row 2 can be approximated as follows:

TABLE 12. DAMAGE CASES ANALYZED FOR DOUBLE LAP JOINT SPECIMEN

| DESCRIPTION                  | CROSS SECTIONAL VIEW OF DAMAGE   |
|------------------------------|--|
| <u>Undamaged Case</u>        |    |
| <u>One Doubler Cracked:</u>  |  |
| $a = 3R_o$                   |    |
| $a = 4.5 R_o$                |    |
| 1 broken ligament            |    |
| 1.5 broken ligaments         |    |
| 2 broken ligaments           |   |
| 3 broken ligaments           |  |
| <u>Two Doublers Cracked:</u> |  |
| $a = 1.5R_o$                 |  |
| $a = 4.5R_o$                 |  |
| 1.5 broken ligaments         |  |
| 2 broken ligaments           |  |
| 3 broken ligaments           |  |



$$\frac{P_{ij}}{P_{ave}} = \begin{bmatrix} -1.0462 & -0.9666 & -0.9495 \\ -1.0242 & -0.9666 & -0.9943 \\ 1.0405 & 0.9822 & 0.9559 \\ 1.0306 & 0.9744 & 0.9637 \end{bmatrix} \quad \text{SYMMETRIC}$$

(a) UNDAMAGED

$$\frac{P_{ij}}{P_{ave}} = \begin{bmatrix} -1.0569 & -0.9659 & -0.9132 & -0.9438 & -0.9751 & -1.0533 \\ -1.0313 & -0.9780 & -0.8805 & -1.0 & -0.9744 & -1.0292 \\ 1.0434 & 0.9780 & 0.9182 & 0.9431 & 0.9836 & 1.0441 \\ 1.0320 & 0.9637 & 0.9431 & 0.9445 & 0.9708 & 1.0349 \end{bmatrix}$$

$$\frac{P_{ij}}{P_{ave}} = \begin{bmatrix} -1.0576 & -0.9908 & -1.0085 & -1.0057 & -0.9879 & -1.0569 \\ -1.0277 & -1.0085 & -1.0199 & -1.0064 & -1.0050 & -1.0277 \\ 1.0420 & 1.0057 & 1.0178 & 1.0135 & 1.0021 & 1.0391 \\ 1.0391 & 0.9993 & 1.0057 & 1.0050 & 0.9972 & 1.0370 \end{bmatrix}$$

(b) DAMAGED

Figure 50. Typical Distribution of Normalized Fastener Loads for the Double Lap Joint Specimen

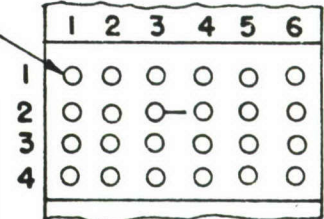
TABLE 13. CALCULATED FASTENER LOADS IN DOUBLE LAP JOINT

(Values shown are normalized fastener forces in cracked doubler for crack of length "a"):

$$\frac{1}{P_{ave}}$$

$$\begin{bmatrix} P_{13} & P_{14} \\ P_{23} & P_{24} \\ P_{33} & P_{34} \end{bmatrix}$$

$R_0$  = HOLE RADIUS



| ONE DOUBLER CRACKED |                  |       | TWO DOUBLERS CRACKED |                  |       |
|---------------------|------------------|-------|----------------------|------------------|-------|
| $a/R_0$             | $P_{ij}/P_{ave}$ |       | $a/R_0$              | $P_{ij}/P_{ave}$ |       |
| 0                   | 0.95             | 0.95  | 0                    | 0.95             | 0.95  |
|                     | 0.994            | 0.994 |                      | 0.994            | 0.994 |
|                     | 0.955            | 0.955 |                      | 0.955            | 0.955 |
| 3                   | 0.91             | 0.945 | 1.5                  | 0.961            | 0.965 |
|                     | 0.88             | 1.000 |                      | 0.950            | 1.000 |
|                     | 0.92             | 0.945 |                      | 0.956            | 0.970 |
| 4.5                 | 0.87             | 0.92  | 4.5                  | 0.91             | 0.945 |
|                     | 0.85             | 1.00  |                      | 0.89             | 1.00  |
|                     | 0.89             | 0.91  |                      | 0.93             | 0.955 |
| 6.0                 | 0.876            | 0.876 | 6.0                  | 0.90             | 0.90  |
|                     | 0.768            | 0.768 |                      | 0.85             | 0.85  |
|                     | 0.880            | 0.880 |                      | 0.93             | 0.93  |

In the cracked doubler when the other doubler is uncracked,

$$\frac{P_o}{P_{ave}} = (0.994 - \frac{a_{34}}{R_o} 0.035) (1 - \frac{a_{32}}{R_o} 0.09) \quad (53)$$

When both doublers are cracked,

$$\frac{P_o}{P_{ave}} = (0.994 - \frac{a_{34}}{R_o} 0.24) (1 - \frac{a_{32}}{R_o} 0.07) \quad (54)$$

## 1.2 Stress Intensities for the Double Lap Shear Joint Specimens

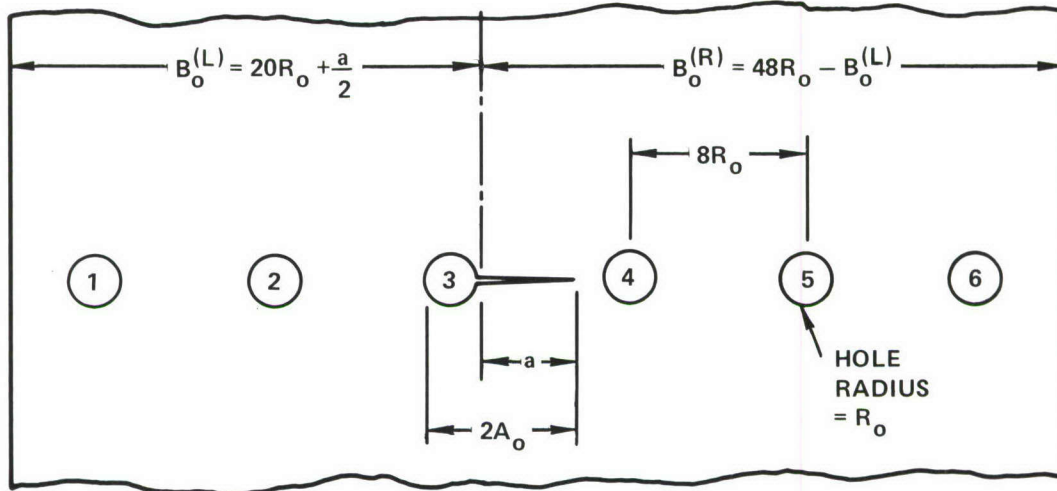
The formulas in Section III can be combined to provide  $K_I$  expressions for the anticipated cracks in the double lap shear joint specimens. The following summarizes these combined  $K_I$  expressions, which are used for the crack growth predictions.

In all cases the stress intensity is formed as the sum of  $K_I^{(F)}$ , the stress intensity due to the fastener load at the hole (or holes) from which the crack is emanating, plus  $K_I^{(R)}$ , the stress intensity due to all other fastener loads:

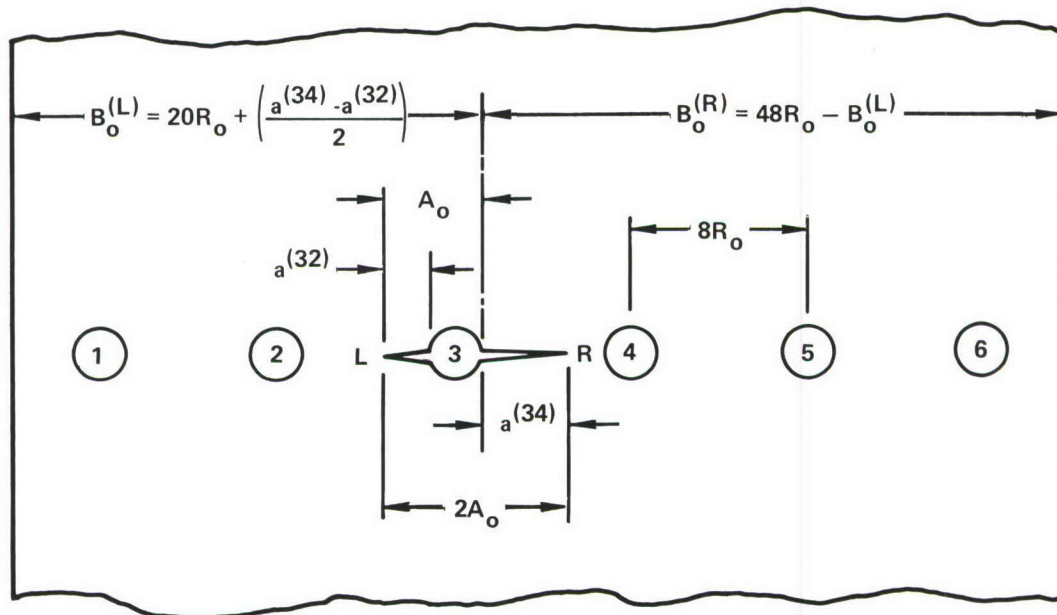
$$K_I = K_I^{(F)} + K_I^{(R)} \quad (55)$$

1.2.1 Crack in the First Ligament. - For much of the estimated crack growth life the initial crack grows across the first ligament independent of other cracks. Therefore the greatest attention was given to this configuration (Figure 51(a)).

The load in fastener 3 of row 2 is approximated by Equation (53) for crack growth only in the top doubler and in Equation (54) for crack growth in both doublers. This is the load magnitude  $P_o$  in Equation (44) for  $Y_{FO}$  for this crack configuration. The expression for  $K_I^{(F)}$  is constructed using



(A) CRACK IN CENTER LIGAMENT ONLY



(B) UNSYMMETRIC DOUBLE CRACK

Figure 51. Anticipated Crack Configuration in Row 2 of the Double Lap Joint Specimens

Equation (18) for the fundamental stress intensity solution and Equations (27), (32), (44), and (28) for the correction factors. Then

$$K_I^{(F)} = K_I^{(1)} Y_{FW} Y_{TR} Y_{FO} Y_{AH} \quad (56)$$

where, from Equation (45), the crack depth  $c$  as used in the expression for  $Y_{TR}$  is given approximately by

$$c = \left( \frac{2 - \theta}{\theta} \right)^2 a \quad (57)$$

All other dimensions are as defined in Figure 51(a). Equation (37) was used along with output from the loads analyses to compute  $K_I^{(R)}$  due to the remote fastener loads for various crack lengths. From this, approximate expressions for  $Y_{RE}$  (Equation (38)) were obtained by curve-fitting the computed points. When only the top doubler is cracked,

$$Y_{RE} = 0.661 - 0.0184 \frac{a}{R_o} + 0.00407 \left( \frac{a}{R_o} \right)^2 \quad (58)$$

When both doublers have equal cracks,

$$Y_{RE} = \begin{cases} 0.661 & \text{for } \frac{a}{R_o} \leq 4 \\ 0.661 + 0.0348 \left( \frac{a}{R_o} - 4 \right)^2 & \text{for } \frac{a}{R_o} > 4 \end{cases} \quad (59)$$

The expression for  $K_I^{(R)}$  is then constructed using Equation (18) for the fundamental stress intensity solution and Equations (27), (32), (28a) and either (58) or (59) for the correction factors. Then

$$K_I^{(R)} = K_I^{(1)} Y_{FW} Y_{TR} Y_{AH} Y_{RE} \quad (60)$$

where  $c = a$  is assumed in the expression for  $\gamma_{TR}$  (effects of transverse bending caused by remote loads are ignored). The other dimensions needed for Equation (60) are as defined in Figure 51(a).

The continuing damage flaws occur at different holes but are otherwise similar to the initial 0.050-inch flaw. During the time that all flaws grow independently, the minor differences are ignored and the continuing damage flaws are analyzed using the identical  $K_I$  expressions that are used for the main flaw, as given above.

1.2.2 Double Unsymmetric Cracking at the Precracked Hole. - The first new crack to initiate is expected to occur on the opposite side of the precracked fastener hole. In general this leads to the crack configuration shown in Figure 51(b). For this configuration two stress intensity factors are needed,  $K_I(L)$  and  $K_I(R)$ , for the left and right-hand crack tips in Figure 51(b).

The expressions for  $K_I^{(F)}(L)$  and  $K_I^{(F)}(R)$  are constructed using Equation (19) for the fundamental stress intensity solution and Equations (27), (44)\* and (28) for the correction factors. Thus

$$K_I^{(F)} = K_I^{(2)} \gamma_{FW} \gamma_{FO} \gamma_{AH} \quad (61)$$

In computing  $K_I^{(R)}$  for the two crack tips it was not considered necessary to recompute the remote fastener force correction factor  $\gamma_{RE}$ . Instead it was assumed as an approximation that  $\gamma_{RE}$  for each crack tip is independent of the length of the crack on the opposite side of the hole. Equations (58) and (59) are thereby applicable, using  $a_{34}$  or  $a_{32}$  in place of  $a$ . The expressions for  $K_I^{(R)}$  are then constructed using Equation (19) as the fundamental stress intensity solution and Equations (27), (28) and either (58) or (59) for the correction factors. Then

$$K_I^{(R)} = K_I^{(2)} \gamma_{FW} \gamma_{AH} \gamma_{RE} \quad (62)$$

---

\*Equation (44) applies to a double crack using  $a = a_{34}$  for the longer crack and  $a = a_{32}$  for the shorter crack.

The crack growth rate curve for 0.188 inch sheet, laboratory air environment, and  $R = 0.1$  is given in Figure 43 of Section IV. The crack growth calculation method utilized follows that diagrammed in Figure 8.

Crack initiation times require expressions for the stress severity factors. Equation (5) is the pertinent expression. It involves knowledge of the stress concentration factor  $k_t$  and of the fastener loads. The fastener loads change as the crack progresses, but these changes are small and inconsequential except at holes adjoined to the crack.

Using the computed fastener loads and linear interpolation, the effects of local load transfer on the stress severity factor can be estimated. The remote loading is assumed to be uniform. The  $k_{tg}$  is obtained as a function of crack size by combining Equations (11), (13) and (16).  $k_{tb}$  is found from Equation (10). The factor  $\theta$  comes from Table 7 or a finite element analysis, whereas  $\alpha$  and  $\beta$  as obtained from the baseline data are given in Table 7.

## 2. SINGLE LAP JOINT SPECIMENS

Essentially the same prediction approach, formulas and baseline data that applied to the double lap joint specimens also apply to the single lap joint specimens. These specimens and the initial damage conditions are shown in Figures 4 and 6 in Section II.

Finite element modeling was again used to generate fastener loads for a sequence of anticipated crack configurations. In selecting these damage conditions it was assumed that the doubler crack would not grow. The computed normalized fastener loads are presented in Table 14.

The stress intensity factor formulas are as given in Equations (56), (60), and (61) or (62). The correction factors  $Y_{RE}$  and  $Y_{FO}$  and the tilt factor  $\theta$  had to be established for the single lap shear joint specimen. A tilt factor of  $\theta = 1.1$  was computed using the profile view finite element model. Equation (37) was used to compute  $K_I^{(RE)}$ , which takes account of fastener loads in Row 2 of the skin as well as the uniform remote skin load. Computed values of  $K_I^{(RE)}/S\sqrt{\pi A_o}$  for both the left and right-hand crack tips are plotted in Figure 52 and fitted with the linear expression

$$Y_{RE} = 0.756 - 0.0053 A_o/R_o \quad (63)$$

TABLE 14. COMPUTED FASTENER LOADS ( $P/P_{avg}$ ) IN SKIN, SINGLE LAP JOINT

|                                  |        |        |         |        |         |        |        |        |  |
|----------------------------------|--------|--------|---------|--------|---------|--------|--------|--------|--|
| UNDAMAGED CASE                   |        |        |         |        |         |        |        |        |  |
| -0.923                           | -0.885 | -0.877 | -0.877  | -0.877 | -0.877  | -0.877 | -0.885 | -0.923 |  |
| -1.136                           | -1.103 | -1.092 | -1.091  | -1.092 | -1.091  | -1.092 | -1.103 | -1.136 |  |
| 1.136                            | 1.097  | 1.070  | 1.066   | 1.070  | 1.066   | 1.070  | 1.097  | 1.136  |  |
| 0.927                            | 0.886  | 0.902  | (0.895) | 0.902  | (0.895) | 0.902  | 0.886  | 0.927  |  |
| $a = 3R_o$                       |        |        |         |        |         |        |        |        |  |
| -0.924                           | -0.885 | -0.877 | -0.876  | -0.877 | -0.876  | -0.877 | -0.885 | -0.924 |  |
| -1.136                           | -1.103 | -1.091 | -1.090  | -1.091 | -1.090  | -1.091 | -1.103 | -1.136 |  |
| 1.144                            | 1.103  | 1.065  | 1.053   | 1.070  | 1.053   | 1.070  | 1.103  | 1.143  |  |
| 0.933                            | 0.891  | 0.907  | (0.860) | 0.905  | (0.860) | 0.905  | 0.890  | 0.931  |  |
| 1 BROKEN LIGAMENT + $a = 1.5R_o$ |        |        |         |        |         |        |        |        |  |
| -0.927                           | -0.885 | -0.875 | -0.873  | -0.875 | -0.873  | -0.875 | -0.885 | -0.927 |  |
| -1.142                           | -1.104 | -1.086 | -1.084  | -1.087 | -1.084  | -1.087 | -1.105 | -1.141 |  |
| 1.195                            | 1.125  | 0.999  | 0.982   | 1.082  | 0.982   | 1.082  | 1.132  | 1.172  |  |
| 0.970                            | 0.927  | 0.841  | (0.785) | 0.926  | (0.785) | 0.926  | 0.914  | 0.950  |  |
| 2 BROKEN LIGAMENTS               |        |        |         |        |         |        |        |        |  |
| -0.935                           | -0.887 | -0.871 | -0.866  | -0.871 | -0.866  | -0.871 | -0.887 | -0.935 |  |
| -1.154                           | -1.107 | -1.078 | -1.071  | -1.078 | -1.071  | -1.078 | -1.107 | -1.154 |  |
| 1.266                            | 1.184  | 0.978  | 0.812   | 0.978  | 0.812   | 0.978  | 1.184  | 1.266  |  |
| 1.020                            | 0.982  | 0.849  | (0.631) | 0.849  | (0.631) | 0.849  | 0.982  | 1.020  |  |
| 3 BROKEN LIGAMENTS               |        |        |         |        |         |        |        |        |  |
| -0.944                           | -0.888 | -0.865 | -0.859  | -0.866 | -0.859  | -0.866 | -0.888 | -0.943 |  |
| -1.169                           | -1.107 | -1.066 | -1.057  | -1.071 | -1.057  | -1.071 | -1.110 | -1.165 |  |
| 1.436                            | 1.136  | 0.771  | 0.701   | 0.999  | 0.701   | 0.999  | 1.253  | 1.326  |  |
| 1.157                            | 1.096  | 0.589  | (0.550) | 0.883  | (0.550) | 0.883  | 1.042  | 1.061  |  |

(Load at precracked hole shown in parentheses)

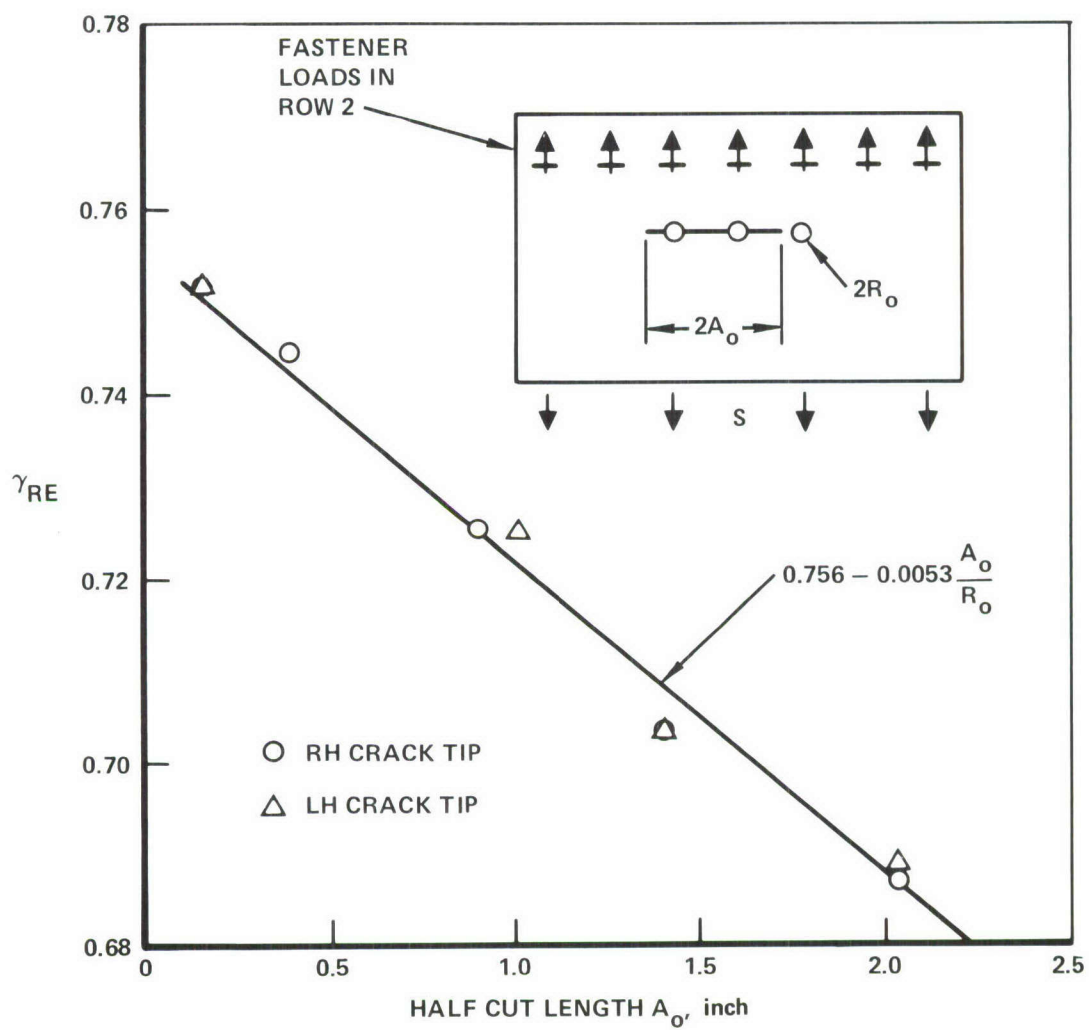


Figure 52. Remote Load Factor  $\gamma_{RE}$  for K for Single Lap Joint Specimen

The only fastener loads in Row 1 that influence the stress intensity are those at holes intersected by the crack. These may be accounted for in the term  $Y_{FO}$ . Using Equation (44) of Section III in conjunction with the computed loads for the sequence of damage conditions of Table 14, the solution for  $Y_{FO}$  for the single lap joint takes the form

$$Y_{FO} = \phi_{FO} \sqrt{\frac{1}{R_o + a} - \frac{1}{2A_o}} \left( \frac{\theta}{10 \sqrt{\pi A_o}} \right) \quad (64)$$

where  $A_o$  and  $R_o$  are as defined in Figure 53, "a" is the crack length measured from the edge of the nearest hole, and  $\phi_{FO}$  is the following linear fit of the computed values shown in Figure 53:

$$\phi_{FO} = 2.3 - 0.38 A_o \quad \text{before the first ligament breaks} \quad (65a)$$

$$\phi_{FO} = 2.0 + 0.4 A_o \quad \text{after the first ligament breaks} \quad (65b)$$

The modified stress severity factor approach described in the preceding section is used to compute reinitiation times for arrested cracks. All the equations in Section V, Paragraph 1 apply without change, using the correct dimensions for the single lap joint specimen and the computed loads given in Table 14.

### 3. Tee-Reinforced Continuous Skin Specimens

The tee-reinforced continuous skin specimen consisted of a 0.188-inch thick tee extrusion fastened at its base with a double row of 0.25-inch diameter aluminum rivets to an 18-inch wide, 0.188-inch thick panel. Cyclic loads were applied parallel to the stringer axis.

The crack growth prediction procedure follows that of Section V, Paragraph 1. The crack growth rate curves for the sheet and tee are given in Figure 43 of Section IV.

If transverse bending effects are ignored, the stress intensity solutions for cracks in the sheet are simpler than the K solutions for joints. For the

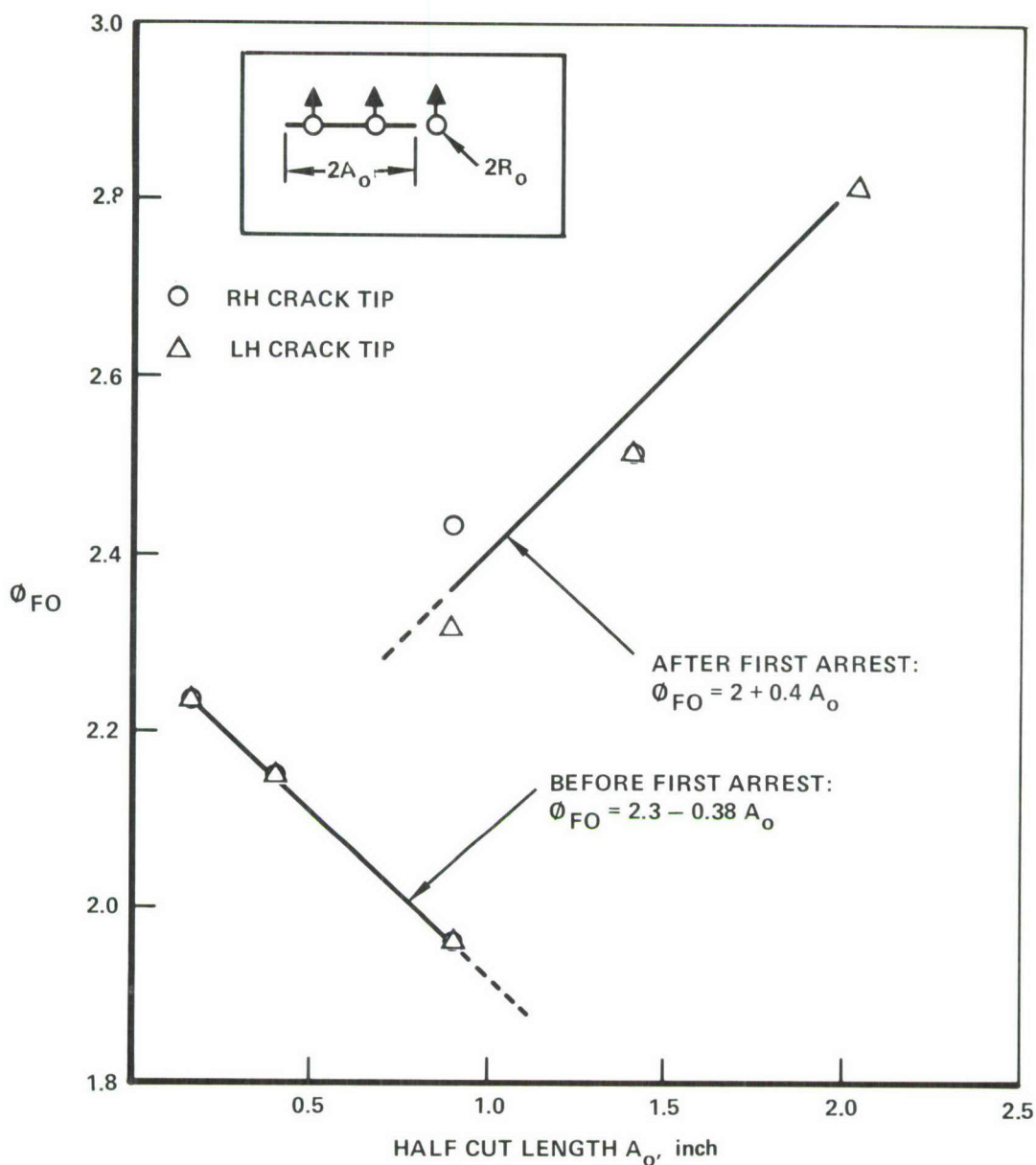


Figure 53. Stress Intensity Correction Factor  $Y_{FO}$  for Fastener Loads on the Crack Line

joints, the fasteners in the crack line transferred significant loads; and the stress intensity factor had two components, one due to the fastener loads along the crack line and one due to the remote loads. For the sheet-stringer specimens, the fasteners in the path of the crack are on the line of symmetry and do not transfer y-direction loads. Hence only the remote-load terms are applicable.

The same symmetry argument applies to the tee in these specimens. However, the fact that the tee is nonplanar complicates the stress intensity analysis. Also, the base of the tee is only 2.625 inches wide and the height of the flange is only 2.25 inches, so there are important free edge effects on stress intensity and a tendency for the tee to eventually fail by net section yielding, without regard to the  $K$  value.

The analysis of tee-reinforced specimens was conducted only up to the time when the secondary cracks initiated. In the tests, the time thereafter until failure was expected to be relatively short, so the effect of this omission would be minimal. However, in 18 of the 26 tests the remaining life after the first secondary initiation exceeded 10 percent of the total test life. Therefore, the subsequent analysis of edge-stringer specimens included the growth period of secondary cracks.

### 3.1 Stress Intensity Factors for the Skin

Before any crack reinitiation and before any significant growth of continuing damage flaws, the only growing skin crack is the primary initial flaw. This flaw begins as a corner flaw at a fastener hole, becomes a through-thickness crack, and grows toward its neighboring fastener hole or toward the free edge of the sheet. Load-shedding between the sheet and stringer may occur as the crack grows. Equation (60) is directly applicable and complete for  $K_I$  for this case.

Similarly for double unsymmetric cracking, Equation (62) is used. This same equation also applies when the crack intersects both fastener holes, and  $Y_{AH}$  is equal to unity.

### 3.2 Stress Intensity Factor in the Tee Stringer

Analysis of the tee stringer is complicated by the thickness change at the vertical flange, the simultaneous growth in both the base and the vertical flange, and the strong finite-width effects.

For the outside crack shown in Figure 54 the following is used:

$$K_I = K_I^{(1)} \gamma_{TR} \gamma_{RE} \gamma_{NE} \quad (66)$$

Equations (18), (32) and (24) from Section III, Paragraph 3 define  $K_I^{(1)}$ ,  $\gamma_{TR}$  and  $\gamma_{NE}$ .

No finite element analyses were conducted for any of the stringer-reinforced specimens to compute the fastener forces that are induced as crack growth alters the relative flexibilities of the skin and the stringer. It was assumed for the predictions that this "load shedding" was zero. Thus,  $\gamma_{RE} = 1.0$  was used in Equation (66).

For the inside crack shown in Figure 54 the following is used:

$$K_I = K_I^{(1)} \gamma_{TR} \gamma_{FW} \gamma_{SF} \quad (67)$$

The width used in  $\gamma_{FW}$  is the width of the base of the tee. The stiffener-flange effect  $\gamma_{SF}$  was estimated using an available solution by Isida (References 54, 43) and the following approximate method based on engineering judgment of reducing  $K$  when the crack grows from a thin to a thicker section:

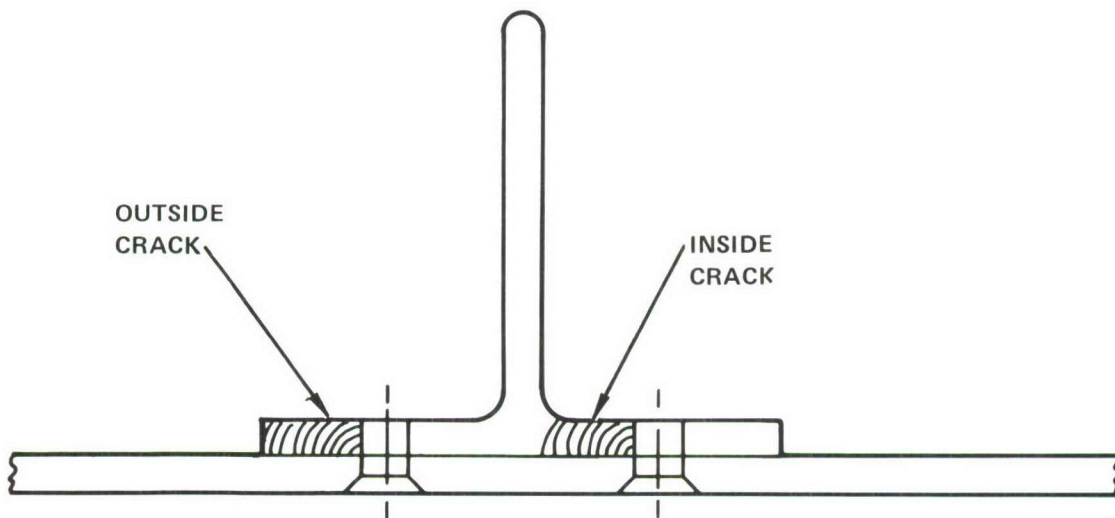


Figure 54. Inside Cracks and Outside Cracks in the Stringer

The strain energy release rate  $\mathcal{G}$  for any crack is

$$\mathcal{G} = \frac{\partial W}{\partial A} = \frac{\partial W}{\ell \partial a} \quad (68)$$

where  $\ell$  is the length of the crack front. Since  $\mathcal{G}$  is proportional to  $K^2$ , the stress intensity should be inversely proportional to the square root of  $\ell$ . Hence it is assumed

$$\gamma_{SF} \doteq \sqrt{A/(2A_o \ell)} \quad (69)$$

where  $A$  is the total fracture surface area and  $A_o$  is crack length.

It was assumed that the crack front shape for the inside tee crack would develop as depicted in the sketch in Figure 55. The shape was assumed to be approximately quarter-circular at the locations marked (1) and (2) in the figure. In both cases the center of this circle is the point on the base of the tee aligned with the near edge of the vertical flange of the tee. The circle radii are 0.188 for crack (1) and 0.312 for crack (2).

Using equation (69) the estimated values of  $\gamma_{SF}$  are

$$\text{for Crack (1),} \quad \gamma_{SF} = 0.78$$

$$\text{for Crack (2),} \quad \gamma_{SF} = 0.65$$

The corresponding crack lengths as measured from the edge of the origin hole along the base of the tee are  $a = 0.625$  inch and  $a = 0.75$  inch.

These points are plotted in Figure 55. A curve that asymptotically approaches Isida's results for a crack in a plate  $t$  thick approaching a section  $2t$  thick (Reference 54) is fitted through those two computed points. Equation (69) is assumed to continue to apply after the crack breaks through the vertical flange. Assuming equal growth rates in the base and vertical flange (in accord with Poe's recommendation in Reference 26a), the plot of crack size versus  $\gamma_{SF}$  was completed. Failure of the tee was assumed when the net section stress equals the yield stress (80.6 ksi) or when the crack reaches both holes and has broken the vertical flange of the tee.

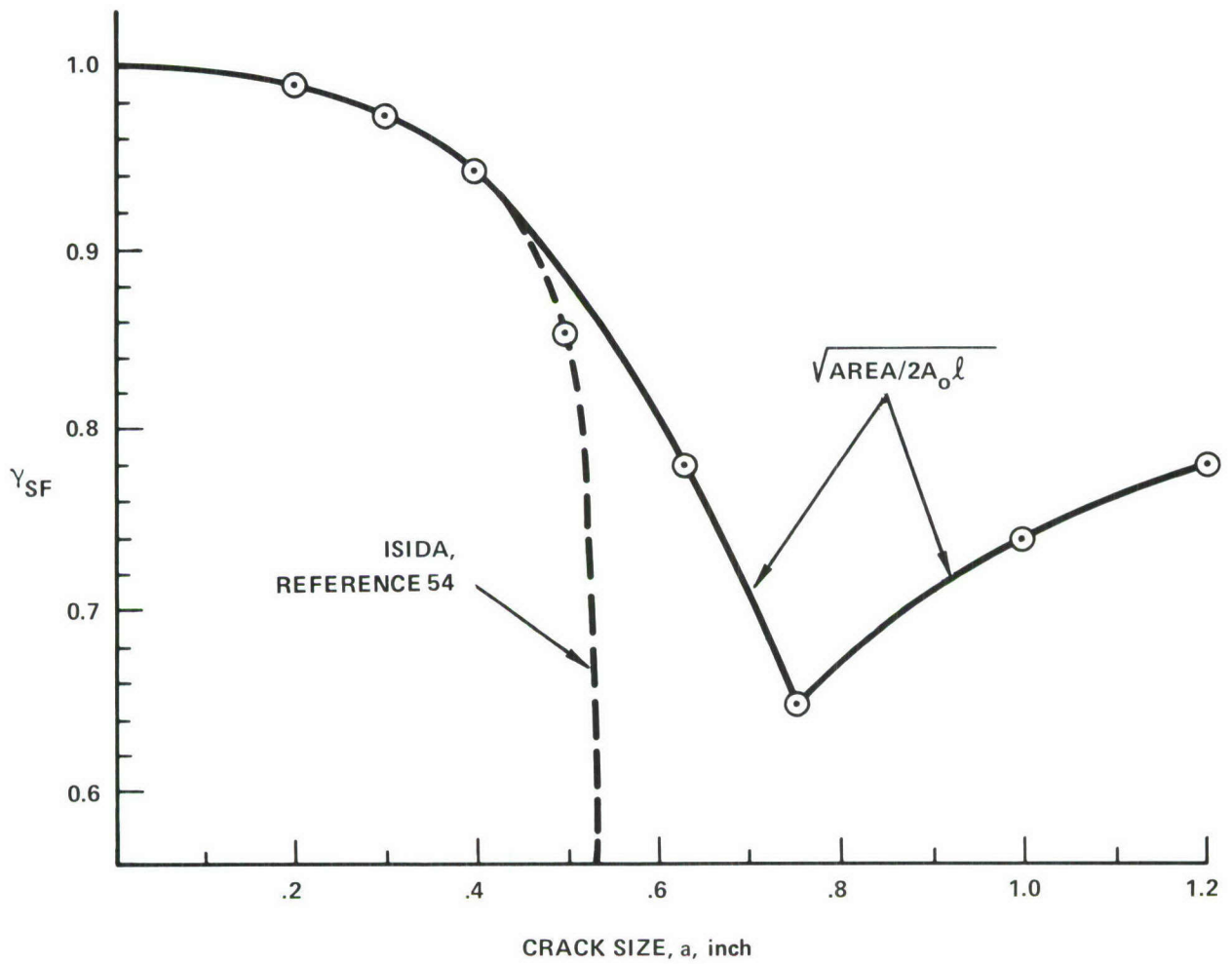
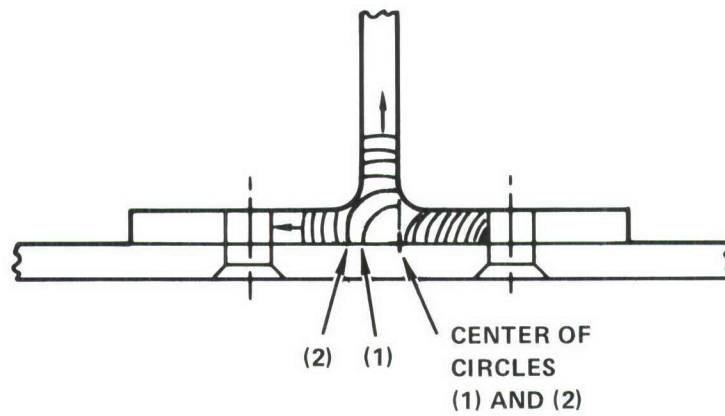


Figure 55. Estimate of Correction Factor  $Y_{SF}$  for Effect of Tee-Stringer Flange on Crack in Stringer Base

### 3.3 Crack Reinitiation

Initiation times of secondary cracks during the growth of primary cracks were predicted from a linear cumulative damage analysis as described in Section III, Paragraph 2.5, using the results of the crack growth prediction and expressions for stress severity factor  $\lambda$ . In all the stringer-reinforced specimens the crack plane is a plane of symmetry so the fastener loads in that plane are zero and

$$\lambda = \alpha \beta k_{tg} \quad (70)$$

The fastener hole diameter was 0.250 inch, so  $\alpha = 1$  was used. The fasteners were either clearance-fit steel Hi-loks, for which  $\beta = 1$ , or aluminum rivets. No baseline tests were done to estimate  $\beta$  factors for rivets; however, standard practice is to assume  $\beta = 1$  for rivets. Thus  $\lambda = k_{tg}$  for fastener holes in the crack plane in these tee-reinforced continuous-skin specimens.

Equations (11), (13), (24), (22), and (16) from Section III, Paragraph 2 are appropriate for expressing  $k_{tg}$  in terms of  $2A_o$ , which is the full "cut length" including the crack plus the fastener hole. The specific cases are as follows:

- For the initiating outside tee crack during growth of the inside tee crack,

$$k_{tg} = k_t^{(1)} \gamma_{o-o} \gamma_{NE} \quad (71)$$

- For the initiating inside tee crack during growth of the outside tee crack toward the free edge,

$$k_{tg} = k_t^{(1)} \gamma_{o-o} \gamma_{QE} \quad (72)$$

- For the same initiating crack after the outside tee crack reaches the free edge (forming an edge notch of depth  $A_o$ ):

$$k_{tg} = 1.1215 k_t^{(1)} \gamma_{o-o} \quad (73)$$

- For an initiating skin crack, either inside or outside,

$$k_{tg} = k_t^{(1)} Y_{o-o} Y_{FW} Y_{RW} \quad (74)$$

#### 4. TEE-REINFORCED SPLIT-SKIN SPECIMENS

The tee-reinforced split-skin specimen (type 4.8-3-X) is shown in Figure B-1 of Appendix B. By its similarity to the continuous-skin specimen (type 4.8-1-X), it presents no significantly new prediction problems.

The fasteners for this specimen are 0.3125-inch steel Hi-loks. Thus, from Table 7 in Section III, the constant  $\alpha$  in Equation (70) is 1.03, and  $\beta = 1.0$  for clearance-fit untorqued fasteners and 0.635 for interference-fit fully torqued fasteners.

The larger hole diameter in the split-skin specimens causes an 8 percent higher initial stress intensity factor in the split-skin specimen than in the continuous-skin specimens. The percent difference diminishes as the crack grows. In predicting crack growth in the tee stringer this small difference was neglected. Furthermore, load shedding effects were neglected in both specimen types. Therefore, the crack growth predictions in the tee for both specimen types were identical.

New predictions were required for the skin because of the free-edge effect at the split. These stress intensity factors are

- For the inside skin crack,

$$K_I = K_I^{(1)} Y_{TR} Y_{NE} \quad (75)$$

- For the outside skin crack,

$$K_I = K_I^{(1)} Y_{TR} Y_{QE} \quad (76)$$

Equation (71) was used to compute the stress concentration factor for the initiating inside skin crack during growth of the outside skin crack. Equations (72) and (73) were used to compute  $k_{tg}$  for the initiating outside skin crack during growth and after arrest of the inside skin crack.

## 5. EDGE-STRINGER SPECIMENS

This section describes the prediction of crack growth for the 12 edge stringer specimens. The configuration of these specimens is shown in Figure B-2 of Appendix B. The 10 different initial damage conditions are shown in Table 3 in Section II.

The fasteners in the path of the crack are on the line of symmetry and do not transfer y-direction loads. Transverse bending effects and effects of load shedding from cracked to less-cracked members were assumed to be negligible.

The prediction for each structural element of a specimen consisted of a crack growth prediction of the growth of the initial crack across the first ligament (to the neighboring fastener hole or free edge) and the initiation times and growths of secondary cracks. The crack growth rate curve for the 0.187-inch sheet and 0.250-inch angle extrusion is given in Figure 43 in Section IV. Continuing damage flaws were regarded as 0.005-inch cracks. The computed failure time of the element with the shortest life was assumed to be equal to the failure time of the entire specimen.

The initiation times were computed using  $\lambda$  [Equation (70)] in place of  $k_t$  in Equation (48), Section IV. For 0.312-inch diameter holes  $\alpha = 1.03$ ; for clearance-fit untorqued fasteners  $\beta = 1.0$ ; and for interference-fit fully-torqued fasteners  $\beta = 0.635$ .

The main effort in the crack growth computation is the selection of formulas for stress intensity factors,  $K$ , and stress concentration factors,  $k_t$ . These formulas are summarized in the following subsections.

### 5.1 Initial Outside Crack in the Angle Stringer

Figure 56(A) shows the general cracked condition of the angle for the crack that begins as an outside corner crack,  $a_L = 0.050$  inch. For the actual specimen, the fixed dimensions defined in Figure 56 are as follows:

$$\begin{array}{ll} L = 0.81 \text{ inch} & R_o = 0.156 \text{ inch} \\ W = 5.0 \text{ inches} & W_{SK} = 18.0 \text{ inches} \\ L_R = 0.63 \text{ inch} & L_L = 1.81 \text{ inches} \\ t = 0.250 \text{ inch} & t_{SK} = 0.182 \text{ inch} \end{array}$$

As shown schematically in the figure, the angle is considered to be equivalent to a plane strip of width equal to the total length of its two flanges (hence,  $W = 5.0$  inches).

When  $a_R = 0$ , the stress intensity for the left-hand crack tip can be approximated by

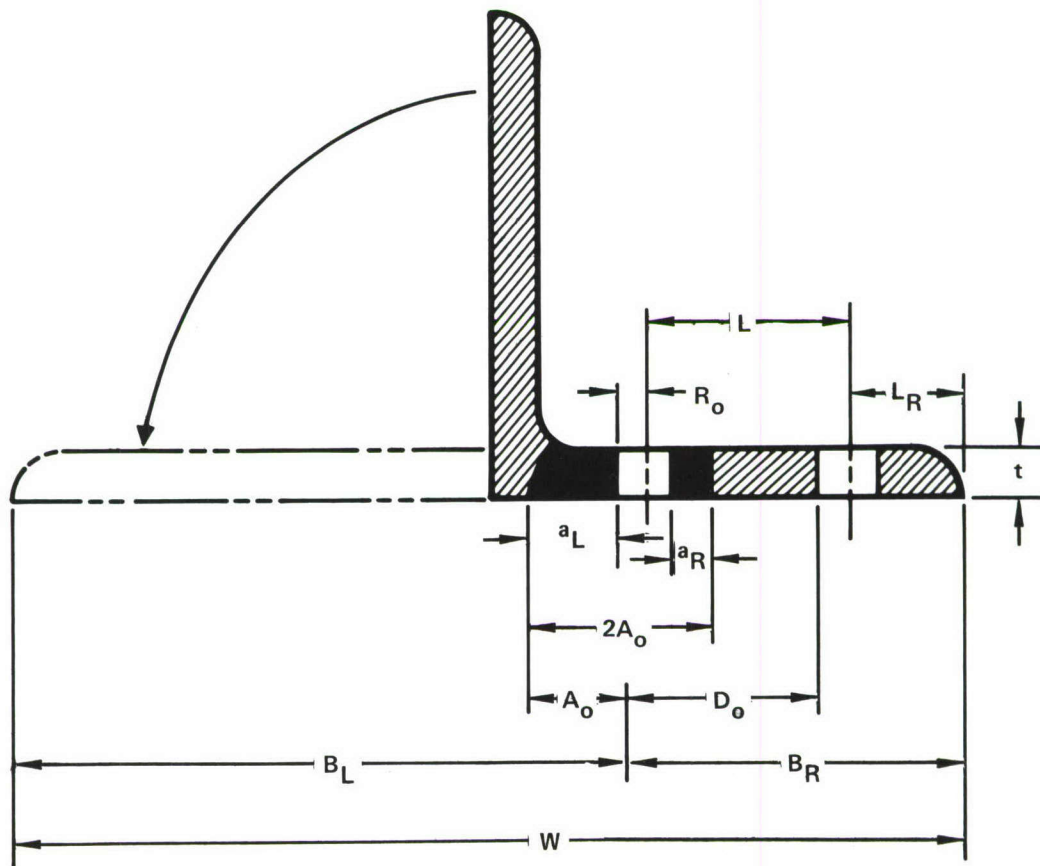
$$K_I = K_I^{(1)} Y_{TR} Y_{FW} \quad (77)$$

Here  $K_I^{(1)}$  is defined in Equation (18) in Section III with  $a = a_L$ .  $Y_{TR}$  is obtained from Equation (32) with  $c = a_L$ . Equation (27) defines  $Y_{FW}$ . Using Equations (11), (13) and (16), the stress concentration factor  $k_{tg}$  at the origin point of  $a_R$  is given by Equation (74).

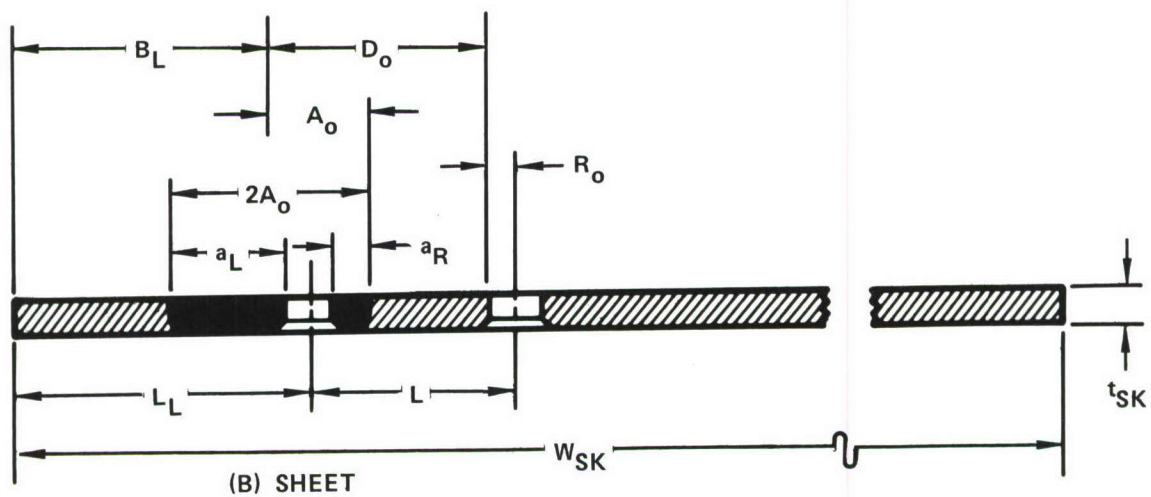
When  $a_R = 0$  the stress intensity for the left-hand crack tip is given by Equation (75), and the stress concentration factor at the origin point of  $a_R$  is given by Equation (72), where Equations (24) and (26) are used for  $Y_{NE}$  and  $Y_{QE}$ , with  $B_o = B_L$ .

After  $a_R$  initiates, the stress intensity for the left-hand crack tip is given by

$$K_I = K_I^{(2)} Y_{TR} Y_{FW} \quad (78)$$



(A) ANGLE STRINGER



(B) SHEET

Figure 56. Dimensions for Outside Cracks, Edge Stringer Specimens

where  $K_I^{(2)}$  is from Equation (19). Using Equation (28) for  $\gamma_{AH}$ , the stress intensity for the right-hand crack tip is

$$K_I = K_I^{(2)} \gamma_{FW} \gamma_{AH} \quad (79)$$

When the crack is arrested at the second fastener hole and then reinitiates, the stress intensity for the left-hand crack tip is still as given in Equation (78), where  $2A_o$  is the total cut length, including the holes. During reinitiation the stress concentration factor is again as given by Equation (74). After reinitiation the stress intensity for the right-hand crack tip is given by Equation (78).

When by analysis the crack breaks through to either free edge, the initially-outside-cracked angle is considered to have failed.

## 5.2 Initial Outside Crack in Skin

Figure 56(B) shows the general cracked condition of the skin for the crack that begins as an outside corner crack,  $a_L = 0.050$  inch. Before  $a_R$  initiates, the stress intensity for  $a_L$  is given by Equation (66).

After  $a_R$  initiates (or for a specimen with continuing damage), the stress intensity for the left-hand crack tip is given by

$$K_I = K_I^{(3)} \gamma_{TR} \quad (80)$$

in which  $a = a_L$  is used. Here  $\gamma_{TR}$  was previously presented, while

$$K_I^{(3)} = \text{MIN} \left[ \frac{k_{tg}}{3} K_I^{(1)}, K_I^{(2)} \gamma_{NE} \right] \quad (81)$$

In Equation (81),  $k_{tg}$  is as defined in Equation (71) assuming  $a_L = 0$  (so that  $A_o = R_o + a_R/2$ ).

Equations (80) and (81) are also applicable to the right-hand crack tip, except that the roles of  $a_L$  and  $a_R$  are interchanged;  $\gamma_{AH}$  is incorporated into Equation (80), and  $\gamma_{QE}$  replaces  $\gamma_{NE}$  in Equations (71) and (81).

If  $a_L$  reaches the free edge before  $a_R$  initiates,  $k_t$  is given by Equation (73) where  $A_o$  is the total cut length (crack plus hole). This formula also applies for the edge crack arrested at the second hole. After  $a_R$  initiates at the first (left-hand) hole, the stress intensity at the tip of this edge crack is

$$K_I = 1.1215 K_I^{(2)} \gamma_{AH} \quad (82)$$

(where  $A_o$  is the cut length). After initiation at the second hole, the same formula applies but  $\gamma_{AH}$  is omitted.

If  $a_R$  is arrested at the second fastener hole before  $a_L$  reaches the free edge, then Equation (72) gives  $k_t$  at the second fastener hole. After  $a_R$  initiates (but before  $a_L$  reaches the free edge) the stress intensity at the right-hand tip is

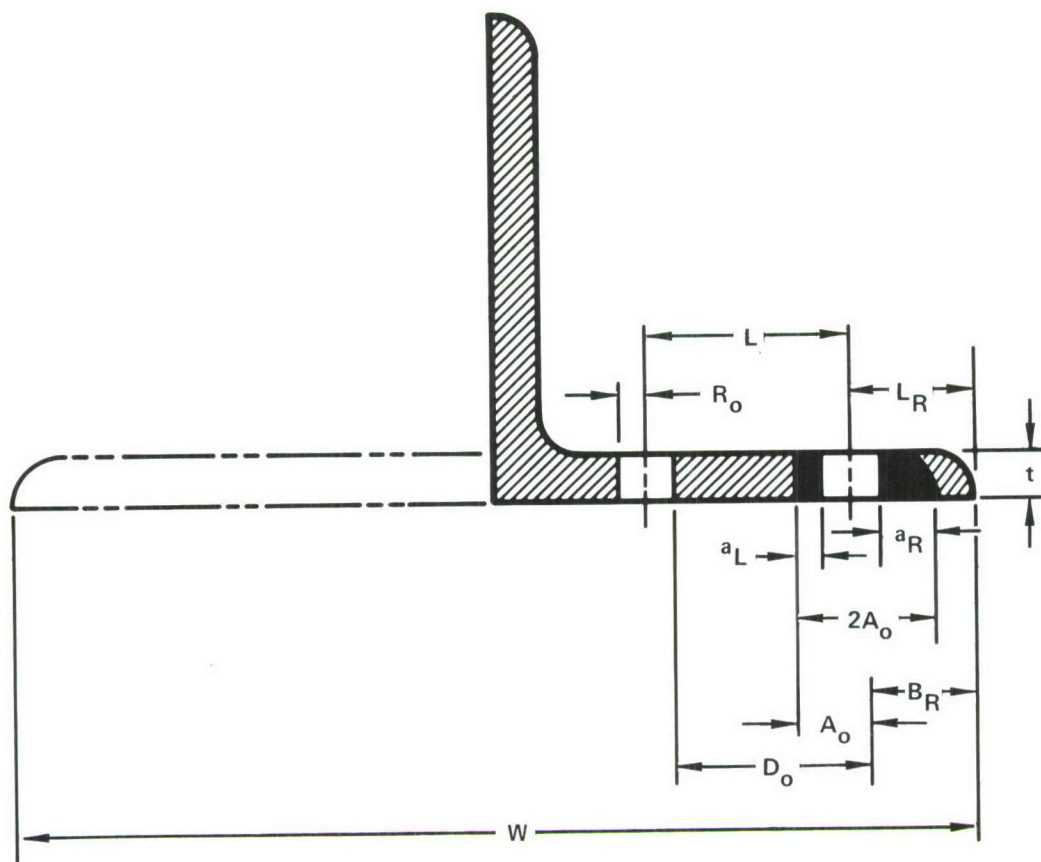
$$K_I = K_I^{(2)} \gamma_{QE} \quad (83)$$

Specimens with outside skin cracks are expected to fail by the time the skin crack is 20 to 25 percent of the way across the width. Thus no correction for the far edge is included in the above equations.

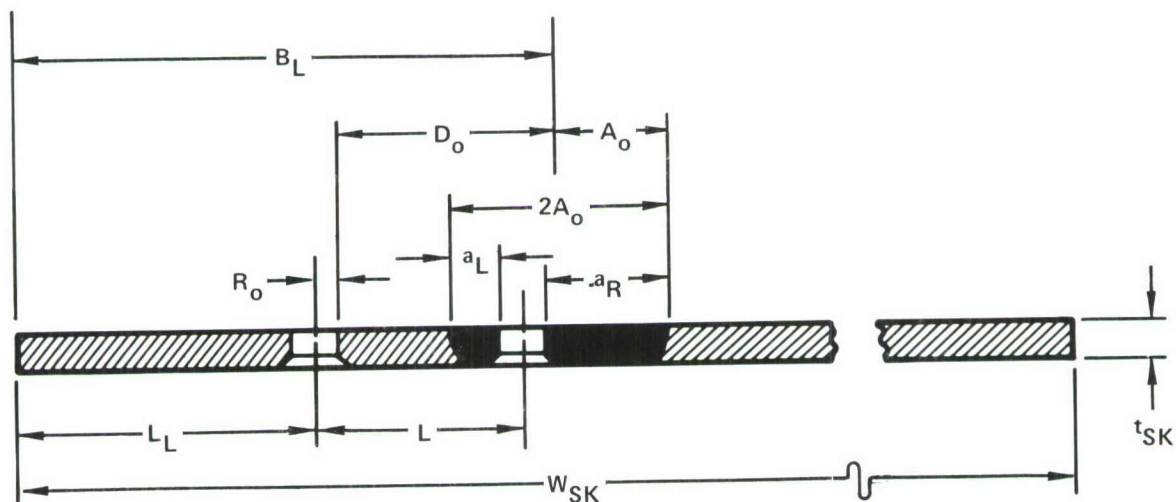
### 5.3 Initial Inside Crack in the Angle Stringer

Figure 57(A) shows the general cracked condition of the angle for the crack that begins as an inside corner crack,  $a_R = 0.050$  inch.

When  $a_L = 0$ , the stress intensity for the right-hand tip is as given in Equation (75), where  $a = a_R$ . The stress concentration at the origin point of  $a_L$  is given in Equation (72), using  $B_o = B_R$ .



(A) ANGLE STRINGER



(B) SHEET

Figure 57. Dimensions for Inside Cracks, Edge Stringer Specimens

When  $a_L$  initiates (or for a specimen with continuing damage), the stress intensity at each tip in the angle is analogous to that defined in Equations (81) and (82) for the outside crack in the skin.

It was known beforehand that right-hand crack  $a_R$  would reach the free edge before  $a_L$  reaches the second hole, because it is initially larger and grows across a smaller ligament toward a free edge, which is a more severe magnifier on  $K_I$  than a hole. Immediately thereafter,  $K_I$  for the left-hand tip is given by Equation (82). After  $a_L$  is arrested at the second fastener hole,  $k_t$  is given by Equation (73). After reinitiation of  $a_L$ , the stress intensity is given by Equation (82) wherein  $\gamma_{AH}$  is replaced by

$$\gamma_{EW} = \sqrt{\text{SEC} \left( \frac{\pi A_o}{2W} \right)} \quad (84)$$

This is the finite width correction factor approximation proposed in Reference 7 for an edge crack in a finite width member fastened to other less-damaged structure.

#### 5.4 Initial Inside Crack in the Skin

Figure 57(B) shows the general cracked condition of the skin for the crack that begins as an inside corner crack,  $a_R = 0.050$  inch.

When  $a_L = 0$  the stress intensity for the right-hand tip is obtained from Equation (76), with  $a = c = a_R$  and  $B_o = B_L$ . The stress concentration factor at the origin point of  $a_L$  is obtained by letting  $B_o = B_L$  in Equation (71).

After  $a_L$  initiates, the stress intensity for the two crack tips are obtained from Equations (80) and (81). For the left-hand crack tip,  $\gamma_{AH}$  is incorporated into Equation (80). For the right-hand crack tip,  $\gamma_{AH}$  is not included but  $a_R$  is used in place of  $a_L$  and  $\gamma_{QE}$  in place of  $\gamma_{NE}$ .

When  $a_L$  is arrested at the second hole, the stress concentration factor is obtained from Equation (71). When  $a_L$  reinitiates, its stress intensity factor is

$$K_I = K_I^{(2)} Y_{NE} \quad (85)$$

By the time  $a_L$  breaks through to the free edge, the skin crack was expected to be unstable.

## 6. CRACK GROWTH LIFE PREDICTIONS FOR SPECTRUM LOADING

In this section two simple methods to predict the crack growth life of a structural specimen subjected to the 80-flight spectrum fatigue loading (Figure 8) are presented. Both methods utilize the baseline constant-amplitude and spectrum data from Section IV and a constant-amplitude fatigue test result for the identical structural specimen configuration that is to be spectrum tested. Baseline fatigue crack initiation data are used in the equivalent  $k_t$  prediction method. Baseline crack growth data are used in the equivalent stress intensity factor method. Otherwise the two methods are very similar.

The two methods are best explained by means of an example. Tests of split-skin stringer reinforced specimens, discussed in Section VIII, are used for this purpose. At the time that a spectrum prediction was required, Specimens 4.8-3-3 and 4.8-3-4 had already been tested under constant-amplitude loading at a maximum gross area stress of 17 ksi and a range ratio of 0.1. The resulting geometric mean life for these two specimens was 24,411 cycles. Two identical specimens, 4.8-3-1 and -2, with the identical system of fasteners and initial flaws, were to be spectrum tested at a reference stress of 30 ksi. A crack growth life prediction for this test was required.

Table 15 demonstrates how the Equivalent  $k_t$  method is applied. For  $\alpha = \beta = 1$ , Equation (48) relates constant-amplitude fatigue life to  $k_t S_{\max}$  for fatigue coupons. A fatigue coupon subjected to  $S_{\max} = 17$  ksi,  $R = 0.1$  and lasting 24,411 cycles would, by Equation (48), have an estimated  $k_t$  value of 5.18. This, then, is the equivalent  $k_t$  value for these structural specimens.

TABLE 15. SPECTRUM CRACK GROWTH PREDICTIONS FOR STRUCTURE  
BY EQUIVALENT  $k_t$  PREDICTION METHOD

| Const. Amplitude<br>( $S_{\max}$ = 17 ksi, R = 0.1) |                               |                               | Spectrum ( $S_{\text{Ref}}$ = 30 ksi) |                     |                            |                                   |                            |
|---|-------------------------------|-------------------------------|---------------------------------------|---------------------|----------------------------|-----------------------------------|----------------------------|
| Specimen Numbers                                    | Geom. Mean Test Life (Cycles) | $k_t S_{\max}$ (ksi) (Eq. 48) | Equivalent $k_t$                      | Specimen Numbers    | $k_t S_{\text{Ref}}$ (ksi) | Predicted Life (Flights) (Eq. 86) | Actual Test Life (Flights) |
| 4.8-3-3 and 4.8-3-4                                 | 24,411                        | 88.1                          | 5.18                                  | 4.8-3-1 and 4.8-3-2 | 155.4                      | 8,200                             | 6600<br>8240               |

TABLE 16. SPECTRUM CRACK GROWTH PREDICTIONS FOR STRUCTURE  
BY EQUIVALENT STRESS INTENSITY FACTOR METHOD

| Const. Amplitude ( $S_{\max} = 17$ ksi, $R = 0.1$ ) |                               |  |  | Spectrum ( $S_{\text{Ref}} = 30$ ksi)          |  |  |  |                            |
|---|-------------------------------|--|--|--|--|--|--|----------------------------|
| Specimen Numbers                                    | Geom. Mean Test Life (Cycles) | $\overline{K}_{\max}$ (Fig. 43)<br>(ksi $\sqrt{\text{inch}}$ ) | $\frac{da}{dN}$<br>$= 10^6 \div \overline{N}$<br>(Microinch Per Cycle) | $K_{\max} \div 17$<br>( $\sqrt{\text{inch}}$ ) | $\overline{K}_{\text{Ref}}$<br>$= 30 \text{ K/S}$<br>(ksi $\sqrt{\text{inch}}$ ) | $\frac{da}{dF}$<br>Fig. 47<br>(Microinch Per Flight) | Predicted Life =<br>$10^6 \div da/dF$<br>(Flights) | Actual Test Life (Flights) |
| 4.8-3-3 and 4.8-3-4                                 | 24,411                        | 40.97  | 18.56  | 1.092  | 32.8   | 80   | 12,500   | 6600<br>8240               |

The equation for a log-log straight line through the geometric mean spectrum fatigue crack initiation life points for Specimens MCT-1 and -2 and MCT-3 and -4 is

$$N = \left( \frac{k_t S_{Ref}}{100 \text{ ksi}} \right)^{-4.0417} \times 48,775 \text{ flights} \quad (86)$$

For a gross area spectrum reference stress of 30 ksi and a  $k_t$  value of 5.18, a fatigue coupon would have an estimated crack initiation lifetime of 8,200 flights, according to Equation (86). By the equivalent  $k_t$  method this was the predicted crack growth life for Specimens 4.8-3-1 and 4.8-3-2.

The Equivalent Normalized Stress Intensity Factor prediction method is utilized in Table 16. The method requires an average crack growth rate to characterize the fatigue test results for structural Specimens 4.8-3-3 and 4.8-3-4. By inspection of the data from these specimens, failure occurred soon after the skin crack or tee crack reached a length of 1 inch. By using 1 inch as the final stable fatigue crack size\*, the average crack growth rate can be obtained by dividing 1 inch ( $10^6$  microinches) by the mean specimen life. The result is 40.87 microinches per cycle. The baseline constant-amplitude crack growth rate curve for 0.188-inch sheet is found in Figure 43. The  $K_{max}$  value corresponding to this rate is 18.56 ksi  $\sqrt{\text{inch}}$ . Thus the equivalent normalized stress intensity factor for this specimen configuration is  $K/S = 1.092 \sqrt{\text{inch}}$ , obtained by dividing 18.56 ksi  $\sqrt{\text{inch}}$  by the maximum gross area stress, 17 ksi.

The spectrum prediction is obtained by inverting this procedure. A value of spectrum reference stress intensity of 32.8 ksi  $\sqrt{\text{inch}}$  is obtained by multiplying  $K/S$  by the reference stress, 30 ksi. The corresponding spectrum crack growth rate, 80 microinches per flight, is estimated from the spectrum crack growth rate data points for Specimens CT5-1 and CT5-2 shown in Figure 47. Finally, dividing  $10^6$  microinches by this rate gives the estimated spectrum life for Specimens 4.8-3-1 and 4.8-3-2, 12,500 flights.

---

\* This is a selected growth increment, not the critical crack size, and is somewhat arbitrary. For example, use of 2 inches instead of 1 inch would have led to a prediction of 10,000 flights in Table 16, instead of 12,500 flights.

The predictions in Table 15 relate best to fatigue crack initiation while those in Table 16 relate best to fatigue crack growth. The failure of the precracked structural specimens results from a combination of crack initiation phenomena and crack growth phenomena. Thus the best life estimate for these structural specimens would seem to be some intermediate value, such as the geometric mean of the two life estimates.

There are, of course, more elaborate prediction methods than the two described above, in which the entire crack growth sequence is calculated as a sequence of crack growth periods and crack initiation and reinitiation periods. During crack growth a stress intensity factor expression and a spectrum crack growth rate curve are used, whereas during crack initiation or reinitiation a stress severity factor expression and a spectrum fatigue crack initiation life curve are needed.

As seen in Section IV, Paragraph 6, spectrum crack growth rate and spectrum crack initiation life curves can be obtained either analytically (by using a retardation or Miner's Rule prediction model and constant-amplitude data) or empirically (by using simple baseline specimens subjected to the identical loading sequence that the structure will see). Likewise, as seen in Figure 25, Section III, Paragraph 3.3.2, it is possible to obtain a stress intensity factor (or stress severity factor) expression empirically, as well as analytically. Such factors, obtained empirically from the constant amplitude test results for structural specimens, can be utilized to predict crack growth and reinitiation for the spectrum tests of similar specimens.

## SECTION VI

### SPECIMEN FABRICATION AND TEST PROCEDURES

#### 1. FABRICATION OF TEST SPECIMENS

The careful and proper fabrication of test specimens is always an important aspect of any experimental investigation. Due to the unusual nature of the test specimens for this program, fabrication required significantly more care, concern and attention than otherwise. Tests are commonly conducted on built-up structure and on cracked specimens, but the testing of complex built-up structure containing well-defined and well-located small initial cracks has been rare.

The typical test specimen in this program consisted of plates or sheets with adjacent elements attached by fasteners. Small (0.050-inch) part-through precracks were required at preselected fastener holes, most often in two adjacent elements at the same hole location. Additional continuing damage razor cut defects were sometimes required at adjacent holes. For the type of precise comparisons required in this program, it was important to have, for each specimen, as much information as possible about the values of fabrication variables that could affect crack growth.

Thus in addition to simply following careful fabrication procedures, information not usually collected about the fabrication was recorded. These data included actual final precrack dimensions (measured to 0.002 inch), growth rates during precracking, hole and fastener diameters (to 0.0005 inch) at cracked and adjacent holes, and any comments regarding variations in any fabrication step. Some of these data are summarized in Section IX of Volume II. Note that none of this information was used in the initial life predictions. However the data are available to help explain any anomalies that occurred in the testing.

## 1.1 Joints

The following step-by-step procedure was used for fabrication of the 26 precracked joint specimens:

- 1) Each plate and doubler were rough cut to size and milled to appropriate outer dimensions  $\pm 0.030$  inch. If a crack was to be placed within 4 inches of a parallel edge, sufficient extra material was left so that the specimen could be easily gripped for precracking in cantilever bending. Final splitting along the centerline of the skin pieces was delayed until after Step 9 in order to leave a gripping area for precracking.
- 2) Grip holes were drilled.
- 3) Specimen components were arranged together as they were to be in the completed specimen and labelled so that they could be assembled in the same orientation at all later points in the fabrication program.
- 4) A small hole was drilled at the site of the hole at which a 0.050-inch fatigue crack was required.
- 5) A starter notch was cut in each undersized hole with a razor blade.
- 6) Each component which was to contain a 0.050-inch crack was subjected to cyclic loads using cantilever bending until a fatigue crack of the appropriate length was obtained. The appropriate length was such that the length of the crack plus the radius of the undersize hole was equal to the radius of the final hole size plus 0.050 inch. The loads used in precracking were chosen to be small enough so that the crack growth rates during precracking were approximately  $10^{-5}$  inch per cycle or slower. This was less than the initial rates expected during the actual tests. This was done to eliminate initial crack retardation effects. The final crack growth rate for each precrack was measured and recorded. (See Section 8 of Volume II.) Thus, checks on retardation elimination are possible.
- 7) Based on the exact location of the crack tip, the center of the cracked hole was located in each component with respect to a machined reference surface. Note that for multiple-cracked structure each crack tip may dictate a different optimum hole center relative to the component exteriors. It was felt that the optimization of the 0.050 inch crack length in each component was more important than the few thousandths of an inch variation in hole pattern location relative to the component edges. In fact, machining tolerances on width dimensions are greater than the error introduced by this locating procedure.
- 8) The hole at the crack location was drilled, eliminating the razor-induced starter flaw and leaving only the 0.050-inch crack. Each of

the component cracked holes were drilled separately for the reasons described in Step 7.

- 9) A locator pin nominally 0.0002 inch less than the drilled cracked hole diameter and the largest pin that can be placed in the drilled hole was used to align the specimen components. The specimen was then clamped and all other fastener holes were drilled. This was followed by countersinking where required.
- 10) The cracked hole and the two adjacent holes in the same row were measured to the nearest 0.0005 inch, and these data were recorded.
- 11) The actual crack lengths in each component are measured and recorded. Crack sizes were held to 0.050 inch  $\pm$  0.008 inch.
- 12) All holes were deburred. (Deburring at the faying surface was a minor deviation from standard assembly practice. Standard practice is to clamp, drill, deburr the exposed side of the holes, and assemble. The faying surfaces are seldom separated after drilling so deburring is impossible. However for these specimens the faying surfaces had to be separated to measure the cracks and induce the continuing damage flaws. It was decided that having been separated, the faying surfaces should be deburred, lest the burrs induce inadvertant scratches and flaws during subsequent handling).
- 13) Where continuing damage was required, 0.020-inch razor cuts were placed at hole corners. The procedure developed and verified in Reference 55 and described in Appendix C was used for making these continuing damage flaw cuts.
- 14) The diameters of the fasteners to be used at the cracked and adjacent holes were measured (to 0.0002 inch) and these data were recorded.
- 15) The fastener was installed in the precracked hole, and all other fasteners were then installed. In the case of interference-fit fasteners, alcohol was used as a lubricant when driving the fasteners into the holes. During installation of these fasteners the torque was limited by the shearing off of a portion of the nut. For clearance-fit fasteners, each fastener was torqued to a common predetermined load corresponding to a "finger-tight" situation. For example, in the case of the large double lap shear specimens it was determined by experiment that the maximum thread friction ran from 15 to 35 inch-pounds for each fastener; based upon this, a uniform torque of 40 to 45 inch-pounds was chosen for this specimen.
- 16) All required strain gages and mounting clips for clip gages were installed.

Prior to actually fabricating the precracked joint specimens, checks on the precracking procedures were made in order to make sure that the flaw shapes would be as intended. Figure 58 shows the result of attempting to induce a 0.05-inch quarter-circular flaw at the corner of a 0.375-inch diameter hole in a 0.188-inch sheet, and at a 0.250-inch diameter hole in a 0.094-inch sheet. As can be seen the shapes are fairly close to quarter-circular.

Different precracking procedures were used for the extrusions, as discussed in the following subsection. These procedures resulted in non-quarter-circular cracks, the depth being substantially greater than the surface length. A typical case shows up in Figure 108, Section VIII. The initial flaw in the tee appears on the fracture surface as a gray quarter-ellipse approximately 0.09-inch deep. Its premeasured length on the faying surface was 0.046 inch.

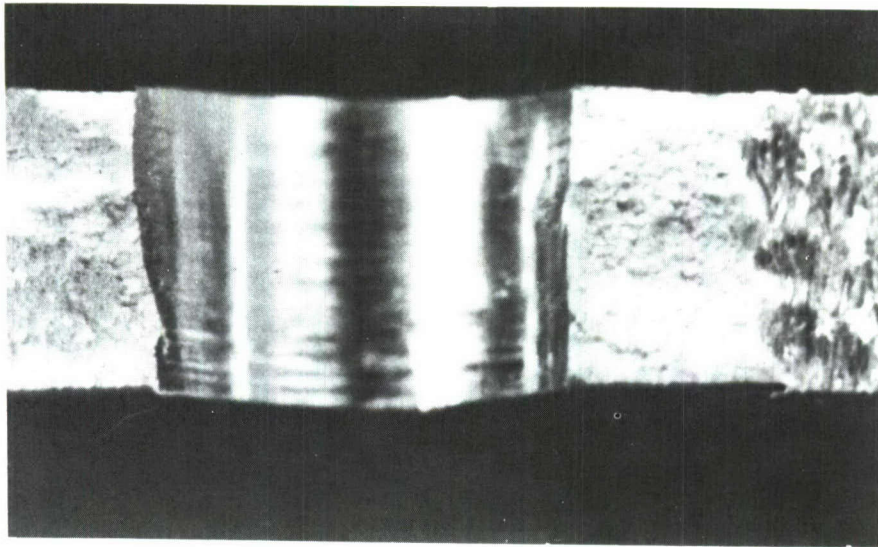
## 1.2 Stringer-Reinforced Panels

The primary difference between the joint specimen fabrication and the skin-stringer specimen fabrication was the requirement to place 0.05-inch cracks in the stringer as well as sheet or plate elements. Additional differences included bonding doublers to the specimens in the grip area and changes in machining sequencing to assure alignment.

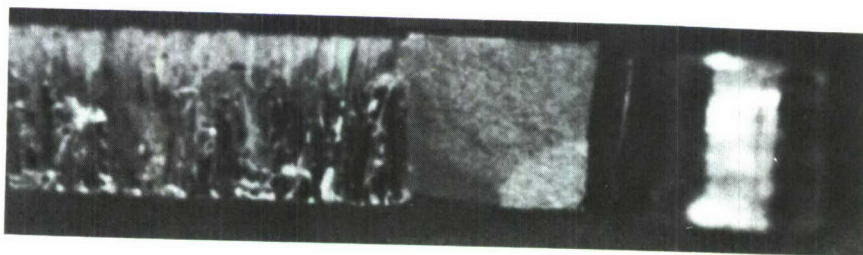
Figure 59 shows the two stringer cross sections used, an angle and a tee extrusion. Although all elements fabricated from sheet and plate materials were precracked in cantilever bending, it was impossible to precrack these stringers in bending. The required location of all stringer precracks was at a hole in the outer face of the base ((a) in Figure 59). Since the location of the neutral axis in both cross sections is in the vicinity of the upper face of the base (b), any attempt to place bending stresses on the order of 20 ksi at the crack site would have resulted in compressive yielding at the top of the vertical leg (c).

The tees for the tee-stiffened specimens were cracked in uniaxial tension. The steps for precracking the tee elements were as follows:

- 1) The tees were reduced in the test section as shown in Figure 59 and holes for gripping during the precracking were drilled. A small hole was drilled at the precrack site and a razor cut placed in the base (a) at the edge of the hole.



(a) 0.188-Inch Sheet, 0.375-Inch Diameter Hole



(b) 0.094-Inch Sheet, 0.250-Inch Diameter Hole

Figure 58. Fatigue-Induced 0.05-Inch Near-Quarter-Circular Corner Flaws at Drilled Holes in 7075-T6 Aluminum Sheet

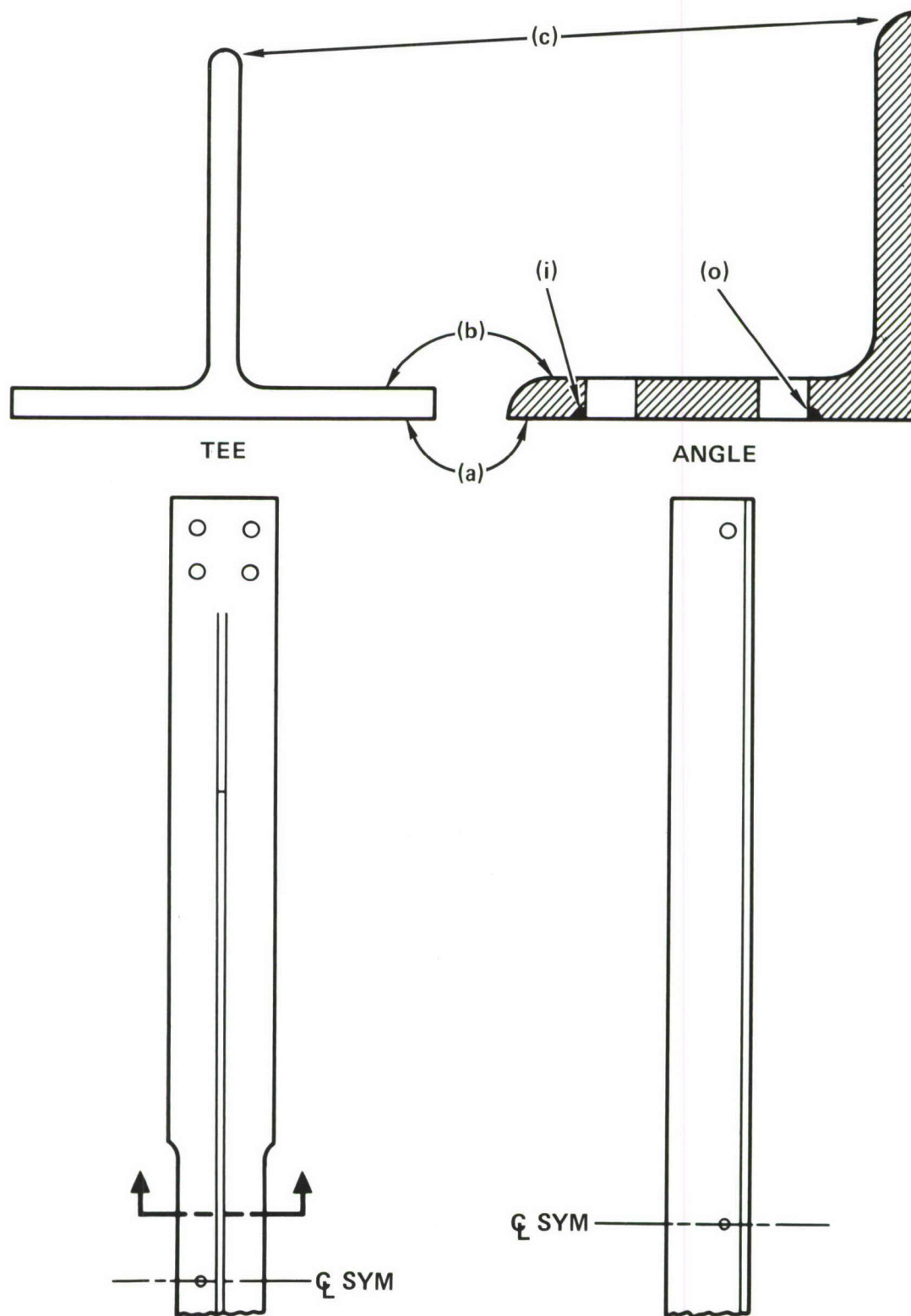


Figure 59. Stringer Configurations for Precracking

- 2) Emory paper was glued to the grips to maximize the load transferred in friction and to minimize the probability of cracking at the grip holes. Care was taken to uniformly tighten the bolts in the grip area and to maintain alignment of the tee in the tensile machine.
- 3) The tee was constrained laterally at the mid-section to maintain a high tensile loading at the precrack location.
- 4) Cyclic tension stressing of approximately  $S_{\max} = 20$  ksi,  $R = 0.1$  was applied. This resulted in a crack growth rate of about 10 microinches per cycle, which tended not to exceed the initial  $da/dN$  in this test, demonstrating that no crack retardation was introduced. The crack length and the crack growth rate were monitored optically during precracking.
- 5) When the appropriate crack length was reached, precracking was stopped. The appropriate length is the length such that the radius of the small initial hole plus the crack length equals the radius of the final hole plus 0.05 inches.

Although care was taken to minimize fatigue problems in the grip area, a large number (approximately 50 percent) of attempts to produce a precracked tee resulted in failure of the tee in the grip section. This difficulty was a result of the relatively close net areas of the test section and grip areas. All apparent avenues for improving upon this situation seemed closed: Further reduction of the tee base would have made it too narrow to accommodate two rows of fasteners; reduction of the vertical section of the tee in the test section would have produced an increased tendency for compression at the potential precrack site; and the use of larger tees reduced to the appropriate size after precracking was prohibitively expensive. With persistence (and some relaxing of the tolerance requirements on the 0.050-inch crack dimension) the required 24 tee stringers were finally precracked.

Precracking of the angles presented additional problems. The width of the base could not be reduced in the test section since there would then not have been room for the double row of fasteners required in the built-up test specimen; reduction in size of the vertical leg in the test section would have introduced a bending component which would work against the precracking; thinning of the base leg in the test area (on the side away from the precrack location) would have also tended to produce adverse bending affects. Since

none of these options were available and since even with a reduced section only a 50 percent acceptance rate was attainable with the tees, the concept of remote tensile loading for precracking the angles was abandoned.

The precracking problem is one of getting loads into the precrack area without producing cracks in other areas. Therefore, it was decided to attempt to put loads directly into the precrack area using pin loading in a hole at the precrack site.

Both single shear and double shear loading was attempted. Although single shear loading tended to produce hole distortion, it proved to be a more consistent method of producing cracks at the desired location. Since the hole was redrilled to a larger size during final assembly, the minor hole damage that occurred was acceptable. During precracking the hole was loaded through a 0.250-inch diameter steel pin which was loaded by a long steel plate (see Figure 60). The steel plate was attached to the test machine by pin loading as was one end of the angle. The grip end of the angle was loaded through a 0.375-inch diameter pin in double shear. Thus the bearing stress in the grip section was considerably lower than that in the precrack section.

The point of peak stress tangential to a pin-loaded hole lies at approximately  $10^\circ$  from a perpendicular to the load line. Therefore, the angle was rotated  $180^\circ$  every few thousand cycles and loaded in the opposite direction to minimize the deviation of the crack line from the desired  $0^\circ$  orientation.

As shown schematically in Figure 59, there were two alternative initial crack locations required in the angles. A razor notch was used as a starter notch for precracking in both cases. The inside precrack (i) readily initiated and grew. In attempting to induce the outside crack (o), however, cracks would often start at other locations. Sometimes they would grow from the opposite side of the hole, and sometimes they would start above or below the starter notch. The net result was that the acceptance rate on these elements was low. It took twelve angles to generate the first four usable stiffeners of configuration (o).

Note that this might imply that crack configuration (o) is a noncritical damage location. Experience during precracking indicated that a fatigue crack is unlikely to initiate at this location, and that when initial damage is introduced by other means, it does not readily grow at this location. However, the

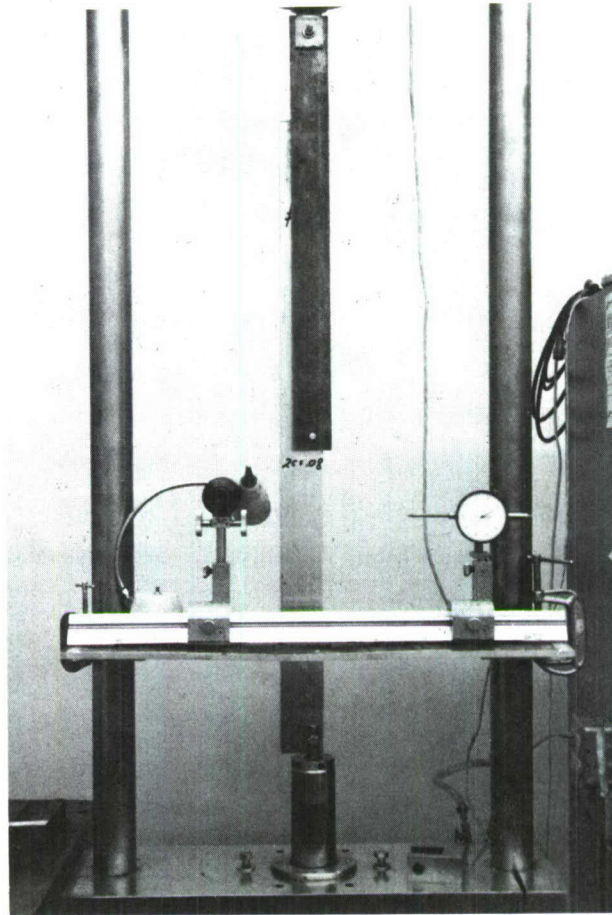


Figure 60. Precracking of the Angle by Pin Loading

precracking experience was based entirely on single shear loading in the manner shown in Figure 60. In typical structure, the angle stringer would be subjected to a combination of remote loading and single lap shear. An examination of the structural test results discussed in Section VIII shows that, although cracks at location (o) in Figure 59 tend to grow somewhat more rapidly, cracks at location (i) also grow and participate in specimen failures.

The overall fabrication sequence for the skin-stringer specimens was essentially the same as that for the joint specimens except that to ensure proper alignment, the grip holes were drilled after assembly. Additionally, just prior to the drilling of the grip holes, doublers were bonded at the grip area of the specimens, using a two-part, room-temperature cure epoxy adhesive.

The last four specimens fabricated for this program were two-bay panels with angles as edge stiffeners and a central tee stiffener. All crack locations were called out to be at the outer fastener hole relative to the stiffener and toward the outer edge of the stiffener. Since precracking the angles for this crack location using the pin-loading technique had proved to be a relatively easy procedure, the same technique was used for the tees. It is worth noting that in addition to not being consistently successful, the prior procedure used for precracking the tees was time-consuming. The setup and dismantling time of the grips was extensive. Once again the pin-loading technique proved to be effective and the acceptance rate on precracks was 100 percent. Since the setup is also rapid, this technique is recommended for use in future studies requiring precracking of stringer extrusions. However, based upon the precracking and testing experience described above, a combination of tension and single-shear pin loading should be attempted for cases where the crack has to grow toward the vertical stiffener segment ((o) in Figure 59).

## 2. TEST PROCEDURES

This section summarizes the procedures used for crack growth monitoring and measurement and the constraints used to limit lateral deflections of the specimens to within the range typical of aircraft structure. The environment for all tests was controlled (Lockheed Rye Canyon) laboratory air ( $72^{\circ} \pm 3^{\circ}\text{F}$ ;  $40\% \pm 10\% \text{ RH}$ ).

## 2.1 Crack Length Monitoring

Due to their complexity, the structural specimens often contained several cracks which grew simultaneously. To allow for the measurement of crack lengths the cycling was stopped intermittently. Past experience with 7075-T6 aluminum indicates that these pauses have no effect on  $da/dN$ .

Cracks were measured visually on external surfaces. In planar areas a traveling microscope and dial gage were used for crack growth measurements with approximately  $\pm 0.002$ -inch accuracy. For more complex contours like the crack growing from the base of an angle stringer, around a fillet radius, and up the protruding leg of the stringer, a flexible plastic ruler graduated in 0.02-inch intervals was bent to follow the contour of the surface. The crack length was read directly, probably within  $\pm 0.002$ -inch accuracy.

In the stringer-reinforced specimens, there was no load transfer in the plane of the initial crack because of symmetry. Clearance-fit Hi-lok fasteners in this plane were removed for crack length measurement. This facilitated the detection of small cracks that would otherwise be hidden by the collar or fastener head and allowed for direct use of the edge of the hole as the zero-crack-length point. After crack measurement the fastener was replaced for subsequent fatigue cycling but the collar was not.

Of course, interference-fit fasteners, rivets, and fasteners with load transfer were never removed during testing. For these, cracks were detected only after they grew beyond the edge of the collar or fastener head. However even for these the crack lengths tabulated in Volume II of this report are as measured from the hole edge. They were computed from the raw data by adding the nominal overhang length of the collar or fastener head to the observed crack length.

For the tee-reinforced specimens marking cycles were useful in providing occasional crack length and crack front shape markings on the fracture surface. Marking cycles were not effective in the joint specimens and were not used in the angle-reinforced specimens. Furthermore the marks seldom showed up for the small cracks at the edge of the fastener holes before they became visible at the surface.

## 2.2 Control and Measurement of Transverse Deflections

The stresses in a structure often depend upon the degree of constraint imposed by adjacent structure against induced lateral bending deflections. Thus it was important that the degree of lateral support in these structural test specimens was typical of aircraft structure and that the resulting stress gradients and lateral deflections were measured.

The double lap joint specimens were symmetric about the plane of the specimen itself. Therefore there was no tendency for lateral deflection to occur, except to a limited extent when the crack in one doubler was longer than the crack in the other. Therefore no lateral supports were used for the double lap joint specimens.

The eccentricity in the single lap joints induces bending stresses even when a lateral constraint is employed. Figure 61 is a photograph of this specimen in the test machine. The lateral constraint was achieved by attaching the transverse tee member of the specimen to a steel channel beam through a pair of flexures. The channel beam was mounted across the vertical columns of the MTS test machine. Because of its span and orientation the beam could bend somewhat. As a result, lateral deflections of 0.0175 inch were measured at the center of the undamaged test specimen for a 17 ksi applied gross area tensile stress. By subsequent beam calculations on the channel it was estimated that approximately 230 pounds of tensile load were exerted by the two flexures.

As shown in Figure 62, no constraints against bending were used for the center tee-reinforced specimens. The protruding leg of the tee was not directly loaded in the grip area. Instead, it was tapered at its end. A system of bonded-on doublers was used at each end of the specimen in an attempt to keep the area centroid of the specimen in the same plane throughout its length. Nevertheless, out-of-plane bending did occur in the tee-reinforced specimens.

The C-clamps shown in Figure 62 are to help prevent the bonded doublers from disbonding. Each clamp clasps through a 0.25-inch flat plate onto the innermost doubler of the specimen to reduce the normal stresses in the bond. These normal stresses were high because the doublers extended far beyond the grip area. It was found that the room-temperature-cure adhesive, even when bonded with great care to a clean, rough, sandblasted metal surface,

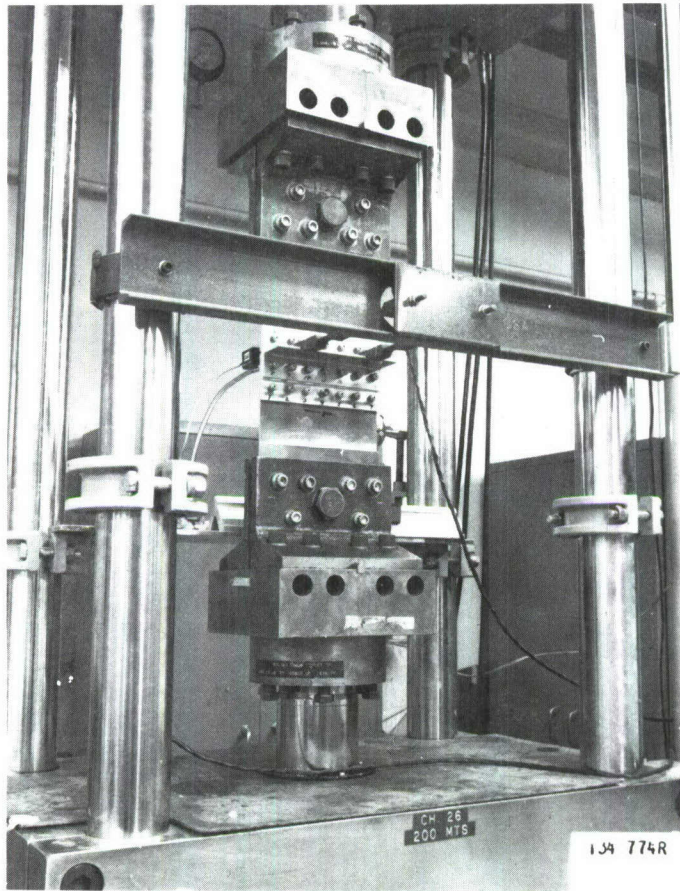


Figure 61. Single Lap Joint Specimen, Showing Lateral Constraint

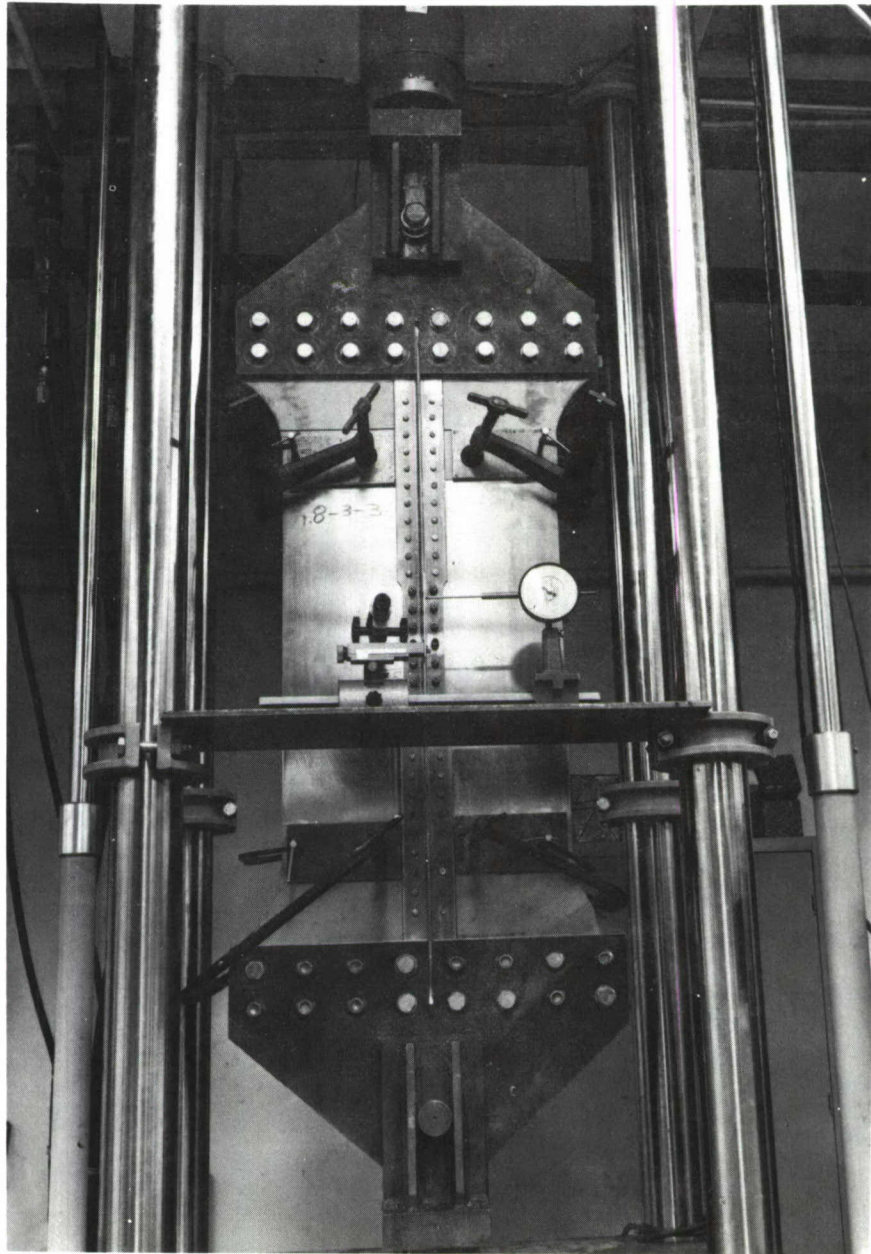
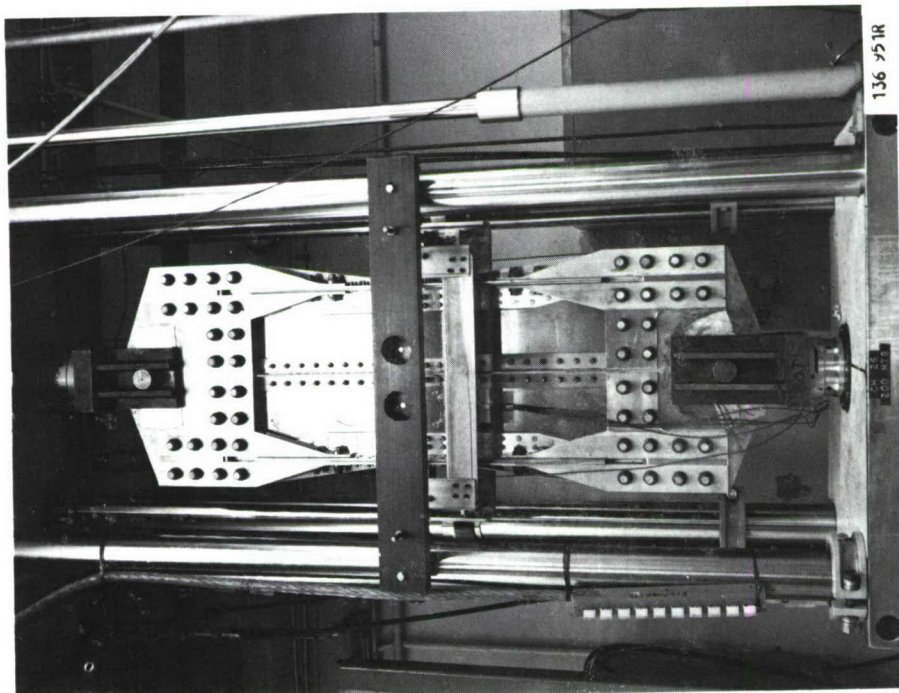


Figure 62. Center-Stringer Specimen in Fatigue Test Machine

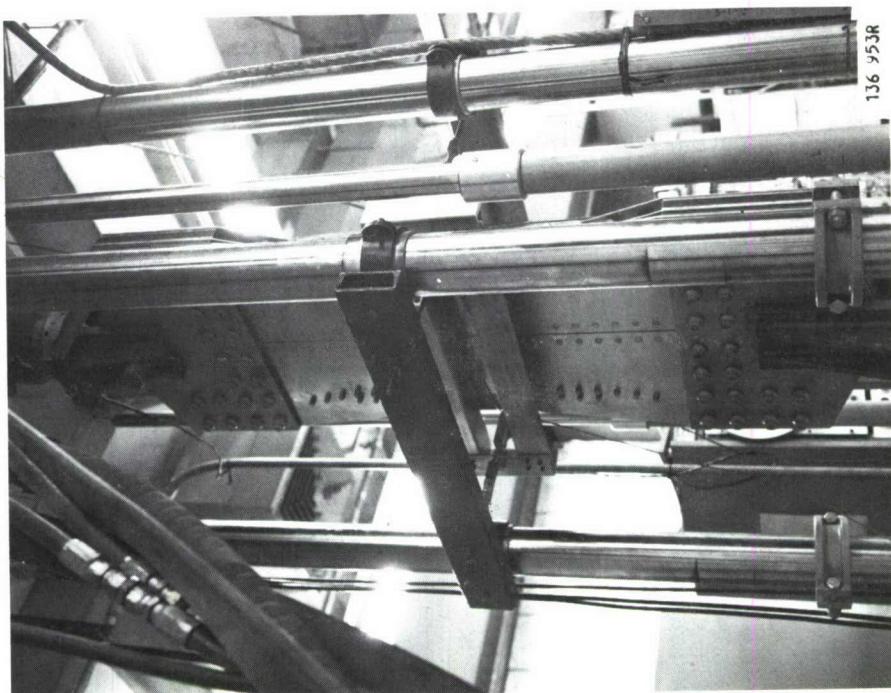
was not well suited for use with these bonded doublers. Fortunately, the partial disbonding of the longer doublers had very little effect on transverse deflections and no noticeable effect on crack growth behavior.

Figure 63 shows three views of the two-bay specimen in the 200-kip MTS machine. The same fixturing was used for the edge-stringer specimens. The specimen was loaded by means of steel plates that clamped to the skin, and pairs of aluminum channels that clamped through the simulated shear web and outstanding leg of the angle. By directly picking up the stringers in this manner, the out-of-plane bending was somewhat alleviated. Two large beams spanning the columns of the MTS machine were connected through flexures to a double rectangular frame which clamped directly onto the specimen. This was provided to limit the lateral deformations that could otherwise occur from eccentricities induced by extensive cracking and from imperfect stringer pickup in the grips.

As a result, according to the strain gage readings discussed in Section VIII, little transverse bending occurred in the two-bay specimens. Some bending occurred in the edge stringer specimens; however, the distribution of stress through the thickness was typical of the stress distribution in aircraft wing structure.

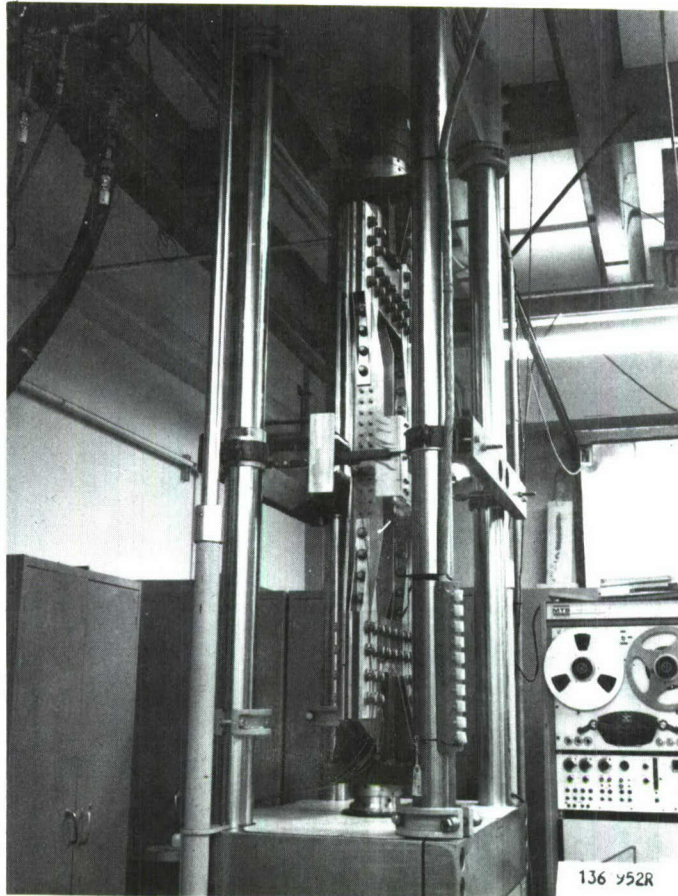


[a] Front View



[b] Back View

Figure 63. Test Setup, Two-Bay Specimens (Same as for Edge-Stringer Specimen)  
(Page 1 of 2)



[c] Side View

Figure 63. Test Setup, Two-Bay Specimens (Same as for Edge-Stringer Specimen) (Page 2 of 2)

## SECTION VII

### TEST RESULTS FOR PRECRACKED JOINTS

Fourteen precracked double lap joints and twelve precracked single lap joints were fatigue crack growth tested to failure. The specimen configurations are summarized in Figures 2, 3, and 4. The initial damage conditions for the 18 Phase I tests are shown in Figures 5 and 6. The conditions for the Phase II tests are summarized in Tables 3 and 4.

The test data and the crack growth predictions are tabulated and plotted in Volume II. These results are reviewed and discussed in detail in this section.

#### 1. TEST OBSERVATIONS FROM PHASE I

Twelve precracked double lap joint specimens and six precracked single lap joint specimens were fatigue crack growth tested to failure in Phase I. Figure 64 shows the crack growth lives of these specimens. The following observations can be made:

- The fatigue life of precracked joints is significantly longer when interference-fit fasteners with full bolt torque are used (at all but the precrack location) rather than clearance-fit finger-tight fasteners. The beneficial effects of interference and clamp-up are more pronounced in the double lap joint specimens with protruding head fasteners than in the single lap joint specimens with flush head fasteners.
- For the joints tested here there was little or no sensitivity to variations in initial flaw condition (single flaw versus multiple flaw, continuing damage versus no continuing damage).

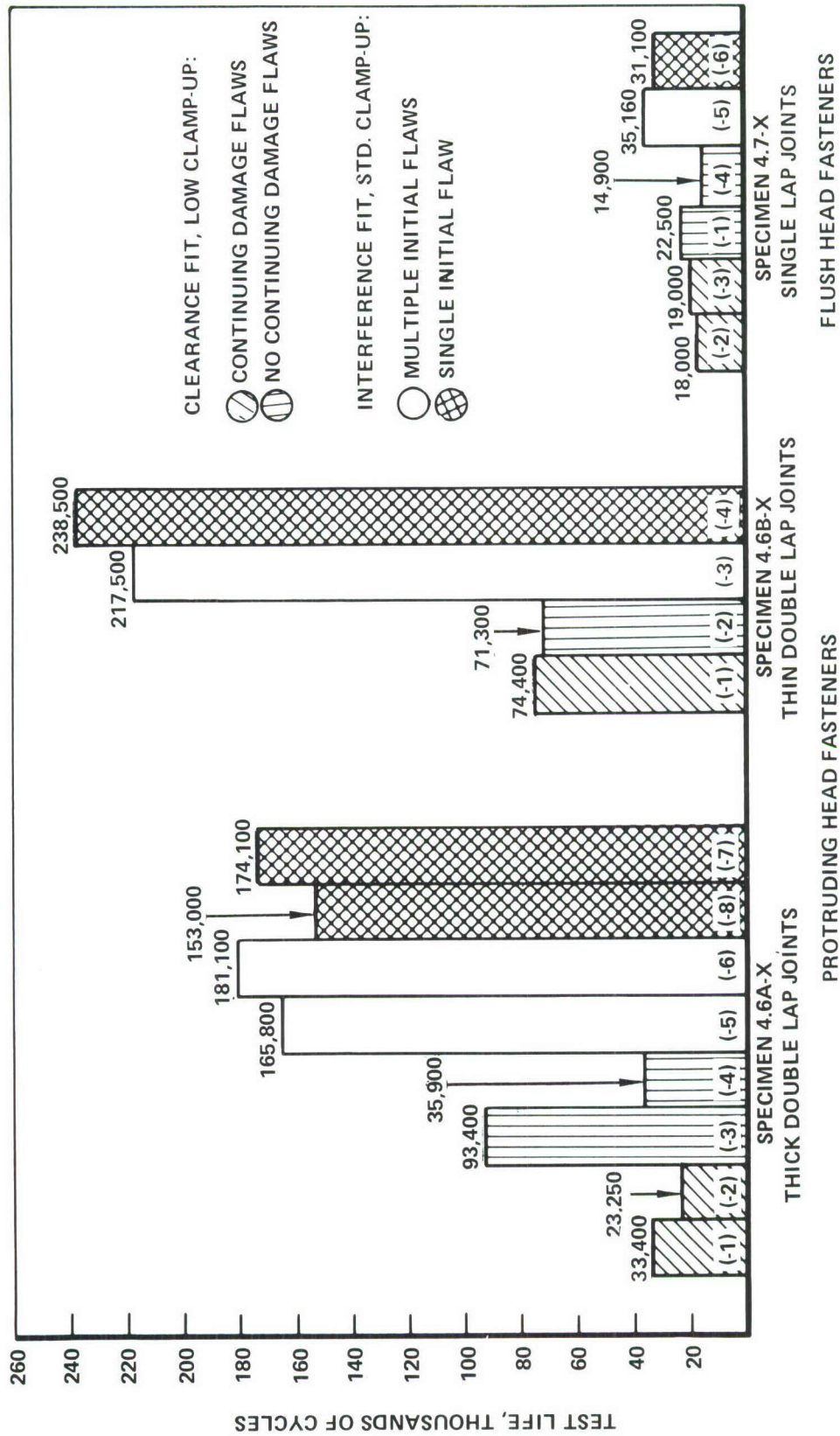


Figure 64. Total Test Lives for Precracked Single Lap and Double Lap Joint Specimens

- Test lives tended to be more reproducible than had been expected. Of the 18 specimens tested, Specimen 4.6A-3 appears to be the only aberration, with a life of 93,400 cycles compared to 35,900 cycles for replicate specimen 4.6A-4.

### 1.1 Double Lap Joint Tests

Figures 65 through 68 compare actual and predicted crack growth histories for the initial 0.050 inch fatigue-induced corner cracks in the thick double lap joint. These cracks grow from Fastener 3 in Row 2 of the doublers to Fastener 4. Side A is the fastener head side and Side B is the collar side. Thus  $a_{34}$  designates a crack in the head-side doubler growing from Fastener 3 to Fastener 4, and  $b_{34}$  is a similar crack in the collar side doubler.

For the test points the crack length is measured from the edge of the hole on the external surface of the doubler. For the prediction the crack size is as would be measured on the faying surface of the doubler. For cracks longer than about 0.25 inch, both should be the same. Thus, the predicted and actual crack growth rates are the same for long through-thickness cracks if the curves have the same slope for crack lengths in excess of 0.25 inch. The predicted and actual growth rates for corner flaws agree if there is agreement in the number of cycles to attain a crack length of 0.25 inch. Specimen 4.6A-12 shown in Figure 66 is a replication of 4.6A-3 and -4 tested under other funding and reported in Reference 71.

Similar comparisons are made in Figure 69 for the thin double lap joint specimens. The doublers are only 0.094 inch thick for these specimens, so cracks longer than about 0.125 inch are probably uniform through-the-thickness cracks. Thus, matched slopes for cracks greater than 0.125 inch indicate that the predicted and actual rates of through-thickness cracks are the same. Agreement in the time to attain a 0.125 inch crack indicates an agreement in the growth rates of corner flaws.

The following are observed from Figures 65 through 69:

- The experimental growth rates of corner flaws are slower than predicted.
- For unclamped joints with clearance fit fasteners the growth rate of long through-thickness cracks is accurately predicted except in

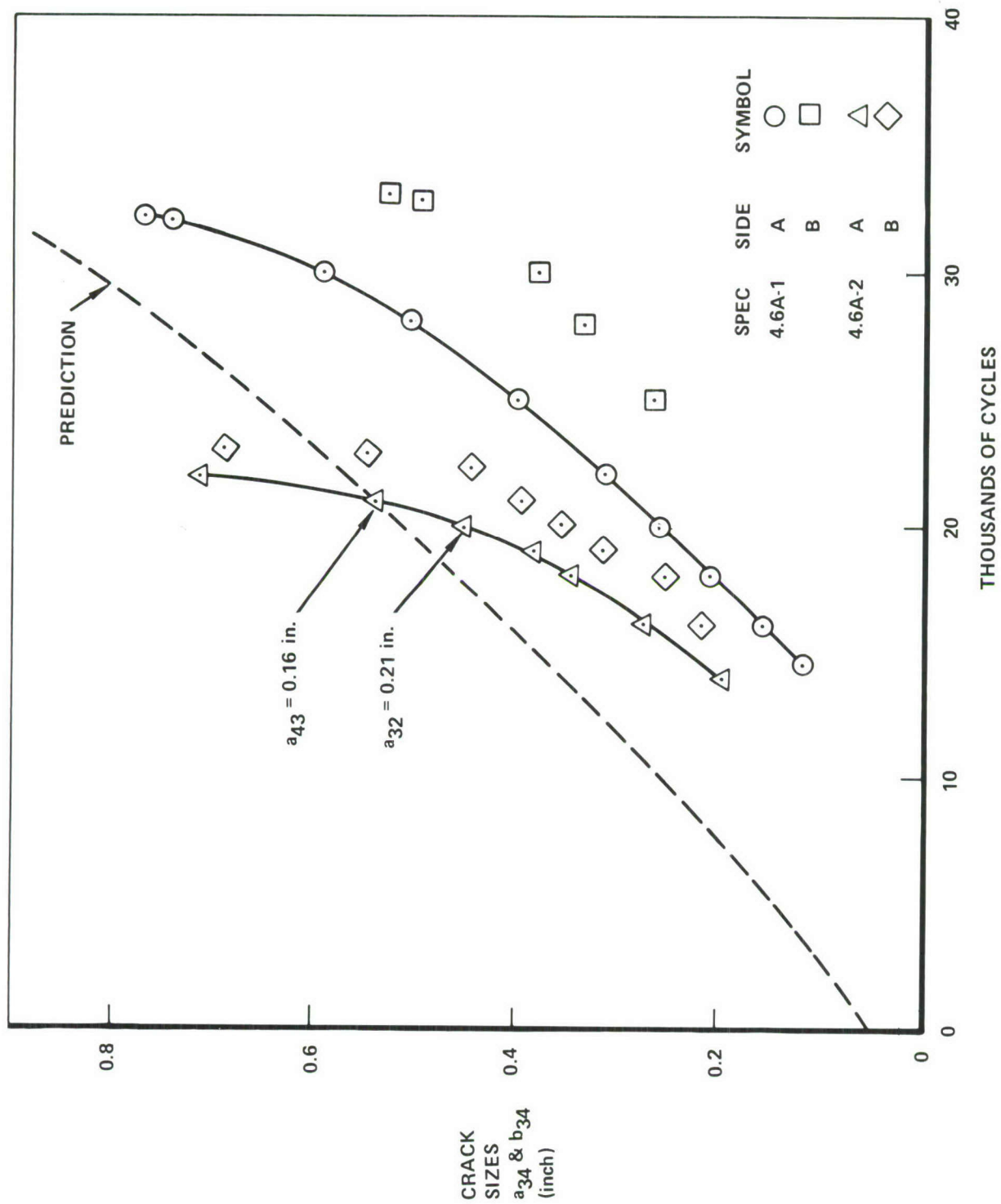


Figure 65. Crack Growth Across the First Ligament, Thick Double Lap Joint Specimens 4.6A-1 and 4.6A-2

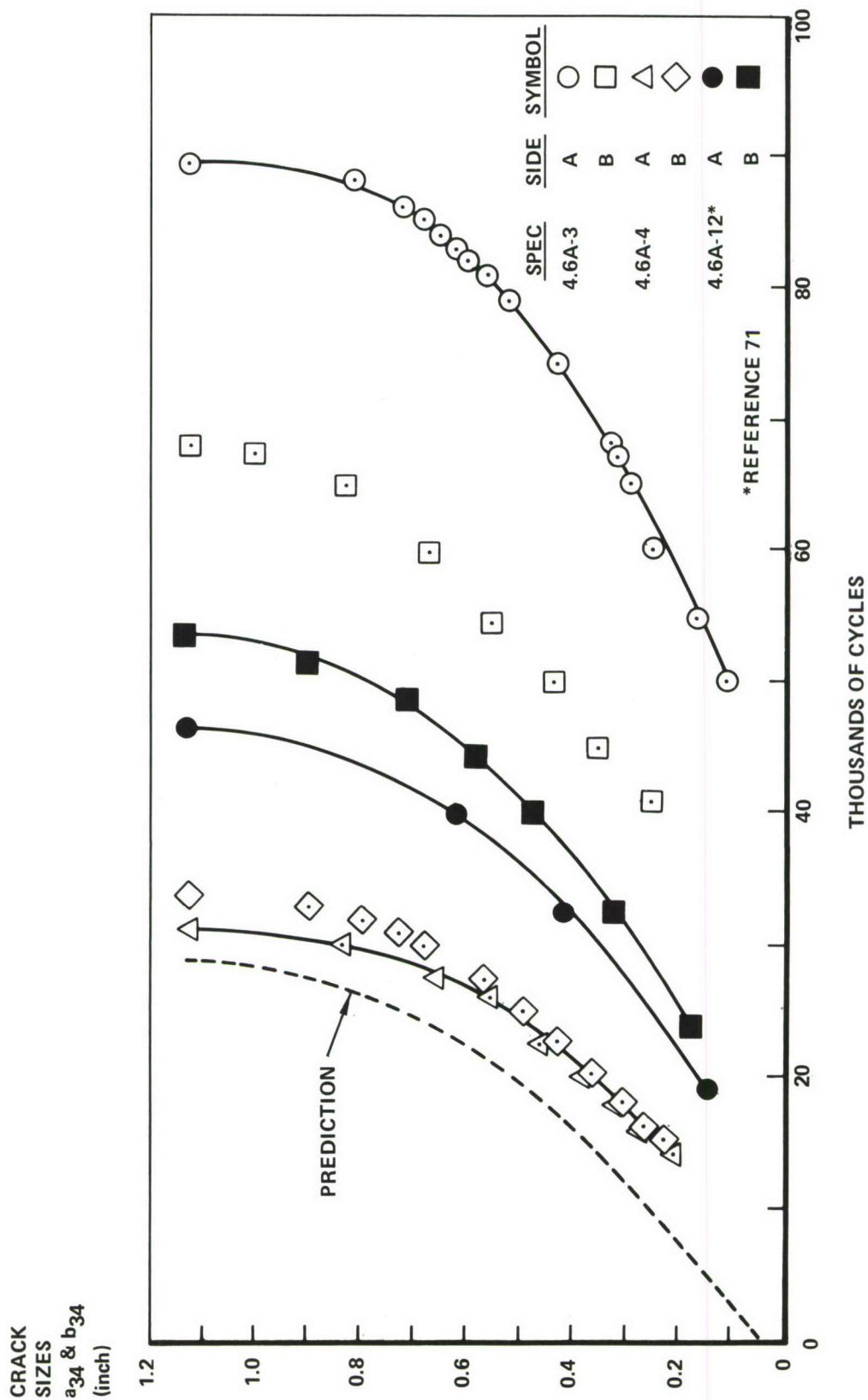


Figure 66. Crack Growth Across the First Ligament, Thick Double Lap Joint Specimens 4.6A-3, 4.6A-4, and 4.6A-12

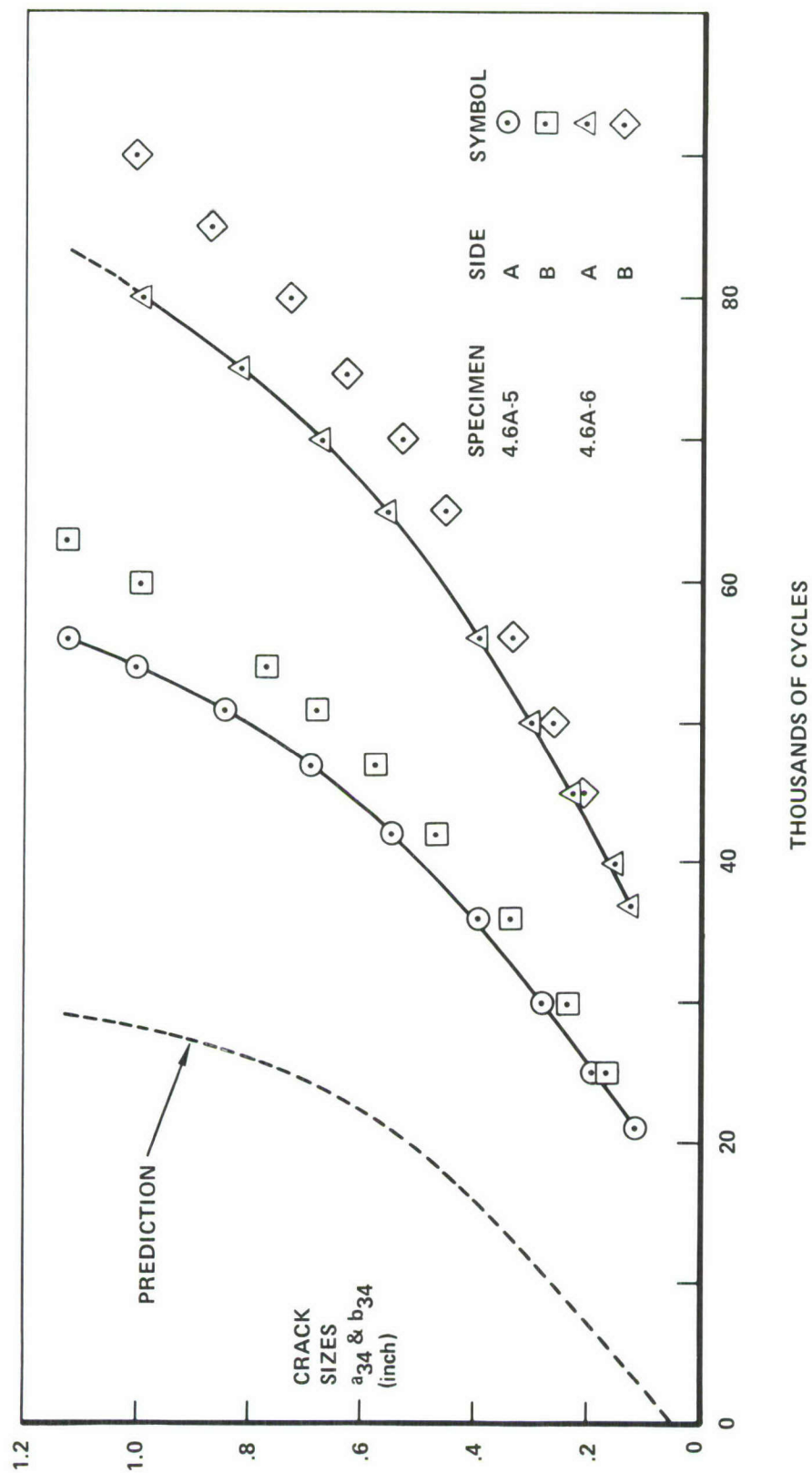


Figure 67. Crack Growth Across the First Ligament, Thick Double Lap Joint Specimens 4.6A-5 and 4.6A-6

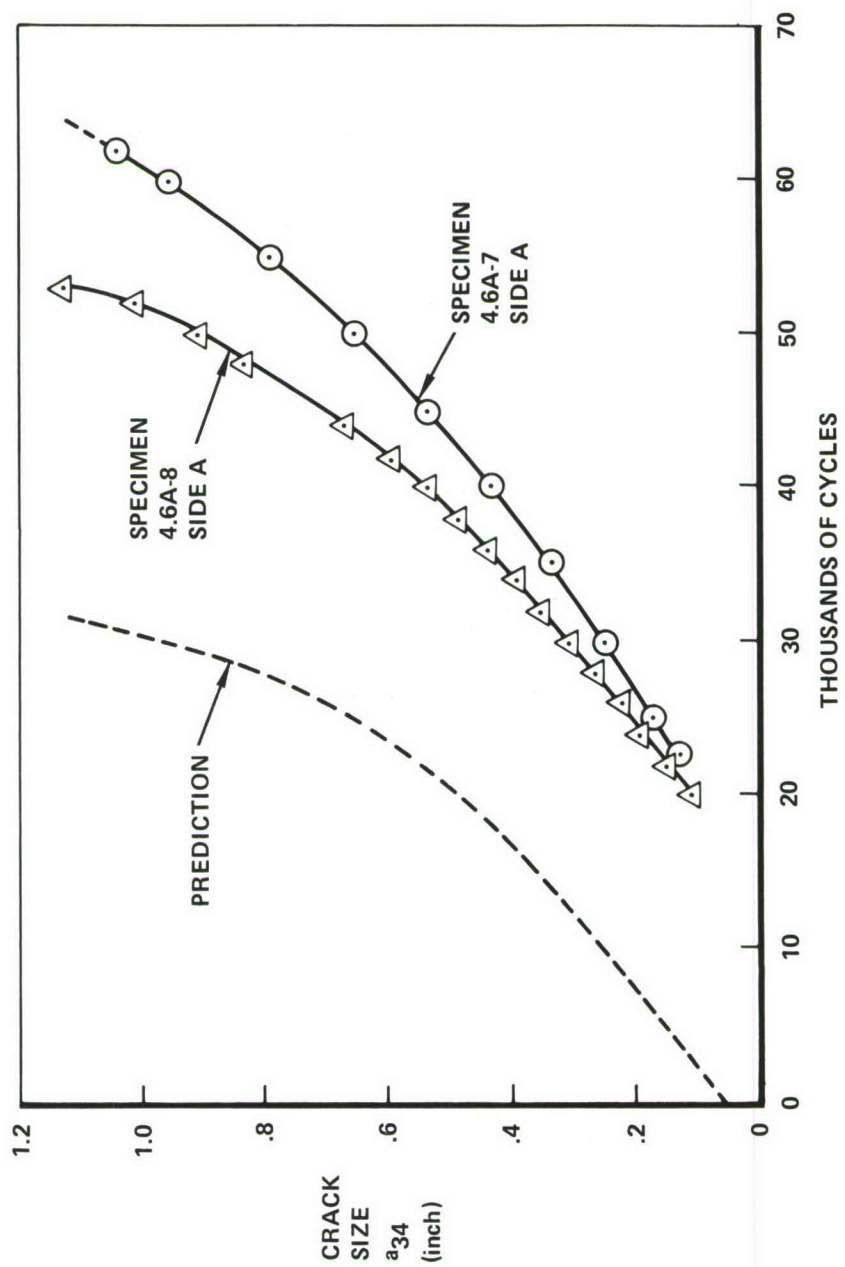


Figure 68. Crack Growth Across First Ligament, Thick Double Lap Joint Specimens 4.6A-7 and 4.6A-8

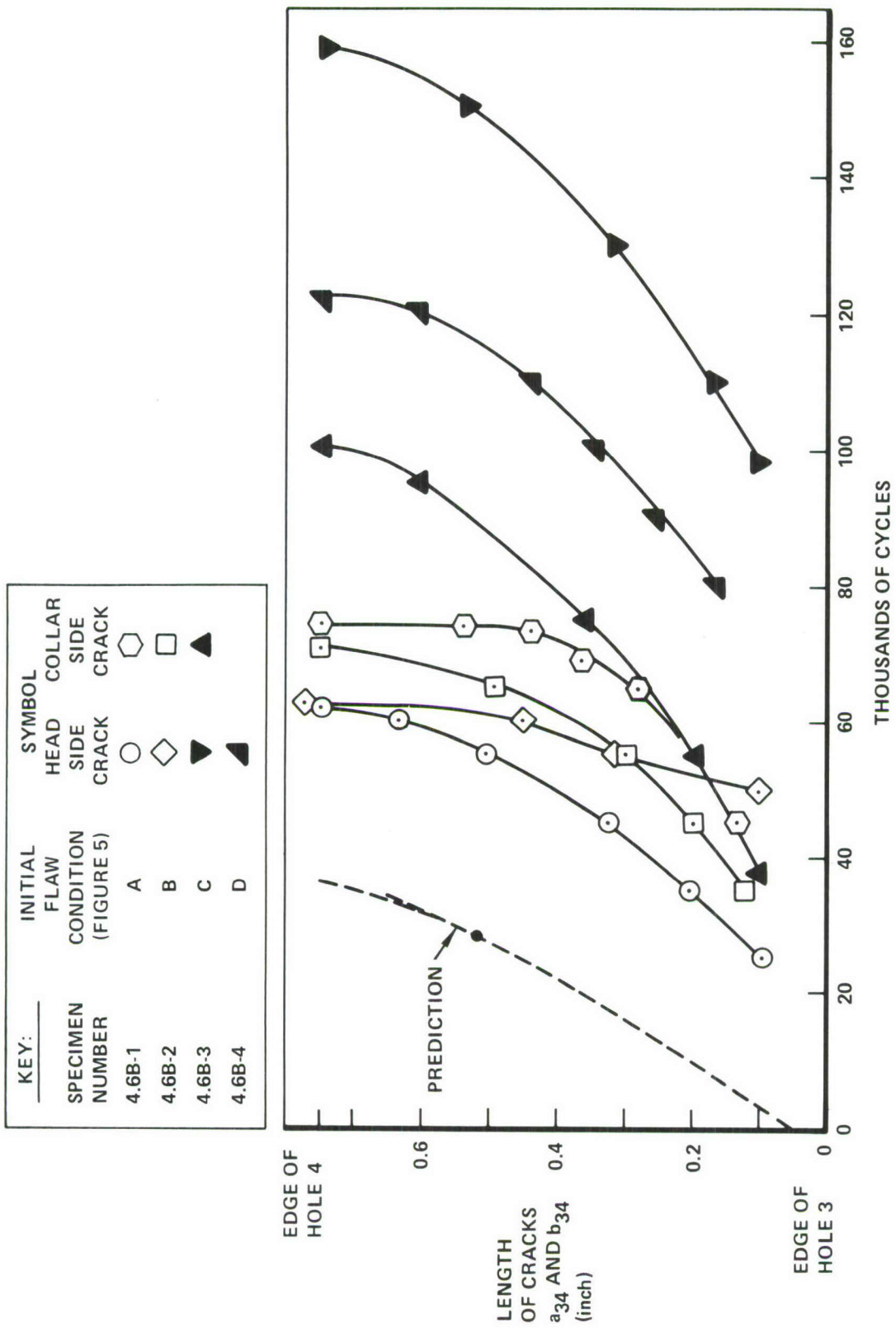


Figure 69. Crack Growth Across First Ligament, Thin Double Lap Joint Specimens

Specimen 4.6A-3, where the entire crack growth history (corner crack and through-thickness crack) is much slower than in replicate Specimen 4.6A-4. The cracks grew slightly faster than predicted in Specimen 4.6A-2 but the acceleration was caused by the presence of secondary cracks  $a_{32}$  and  $a_{43}$ .

- Growth rates of corner flaws and through-thickness cracks are slower in fully-clamped joints with interference-fit fasteners than in unclamped joints with clearance-fit fasteners, and slower than the predicted rates by factors of about 2 to 4.

Displacement gages were placed across the gap of the joint on either edge of the eight thick double lap joint specimens. The time histories of displacement range are shown in Figure 70. The most striking observation is their correlation with fastener interference and torque. The steady-state displacement range for Specimens 4.6A-5 through -8 (with interference-fit, fully-torqued fasteners) was about 0.0031 inch. Displacements for Specimens 4.6A-1 through -4 (with clearance-fit, low-torque fasteners) were significantly higher. Data from Specimens 4.6A-1, -2, -3, and -8 indicate that the initial displacement range was higher than the steady-state value.

Note that the steady-state value of displacement range for Specimen 4.6A-3 was about 0.0047 inch, while those of 4.6A-1, -2, and -4 were about 0.0063 to 0.0075 inch. This lower displacement value is consistent with the unexpectedly long life for this specimen, since the lower the displacement range, the lower the strain range in the doublers, and consequently the longer the crack growth life in the doublers.

Strain gages were installed on Specimen 4.6A-8 to detect initial strain nonuniformities and to observe changes in local strains as cracking developed. Figure 71 summarizes these strain gage results.

The numbers in parentheses are normalized values of the strain range  $\Delta\epsilon$ , equal to  $E \Delta\epsilon / \Delta S$ , where  $E = 10^7$  psi and  $\Delta S = 15,300$  psi. If the strain distribution had been completely uniform, the normalized strain range values would all have been 1.0. Note by comparison of the initial readings of Gages 1, 2, and 3 that there appears initially to have been both in-plane and transverse bending in this particular specimen. Interestingly, a fretting crack eventually originated at the faying surface near Gage 1, although the Gage 2 strains were consistently 30 percent higher than the Gage 1 strains.

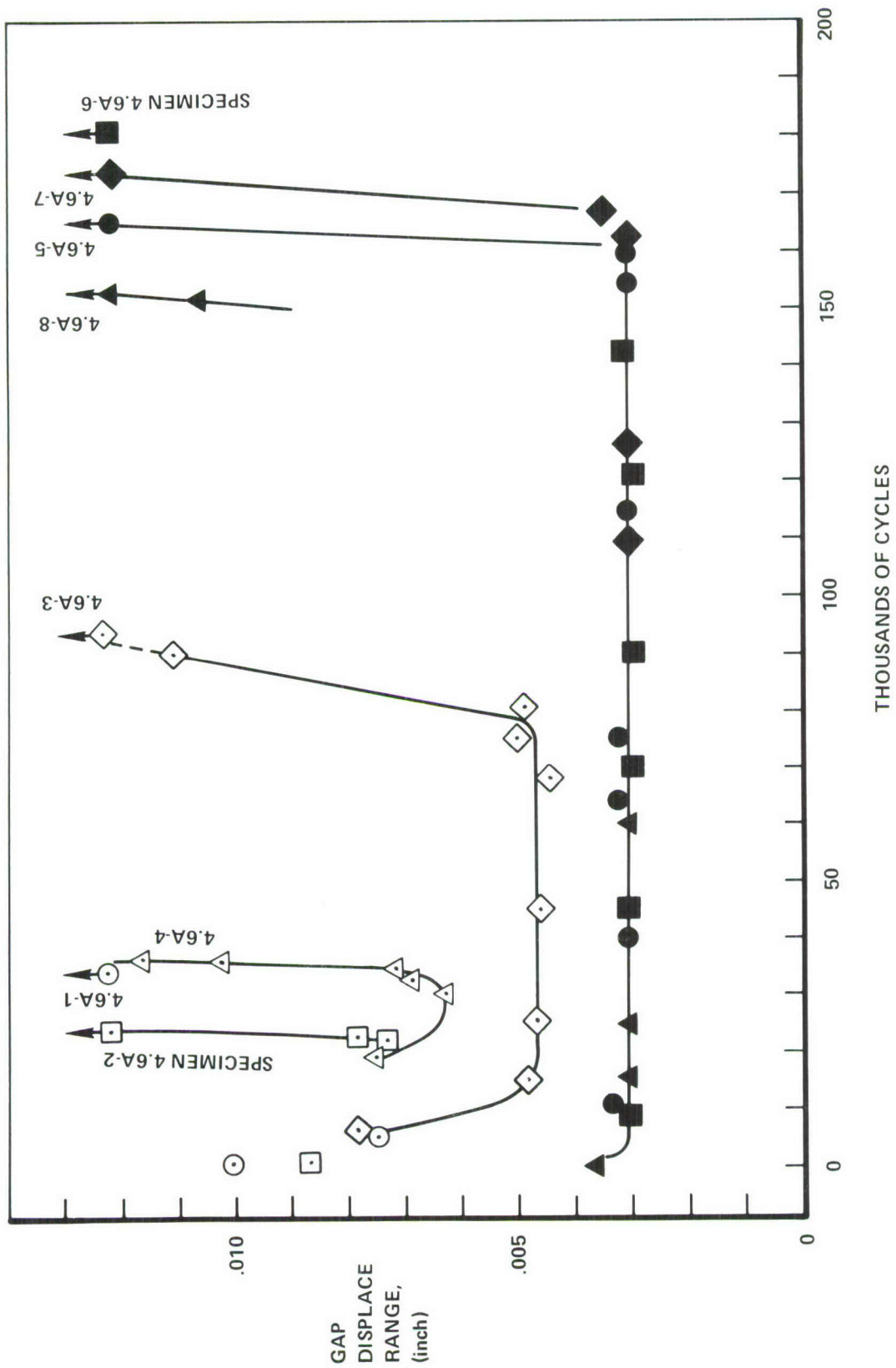


Figure 70. Gap-Opening Displacement Range in the Thick Double Lap Joints

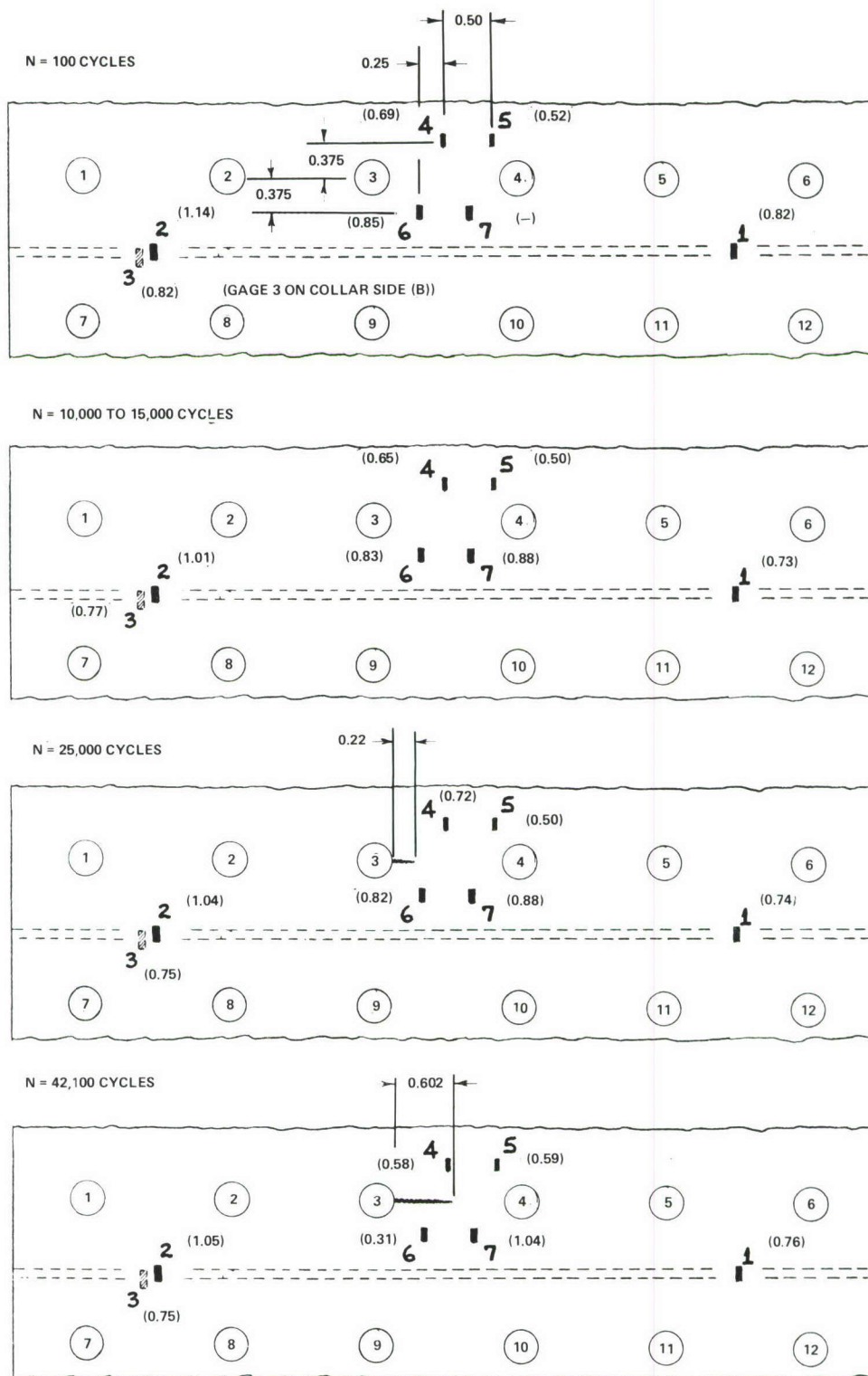


Figure 71. Strain Gage Results, Double Lap Joint Specimen 4.6A-8 (Sheet 1 of 2)

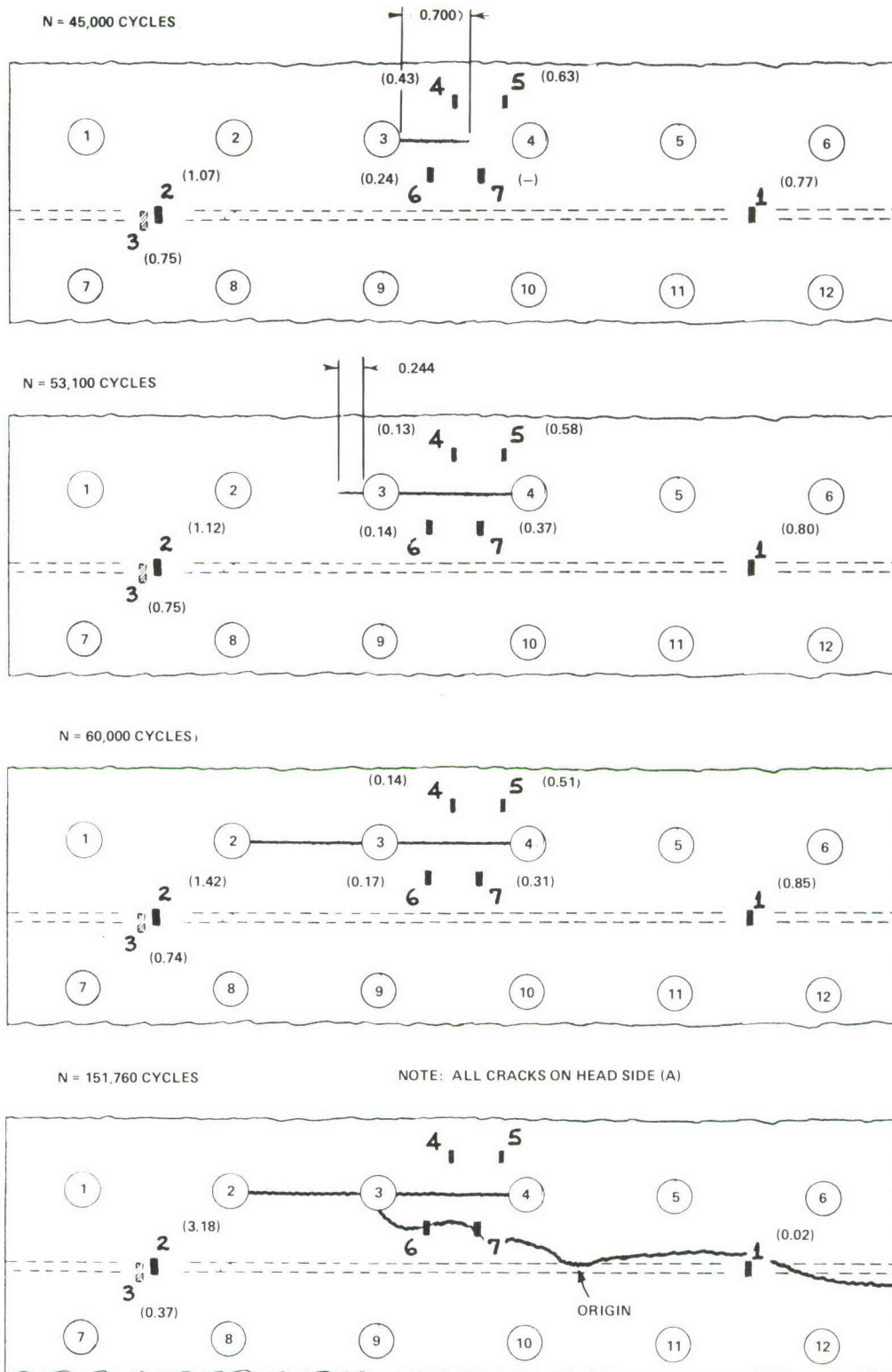


Figure 71. Strain Gage Results, Double Lap Joint Specimen 4.6A-8 (Sheet 2 of 2)

Note also that the average strain range from Gages 1, 2, and 3 is only 0.84, not 1.0. Since these gages are on the outer surface, this suggests the possibility that each doubler bent individually and that perhaps the tension stress was approximately uniform across the width but the bending stress was not. Thus, at the faying surface beneath Gage 1 the normalized initial strain range might have been 1.18,  $(2.0 - 0.82)$  whereas beneath Gage 2 it might have been 0.86  $(2.0 - 1.14)$ . This would be consistent with the location of the fretting crack origin.

## 1.2 Single Lap Joint Tests

Figure 72 is a plot of the crack growth data on the six single lap joint specimens. All fasteners in specimens 4.7-1 through -4 are clearance fit with finger-tight torque. All fasteners in specimens 4.7-5 and -6, except the one in the precracked hole, are interference fit with standard torque. There are continuing damage flaws in duplicate specimens -2 and -3, but none in duplicates -1 and -4. Specimen -5 has a second precrack in Row 1 of the doubler but is otherwise the same as -6. Since only the skin cracks grow in Row 1, specimens -5 and -6 can also be regarded as duplicates.

Compare the curves for specimens 4.7-2 and -3 with those of -1 and -4. There is no apparent effect of the secondary continuing damage flaws on the growth rate of the main crack.

However, comparing these four to the curves for specimens 4.7-5 and -6, there is a significant effect of the torque and interference of the secondary fasteners on the growth rate of the primary crack.

A specimen life comparison is made in Figure 73 between the predicted life and the actual test life of the different conditions. The predictions of crack growth across the first ligament (between adjacent fasteners) is compared to the test data in Figure 72.

When clearance-fit low-torque fasteners are used, the specimen life is not significantly affected by the initial damage condition. This is clearly shown by examining the predictions and test data in each figure. According to the test results as well as the predictions, the use of interference-fit, fully torqued fasteners increased the specimen life by about 50 percent.

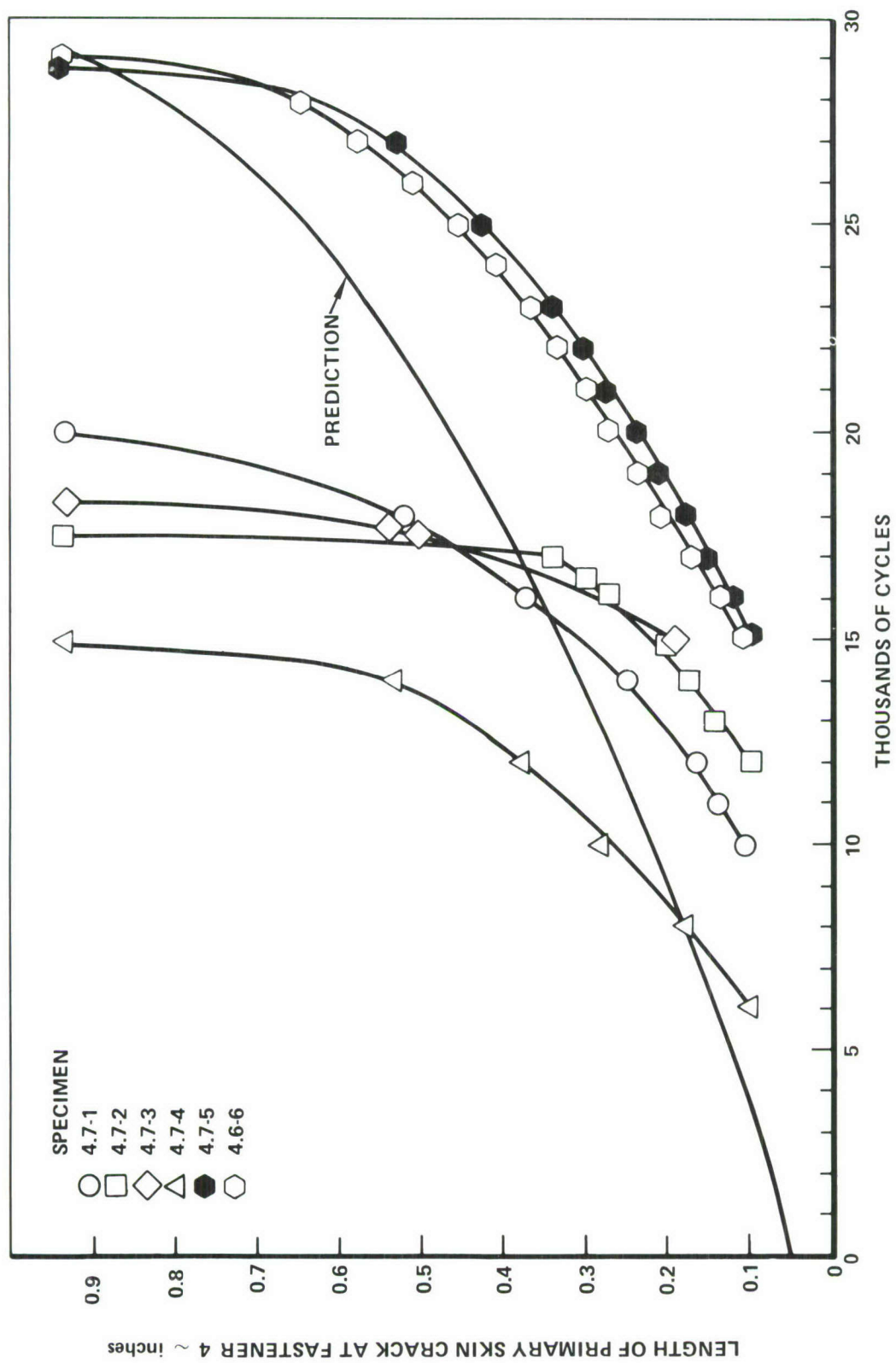


Figure 72. Crack Growth Results, Single Lap Joint Specimens

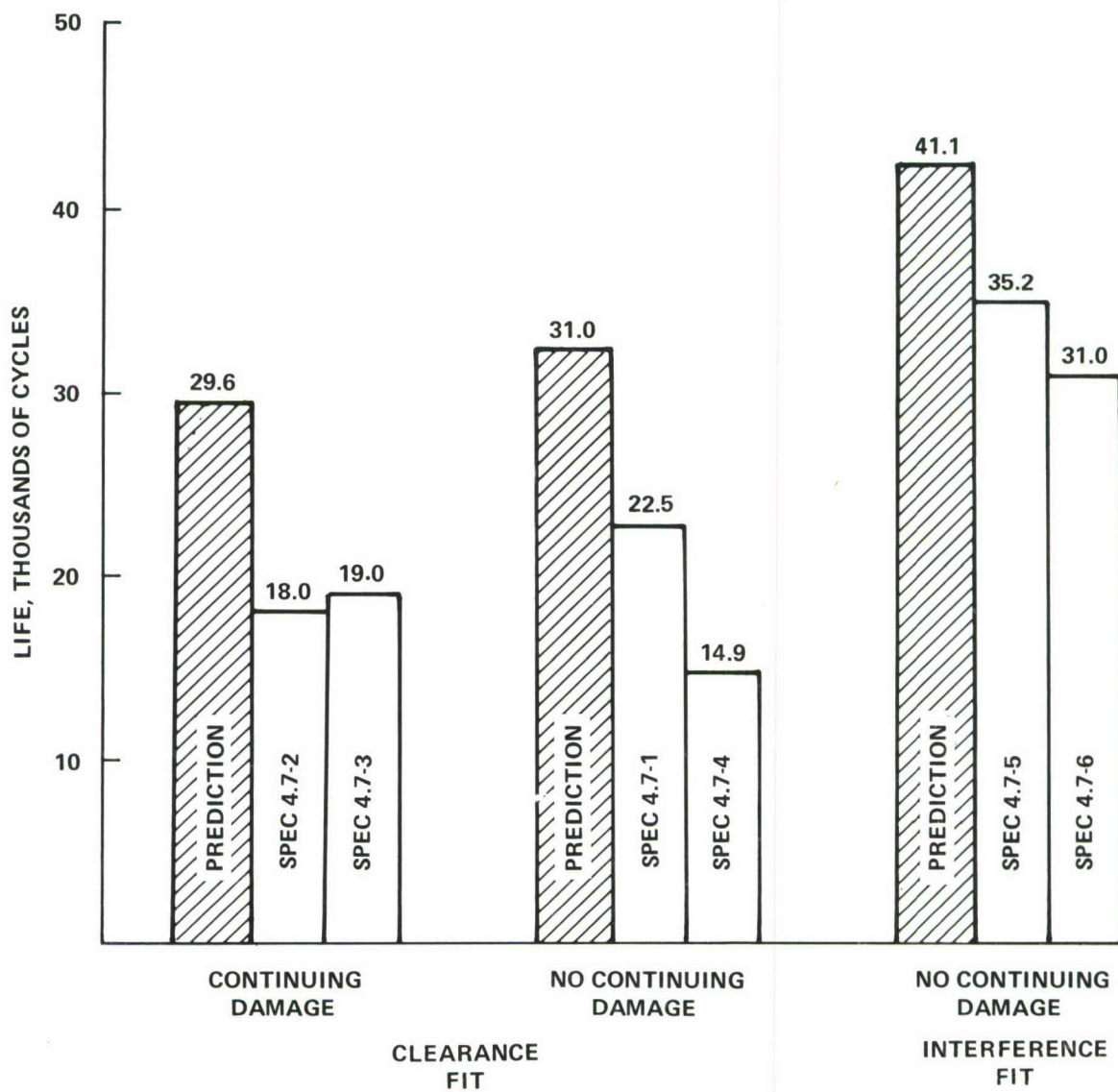


Figure 73. Predicted and Actual Crack Growth Lives, Single Lap Joint Specimens

The predictions for the single lap joint specimens tend to be unconservative, overestimating crack growth lives by a factor of roughly 1.5. The most likely explanation is that the transverse bending stresses have been inadequately considered in the prediction.

The strain gage measurements on Specimen 4.7-3 indicated that substantial transverse bending occurred in the single lap joint specimen despite the lateral constraints shown in Figure 61, Section VI.

The bending strains were measured on Gages 2 and 3 which were mounted back to back as shown in Figure 74. The number in parentheses alongside each gage is the normalized strain range,  $E \Delta\epsilon/\Delta S$  (where  $E = 10^7$  psi and  $\Delta S = 15,300$  psi). Gage 3, located on the faying surface side of the skin just below the end of the doubler, had an initial normalized value of 1.43.

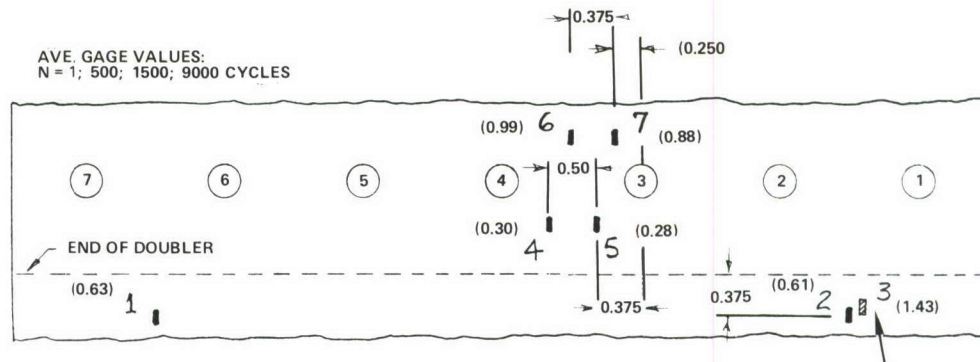
Figure 75, which summarizes the strain gage results from Specimen 4.7-7, a Phase II single lap joint specimen, confirms the presence of bending strains. This specimen was the same configuration as 4.7-3 but the fasteners were interference-fit, fully-torqued protruding head Hi-loks. Back-to-back Gages 1 and 5 indicate that transverse bending causes a 30 to 40 percent increase in the peak value of the strain range in the faying surface side of the strain.

Thus, the bending in the single lap shear joint specimen apparently increases the peak tension stress by about 40 percent in the skin at the faying surface. Using as a rule of thumb

$$\frac{da}{dN} = C_o \Delta K^{3.25} \quad (87)$$

the stress factor of 1.4 would increase the crack growth rates by a factor of 3.0.

It is evident from Figures 72 and 73 that when the bending stresses are neglected, the crack growth rates are underestimated. However, if it were assumed in computing  $da/dN$  that the effective uniform stress is the applied tension plus the peak induced bending stress, the crack growth rates would be overestimated, as they were in the double lap joints.



NOTE: GAGE 3 ON DOUBLER SIDE OF SKIN. ALL OTHERS ON OPPOSITE SIDE.

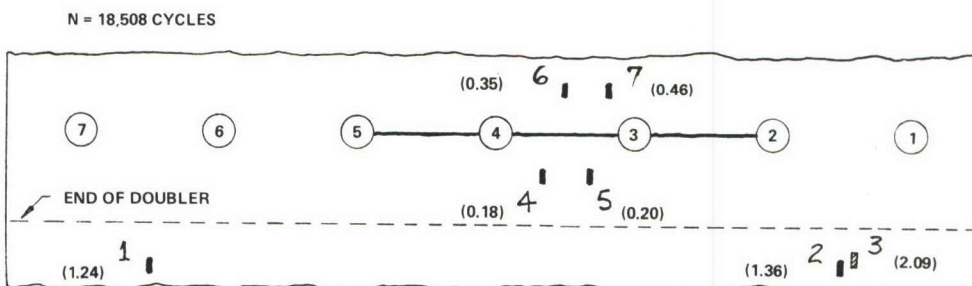
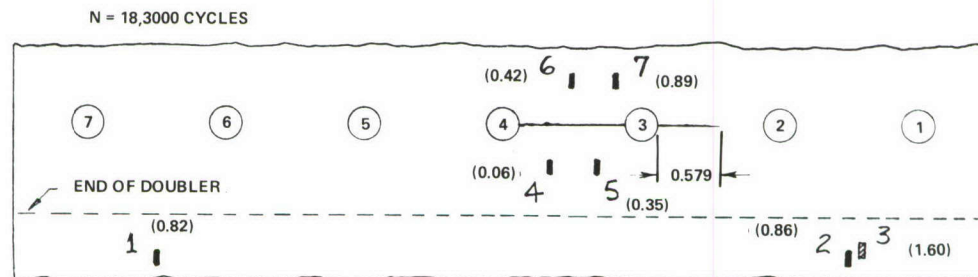
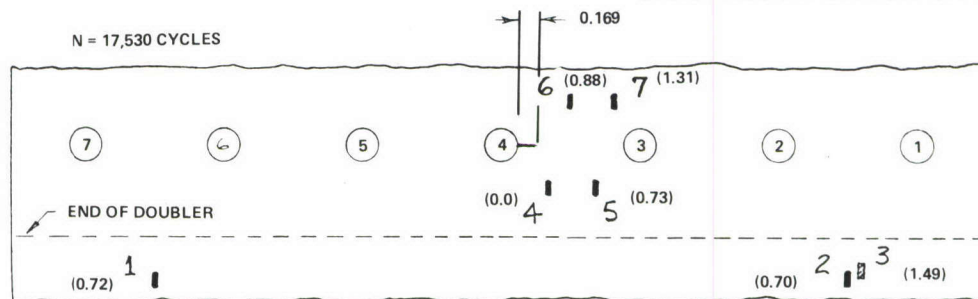


Figure 74. Strain Gage Results, Single Lap Joint Specimen 4.7-3

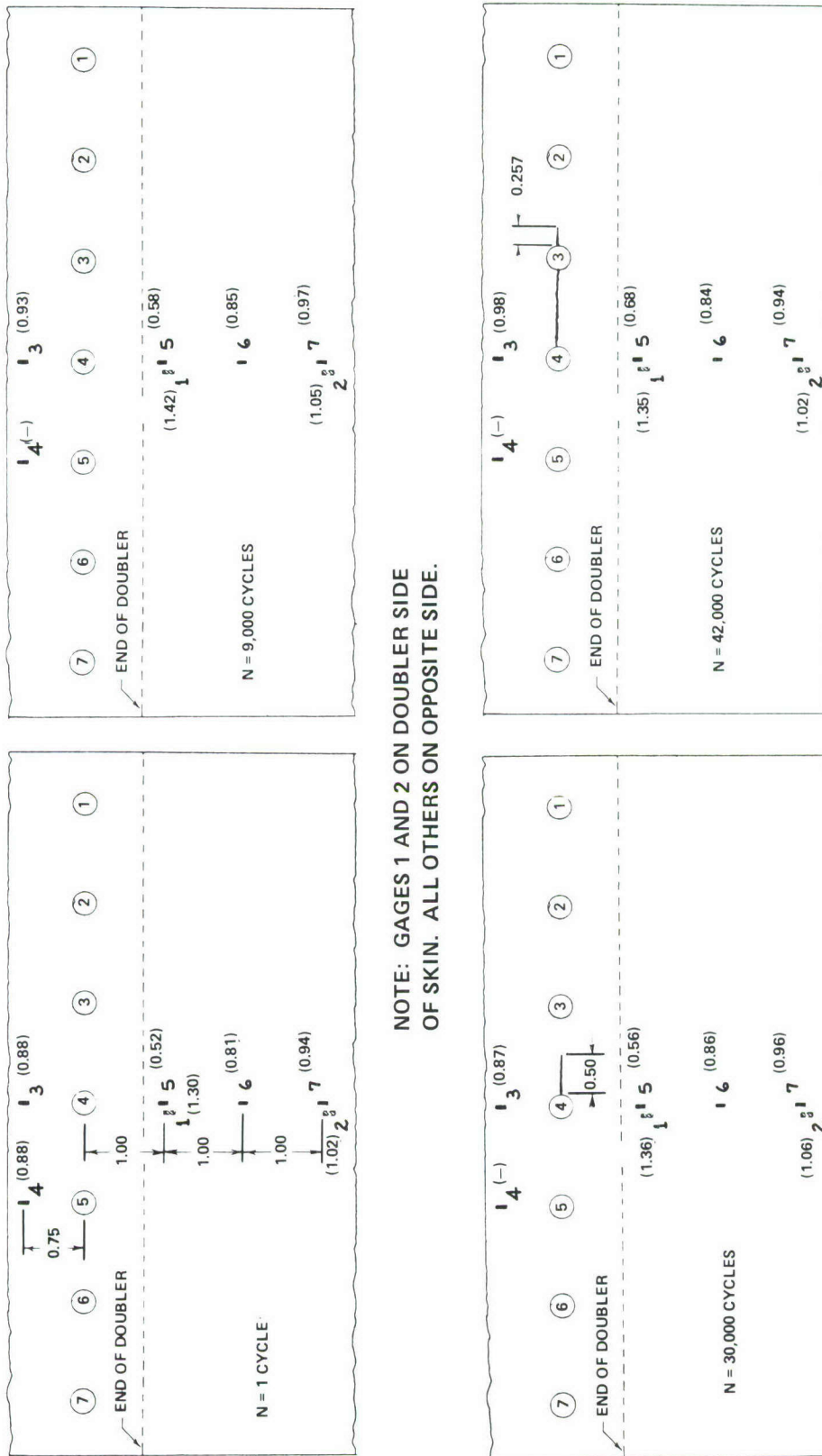


Figure 75. Strain Gage Results, Single Lap Joint Specimen 4.7-7

## 2. DISCUSSION OF RESULTS FROM PHASE I

The greatest error in predictions was in estimating crack arrest periods for the double lap joints. Figure 76 compares predicted and actual crack arrest periods at the interference-fit fully-torqued fasteners in the immediate path of the preflaw. The crack arrest period is defined as the number of cycles from the time of crack arrest at the hole until reinitiation on the opposite side of the hole or, if the crack does not reinitiate, until specimen failure. In most of the double lap joint cases the crack did not reinitiate and failure occurred by fretting nearby. The theory and baseline data failed to predict the long crack arrest periods for these double lap joints.

The applicable baseline crack initiation data consisted of the results from two one and one-half dogbone specimens (Specimens 2B-2-4 and 2B-1-3, Table 9). The specimen configuration is shown in Figure 34. Each specimen had a fully-torqued 0.375-inch diameter interference-fit protruding-head Hi-lok fastener. It is significant to note that anti-friction teflon tape was placed in the faying surface of these specimens to prevent fretting and force the failure to occur at the fastener hole instead. It was originally intended that the tape be placed on the leading edge of the 1/2-dogbone component only. However, the tape was inadvertently placed across the entire faying surface. Thus, these baseline test results failed to adequately reflect the life-extending benefits of faying surface friction for a non-lubricated joint. In that light, these tests were inadequate for the analytical purpose used.

Long crack arrest periods were not always observed, as seen in Figure 76. The crack arrest periods are very long for the double lap joint specimens with protruding head fasteners but very brief for the single lap joint specimens with flush head fasteners.

A notable crack growth sequence occurred in Specimen 4.6.A-5, a thick double lap joint specimen with 0.050-inch precracks in both doublers. A plot of the crack growth history for the collar-side doubler of this specimen is shown in Figure 77. Typical of all specimens the initial crack grew from

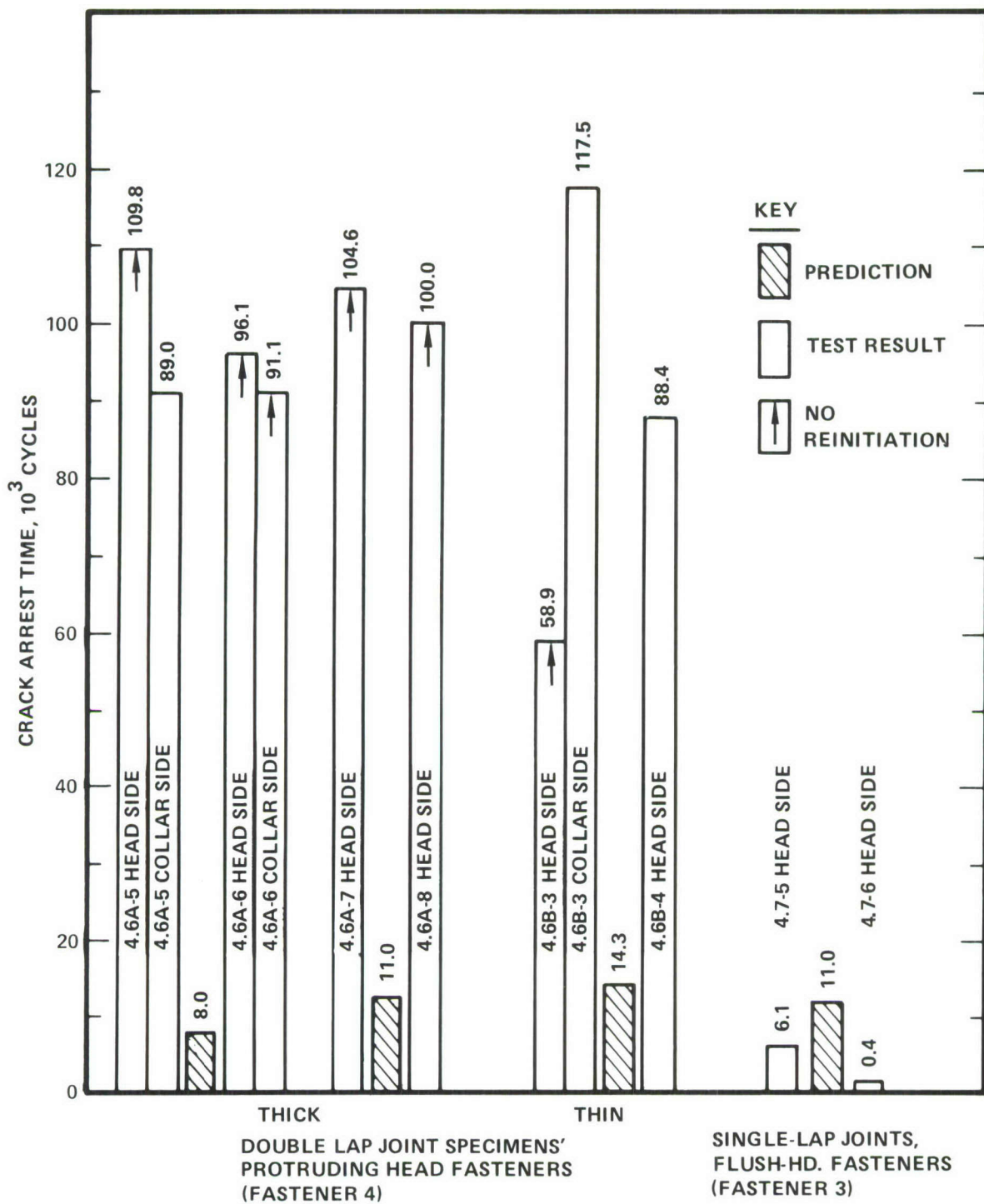


Figure 76. Comparison of Arrest Times at the Torqued, Interference-Fit Fastener in the Precrack Path

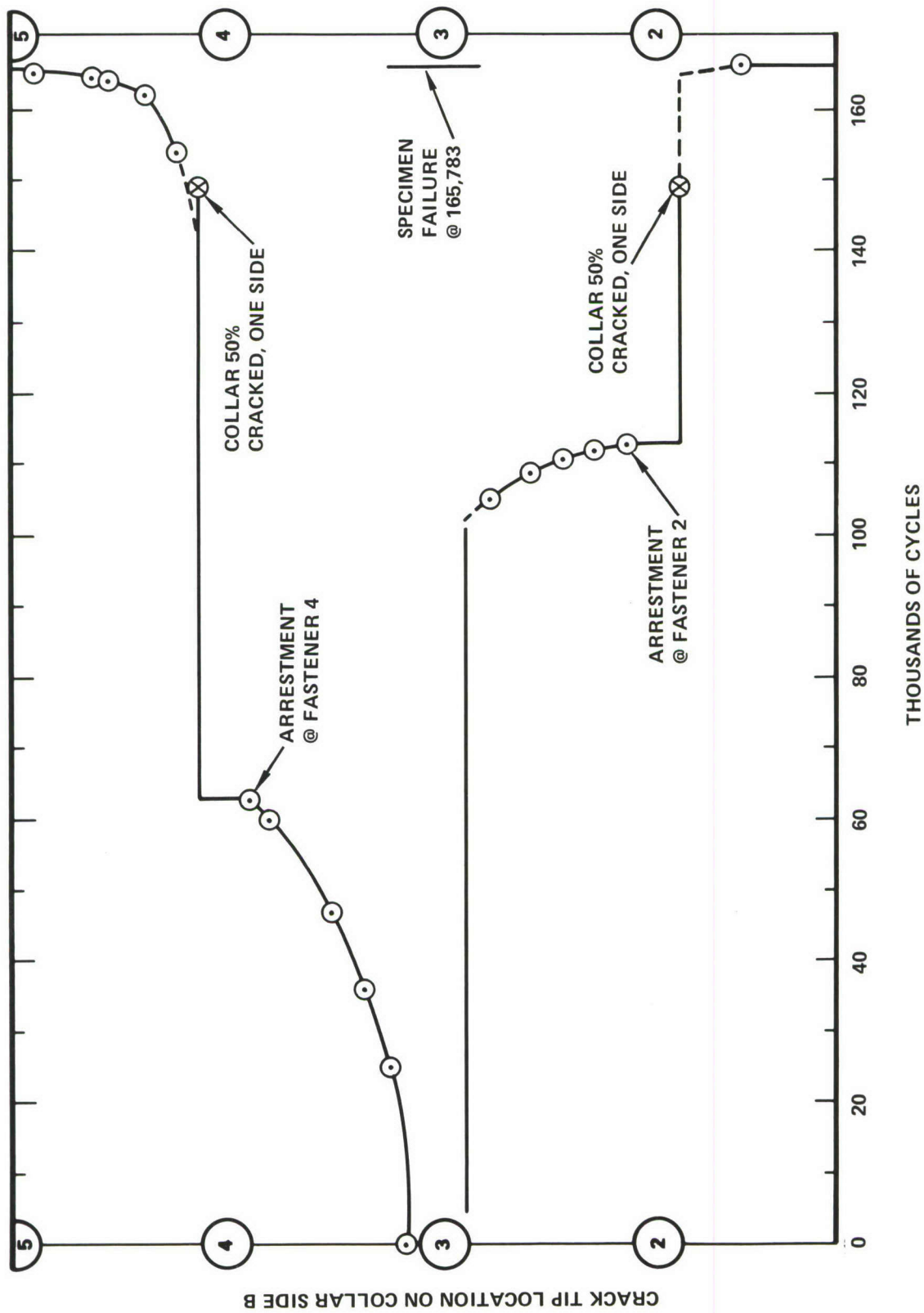


Figure 77. Crack Growth History in the Collar-Side Doubler of Specimen 4.6A-5

Fastener Number 3 to Fastener 4 and arrested in 63,000 cycles. Since Fastener 3 was an untorqued clearance fit fastener, a secondary crack initiated on the unflawed side of Fastener 3 and grew to Fastener 2 and arrested at 112,500 cycles. Continued cycling produced no further evidence of damage until 149,000 cycles, when it was noted that cracks had developed in the aluminum Hi-lok collars of both Fastener 2 and Fastener 4. A mere 5000 cycles later at 154,000 cycles, a reinitiated crack appeared on the opposite side of Fastener 4. This crack grew slowly across the ligament and arrested at Fastener 5 at 165,000 cycles. Specimen failure occurred within 800 cycles, but not before a crack had also reinitiated at Fastener 2 beneath the other cracked collar and propagated across the ligament to Fastener 1.

Figure 78 is a photograph of a portion of the fracture surface from this specimen, showing the collar crack at Fastener 4. Note the fretting-induced surface flaw in the head-side doubler. Fretting flaws of this type, located on the split line of the joint just above Fastener 4, contributed to the failures of all four of the thick double lap joint specimens with fully-torqued interference-fit fasteners.

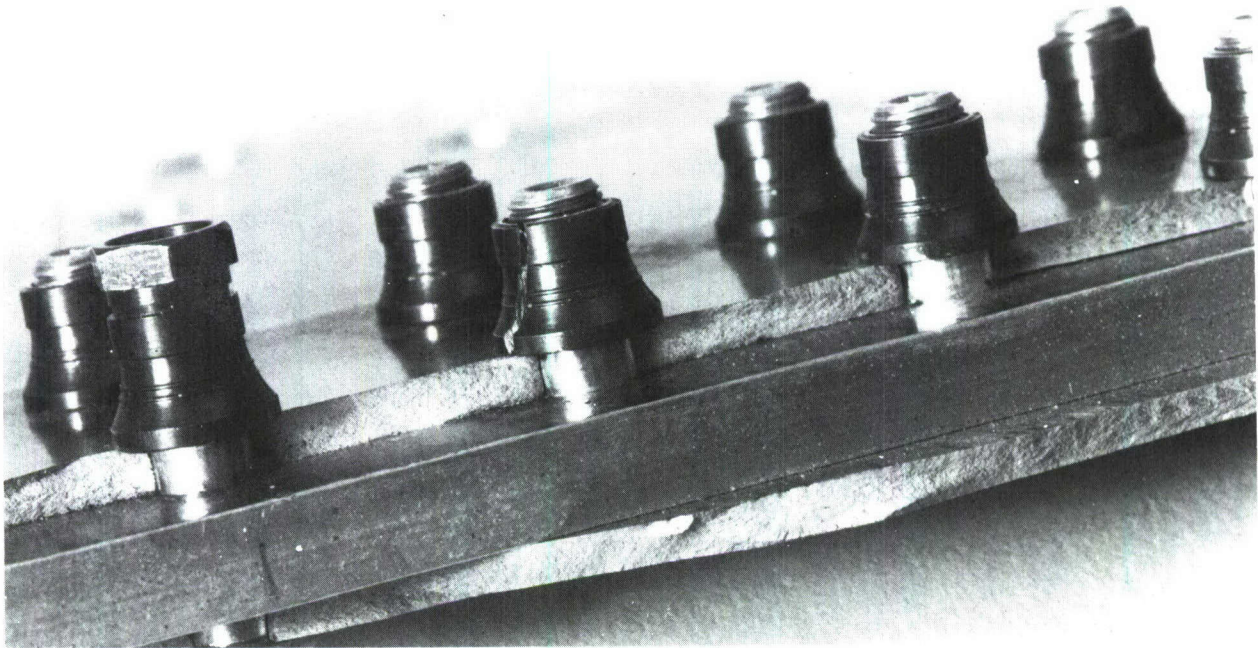


Figure 78. Specimen 4.6A-5: Cracked Collar and Fretting-Induced Surface Flaw

In five of the six double-lap joints with clearance fit, finger-tight fasteners, cracks initiated during the test at fastener locations remote from the main propagating crack. So many of these random initiations occurred in Specimen 4.6B-2, in fact, that the final failure occurred in fastener Row 3 rather than in Row 2. (Rows 2 and 3 are nominally identical except that preflaws are induced in Row 2).

The test data seemed to emphasize two main points about crack growth in mechanically fastened joints. First, there appears to be little sensitivity to variations in initial flaw conditions. On the other hand, there appear to be major effects of fastener torque in slowing down and arresting fatigue cracks. While effects of torque on fatigue initiation have been discussed in the literature, the large affect of fastener torque on the crack growth and reinitiation had not been previously recognized.

## 2.1 Insensitivity to Initial Flaw Conditions

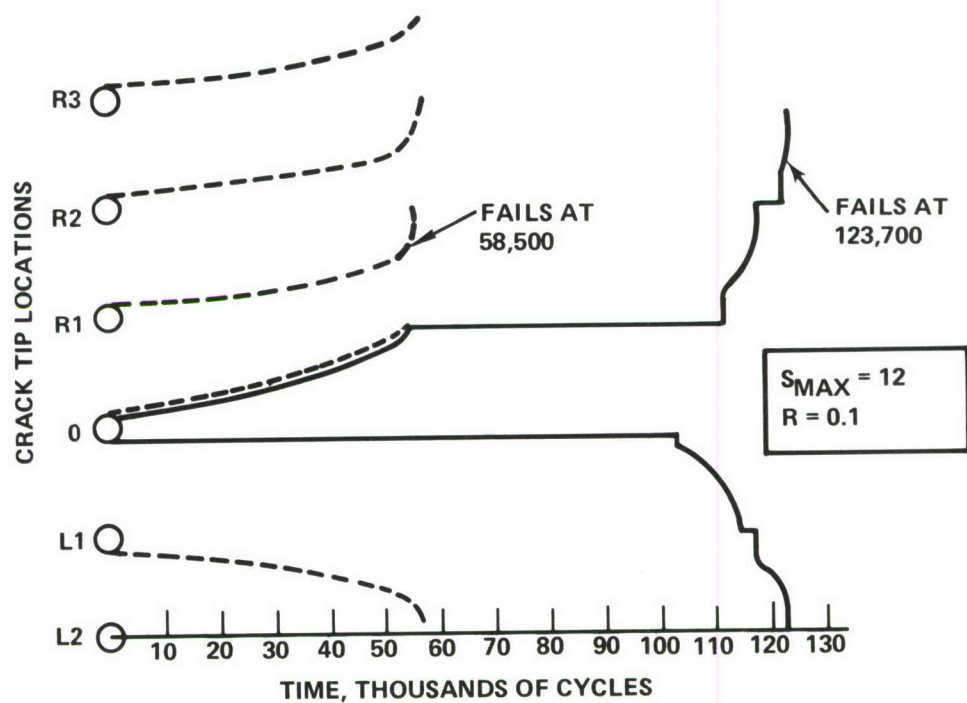
For joints with finger-tight, clearance-fit fasteners and a 0.050-inch initial fatigue crack, the fatigue crack initiation periods at each (unflawed) fastener hole are short compared to the propagation period of the one crack growing from hole to hole across the joint. Cracks therefore initiate independently at several fastener locations during the test. Because of this, for clearance-fit unclamped joints there was no significant difference in life between specimens with simulated 0.005-inch continuing damage flaws and similar specimens without continuing damage flaws. This conclusion, however, must be understood to be valid only at stress levels equal to or greater than  $S_{\max} = 17.0$  ksi,  $R = 0.1$ . At lower stresses than used here, initial flaw conditions may play a more significant role.

Consider for example, the hypothesis that lower stress levels would have magnified the effects of continuing damage flaws. Fatigue tests of the crack-growth-along-a-row-of-holes specimen, shown in Figure 10, run prior to the start of this program (Ref. 9), had long arrest times at each hole, creating the impression that continuing damage flaws (which would reduce this arrest time) would significantly shorten the total crack growth life. This

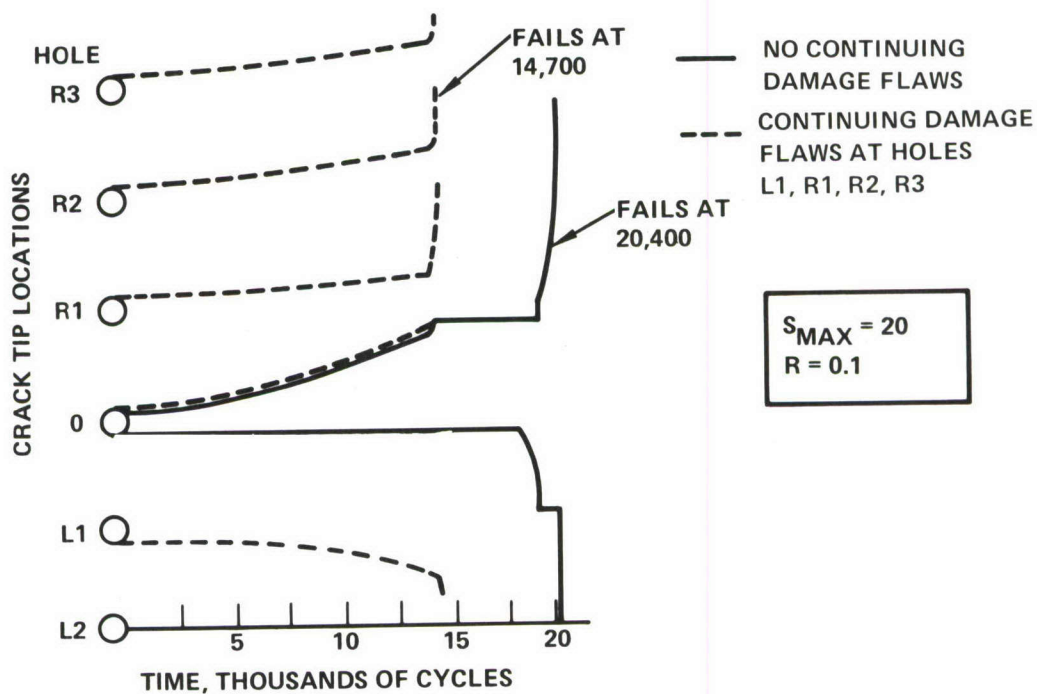
life reduction would occur even if the continuing damage flaws were not placed at the critical locations on the opposite side of the precracked hole. These tests were run at low cyclic stresses, ( $R = 0.1$  and  $S_{\max} = 10$  ksi or 13.8 ksi). Analyses of this specimen for  $R = 0.1$  and  $S_{\max} = 12$  ksi and 20 ksi are shown in Figure 79. The scale of the abscissa has been chosen so that the cycles for the 0.05-inch crack to grow to the adjacent hole align visually for both stress levels. As the figure shows, the reinitiation times are more significant at the lower stress level and thus the continuing damage flaws have more impact on crack growth life at 12 ksi than at 20 ksi.

For specimens with interference fit, fully-torqued fasteners everywhere (except at the location of the precracks, where a clearance fit, untorqued fastener was always used) there was no significant difference in life between specimens with multiple initial cracks (cracks in all members at a common fastener hole) and single initial cracks. In the single lap joint specimens this was expected: The stresses are much lower in the doubler than in the skin along the row of fasteners where the precrack was introduced so the doubler crack does not grow. In the double lap joint specimens the specimen life was so strongly dominated by clamp-up and/or interference effects that multiple flaw effects, if present, were not identifiable. That is in the test comparing single versus multiple flaws in which the nonprecracked holes had fully-torqued interference-fit fasteners, the final failure was precipitated by either fretting cracks or collar failures, and thus the multiplicity of flaws had little or no effect.

Had a comparison between single and multiple crack configurations with all clearance-fit untorqued fasteners been made, it is probable that little difference would have been observed as well, because of relatively rapid crack initiation and relatively slow crack growth. However, that conclusion would be stress dependent as just discussed.



(a) LOW STRESS LEVEL



(b) HIGH STRESS LEVEL

Figure 79. Analytical Crack Growth Predictions, Hole-to-Hole Specimen

## 2.2 Effects of Fastener-Head Friction on Crack Arrest

The fatigue life of the double lap joints with interference-fit, fully-torqued protruding-head fasteners is much longer than predicted and much longer than comparable specimens with untorqued clearance-fit fasteners. Much of the difference is attributable to the nearly certain and permanent crack arrestment at the fully-torqued, interference-fit fasteners on either side of the preflawed fastener hole. Predictions based on the stress severity concept and baseline data on two one and one-half dogbone specimens with a fully-clamped interference fit protruding-head fastener and teflon tape in the faying surface had been used to predict reinitiation times of about 6000 cycles for these arrested cracks. In contrast these arrested cracks were subjected to approximately 100,000 cycles without reinitiation, the final failures occurring due to nearby fretting cracks like the one shown in Figure 78.

Positive crack-closing due to friction beneath the fastener head or collar of the fully-torqued, crack-arresting fastener is hypothesized to be the necessary condition for long periods of crack arrestment such as were observed in the double lap joints. Best evidence for this is the crack-arresting history of Specimen 4.6A-5, Figure 78, where the crack arrested at Fastener Number 4 and did not reinitiate for 86,000 cycles, when a radial crack developed in the collar. The collar cracking was evidence of substantial cyclic load transfer by friction between the collar and the cracked doubler piece. This frictional force reduced the cyclic deformation of the arrested crack near its tip, prolonging the reinitiation time. When finally the collar cracked it was free to deform compatibly with the cracked doubler; the cyclic friction force dropped off; and reinitiation was able to occur in a relatively few cycles.

At full clamp-up the 0.375-inch diameter fastener has a nominal bolt tension of approximately 3575 pounds. If the coefficient of friction is 0.26, this corresponds to a total friction force capability of 930 pounds. Thus the collar could exert about 465 pounds of force on each side of the arrested crack and on each face of the 0.182-inch doubler to resist the cyclic deformation of the crack.

Consider the problem, sketched in Figure 80, of a crack arrested at a fastener hole of radius  $R_o$  in a sheet of thickness  $t$ . The main component of the stress  $\sigma_p$  at point P at the edge of the hole is due to the remote stress. The solid line in Figure 80 depicts the time history of this component when the remote stress is cycled at a range ratio of 0.1.

Assume a fastener is present in the hole, and the fastener torque has put an axial preload of magnitude  $P_N$  in the fastener. This will create a distributed frictional force around the hole periphery. When the remote load is cycled the direction of the frictional force is always so as to oppose the motion of the crack surfaces. When the remote-load and frictional-load effects are combined, the time history of the stress at the edge of the notch is reduced to the magnitude shown by the dashed line in Figure 80.

Note that both the minimum and the maximum of the cycle are truncated due to the frictional force. The magnitude of the averaged-through-the-thickness friction-imposed change in the stress at the edge of the notch is approximately proportional to  $P_N/(R_o t)$ :

$$S_f = \beta_f \frac{P_N}{R_o t} \quad (88)$$

The nondimensional factor  $\beta_f$  depends on the coefficient of friction  $\mu_f$  and the unknown distribution of the frictional force. Assuming a uniform distribution across the hole diameter on both faces of the sheet, the theoretical relationship  $\beta_f = \frac{2\mu_f}{\pi}$  can be derived from Equation (47) and from the stress intensity factor solution on page 3.7 of Reference 43. A friction coefficient of about 0.26 is found by setting a fastener or collar on the surface of an aluminum sheet, tilting the sheet until sliding occurs, and measuring the tangent of the angle with the horizontal. Using this value  $\beta_f$  is approximated as 0.166. However, a preferred way of measuring  $\beta_f$  is empirically using appropriate fatigue data.

An appropriate series of supplementary baseline fatigue tests was conducted to measure the crack-arrest capability of a fully-torqued Hi-lok

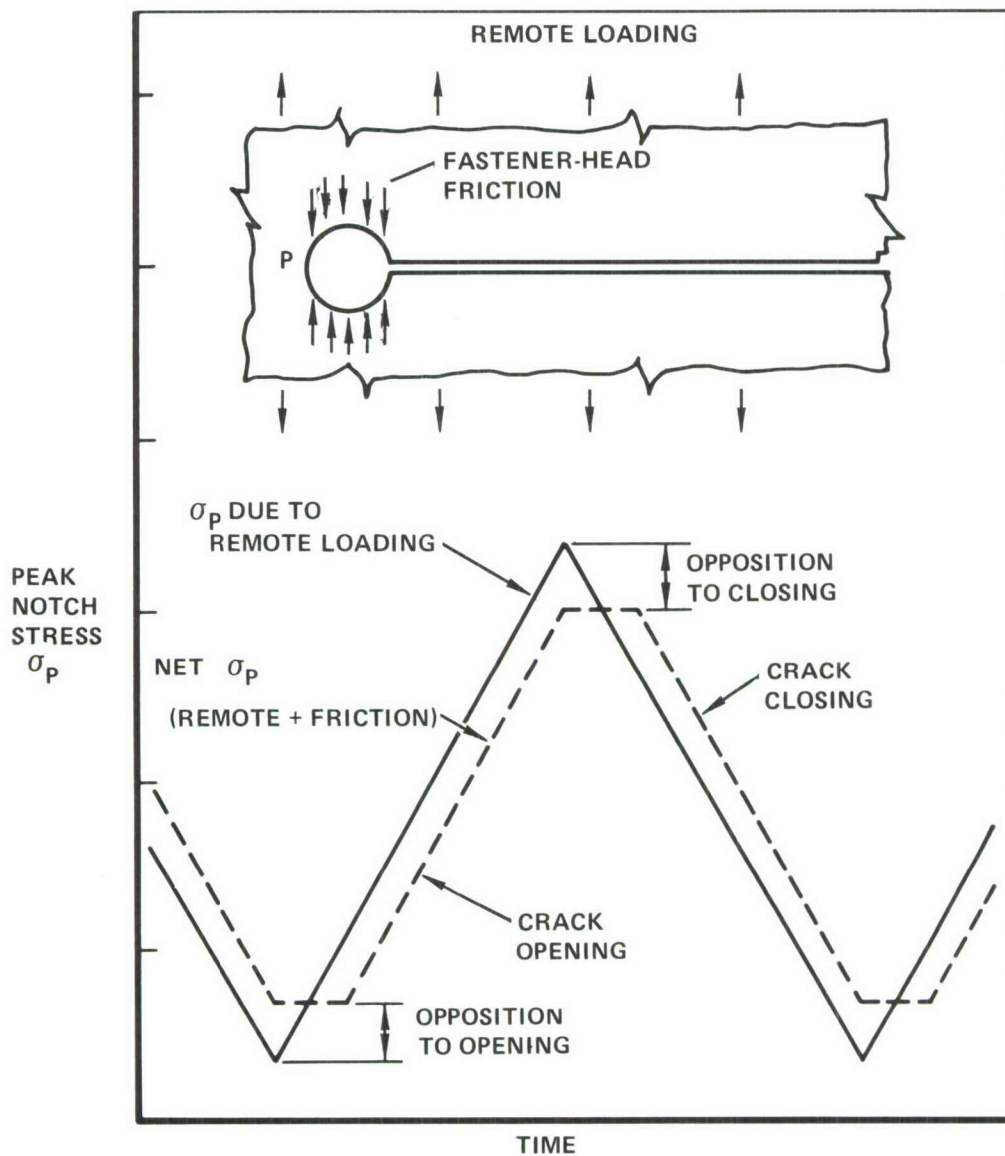


Figure 80. Reduction of Cyclic Notch Stress by Friction Beneath the Head of a Torqued Fastener

fastener. These tests are summarized in Table 17. The modified compact tension specimen with  $W = 5.0$  inches was used. In specimens N-1, N-2, A, B, and C, the 0.25-inch diameter hole was at the end of the slot, and in specimens A, B, and C, a fully-torqued clearance fit fastener was inserted in the hole. In specimens D, E, and F, a ligament of material of length  $b_e = 0.25$  inch was left between the end of the slot and the edge of the hole, and a fully-torqued interference-fit fastener was inserted in the hole. (The 0.25-inch ligament broke after a few hundred cycles, which were not included in the tabulated crack initiation times.) In specimens B through F a square washer  $1 \times 1 \times 0.182$  inch was used to simulate the fastening of a cracked member to an uncracked member.

The test results are shown in the last column of Table 17. The presence of the fully-torqued fastener improved the fatigue life significantly in all cases (by factors ranging from 2.0 to 36.2). Of all tests with fasteners, Specimen C with a flush-head clearance-fit fastener had the shortest life, 16,500 cycles. However, this result may be misleading due to the fact that  $b_e$  was zero. The reason for having  $b_e$  equal to 0.25 inch in specimens D, E and F was to allow the fastener interference to be developed properly. However with  $b_e$  equal to zero, the tapered head of the fastener in specimen C would simply spread the hole upon installation in a manner unlike anything actually seen on the structure, thus significantly affecting the reliability of the specimen C result. Specimen D with an interference-fit flush-head fastener had a substantially longer life, 140,160 cycles.

These test results substantiate that friction under the head of a torqued fastener is responsible for significant extensions in crack initiation time when a crack arrests at the fastener hole. However, there are insufficient data from these 6 tests to confidently identify consistent differences in the crack-arrest capabilities of protruding heads, flush heads and aluminum collars.

The geometric mean life of specimens A through F was 88,900 cycles, compared to 8,100 cycles for the identical open-hole specimens, N-1 and N-2, a factor of 11.0 improvement in life due to fastener torque. This extended

TABLE 17. MODIFIED COMPACT TENSION SPECIMEN FATIGUE TESTS

| Specimen Number | Fastener Fit |            |            | Side of Fastener Contacting Specimen |               |                 | $b_e$<br>(Inches) | 1 x 1 In.<br>Washer<br>Used | Fatigue Life<br>(Cycles) |
|-----------------|--------------|------------|------------|--------------------------------------|---------------|-----------------|-------------------|-----------------------------|--------------------------|
|                 | Open Hole    | Clear. Fit | Inter. Fit | Flush Head                           | Protrud. Head | Aluminum Collar |                   |                             |                          |
| N-1             | x            |            |            |                                      |               |                 | 0                 | No                          | 7,570                    |
| N-2             | x            |            |            |                                      |               |                 | 0                 | No                          | 8,671                    |
| A               |              | x          |            |                                      | x             | x               | 0                 | No                          | 49,253                   |
| B               |              | x          |            |                                      | x             |                 | 0                 | Yes                         | 292,910                  |
| C               |              | x          |            | x                                    |               |                 | 0                 | Yes                         | 16,580                   |
| D               |              |            | x          | x                                    |               |                 | .25               | Yes                         | 140,160                  |
| E               |              |            | x          |                                      |               | x               | .25               | Yes                         | 64,650                   |
| F               |              |            | x          |                                      | x             |                 | .25               | Yes                         | 227,760                  |

$\frac{P_{max}}{B} = 8665 \frac{lb}{in}$   
 $k S_{t max} = 113.4 \text{ ksi}$   
 $R = 0.1$

Fasteners Used:  
HL50-8-3  
HL50-8-6  
HL51-8-6

Collars:  
HL90LP-8

Washer: 1 x 1 x 0.182 inch  
7075-T6 Aluminum

Spec. Thickness  $\cdot B = 0.182 \text{ inch}$

(MODIFIED CT SPECIMEN)

life can be used to estimate the constant  $\beta_f$  in Equation (88) and thereby account for fastener head friction in the analysis. By interpolation in Table 11, the value of  $k_t \Delta S_{eff}$  corresponding to a life of 88,900 cycles is 64.64 ksi. The remotely-applied values of  $k_t S_{max}$  and  $k_t S_{min}$  are 113.4 ksi and 11.34 ksi respectively. To reflect the effects of friction it is necessary to subtract  $S_f$  from  $k_t S_{max}$  and add  $S_f$  to  $k_t S_{min}$ , as seen in Figure 73. Then, using  $m = 0.5$ , substituting into Equation (52), and squaring both sides, the following quadratic equation for  $S_f$  is obtained:

$$64.46^2 = (113.4 - S_f)[(113.4 - S_f) - (11.34 + S_f)] \quad (89)$$

From this,  $S_f = 27$  ksi is obtained. Then from Equation (88) with  $P_N = 1.865$  kips and  $t = 0.182$  inch,  $\beta_f$  is estimated to be 0.33. This test result is about twice as high as the previous approximation. This is to be expected due to the conservative elements in the approximation, for example, it is assumed that the friction force produces a uniform stress through the thickness, whereas it probably concentrates its effect at the surface where the flaws reinitiate.

The above results ( $\beta_f = 0.33$ ) can be used to estimate reinitiation times of arrested cracks in joints. An effective notch stress is estimated from Equation (5), except that  $\beta = 1.0$  is used. This cyclic stress corresponds to the solid line in Figure 80. The reduction in stress due to fastener clamp-up is calculated from Equation (88). In the double lap joints for example, 0.375 inch diameter fasteners are used,  $t = 0.182$  inch, and  $P_N = 3.575$  kips so  $S_f = 34.5$  ksi. This is subtracted from the maximum and minimum cyclic notch stresses  $S_\lambda$  found by means of Equation (5), and Table 11 is used to estimate the crack reinitiation times. Unfortunately, the estimates are again too short by a factor of about 10 compared to the data. This result is essentially the same as had been obtained by the stress severity factor equation, Equation (5), with  $\beta = 0.635$  for fully-torqued interference fit fasteners.

The clamp-up of the joint leads to load transfer by faying surface friction, making the stresses along the precracked fastener row much milder than assumed in the analytical model. The method described above is sensitive to

small reductions in stress magnitude because it involves the subtraction of a relatively large stress term,  $S_f$ . Thus if the "remote stress" term in Figure 73 were appropriately reduced to account for load transfer by faying surface friction prior to subtraction of  $S_f$ , the predicted crack reinitiation times would probably correlate more accurately. Faying surface friction is discussed in Section VII, Paragraphs 2.3 and 2.4. However it is worth noting here that faying surface friction can transfer over 40 percent of the load in these tests. This large a reduction can easily account for the factor of 10 error in reinitiation time predictions.

It seemed significant in view of the short crack reinitiation times and test lives of the single lap joints compared to the double lap joints that the single lap joints had flush-head fasteners. The tests described above appear to show some superiority of the protruding head fastener. However, the flush-head fastener seems capable of some degree of crack arrestment by friction beneath the head. The significance of fastener head type was further investigated by testing single lap joints during Phase II, as discussed in Section VII, Paragraph 3.1.

The crack arrestment capability of fasteners has been used in the testing of the stringer-reinforced specimens as discussed in Section VIII. In 19 of these specimens the skin crack growing away from the stringer began growing at a high fatigue rate. It was desired to postpone instability of this crack and allow time for secondary damage to initiate and grow in the region near the stringer. Therefore, the skin crack was stop drilled and a fully-torqued 0.375 inch clearance-fit protruding-head steel Hi-lok fastener was inserted in the hole. (A stack of steel washers had to be used between the collar and the specimen surface because the shank length of the shortest available 0.375 diameter Hi-lok was more than the sheet thickness.) In all 19 cases the crack was arrested very effectively by this procedure.

### 2.3 Faying Surface Friction Effects

Faying surface friction also appears to have been important in prolonging the life of the joint specimens. The crack growth rates were much slower in clamped joints than unclamped. The implication is that much of the load is

transferred by friction between the doubler and the skin at points beyond the plane of cracking, so that the nominal stress in the plane of cracking is lower than expected.

The predictions of crack growth and reinitiation times for cracks arrested at fastener holes in the double lap joint specimens were conducted neglecting faying surface friction. All the load transfer was assumed to be by shear in the fasteners. When the Hi-lok fasteners were fully torqued, the actual crack growth rates and crack reinitiation rates were much slower than predicted. One possible reason for this consistent conservatism in prediction is the faying surface friction.

A special test was conducted in a related program (Reference 71) to measure faying surface friction as a function of fastener torque. The thick double lap joint specimen configuration shown in Figure 2 was used. The specimen was not precracked. The nominal fastener hole diameter was 0.385 inch for all holes, creating a 0.010 inch diametrical clearance for the 0.375-inch protruding head Hi-lok fasteners.

The test procedure was as follows. With the fasteners in place but the collars loose, the joint was gently compressed to slide the fasteners into the position shown in Figure 81. All fasteners were equally torqued to a pre-assigned torque, ranging from 30 inch-pounds to the full break-off torque of approximately 200 inch-pounds. A tensile load was applied monotonically and a load-displacement record made. (Displacement is as measured from C.O.D. gages placed across the gap between the two 0.3750 inch skin pieces, as shown in Figure 81.) The load was removed and the fasteners loosened. The test was repeated for a new torque value.

Figure 82 shows a typical load-displacement record. As the load was increased, small gap-opening displacements occurred due to elastic deformations of the joint. Then at a load of about 6.5 kips the displacements suddenly changed. This sudden change indicated that the minimum faying surface friction forces had been overcome and slip was occurring between the skin and the doublers. As Figure 81 shows there were initially four independent 0.010-inch gaps between the fasteners and the bearing surfaces of the holes, so that the total possible

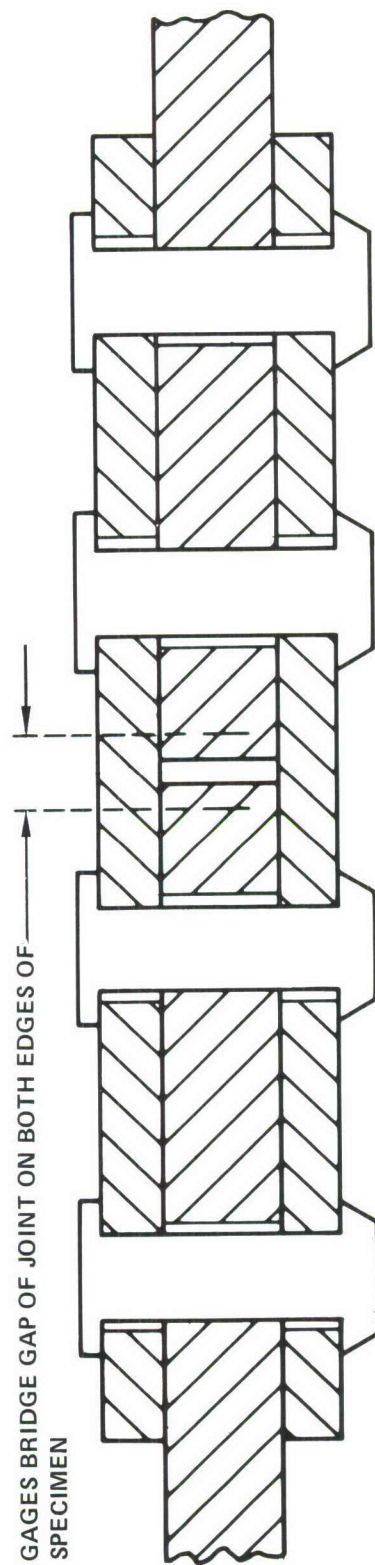


Figure 81. Side Sectional View of Precompressed Joint Prior to Tension Test

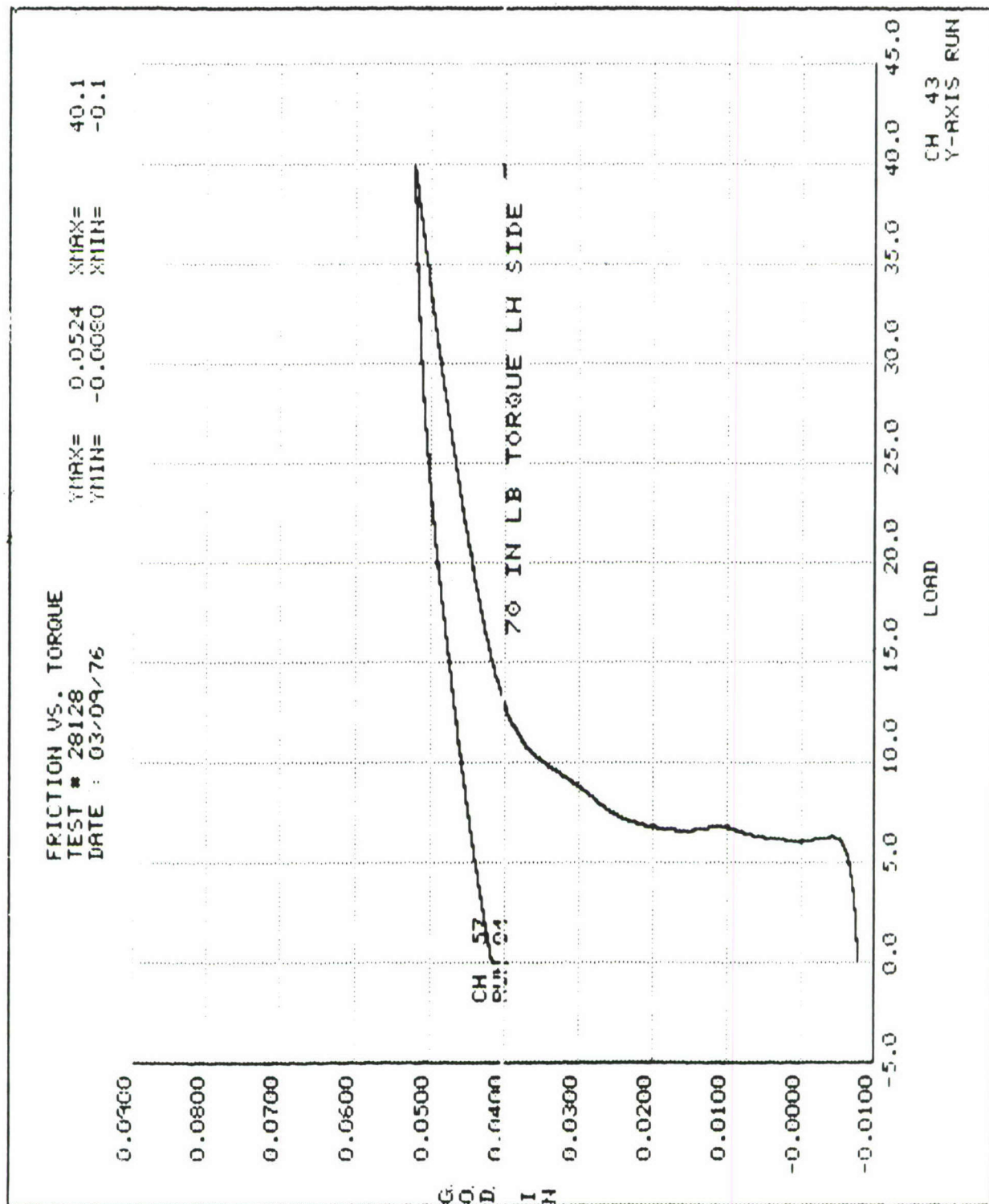


Figure 82. Load-Displacement Curve for Faying Surface Slip Test, Double Lap Joint

slip was about 0.040 inch. The friction load required to complete the slip process was higher than the load required to initiate it. At a load of about 11 or 11.5 kip and after slightly more than 0.040 inch of slip, the slope of the load-deflection curve was again steep. This suggested that the slip process was complete. Thus for a fastener torque of 70 inch-pounds, the upper and lower estimates for the total friction forces in the joint are, respectively, 11.3 and 6.5 kips.

The results of this series of tests are plotted in Figure 83. A straight line is fitted to the lower estimates of friction force as a function of fastener torque. At full break-off torque the lower estimate of friction force is 23.5 kips. This is 42 percent of the 55.7-kip load corresponding to  $S_{\max} = 17$  ksi, the maximum stress used in the fatigue test of these joints.

Note that the marking cycles discussed in Section II, Paragraph 2.1 ( $S_{\max} = 17.0$  ksi,  $R = 0.82$ ) have such a low applied load range ( $\Delta P = 10.0$  kip) the entire cyclic deformation during marking occurs by faying surface friction. This leads to much milder cyclic stress intensity factors than would occur by cyclically loading through the fasteners, as assumed. Consequently there was no detectable growth during marking cycles in the joint specimens.

The growth rate of corner cracks from loaded holes is sensitive to the magnitude of the fastener load. One first-order way to consider faying surface friction effects would be to assume that all fastener loads are reduced equally by the percentage amount of the friction force. Accordingly, all the fastener loads would be assumed to be reduced by 42 percent when the fasteners are fully torqued. The friction load would be assumed to be uniformly induced throughout the area of contact. This would undoubtedly improve the accuracy of crack growth computations for small cracks.

The double-lap joint tests appeared to show sensitivity to friction effects. It should be added that in actual aircraft joints faying surface sealant is sometimes used, or fasteners are installed wet. These could have quantitative effects not covered in this test program, as discussed in the following.

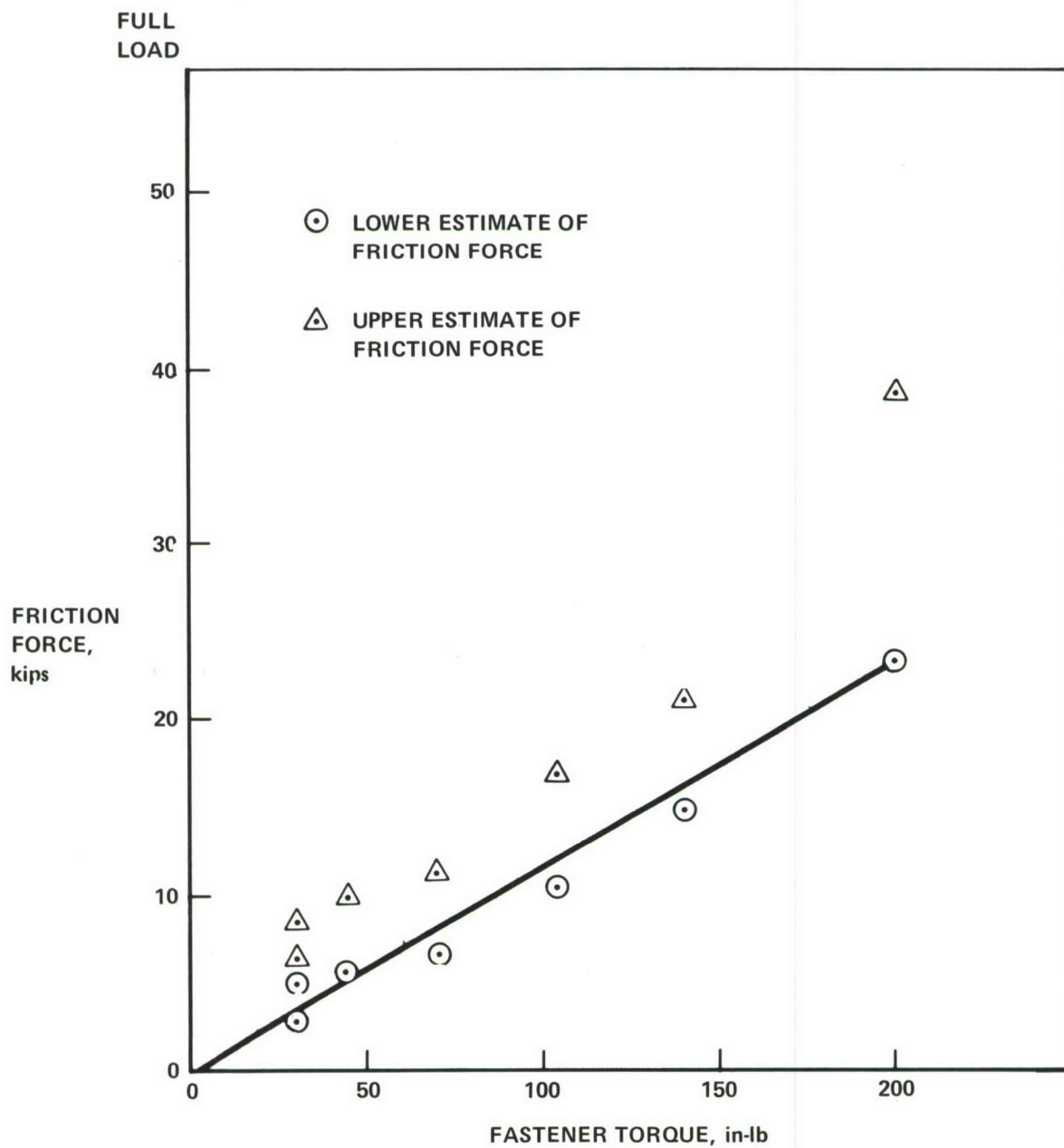


Figure 83. Effect of Fastener Torque on Faying Surface Friction Force in the Double Lap Shear Joints

## 2.4 Effects of Faying Surface Sealant, Environment, and Compressive Stressing

Fatigue tests of ten precracked double lap joints were conducted under other funding and reported in Reference 71. The purpose of these tests was to investigate the effects of the following variables:

- Interference-fit fully-torqued fasteners versus clearance-fit lightly-torqued fasteners.
- Sealant on the faying surface and fastener shank versus no sealant.
- Immersion in 3.5 percent NaCl Solution and a cyclic rate of  $f = 0.2$  Hz versus laboratory air environment and  $f = 4$  Hz.
- Tension-tension cycling ( $R = 0.1$ ) versus compression-tension cycling ( $R = -0.6$ ), at equal values of effective stress  $\Delta \bar{S}$ , where (References 67-68)

$$\Delta \bar{S} = S_{\max} [1 - \text{MAX} (R, R_c)]^m \quad (90)$$

For 7075-T6 Aluminum,  $m = 0.5$  and critical range ratio  $R_c = -0.12$ . The function MAX takes the value of the larger of its arguments.

In order to provide a basis for direct comparison of the test data, details of the test program were carefully planned so as to use the same lot of material, specimen configuration, initial flaw size, and stress level as used in this contract research program. In addition, the same personnel, procedures and facilities were used for specimen machining, precracking, assembly and fatigue testing. Fabrication procedures were as summarized in Section VI, Paragraph 1.

Table 18 summarizes the test matrix. Ten double lap joint specimens with 0.050-inch initial corner cracks were fabricated. In addition, data from four specimens from Phase I, Specimens 4.6A-3, -4, -5 and -6, were directly applicable for data comparisons.

Test scatter was reasonably low in the Phase I testing discussed earlier. Therefore in this test program it was possible to test one specimen at each condition, yet feel confident that the scatter would not obscure the actual test variable effects.

TABLE 18. TEST PLAN FOR PRECRACKED DOUBLE LAP JOINTS  
FROM REFERENCE 71

|                | Tension-Tension<br>S <sub>max</sub> = 17.0 ksi, R = 0.1 |                       | Compression-Tension<br>S <sub>max</sub> = 15.25 ksi, R = -0.6 |         |
|----------------|---|-----------------------|---|---------|
|                | Fastener/Precrack Condition, Figure 5:                  |                       |   |         |
|                | B   | C                     | B   | C       |
| Laboratory Air | 4.6A-3 <sup>(1)</sup>                                   | 4.6A-5 <sup>(1)</sup> |   |         |
| No Sealant     | 4.6A-4 <sup>(1)</sup>                                   | 4.6A-6 <sup>(1)</sup> | 4.6A-11   | 4.6A-13 |
| f = 4 Hz       | 4.6A-12   |                       |   |         |
| Laboratory Air |   | 4.6A-15               |   |         |
| Sealant        | 4.6A-14   | 4.6A-20               | 4.6A-16   | 4.6A-17 |
| f = 4 Hz       |   |                       |   |         |
| 3.5% NaCl      |   |                       |   |         |
| Sealant        |   | 4.6A-18               |   | 4.6A-19 |
| f = 0.2 Hz     |   |                       |   |         |

(1) Tested in Phase I of this program.

Figure 84 summarizes the crack growth lives. There are several conclusions that can be drawn from this figure.

Compression-tension cycling effects seem to be adequately covered by the effective stress concept, Equation (90). Five comparisons can be made between test lives for identical test specimens run at the same effective stress ( $\Delta S = 16.13 \text{ ksi}$ ) but different range ratios,  $R = 0.1$  (tension-tension) and  $R = -0.6$  (compression-tension). All pairs of test lives agreed within about 20 percent.

The use of faying surface sealant in laboratory air substantially reduces the crack growth lives. However the sealant probably provides substantial protection against environmental effects. The crack growth lives in 3.5 percent salt water at 0.2 Hz in the fully clamped and sealed joint were only slightly shorter than in the identical joint tested in laboratory air at 4 Hz.

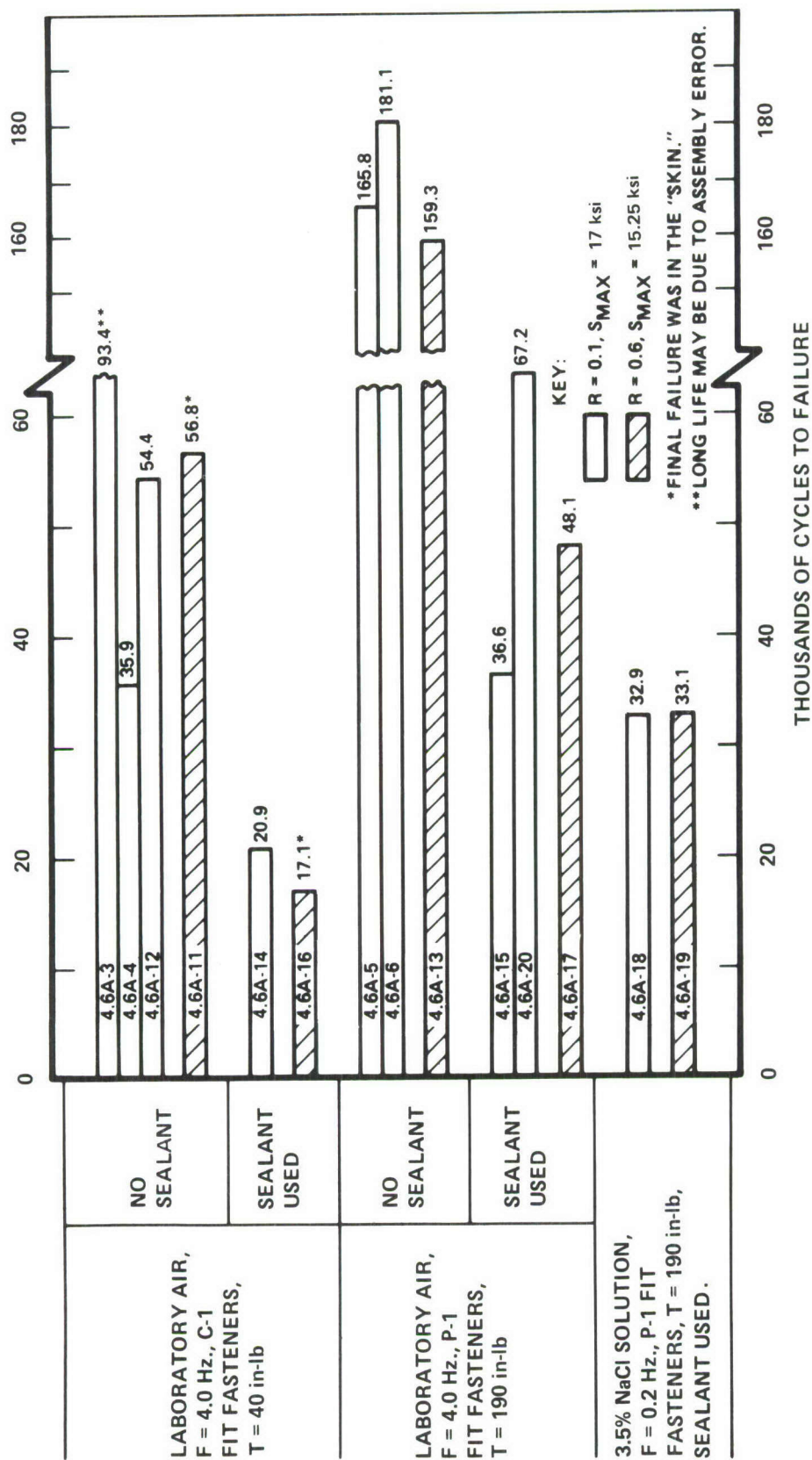


Figure 84. Summary of Test Results on Precracked Double Lap Joints From Reference 71

This difference appears to be due primarily to faster growth rates of through-the-thickness cracks in salt water. The initiation and early growth rates of part-through cracks were about equal.

Fastener torque and interference, shown to extend the crack growth life significantly in dry joints (no sealant), also extended the crack growth life in joints with faying surface sealant. The benefits in sealed joints were not as striking as in the dry joints, but were still very significant.

### 3. PHASE II TESTS OF JOINTS

#### 3.1 Fastener Head Investigation in Single Lap Joints

One of the goals of the Phase II testing was to examine the effect of fastener head type on crack growth and arrest in a fully-clamped precracked single lap joint. Eight specimens were considered in this study as shown in Table 19. Of these, Specimens 4.7-5 and 4.7-6 were tested in Phase I.

The main motivation for these tests was the long crack arrest times at fastener holes in double lap joints with fully torqued protruding-head Hi-lok fasteners contrasted with the short arrest times in single lap joints with fully torqued flush-head Hi-lok fasteners. It was desired to find out how much of this difference is attributable to the type of fastener head used.

TABLE 19. TESTS OF SINGLE LAP JOINT SPECIMENS  
FOR EFFECT OF FASTENER HEAD TYPE

|  | Constant Amplitude<br>$S_{max} = 17 \text{ ksi}, R = 0.1$ |                   | 80-Flight Spectrum |                    |                    |
|--|---|-------------------|--------------------|--------------------|--------------------|
|  | Spec. No.   | Cycles to Failure | Spec. No.          | $S_{Ref}$<br>(ksi) | Flights To Failure |
| HL51-10 Flush-Head Hi-lok Fasteners      | 4.7-5   | 35,200            | 4.7-10             | 25                 | 28,840             |
|  | 4.7-6   | 31,100            | 4.7-11             | 30                 | 18,119             |
| HL50-10 Protruding-Head Hi-lok fasteners | 4.7-7   | 44,800            | 4.7-12             | 30                 | 20,440             |
|  | 4.7-8   | 58,600            | 4.7-13             | 30                 | 17,870             |

Figure 85 shows the results for the constant-amplitude tests. The specimens with protruding-head fasteners had slower crack growth rates and longer crack reinitiation times than those with flush-head fasteners. The differences in crack reinitiation times (cross-hatched area in Figure 85), however, were not as striking as the reinitiation time differences between the single lap and double lap joints. The bending stresses that are essentially absent in double lap joints but present in the single lap joint specimens apparently had a substantial effect on these crack reinitiation times.

Four specimens were spectrum tested, two identical specimens with flush-head fasteners and two with protruding head fasteners. It was originally planned to test one of each type at each of two reference stress levels, 25 ksi and 30 ksi. As Table 19 shows, both specimens with protruding head fasteners were tested at 30 ksi, however. The change was made because Specimen 4.7-10, tested at 25 ksi, failed in an unintended location. Failure occurred in the doubler in fastener row 3 rather than in the skin in Row 1, where the initial crack was located. The fracture surface of the failed doubler is shown in Figure 86. Failure occurred due to multiple fretting cracks which originated in the vicinity of both sides of all seven fastener holes in Row 3. Since this row of the doubler was hidden from view between the skin and the tee, no crack growth data were obtained in the failure plane of this specimen. Without these comparative data, the corresponding 25 ksi test of a specimen with protruding head fasteners seemed pointless. Therefore, a replication was run at a reference stress of 30 ksi instead.

As seen in Table 19, the lives of specimens 4.7-11, 4.7-12, and 4.7-13 were nominally the same. This is in contradiction to the differences in the constant amplitude results shown in Table 19, where the protruding head fasteners furnished slightly longer lives. Examination of the spectrum-tested specimens showed that in all four cases the cause of failure was fretting. Failure was not caused by the steady progression of the initial fatigue crack but rather by the independent initiation and growth of several fretting cracks.

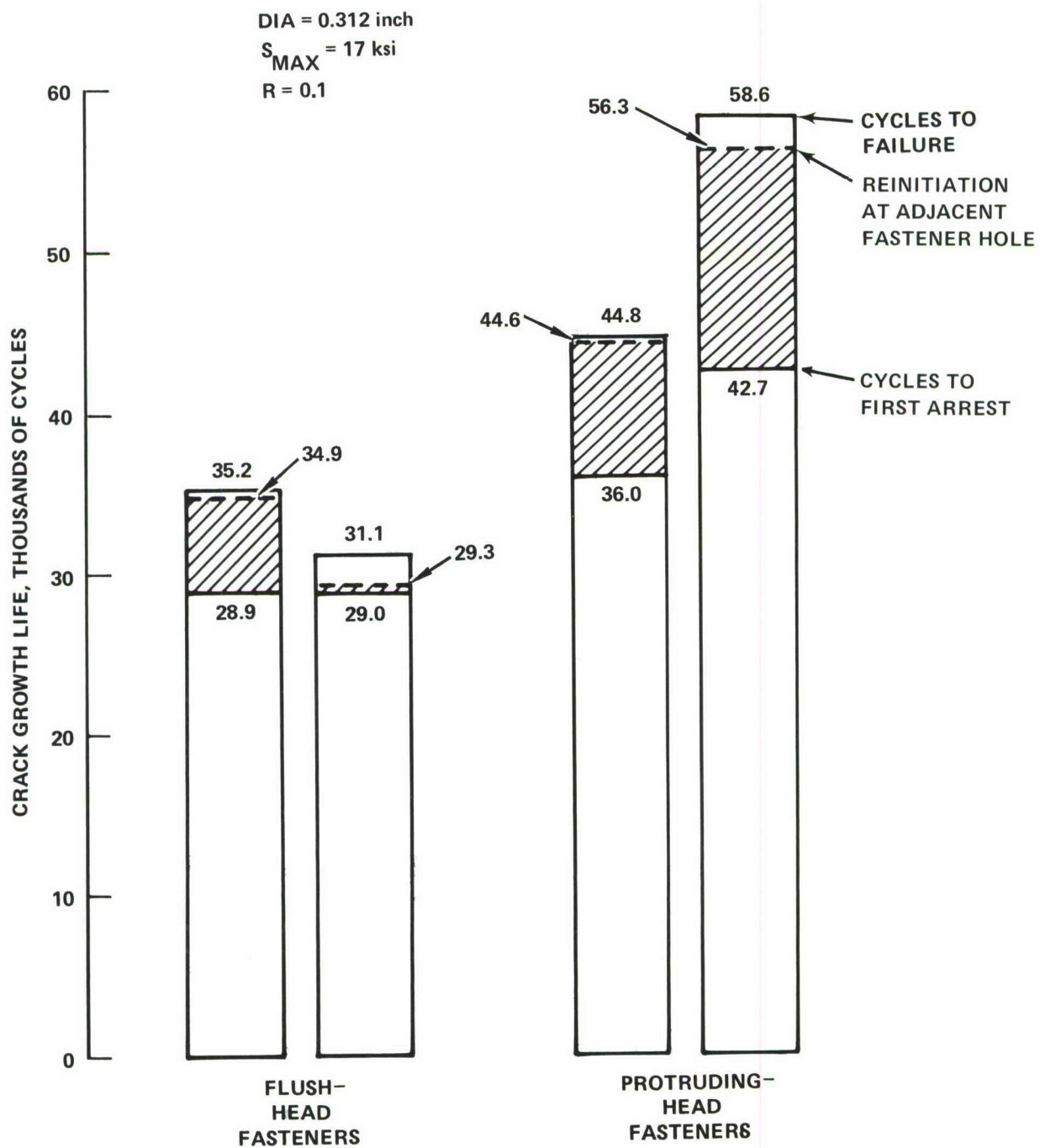


Figure 85. Effect of Fastener Head Type in Constant Amplitude Tests of the Single Lap Joint Specimen

Figure 87 shows some fretting crack origins on the fracture surfaces of specimens 4.7-12 and -13. Note in particular the thin loop of material left on the periphery of the second hole in both specimens, when the crack origin avoided the hole. Fretting cracks were present in virtually all fastener rows. The conclusion is that specimen 4.7-10 which failed in row 3 was not significantly different from the others. Fretting cracks in that specimen were also present in row 1. Although the other three specimens failed in row 1, fretting cracks were present in rows 2 and 3. In general, whether or not the actual failure occurred in row 1 or row 3 was somewhat a matter of chance. Examination of specimens 4.7-5, 4.7-6, 4.7-7, and 4.7-8 revealed fretting also, but it was not as extensive as in the specimens subjected to the spectrum loads.

The conclusion from all tests is that the protruding head fasteners seem to offer a slight advantage with respect to fatigue crack reinitiation and propagation. However, the primary differences between the results of the single lap and double lap joint tests of Phase I were due to bending. Moreover, if failure is caused primarily by fretting at the faying surface, little if any advantage can be gained by using protruding head fasteners. It should be pointed out that the differences shown between the flush head and protruding head constant-amplitude test results (4.7-5, 4.7-6, 4.7-7, 4.7-8) are on the order of what could be predicted by considering the increase in net section stress caused by the countersink for the flush head fasteners.

### 3.2 Spectrum Tests of Joint Specimens

The 80-flight loading sequence discussed in Section II, Paragraph 3.1 was used to test four single lap joints, as tabulated in Table 19, and two double lap joints. The two double lap joints, Specimens 4.6A-9 and 4.6A-10, were identical to Specimens 4.6A-3 and -4, which were constant amplitude tested. There was a 0.050-inch corner crack in Fastener 3 of Row 2 of each doubler. All fasteners were clearance-fit Hi-loks with a low installation torque of 40 to 45 inch-pounds. There were no razor-induced continuing damage flaws. This is damage condition B in Figure 5.

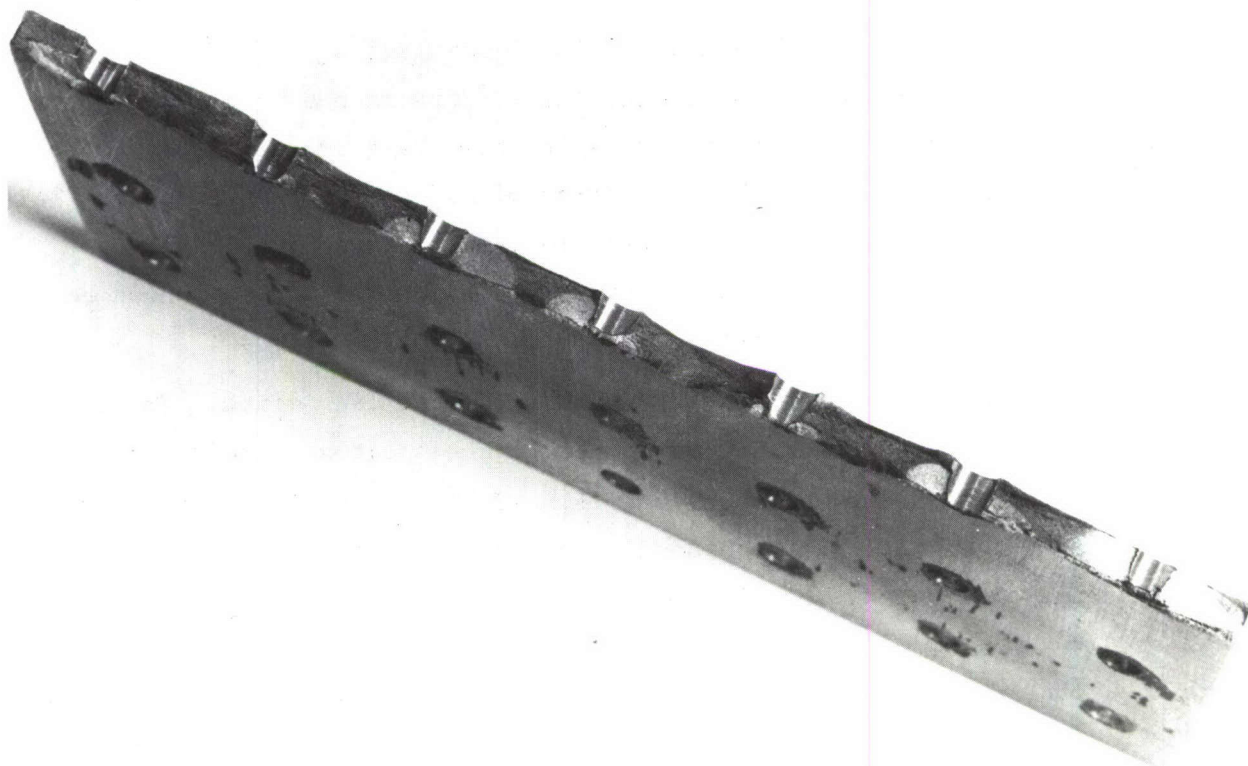


Figure 86. Two Fretting Cracks at Each Hole in the Fracture Surface of the Doubler of Specimen 4.7-10.

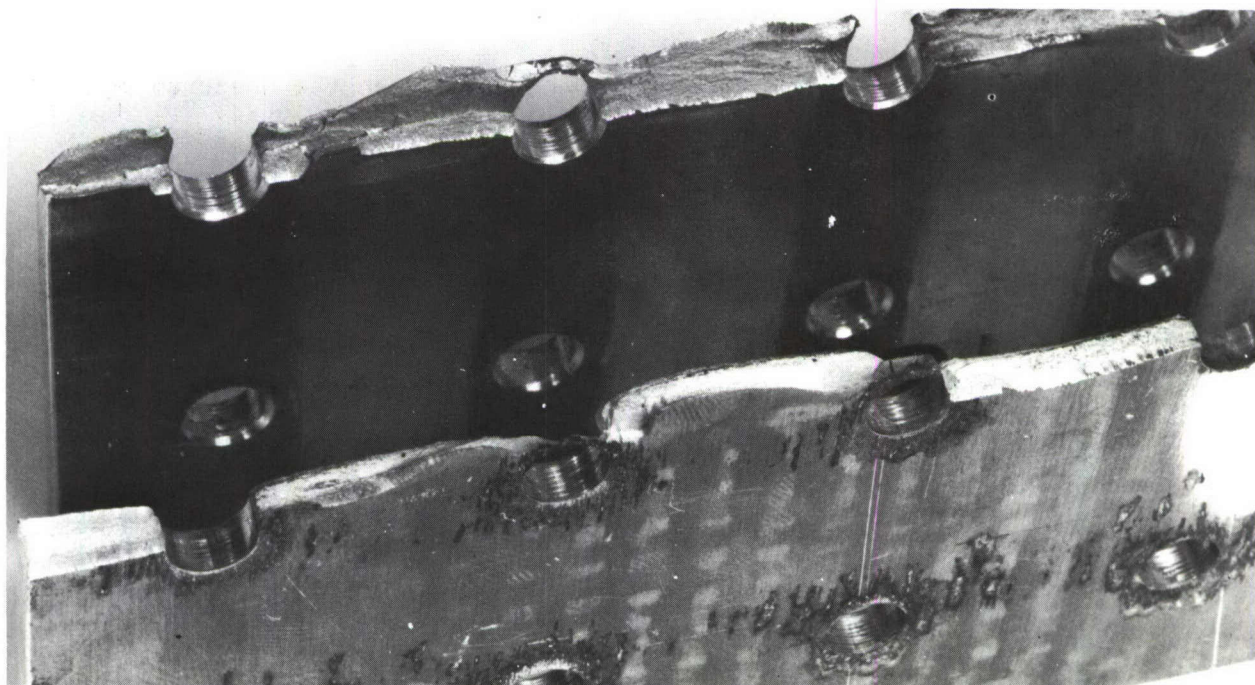


Figure 87. Fretting Crack Origins in the Skin Near the Hole Periphery in Specimen 4.7-12 (Front) and 4.7-13.

Thus for all spectrum tests of joints there were prior constant amplitude test results for the same configuration. The Equivalent  $k_t$  and Equivalent Stress Intensity Factor methods described in Section V, Paragraph 6 were used to predict the crack growth lives. As seen in Figure 88, results from these two first-order prediction methods were within about a factor of 2.0 of the test results. This agreement was achieved despite the greater tendency toward fretting in the single lap joints when subjected to spectrum loading. The methods would be expected to break down when a change in failure mechanism occurs.

The predictions were least accurate for the double lap joints. For this case the prediction was based only on the constant amplitude result for Specimen 4.6A-4, since the replicate specimen, 4.6A-3, lasted much longer and seemed inconsistent with all the other data as discussed in Section VII, Paragraph 1. However, consider in Figure 84 the result from the third replication of this test. Specimen 4.6A-12 from Reference 71 had a life significantly longer than 4.6A-4, suggesting that 4.6A-4 was on the short-life end of the probability distribution. If the spectrum predictions for Specimens 4.6A-9 and -10 were recomputed based on the average constant amplitude life of either all three specimens or just Specimens 4.6A-4 and 4.6A-12, the predictions would be much more accurate.

The degree of difference in failure mechanism between the spectrum and constant amplitude single lap joint tests was discussed in the preceding subsection. There was an increased tendency to develop fretting cracks remote from the initial crack in the spectrum tests. However for both loading conditions the initiation of multiple cracks at random locations was evident.

Similarly in the double lap joints, one of the two specimens that was spectrum tested failed across Row 4 in the skin instead of through Row 2 in the doublers where the precracks were located. There appear to have been no skin cracks in the corresponding constant amplitude specimens, 4.6A-3 and 4.6A-4. In both these specimens however, cracks independent of the main initial cracks did occur. These cracks were in the doublers in Fastener Row 3, but the final failures of the doublers occurred in the precrack plane in Row 2.

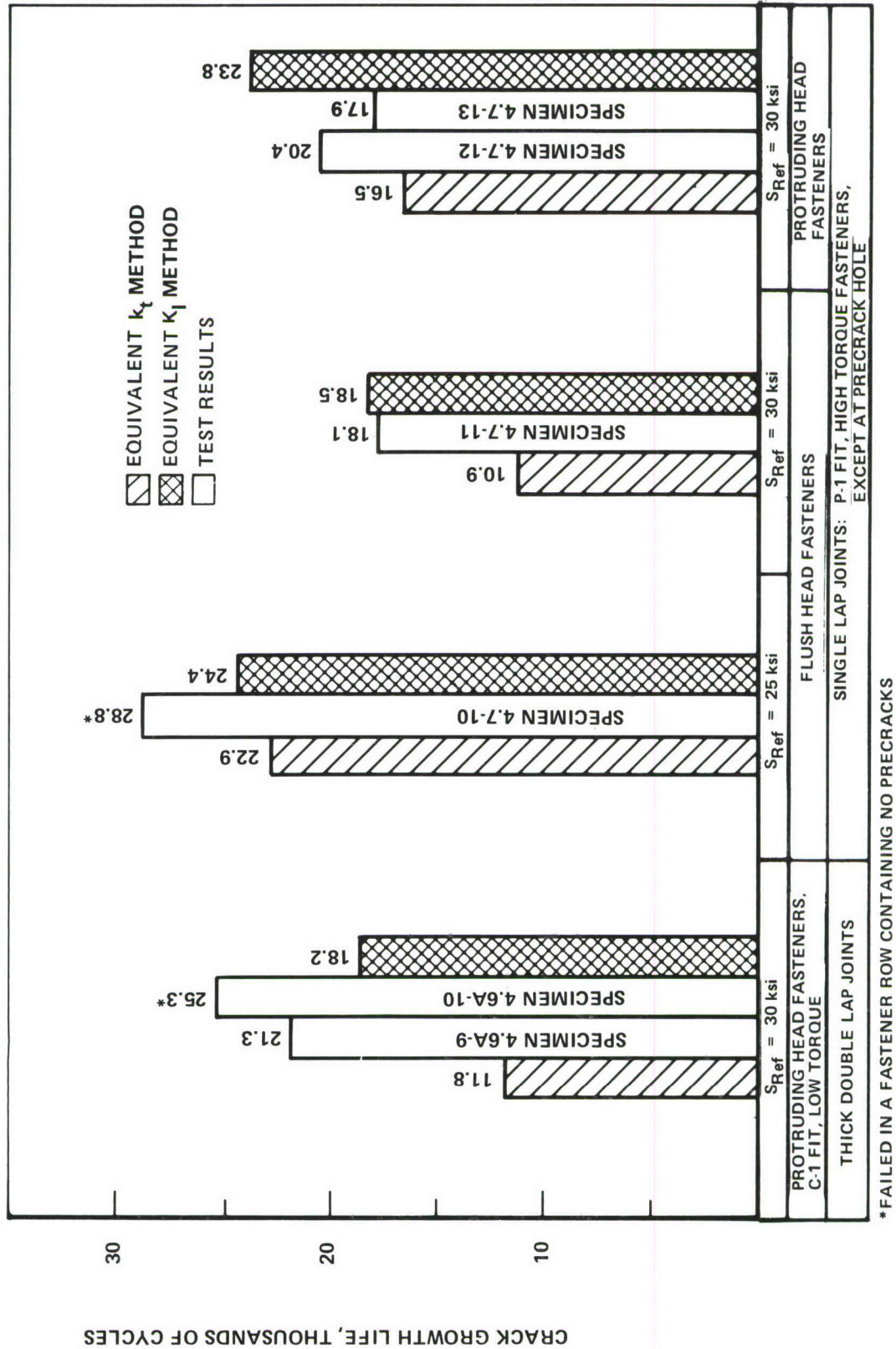


Figure 88. Spectrum Test Lives and Life Predictions

The fracture surface of the failed skin in Specimen 4.6A-10 (Figure 89) shows fatigue cracking from the outermost hole to the edge. On the opposite side of that hole, three surface flaws about 0.070 inch deep combined, tunneled ahead another 0.070 inch in one jump, and did not even break through the thickness before propagating unstably to the next hole. The unstable fatigue crack evident at the next adjacent hole is a mid-thickness surface flaw only about 0.03 inch deep and 0.1 inch long in the thickness direction. The rest of the fracture surface is a static fracture except for surface flaws 0.01 inch or less along the edges of some of the holes.

From these considerations of the fracture surface it is concluded that the failure resulted primarily from the skin crack that initiated at an outer fastener hole and grew to the specimen edge. The reinitiation and subsequent growth of this crack led rapidly to total specimen failure. It seemed surprising that so small a crack could be so critical, but the following analysis verifies the possibility.

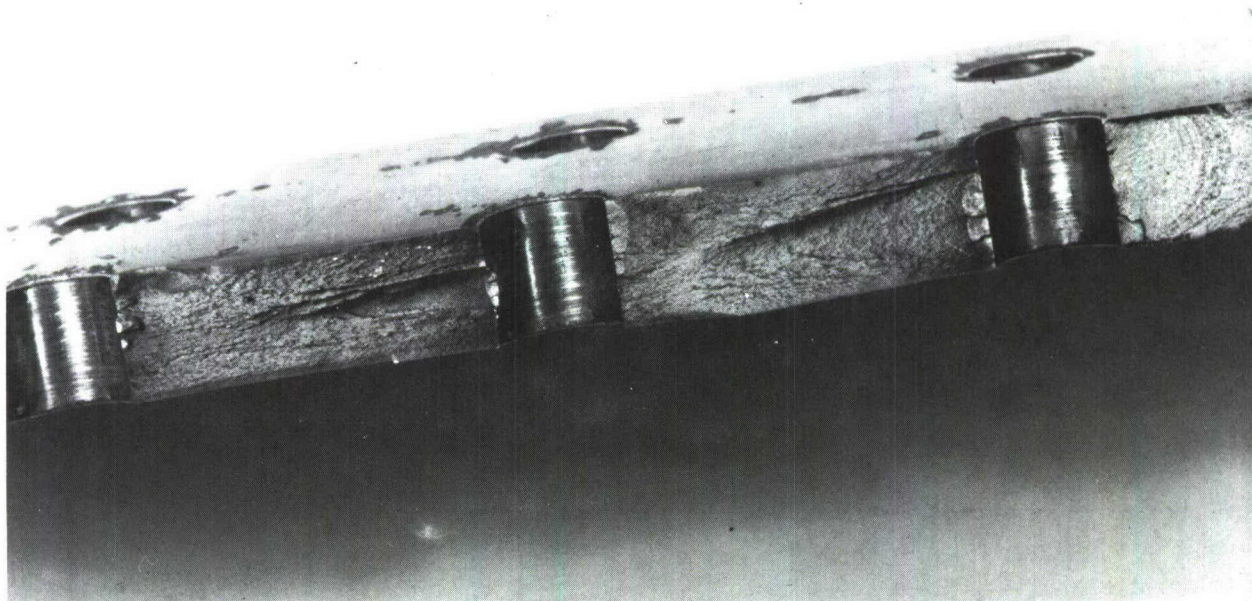
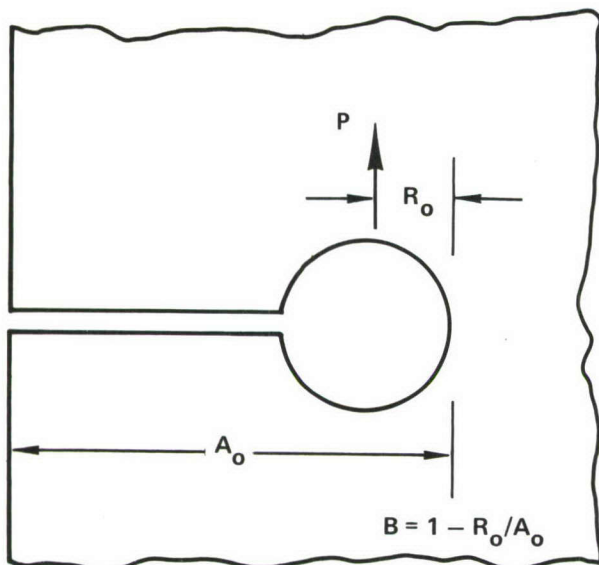
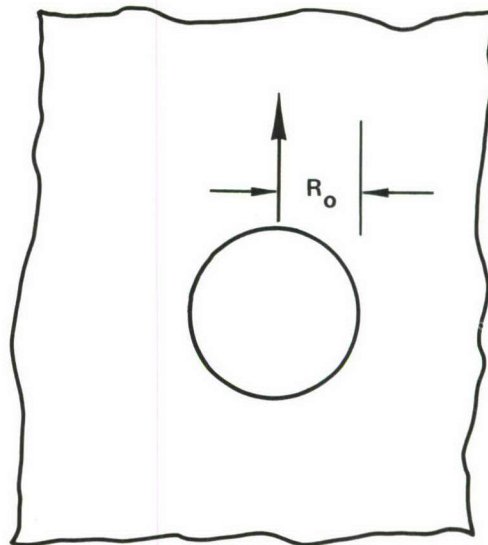


Figure 89. Failed Skin in Spectrum-Loaded Specimen 4.6A-10.



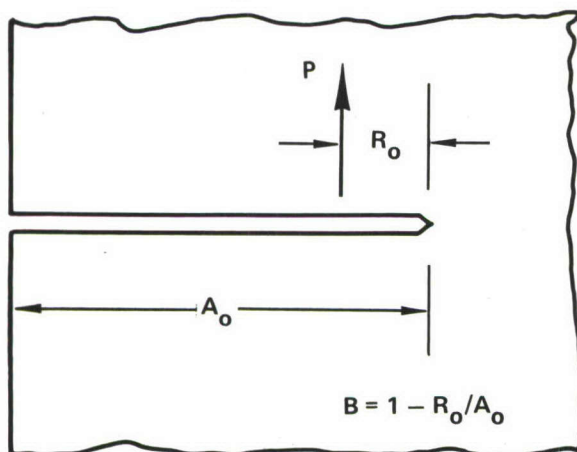
$$k_{tb}^{(A)} = k_{tb}^{(B)} \frac{K_I^{(C)}}{K_I^{(D)}}$$

$$k_{tb}^A = \frac{2.6 - 1.08B^2 + 0.48B^3}{\sqrt{1+B}}$$



$$k_{tb}^{(B)} = 1.0$$

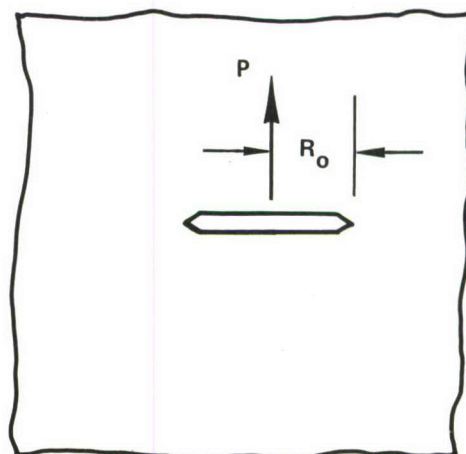
(REFERENCE 49)



$$K_I^{(C)} = \frac{P}{t \pi A_o} \left[ \frac{(1.3 - 0.54B^2 + 0.24B^3)}{\sqrt{1-B^2}} \right]$$

(REFERENCE 43)

(THE TERMS IN PARENTHESES ARE A POLYNOMIAL FIT TO A PLOT APPEARING IN REFERENCE 43)



$$K_I^{(D)} = \frac{P}{2t \sqrt{\pi R_o}}$$

(REFERENCE 43)

Figure 90. Bearing  $k_t$  for a Fastener Hole with a Crack from Hole to Edge (by Ratio Method of Figure 14)

The stress severity factor  $\lambda$  at the hole when the crack reached the edge is calculated from Equation (5) assuming equal load transfer at every fastener and using the following:

$$\alpha = 1.06, \beta = 1.0, \theta = 1.07 \text{ (Table 6)}$$

$$A_o/R_o = 5$$

$$k_{tg} = 1.1215 k_t^{(1)} \gamma_{o-o} = 6.35 \text{ (Equations (11, 13))}$$

$$k_{tb} = k_{tb}^{(A)} = 1.61 \text{ (Figure 90)}$$

From this a value of 8.7 is computed for  $\lambda$ , and the effective peak notch stress for  $S_{Ref} = 30$  ksi is  $\lambda S_{Ref} = 261$  ksi. From Figure 48 this corresponds to a crack initiation time of under 700 flights. Crack instability for this reinitiated crack occurs when the stress intensity versus crack length curve (calculated for short cracks from Equation (20) using  $\lambda/\alpha\beta$  in place of  $k_t$ ) is tangent to and above the crack growth resistance curve for the 0.386 inch plate in Figure 46. For a stress of 30 ksi the unstable crack size, measured from the edge of the hole, is thereby calculated to be 0.003 inch. The next fastener hole in the crack path would not be expected to arrest this running crack for more than a few flights if at all.

#### 4. SUMMARY OF CONCLUSIONS FROM TESTS OF JOINTS

The following observations and conclusions result from the testing and analysis of these joints:

- Fastener torque and faying surface friction effects in an unsealed joint can lead to long crack growth lives and shift the failure mechanism from failure by progressive cracking across the fastener holes to failure due to fretting cracks. Faying surface sealant (Reference 71) seems to protect small cracks against environmental attack but compromises the beneficial effects of faying surface friction. Analytical methods are not currently available to account for the effect of fastener torque and faying surface friction.
- If there are high bending stresses, there is an increased tendency for multiple cracks to initiate at the fastener holes. For example, while the central fastener in Row 1 of the skin contained the

precrack in single lap joint specimen 4.7-10, failure occurred in the doubler across Row 2 by the coalescence of 14 cracks, one on each side of all seven holes in the failed row.

Similarly, when the fasteners are not fully torqued in the double lap joints the crack initiation time at the holes becomes less than the growth time from hole to hole. For example, at  $S_{\max} = 17$  ksi,  $R = 0.1$  and low fastener torque, there was little difference between test lives for double lap joint specimens with or without continuing damage flaws because of such multiple crack initiations.

For both of these cases, the initial flaw condition was unimportant, because failure occurred due to independent cracks at several fastener holes.

- Friction under the head or collar of the fully-torqued fastener helps to retard the reinitiation of the crack. Faying surface friction also has a role in postponing reinitiation. Occasionally the collar can crack, allowing the opening and closing deformations that lead to reinitiation. Improvements to the fatigue design of the Hi-lok collar may be worth considering.
- Spectrum loading was observed to have three possible effects:
  - Caused more of a tendency toward fretting cracks near the holes in single lap joints.
  - Had a predictably shorter critical crack size due to a spectrum maximum stress of 30 ksi compared to a constant amplitude maximum stress of 17 ksi.
  - Had a fairly predictable crack growth life, based on the complementary constant amplitude test result, even when the failure mechanism was different from the anticipated.
- Standard prediction techniques were accurate within about a factor of two for joints, except in dry (unsealed) fully-clamped joints without much transverse bending where faying surface friction and fastener head friction must be accounted for. When bending is present, it seems to accelerate both crack initiation and growth. From Reference 71, compression - tension loading of a double-lap joint can apparently be accounted for using the effective stress concept, Equation (90).

- Scatter in these tests was reasonably low, except for replicate specimens 4.6A-3 (93,400 cycles to failure), 4.6A-4 (35,900) and 4.6A-12 (54,700). (Specimen 4.6A-12 was fabricated and tested later for Reference 71.) When speaking of scatter, it is important to emphasize that some of the controls on machining and assembly of these specimens were more stringent than the controls used in machining and assembly of aircraft structure. Also, except for Specimen 4.6A-12, each pair of replicate specimens was precracked, machined and assembled at about the same time and on the same setup. Therefore it would be wrong to assume that the scatter in these tests is equal to the scatter of crack growth in aircraft structural joints.

## SECTION VIII

### STRINGER-REINFORCED PANELS

Forty-two stringer-reinforced panels with 0.050-inch fatigue-induced precracks were fatigue tested to failure. The test variables and test plan are discussed in Section II. Sections III, IV and V give the background on predictions and the baseline data. Fabrication and test procedures are described in Section VI. Volume II of this report contains a specimen-by-specimen tabulation of the test data and graphical comparison of the experimental crack growth to the predicted crack growth.

As discussed in Section II, four different 18-inch-wide specimen configurations were tested. Two had a central tee stringer only, the continuous-skin reinforced panel (type 4.8-1-X) and the split-skin reinforced panel (type 4.8-3-X). The edge stringer specimen (type 4.9-X) contained 0.250-inch angle stringers on either edge, each with a 3.25-inch-wide strip attached to the protruding leg to simulate the presence of a shear web at the front or rear spar of an aircraft wing. The two-bay specimen (type 4.10-X) was a split-skin type having both a central tee stringer across the split line and edge angle stringers with simulated shear webs on either edge of the panel.

#### 1. CENTER STRINGER SPECIMENS

##### 1.1 Panel Strains and Lateral Deflections

The design of Specimen types 4.8-1 and 4.8.3 included a system of doublers in the grip. One purpose of these doublers was to increase the load-carrying area of the specimen near the grips. Also, the doubler thicknesses were selected so that the average centroid in the test section was coplanar with the centroids at the two grips. This minimized the transverse bending. However, bending was not eliminated.

Figure 91 shows maximum lateral deflections measured in the test section at various points across the specimen width. The across-the-width variation in the location of the elemental centroid causes the specimen center to deflect one way and its edges to deflect oppositely.

Strain gages were placed on Specimen 4.8-1-2 in the locations shown in Figure 92. Measurements were taken at various times throughout the test. The measured strain ranges,  $\Delta\epsilon$  are presented in normalized form in Figure 92. The numbers in parentheses are  $E\Delta\epsilon/\Delta S$  where  $E = 10^7$  psi and  $\Delta S$  is the applied gross area stress range, 15.3 ksi. These parenthetical numbers would all be 1.0 if the strains in the specimen were all uniformly distributed and there were no holes or cracks.

The strain gage readings prior to macrocracking indicate that the strains were lower in the stiffened central region. These lower strains probably occurred because the protruding flange of the stringer was not picked up directly by the grips, and the specimen length between grips was too short to fully compensate for this. The nonuniformity of initial strains was not taken into account in the crack growth predictions.

## 1.2 Test Results, Continuous Skin Specimens

Twelve continuous-skin tee-reinforced specimens were cycled at constant amplitude at a maximum gross area stress of 17.0 ksi and  $R = 0.1$ . At various times throughout the tests marking cycles ( $S_{\max} = 17.0$  ksi,  $R = 0.82$ ) were used in an attempt to mark the fracture surface. These marking cycles had not been successful in testing the joints but were successful for these center-stringer tests.

Figure 93 summarizes the test lives for these specimens. The lives ranged from 19,000 cycles for Specimen 4.8-1-8, which had double outside cracks and continuing damage flaws, to 55,400 cycles for Specimen 4.8-1-6, which had a single inside crack in the tee only.

The analysis described in Section V, Paragraph 3. was applied to predict the growth of the initial crack and the crack initiation time on the opposite side of the precracked hole. The predicted and actual crack growth histories are

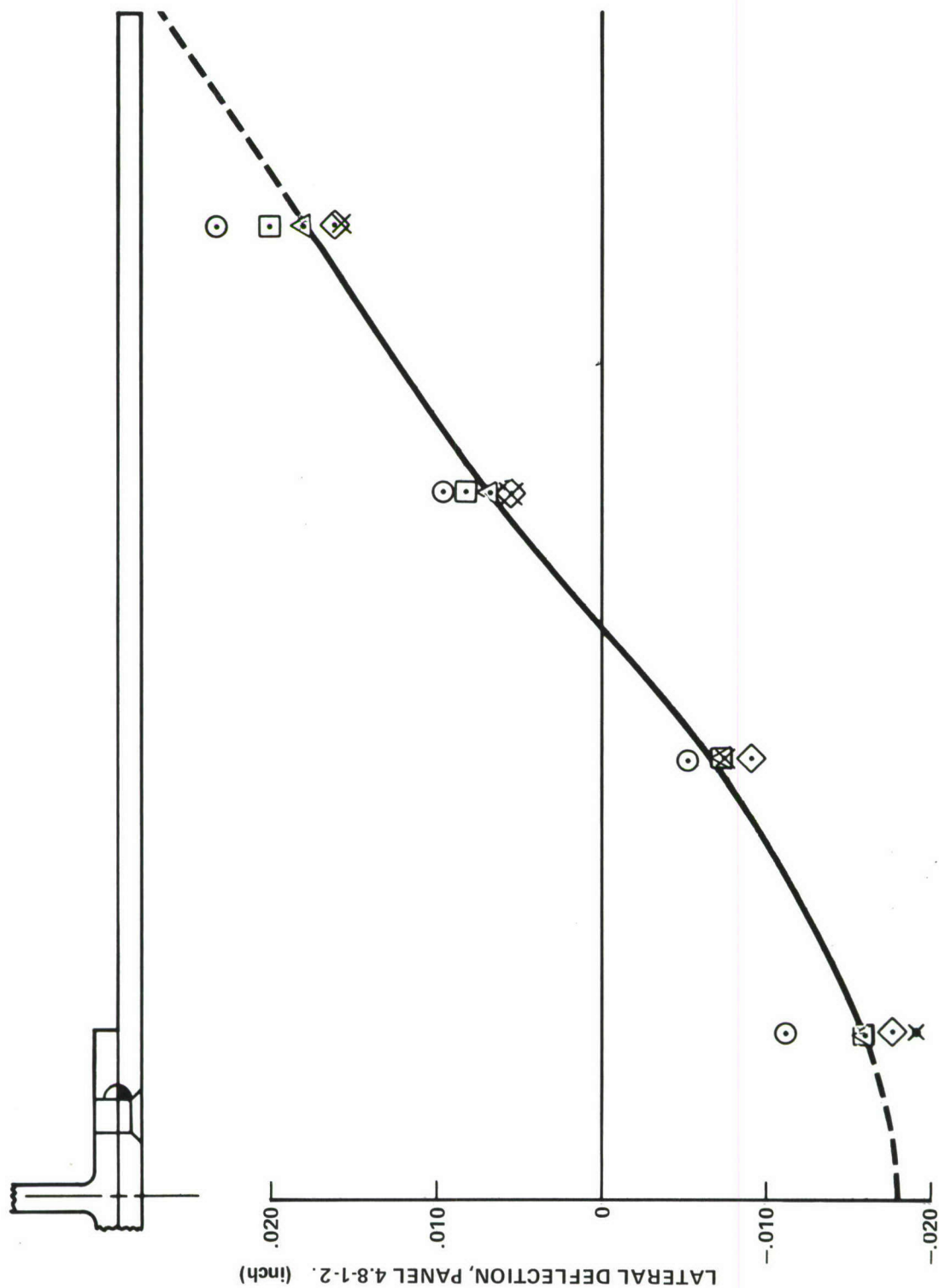


Figure 91. Lateral Deflection of Points Across the Width of the Test Section, Specimen 4.8-1-2

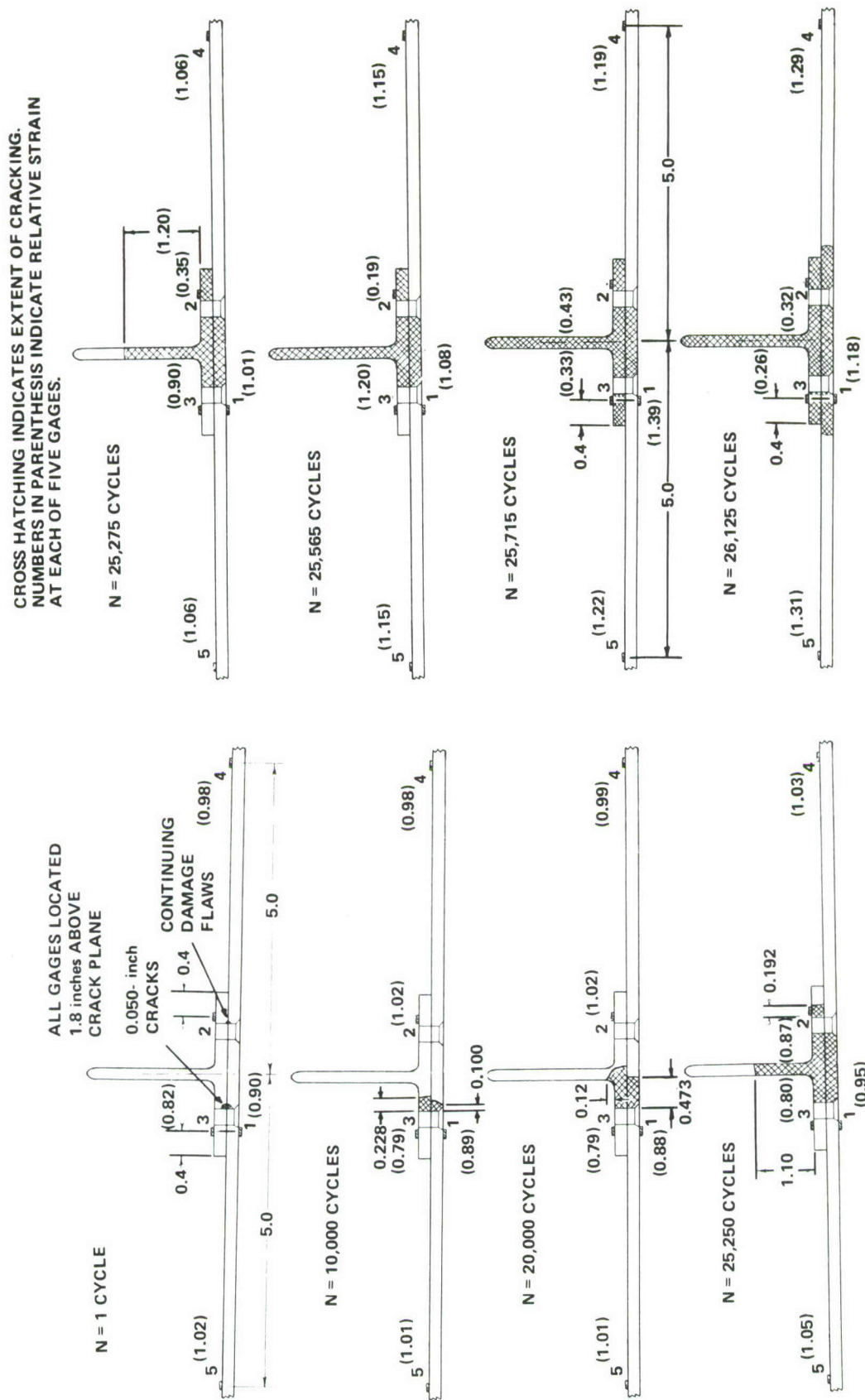


Figure 92. Strain Gage Data for Tee-Reinforced Specimen 4.8-1-2



compared in Figures 94 through 97. Figure 98 compares the predicted and actual crack initiation times.

The term crack length does not have a unique definition. For the purpose of predictions the crack length is as would be measured on the faying surface. The initial length of this crack was 0.050 inch. The test data, however, are visual observations, taken on visible outer surfaces. The initial visible crack length was always zero. Thus even a perfect prediction would appear to overestimate crack size for about the first 0.20 inch of crack growth. Thereafter the crack was through-the-thickness and of approximately equal length on both surfaces.

Differences in the type of fastener used in the hole adjacent to the flawed hole did not lead to differences in crack growth behavior or crack growth life. (Compare 4.8-1-3 and -4 with -5 and compare 4.8-1-9 with -11.)

Specimens with a crack in both members had much shorter crack growth lives than comparable specimens with a crack in just one member. (Compare 4.8-1-3, -4 and -5 with -6 and compare 4.8-1-9 and -11 with -12.)

Specimens 4.8-1-7 and -8 with continuing damage flaws on the opposite side of the precracked hole had significantly shorter lives than comparable specimens 4.8-1-9 and -11 without continuing damage flaws. However, crack growth for Specimens 4.8-1-1 and -2 with continuing damage flaws only at the hole adjacent to the precracked hole was not significantly different from that for Specimens 4.8-1-3, and -4 and -5.

Scatter between duplicate tests was low except for a factor of 1.6 difference in crack growth life between Specimens 4.8-1-9 and -10. The difference, as seen in Figure 96, was in the time required for the flaw to reinitiate on the opposite side of the precracked hole. In Specimen 4.8-1-9 this flaw did not initiate until after 31,600 cycles. By that time the skin crack was 1.1 inches long and the tee crack had long since broken through to the free edge. In specimen -10 this flaw initiated almost immediately. Figure 99 shows that this secondary flaw became visible even earlier than did the continuing damage flaws in Specimens 4.8-1-7 and -8. Note, in fact, that the entire behavior of Specimen 4.8-1-10 was similar to that of the continuing damage cases. Even the total test lives agreed.

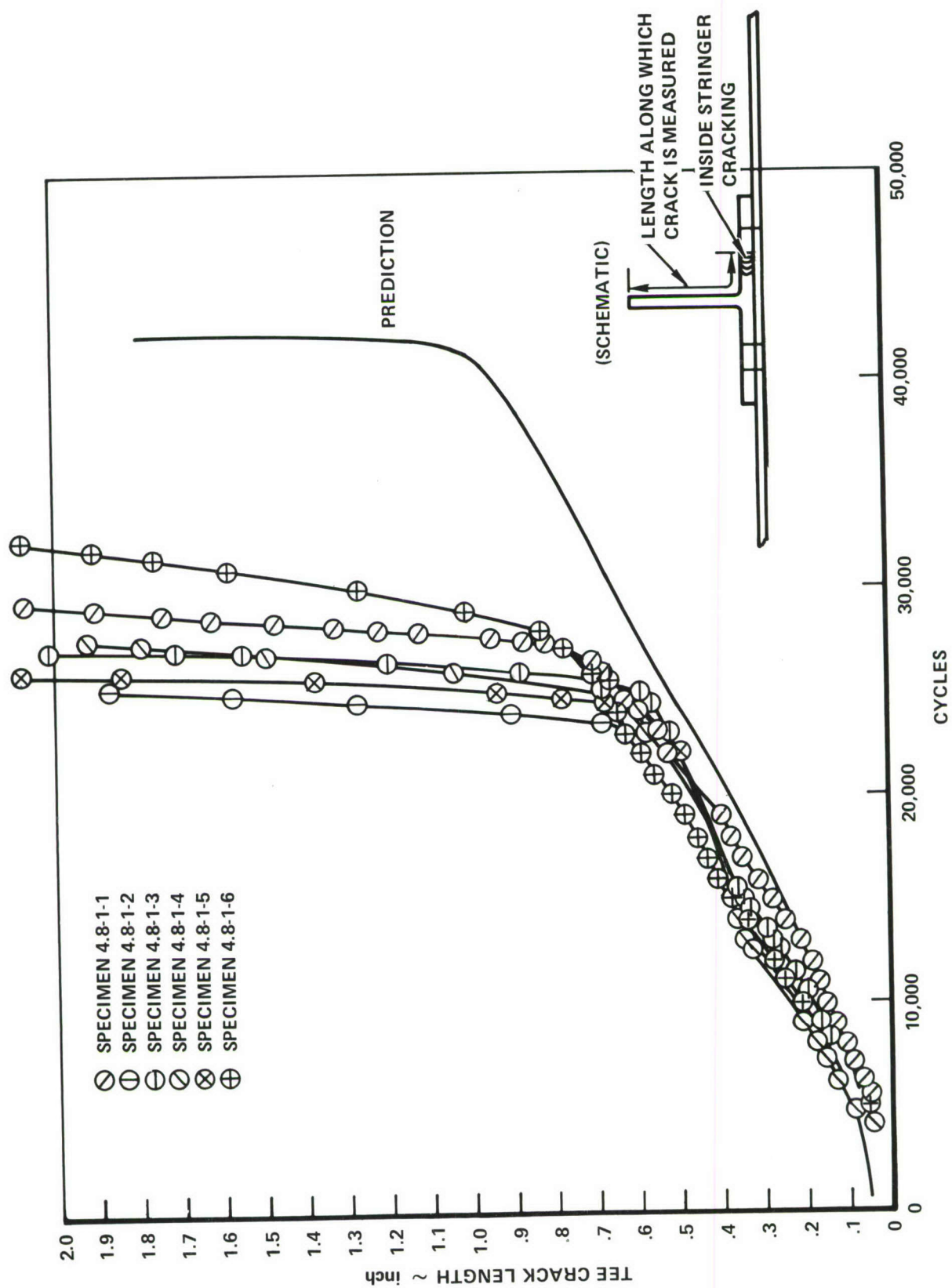


Figure 94. Crack Growth Prediction and Test Results, Inside Crack in Tee

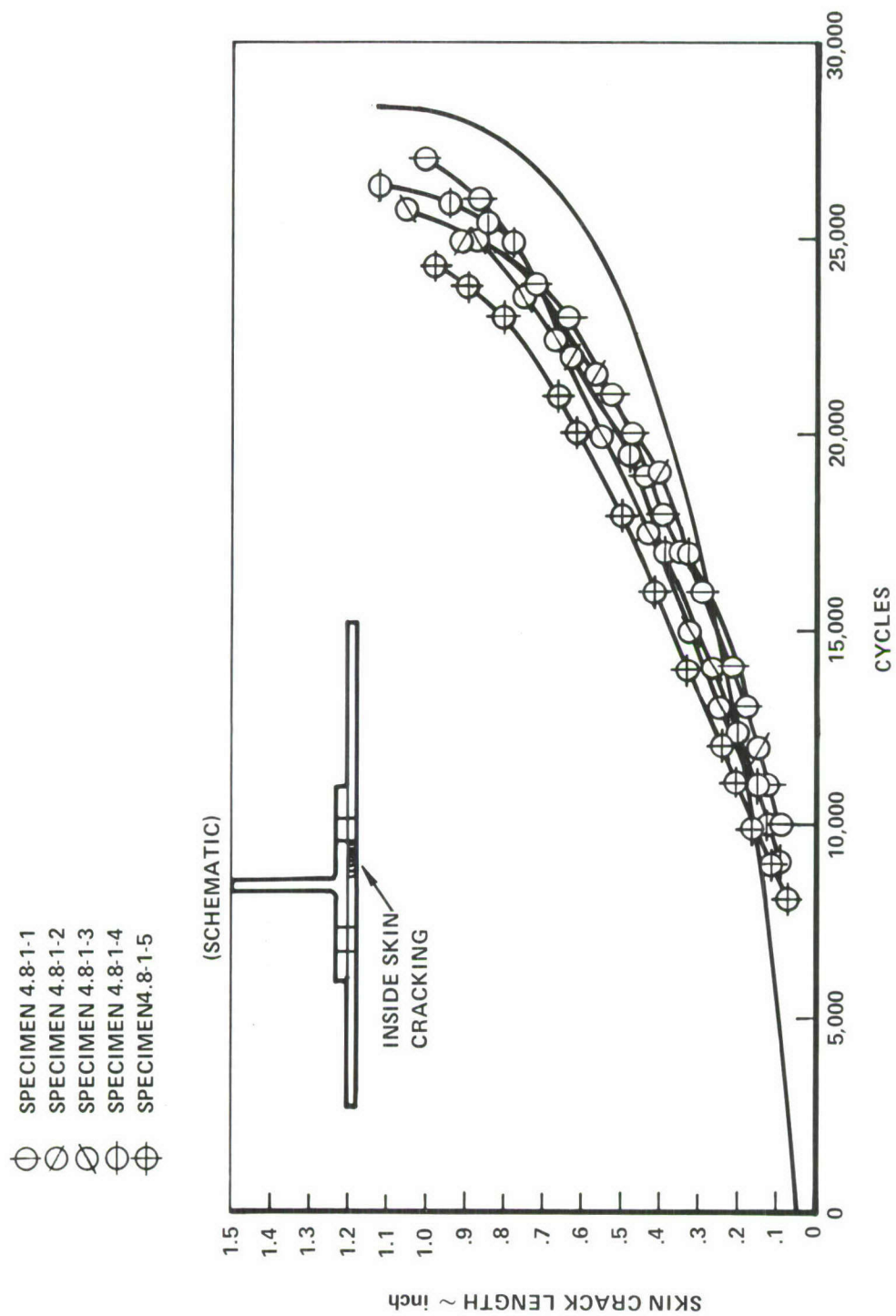


Figure 95. Crack Growth Prediction and Test Results, Inside Crack in Skin

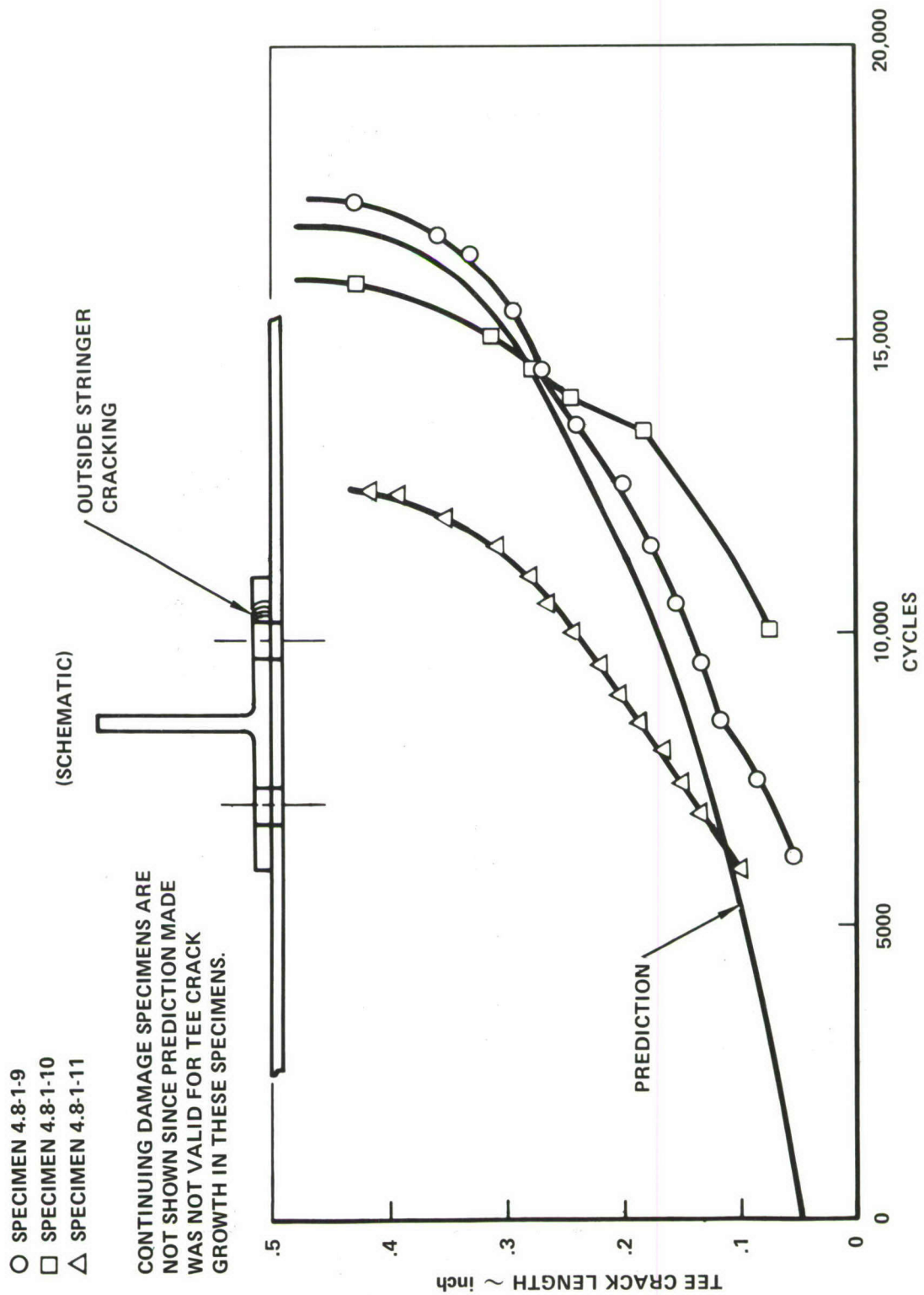


Figure 96. Crack Growth Prediction and Test Results, Outside Crack in Tee

# SKIN CRACKING, PREDICTION VS. TEST, OUTSIDE CRACKING

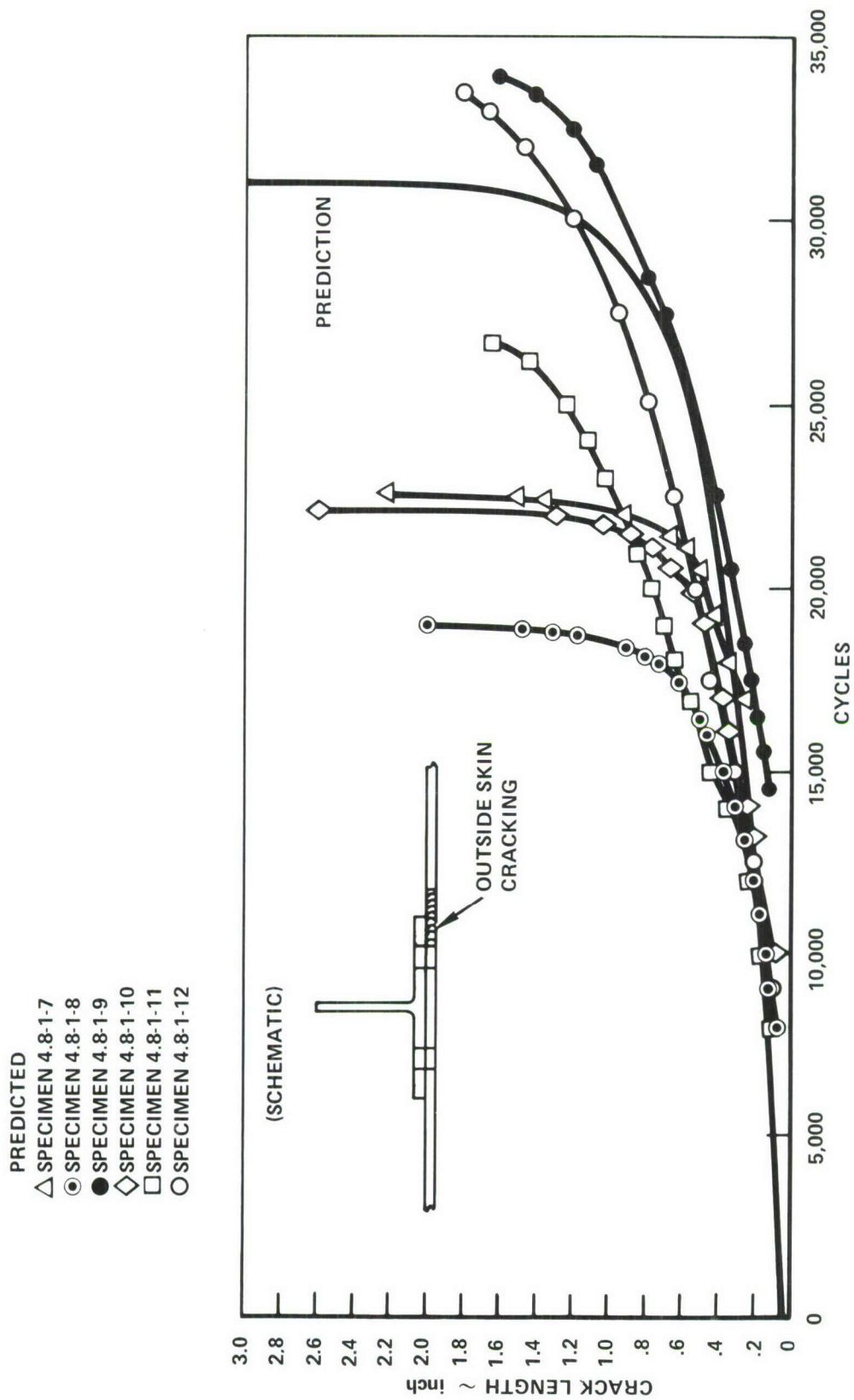


Figure 97. Crack Growth Prediction and Test Results, Outside Crack in Skin

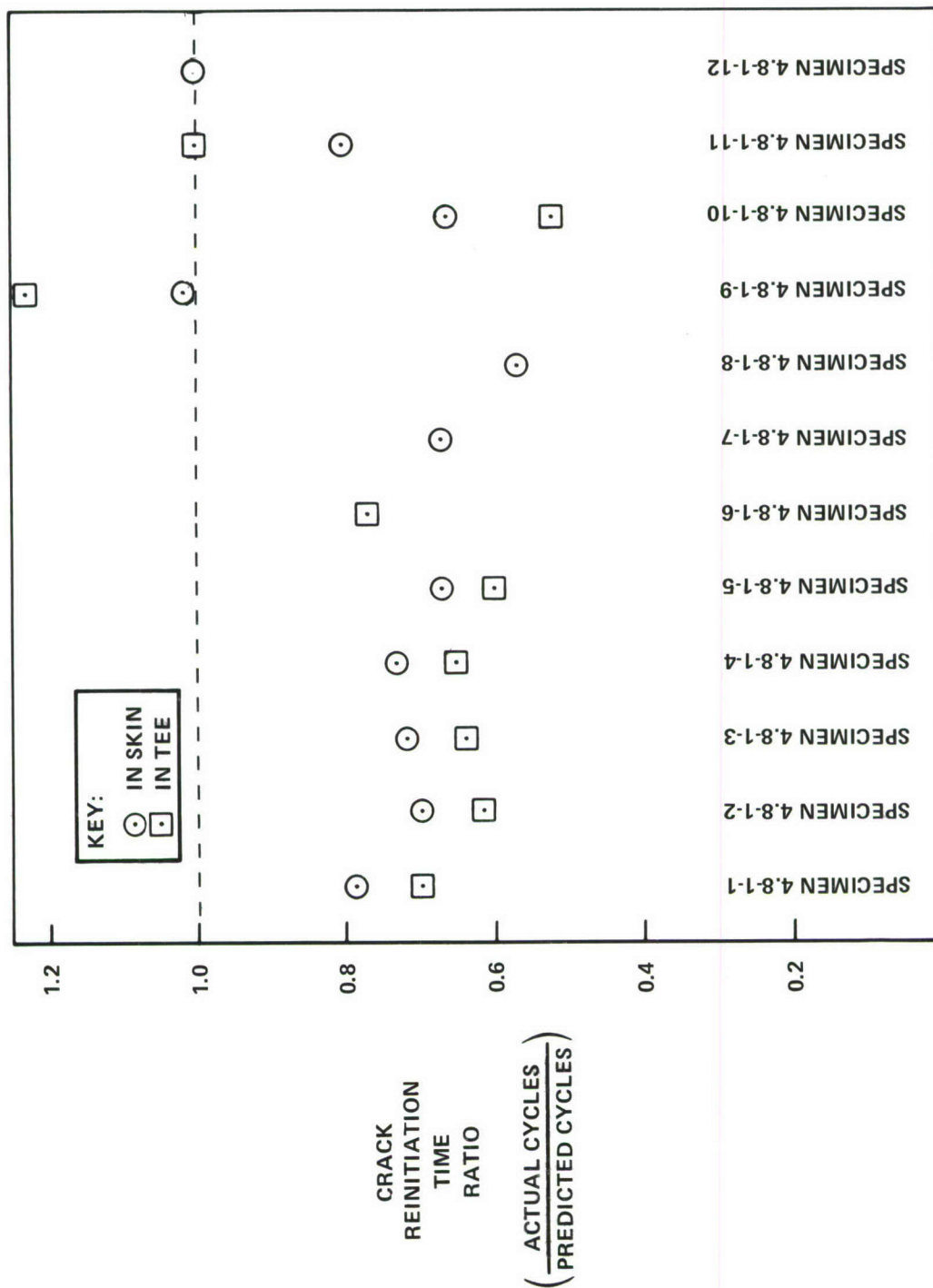


Figure 98. Crack Reinitiation Times on the Undamaged Side of the Precracked Hole, Specimen Type 4.8-1

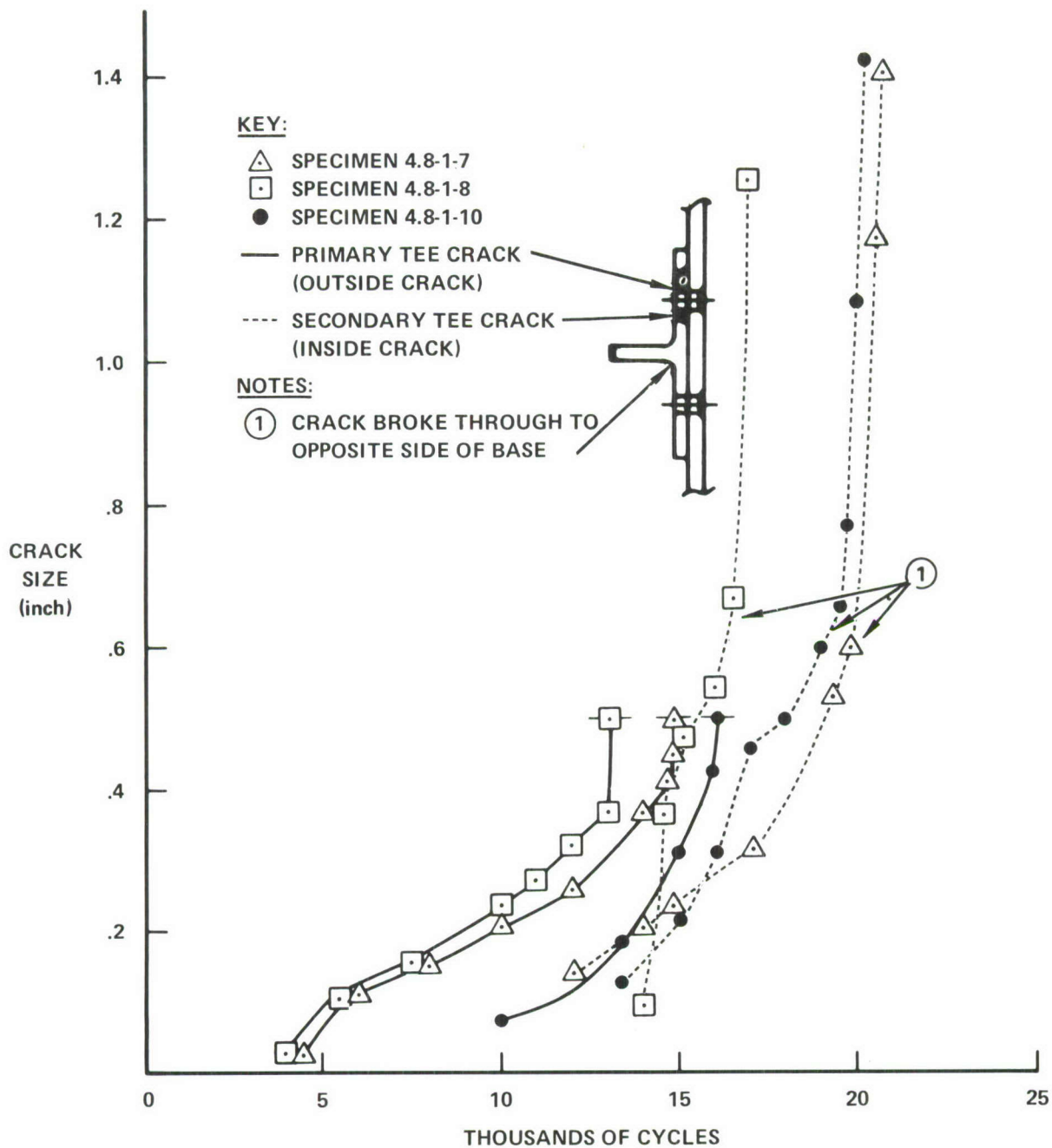


Figure 99. Comparison of Crack Growth in Tee Stringer in Specimens 4.8-1-7, -8 and -10

Since the data seemed to suggest that a defect of some sort had been present at the origin site of the secondary flaw in the tee stringer of Specimen 4.8-1-10, the fracture surfaces were examined. It appears that the secondary crack originated at a material defect. On one fracture surface there appears to be a void about 0.015 inch across, located on the edge of the hole, about 0.010 inch from the faying surface. A congruent inclusion appears to be present at the same location on the opposite fracture surface. Judging from the data, this material defect in the tee extrusion is comparable in severity to a 0.005 inch continuing damage crack.

### 1.3 Test Results, Split Skin Specimens

In Phase I testing 12 split-skin, tee-reinforced specimens were cycled at constant amplitude with  $S_{\max} = 17.0$  ksi and  $R = 0.1$ . Marking cycles ( $S_{\max} = 17.0$  ksi,  $R = 0.82$ ) were used successfully at selected times during the testing. Predictions and crack growth data for these specimens are compared in Figures 100 through 103.

A predicted crack growth sequence for the inside skin crack is plotted in Figure 100. The 0.050-inch initial corner crack was predicted to start at the fastener hole and grow to the edge of the skin, where it is arrested. According to the prediction, it is another 8,924 cycles before the crack reinitiates on the opposite side of the hole. It then quickly grows to the outer edge of the skin, causing the specimen to break.

This prediction turned out to be excellent for Specimens 4.8-3-3, -4, and -5, which had an initial 0.050-inch crack in both the tee and the skin. All three specimen lives were predicted within 13 percent.

This prediction is not applicable to the other three inside crack cases. Specimen 4.8-3-6 had no initial skin crack, only a crack in the tee. Specimens 4.8-3-13 and -14 had initial continuing damage flaws in the skin on the opposite side of the fastener hole containing the primary flaw. Both skin flaws grew simultaneously and unsymmetrically in each of these two specimens.

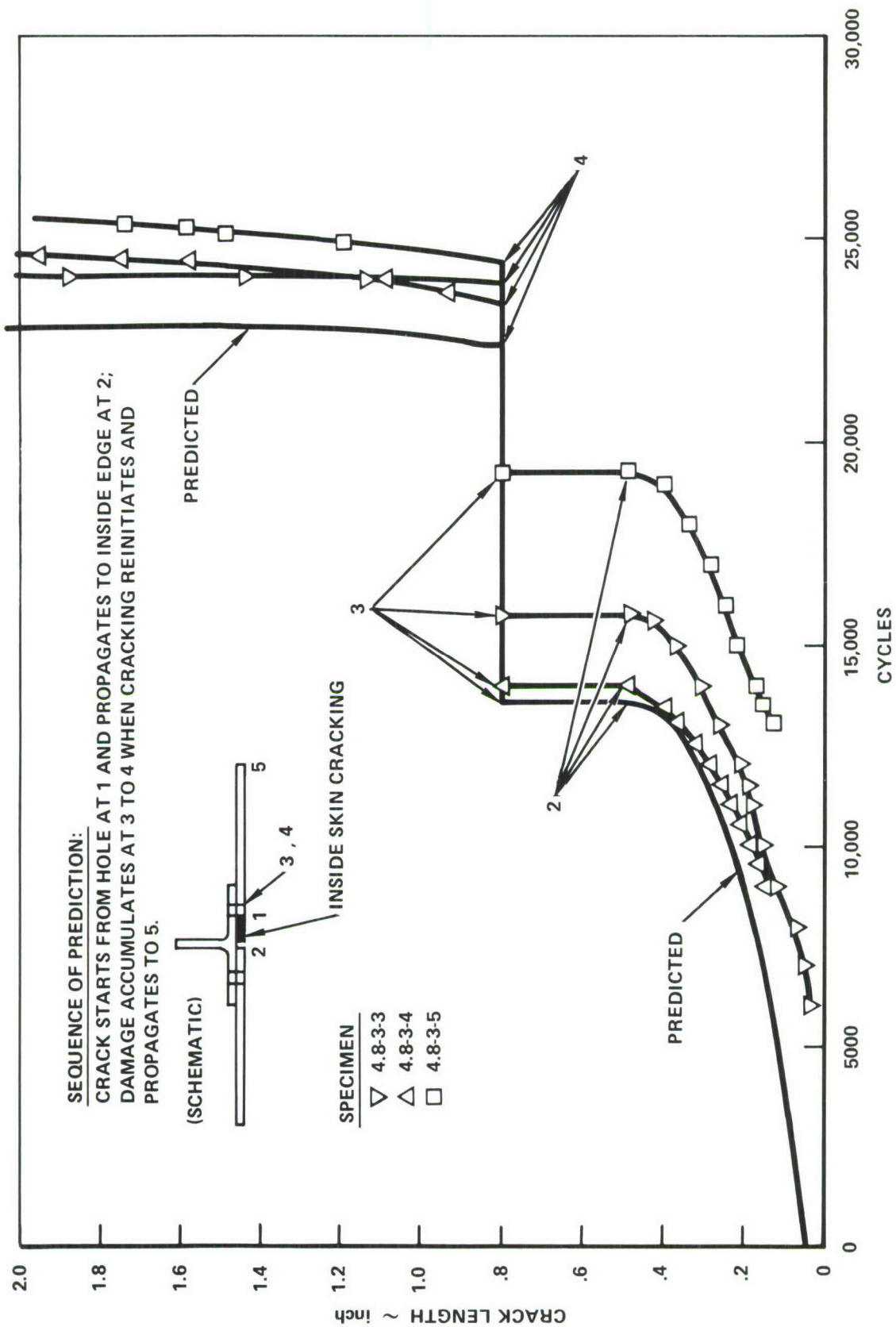


Figure 100. Crack Growth Results, Inside Crack in Skin, Spanwise Splice Specimens

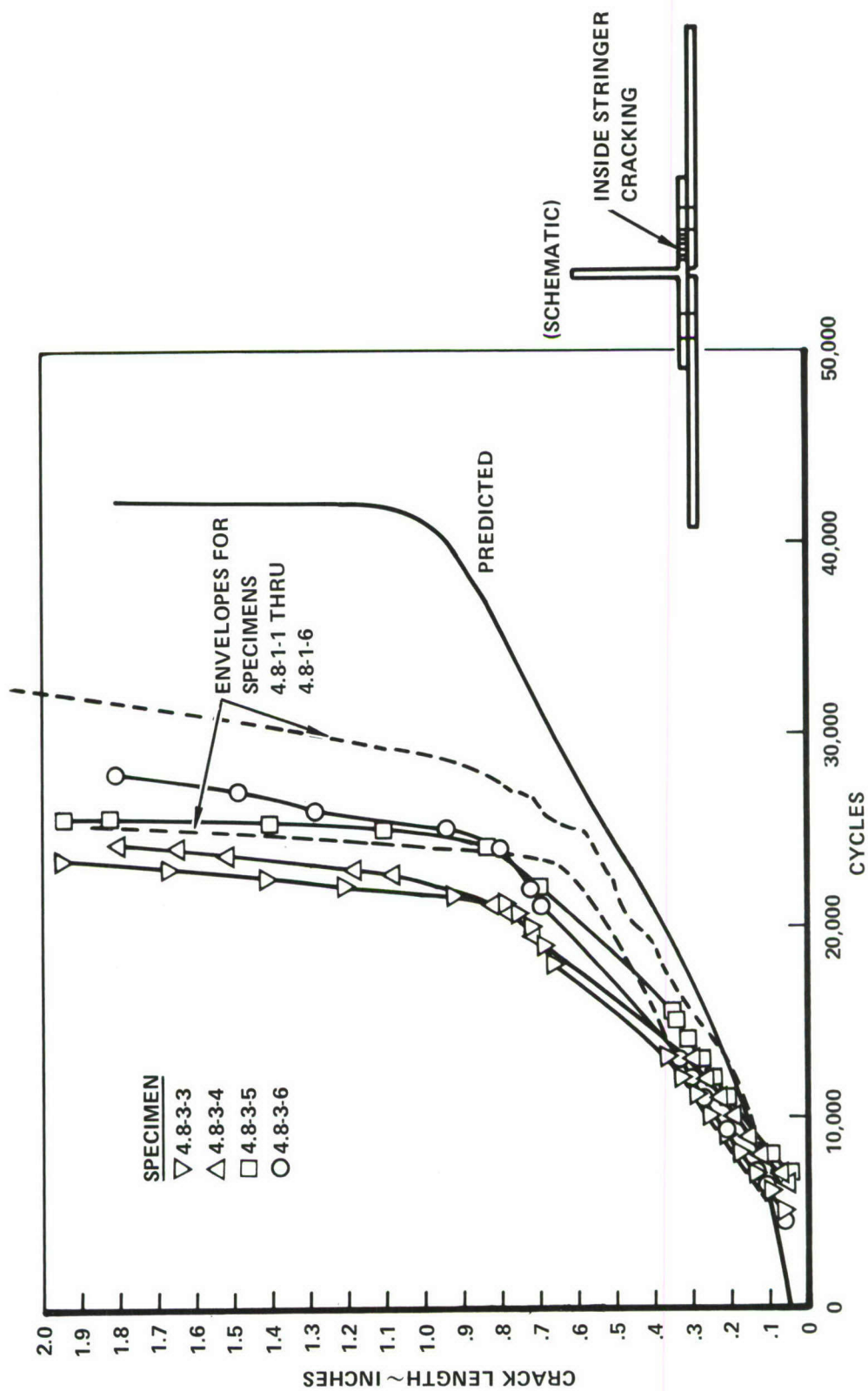


Figure 101. Crack Growth Results, Inside Crack in Tee, Spanwise Splice Specimens

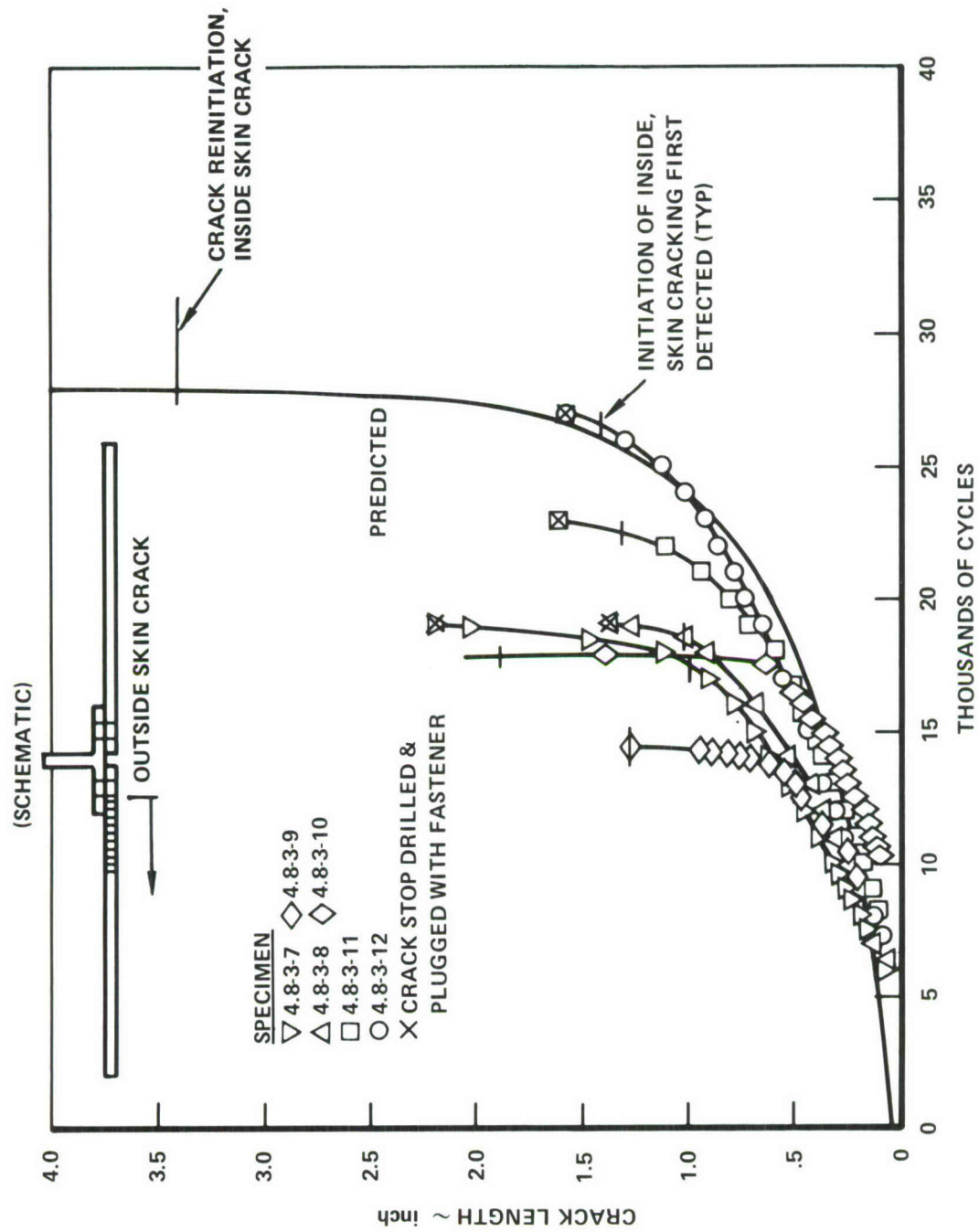


Figure 102. Crack Growth Results, Outside Crack in Skin, Spanwise Splice Specimens

SPECIMEN  
 ▽ 4.8-3-7  
 △ 4.8-3-8  
 □ 4.8-3-11

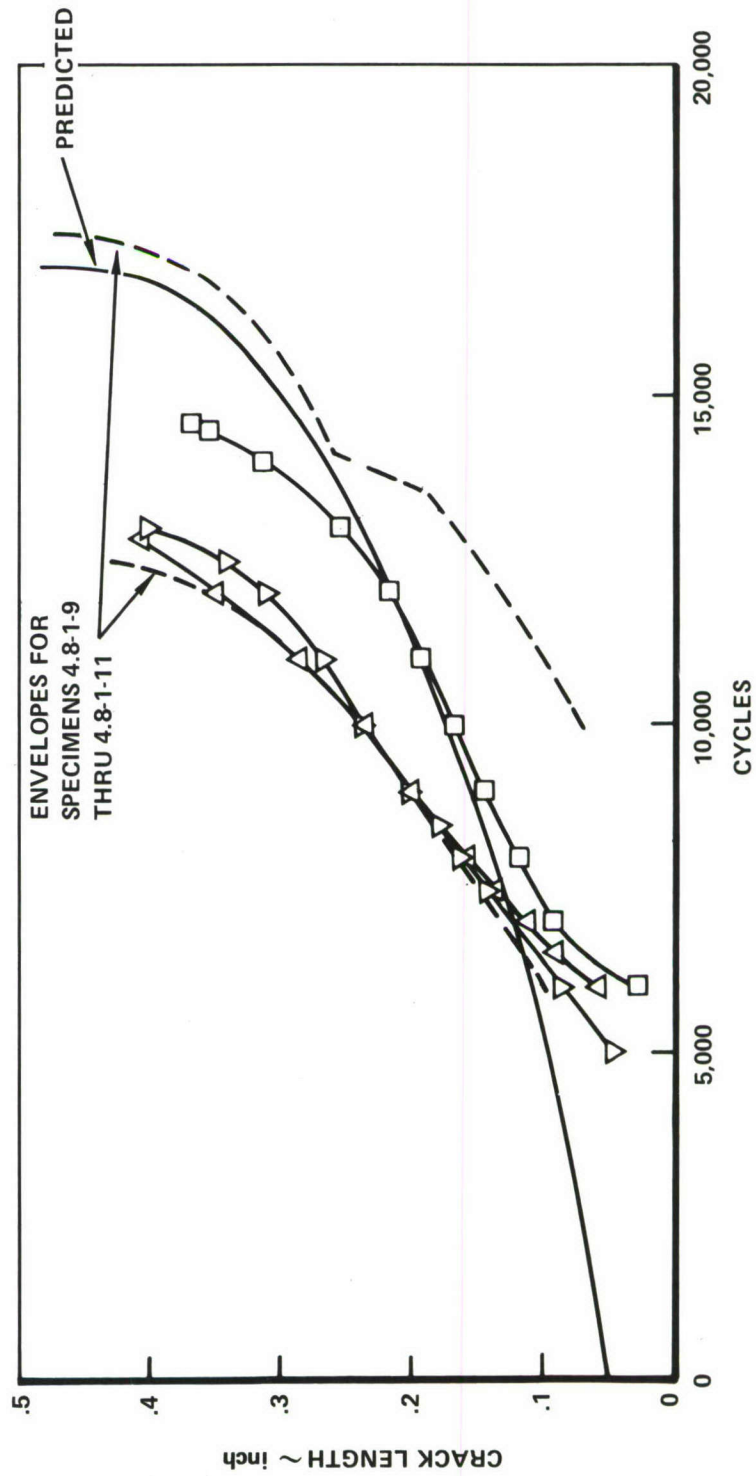
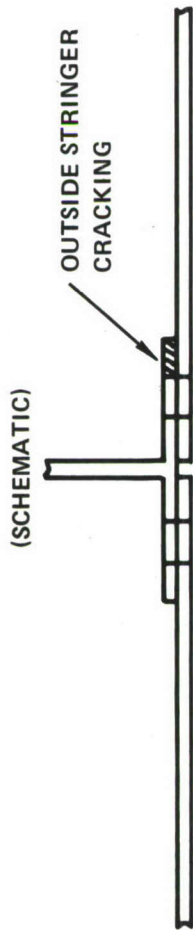


Figure 103. Crack Growth Results, Outside Crack in Tee, Spanwise Splice Specimens

The prediction shown in Figure 101 for the inside crack in the tee is the same curve that is shown in Figure 94. This curve was originally calculated for the continuous skin-type Specimens, 4.8-1-1 through -6. The same geometry was used for the tee on the spanwise-splice specimens except that 0.3125-inch-diameter fasteners were used instead of 0.250-inch fasteners. This prediction was previously seen to underestimate the crack growth rates. The dashed lines show the envelope of the data from prior Specimens 4.8-1-1 through 4.8-1-6. The new data for Specimens 4.8-3-3 through -6 are close to this envelope but crack growth is slightly faster. It is clear that the stress intensity expression for this case, described in Section V, Paragraph 3.2, underestimates the true stress intensity. The data themselves can be used to estimate an improved K expression, as described in Section VIII, Paragraph 1.4.

Specimen 4.8-3-6 contained an initial flaw in the tee only. No crack was observed in the skin until 38,500 cycles, almost 10,000 cycles after the protruding leg of the tee had broken. This is in total contrast to Specimens 4.8-3-3, -4, and -5, where there were initial cracks in both the skin (Figure 100) and the tee (Figure 101) which grew simultaneously. Despite this difference, there was little difference in the growth rates of the tee cracks among these four specimens.

Figure 102 shows the prediction and test results for the growth of the outside skin crack in Specimens 4.8-3-7 through -12. The prediction tended to slightly underestimate the crack growth rates for all specimens except 4.8-3-12, the specimen with no initial flaw in the tee.

While the outside skin crack propagated, the inside skin crack was initiating on the opposite side of the preflawed fastener hole. By prediction, the inside crack should have initiated when the outside crack reached a length of about 3.4 inches. This prediction is contrasted to the experimental points at which the inside crack was first observed in Specimens 4.8-3-7 through -12. As Figure 102 shows, the primary crack was always between 0.9 and 1.9 inches when the secondary crack initiated. No explanation is presently available for this discrepancy.

There appears to be some effect of the degree of secondary initial damage on the rate of growth of the outside skin crack. Specimen 4.8-3-12

had only the initial skin crack and no initial crack in the tee. Specimens 4.8-3-7, -8 and -11 had initial 0.050-inch cracks in both members but no continuing damage flaws. Specimens 4.8-3-9 and -10 had additional razor-induced continuing damage flaws in the tee and the second skin member.

The outside skin crack was stop-drilled in four of these specimens to prevent further growth and allow time for cracks to initiate and grow in the tee and other skin members. An X in Figure 102 denotes the stop-drilling time and crack size. A 0.375-inch-diameter steel Hi-lok fastener (HL50-12-6) was put in the 0.378-inch stop-drill hole (clearance fit) and the collar (HL90LP-12) was fully torqued to maximize the crack arrestment. Full arrestment of the stop-drilled end of the crack was always achieved until the moment of specimen fracture. (Note: A stack of steel washers was used under the collar because the only available 0.375-inch-diameter Hi-lok fasteners had a 0.375-inch shank, whereas the sheet thickness was only 0.182 inch). The success of the use of torqued fasteners here provided further evidence that fastener clamp-up enhances crack arrest at a hole. (See Section VII, Paragraph 2.2.

The prediction shown in Figure 103 for the outside crack in the tee is the same curve that is shown in Figure 96. As in Figure 101, the effect of a small discrepancy in fastener diameter was neglected to avoid having to recalculate this prediction. The envelope for the continuous skin Specimens, 4.8-1-9 through -11, is indicated by a dashed line. The new data for Specimens 4.8-3-7, -8, and -11 are within this envelope but on the faster crack growth side.

Note that in both Figures 102 and 103, the crack growth rate for Specimen 4.8-3-11 is slower than for Specimens 4.8-3-7 and -8. These three specimens are identically fabricated and precracked, except that Fastener No. 2, the fastener in the crack plane adjacent to the preflawed fastener hole, was a fully torqued interference-fit Hi-lok fastener for Specimen -11 and a fingertight clearance fit Hi-lok fastener for Specimens -7 and -8. It is unlikely that a difference in Fastener No. 2 would affect the early crack growth rates at Fastener No. 1. Data scatter cannot be ruled out as an explanation since Specimen 4.8-3-11 was not replicated.

#### 1.4 Empirical Stress Intensity Analysis for the Tee Stringer

The most inaccurate crack growth rate prediction for the center-stringer specimens was for the inside crack in the tee, Figure 94 and 101. This error was no surprise, because the stress intensity analysis discussed in Section V, Paragraph 3.2 was not straightforward; no solutions exist in the literature that are clearly appropriate for this case. Particularly problematic is the crack growth period after the crack front reaches the junction between the base and the protruding leg of the tee.

In Section III, Paragraph 3.3.2 the empirical semiinverse approach was used to estimate  $K$  as a function of crack length for a corner crack at the edge of the center hole in a standard  $k_t = 3.1$  fatigue coupon. This same empirical approach is now used to estimate  $K$  for the inside tee crack.

Measurements of crack growth rate as a function of crack length for the inside tee crack are easily derived from the crack length versus cycles data. An applicable relationship between crack growth rate and  $K_{\max}$  is given in Figure 43 in Section IV. The  $K_{\max}$  versus crack length relationship is easily obtained by matching the observed  $da/dN$  to the corresponding value of  $K_{\max}$  from interpolation on Figure 43.

Data from Specimens 4.8-3-3 and -4 were used for obtaining stress intensity versus crack size for the inside tee crack by this procedure. This empirical result is compared in Figure 104 with the prior analytical  $K$  estimate. The data show that the stress intensity was significantly underestimated, especially for crack lengths between 0.75 and 1.25 inches, as measured from the edge of the fastener hole along the visible surface of the tee.

#### 1.5 Spectrum Tests (Phase II)

Two tee-reinforced, split-skin specimens were spectrum tested using the 80-flight loading sequence introduced in Section II, Paragraph 3.1 at a reference maximum stress of 30 ksi. The purposes of these spectrum tests were

- To mark the fracture surface as in Figure C-5 of Appendix C.
- To verify that the crack growth behavior for constant amplitude loading was the same as for spectrum loading.

- To test the accuracy of predictions made using the baseline spectrum data (Section IV, Paragraph 6) and the equivalent  $k_t$  and equivalent stress intensity factor methods (Section V, Paragraph 6.).

Figure 105 compares the actual and predicted crack growth lives for the spectrum tests of structural specimens. The equivalent  $k_t$  method agreed closely with the experimental results for the tee-reinforced split-skin specimens.

The skin crack in tee-reinforced Specimen 4.8-3-1 was about to be repaired (by stop-drilling and insertion of a 0.375-inch-diameter fully torqued Hi-lok fastener) when it propagated unstably, causing the specimen to fail. Just before failure, the tee crack had propagated only part of the way across the thickness of the outstanding leg of the tee at the base of that leg. The repair, which in retrospect should have been done after 6560 simulated flights, would have arrested the skin crack and allowed time for the tee crack to propagate. The skin crack in duplicate Specimen 4.8-3-2 was repaired after 8000 simulated flights, and the growth of the tee crack was fully recorded both by visual monitoring during the test and by clearly identifiable markings on the fracture surface.

Figures 106 and 107 are photographs of the fracture surface of tee-reinforced Specimen 4.8-3-2. The largest tensile loading in the 80-simulated-flight periodic sequence, which occurs in the 39th flight, causes the crack front to jump ahead, especially at mid-thickness. The dark gray areas or bands on the fracture surface show the length of each such jump. The thin silvery bands separating them indicate fatigue crack growth during the other (smaller) 1079 cycles that recur each 80 simulated flights.

Except near the end of the test, only the largest tensile loading (the one occurring in the 39th flight) causes visible jumps in crack growth. Therefore, the crack growth rates, and in fact the entire crack growth history, can be identified by counting or measuring the spacing of these fracture surface markings. In general they are spaced 80 flights apart. Furthermore, final specimen failure always occurred upon the application of the largest tensile loading.

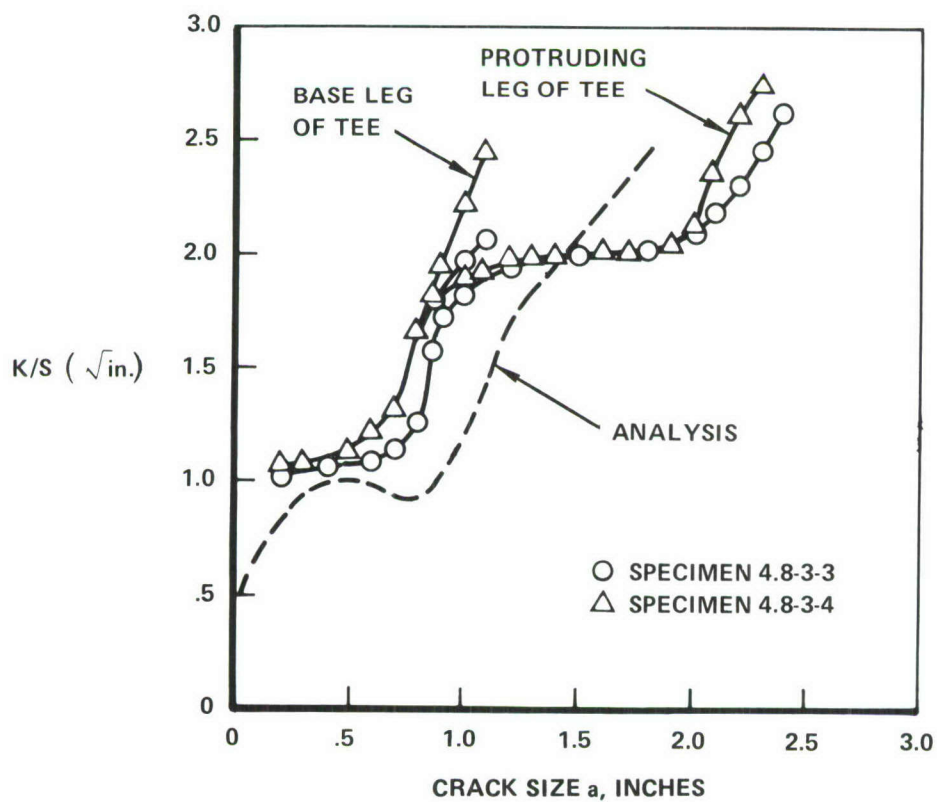
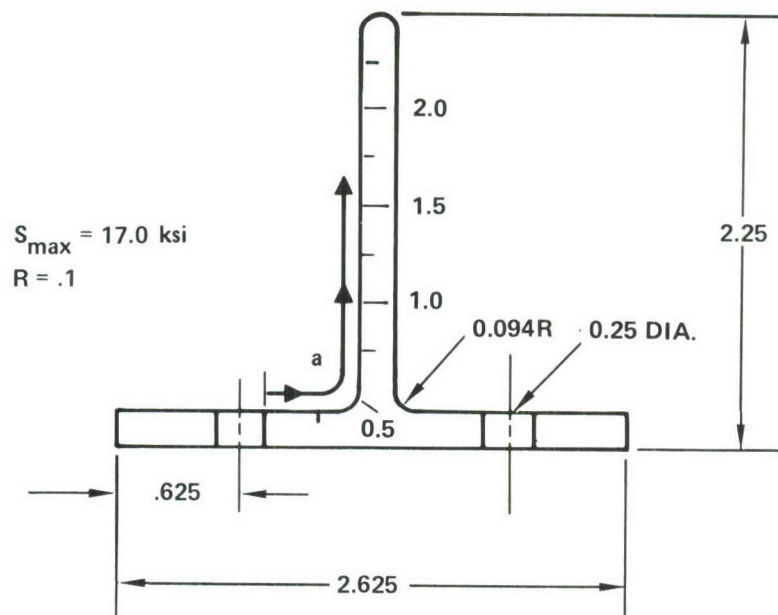


Figure 104. Empirical and Analytical Stress Intensity Factor, Inside Crack in Tee

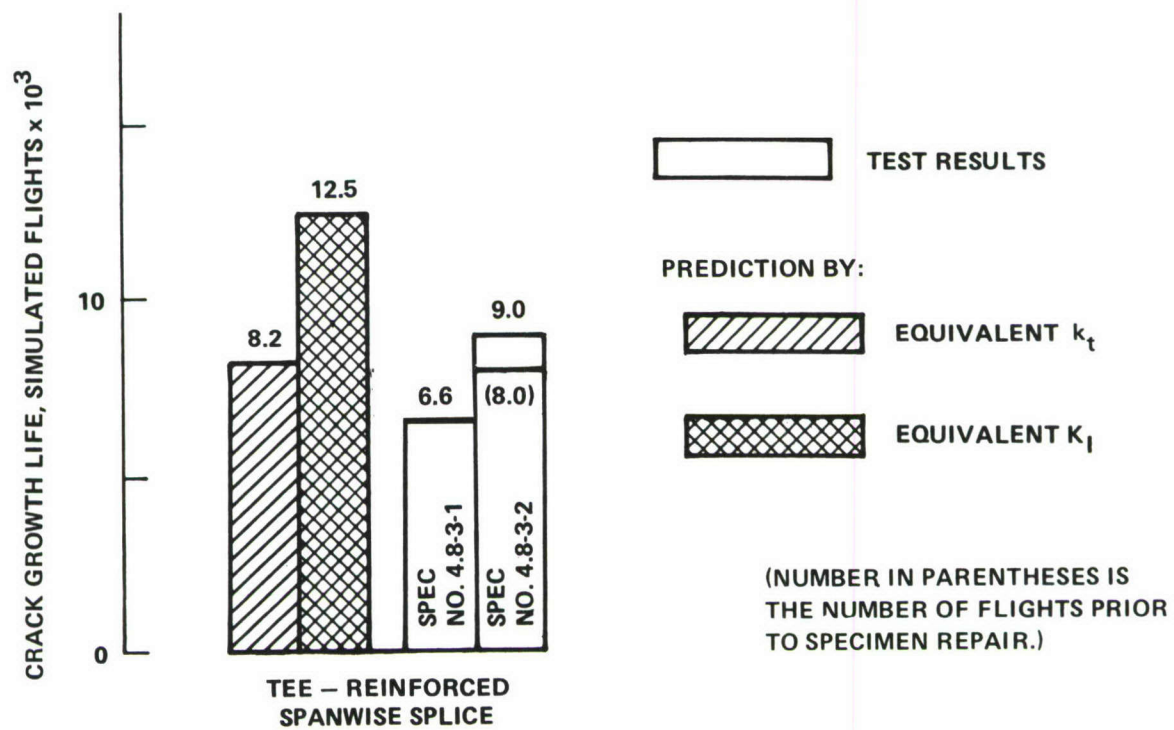


Figure 105. Predicted and Test Lives of Spectrum Loaded Tee-Reinforced Split-Skin Specimens

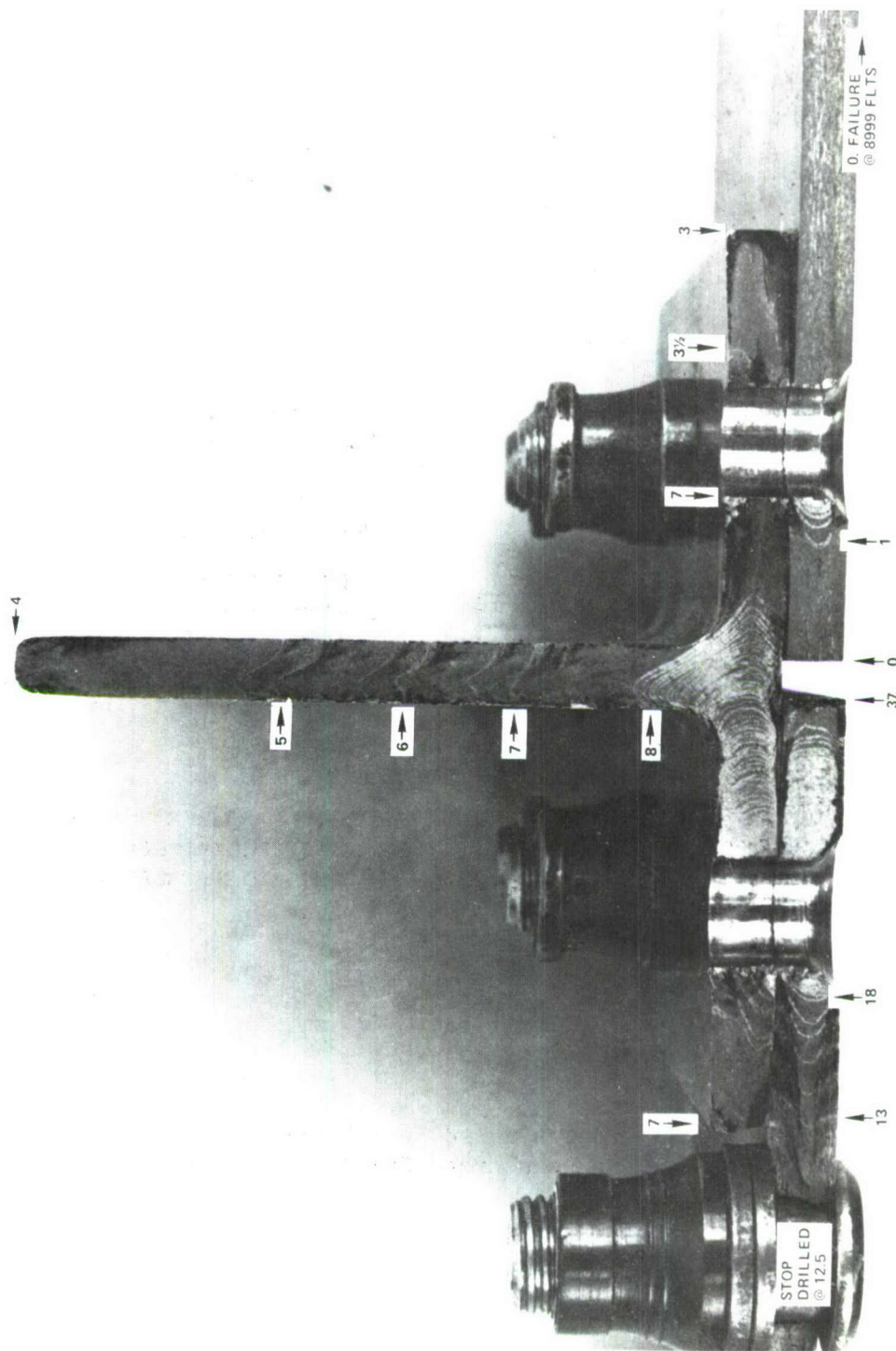


Figure 106. Fracture Surface of Specimen 4.8-3-2 Showing Failure Sequence

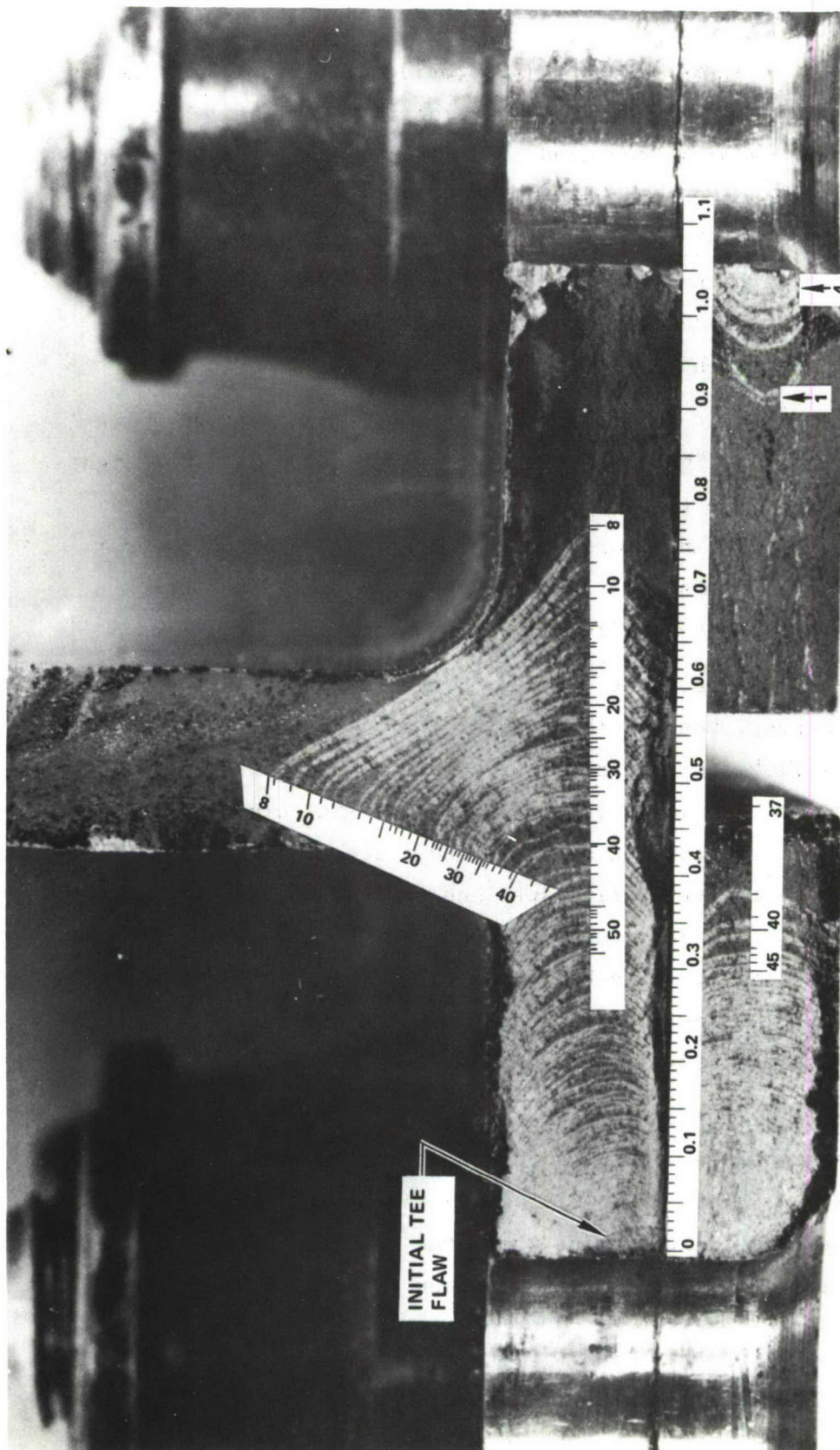


Figure 107. Close-Up of Fracture Surface Markings on Specimen 4.8-3-2

The integer numbers in Figures 107 and 108 provide a countdown of the number of 80-flight sequences remaining until failure of the specimen. For example, the fracture surface marks numbered 7 in Figure 106 identify the locations of the three crack fronts in the tee 560 (7 x 80) flights prior to specimen failure. At that instant the cracks had just jumped to about one-third of the way up the protruding leg of the tee, broken through from the crack-origin hole to the left-hand tee edge, and broken through to the adjacent fastener hole on the right-hand side.

Thus the failure sequence is evident in Figure 106. The protruding leg of the tee broke 320 (4 x 80) flights prior to failure, leaving only the right-hand ligament at the base of the tee intact. At that time there was only a short corner crack (about 0.090 inch long) in that ligament, protruding from the fastener hole. Eighty flights later (240 prior to failure) that crack jumped across the ligament and the entire tee was broken.

By then there was a crack (not yet visible to the operator) in the previously undamaged skin member, beneath the head of the flush-head fastener. By 80 flights prior to failure this crack had reached a length of about 0.2 inch and a very small crack had nucleated on the opposite side of the same hole. On the next application of the highest spectrum load these two cracks propagated unstably, triggering specimen failure. There was no evidence of an initiated fatigue crack at the stop-drill hole. At 1000 flights prior to failure this hole had been drilled and a clearance-fit 0.375-inch-diameter Hi-lok fastener had been inserted and fully torqued (about 200 inch-pounds). This fastener is shown on the left-hand side of Figure 106.

Figure 107 provides detailed data on both the growth rate and flaw shape of this tee crack. At about 3000 (37.5 x 80) flights prior to failure the crack reached the fillet radius where the base and protruding leg intersect. At that time its length (measured at mid-thickness)

was about 0.46 inch. The growth rate had become about 290 microinches per flight. It soon slowed to a minimum growth rate of 50 microinches per flight and grew in a somewhat circular arc. When it had grown about halfway across the base (length = about 0.55 inch) it began tunneling ahead in two directions, up the protruding leg of the tee and across the base. Eventually these seem to have become two almost separate cracks, tending to pull the rest of the crack front behind them as they grew. The growth rates of these two gradually increased until, at 560 flights prior to failure, there was the large jump in the growth of both cracks discussed previously.

In the constant amplitude tests, the crack front shape in this region of the tee was almost perfectly quarter-circular. Marking cycle marks on the fracture surfaces of several specimens clearly showed this. The difference in crack front shape occurs because crack front tunneling is more prevalent at the higher stress levels (30 ksi versus 17 ksi) used in the spectrum tests.

More important than details like crack front shape is the high degree of damage tolerance of the structure, particularly for the period after the repair. At the time that the skin crack was stop drilled and a fastener was inserted, crack instability was imminent. Specimen 4.8-3-1 had failed at almost exactly the same damage condition. Yet after the repair, the structure lasted another 1000 simulated flights. The cyclic stress levels applied were typical of those seen in fighter aircraft except that the higher stress cycles, occurring less than once per 80 flights, were truncated. On the other hand the repair, made on only one side of the crack, would have been even more effective had both crack tips been repaired.

## 2. EDGE STRINGER SPECIMEN

Twelve edge-stringer reinforced panels with 0.050-inch corner precracks were fatigue tested at a nominal gross area stress of  $S_{\max} = 17.0$  ksi,  $R = 0.1$ , and  $f = 4.0$  Hz in laboratory air ( $T = 72^{\circ}\text{F} \pm 3^{\circ}\text{F}$ ,  $\text{RH} = 40\% \pm 10\%$ ). The purposes of these tests and the accompanying analyses were to examine:

- The effect of initial flaw location and multiplicity on crack growth sequence and fatigue life of the preflawed structure.
- The accuracy of crack growth predictions for the structure and initial flaws.
- The effect of continuing damage flaws on the crack growth sequence and life of the structure.

### 2.1 Strain Gage Survey

Strain gages were used on Specimen 4.9-7 to determine the actual stress distribution near the test section of the specimen. The gage locations and strain gage readings are shown in Figure 108. Prior to the test a strain survey was conducted for a preliminary loading of  $S = 7.2$  ksi, to check out the specimen and test grip design. Succeeding surveys were conducted on the first cycle and Cycle No. 13952, right after the ligament broke between the edge of the angle and the first fastener hole. The inside skin crack at that time was 0.32-inch long.

The strain gage readings in Figure 108 are all normalized, and would be 1.0 if the stress were uniform. For example, numbers less than 1.0 for Gages No. 7 and 8 indicate lower strains in the outstanding leg of the angle and in the simulated shear web. Thus the stringer pickup in the grips was not fully effective and the stress distribution, rather than uniform, consisted of combined tension and transverse bending. Although not intended, this does simulate a typical mix of tension and bending for a wing surface.

Important in the strain gage readings for Cycle No. 1 (when there were no cracks except the small initial cracks) was the stress magnification in the skin. In particular, the average of Gages No. 2 and 4 on the Cycle No. 1 indicated a local stress 18 percent higher than nominal in the immediate path

| GAGE NO. | GAGE LOCATION, INCHES      |                     |                           | *NORMALIZED STRAIN RANGE, $E\Delta\epsilon / \Delta\sigma$                       |                                      |   |
|----------|----------------------------|---------------------|---------------------------|--|--------------------------------------|---|
|          | x<br>FROM SIDE<br>OF ANGLE | y<br>FROM $\bar{C}$ | z<br>FROM BACK<br>OF SKIN | PRELIMINARY<br>LOADING<br>$\Delta\sigma = 7.2$ ksi<br>(0.05 INCH INITIAL CRACKS) | CYCLE 1<br>$\Delta\sigma = 15.3$ ksi | CYCLE 13,952<br>$\Delta\sigma = 15.3$ ksi<br>**SKIN &<br>ANGLE CRACKS |
| 1        | 8.25                       | 0.6                 | 0                         | 1.071  | 1.069                                | 1.050   |
| 2        | 3.37                       | 0.6                 | 0                         | 1.138  | 1.246                                | 1.232   |
| 3        | 1.34                       | 0.6                 | 0                         | 1.032  | 1.020                                | 1.086   |
| 4        | 3.37                       | 0.6                 | 0.182                     | 1.119  | 1.114                                | 1.213   |
| 5        | 1.34                       | 3.0                 | 0.432                     | 0.989  | 1.029                                | 0.996   |
| 6        | 1.34                       | 0.6                 | 0.432                     | 0.896  | 0.903                                | 1.356   |
| 7        | 0.250                      | 0.6                 | 1.52                      | 0.914  | 0.894                                | 0.970   |
| 8        | -0.182                     | 0.6                 | 1.52                      | 0.896  | 0.901                                | 0.931   |

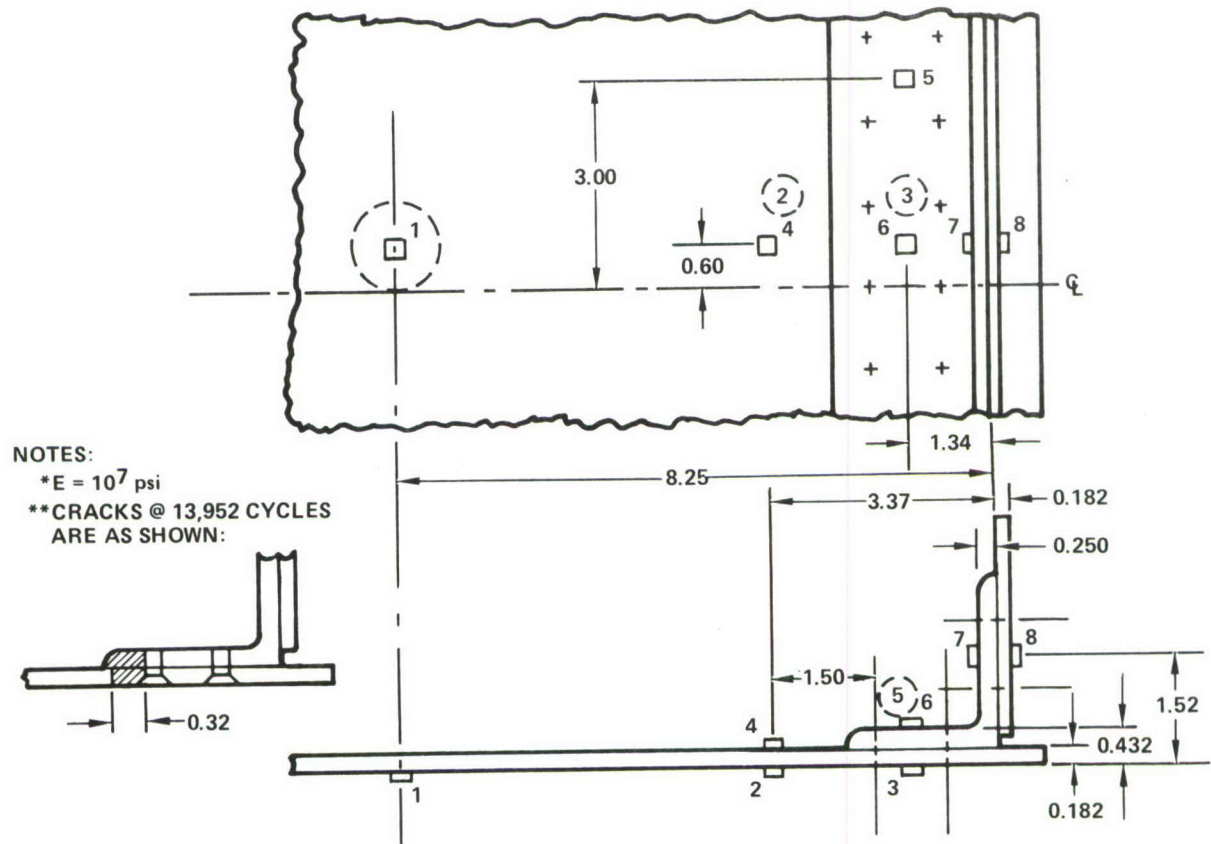


Figure 108. Strain Gage Locations and Results on Edge Stringer Specimen 4.9-7

of the inside skin crack. Note also for Cycle 13952 that the cracking substantially magnified the gage reading for Gage No. 6 while affecting the others to a lesser extent.

## 2.2 Discussion of Results

Figure 109 summarizes the crack growth lives for the edge stringer specimens. The initial damage conditions are shown for each specimen, and the predicted crack growth lives are compared to the test lives. In the tests, specimen failure always occurred soon after one member failed. This agreed with the preselected failure criterion for the prediction: When one member fails the specimen fails.

All eight specimens with initial cracks in both the angle and the skin had nearly identical crack growth lives, ranging from 17,300 cycles for Specimen 4.9-8 to 23,000 cycles for Specimen 4.9-5. Among those eight the most significant variable was initial crack location. Lives for the four specimens with outside initial cracks in both members ranged from 19,600 cycles to 23,000 cycles, whereas test lives for the four specimens with inside initial cracks in both members ranged from 17,300 to 18,400 cycles. For the outside initial cracks, continuing damage flaws if present seemed to have a small detrimental effect, whereas the interference and torque on the secondary fastener (F2) in the crack plane seemed to have a beneficial effect. Neither continuing damage flaws nor torque and interference on the secondary fastener appeared to significantly affect the crack growth life for specimens with double inside initial cracks.

Specimens with an initial crack in just the angle or just the skin lasted longer than specimens with initial cracks in both the angle and the skin. This life extension resulted from the natural transfer of load from the cracked member to the uncracked member, which slowed the growth rate of the crack. This occurred to some extent in all four specimens with single initial cracks. However, the resulting life extension was small in Specimen 4.9-12 because the inside skin crack grew out of the region of influence of the angle (necessitating stop drilling) before the load transfer from the skin to the angle became very large.

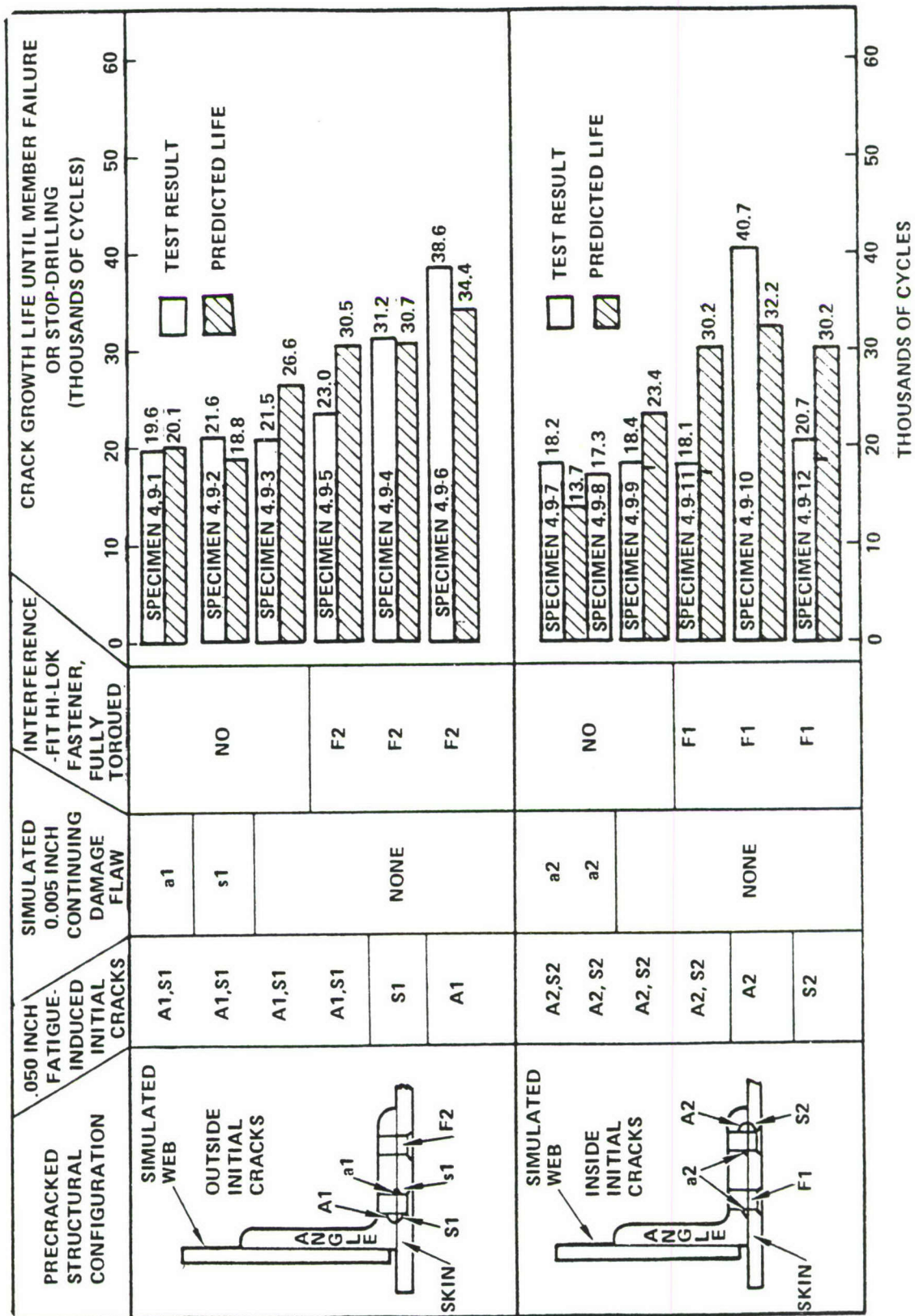


Figure 109. Summary of Crack Growth Lives for Edge-Stringer Reinforced Specimens

Except for those of Specimens 4.9-11 and 4.9-12, all of the predicted crack growth lives were within a factor of 1.33 of the actual test lives. This accuracy is achieved without accounting for load shedding from cracked to less-cracked members. Accounting for load shedding could make predictions more accurate in some cases and less accurate in others.

The somewhat larger error in the predictions for Specimen 4.9-11 and -12 is caused by underestimating the growth rate of the inside crack in the skin. A uniform gross area stress of  $S_{\max} = 17$  ksi was assumed for the prediction. Recall from Figure 109 that the strains at gage locations No. 2 and 4 were higher than the average. For Cycle No. 1, the stress value indicated by use of the average of strain Gages 2 and 4 is calculated as follows:

$$S_{\max} = 17.0 \times \frac{1}{2} (1.246 + 1.114) \text{ ksi} = 20.06 \text{ ksi} \quad (91)$$

The prediction of the growth of the inside skin crack was redone using  $S_{\max} = 20$  ksi,  $R = 0.1$ . The result was applicable to Specimens 4.9-7, -8, -9, -11, and -12 and is shown for these specimens in the respective data plots in Volume II. The revised crack growth estimate for the inside skin crack closely follows the data in all cases. The life predictions for Specimens 4.9-7 and -8 are unaffected because, with continuing damage flaws in the angle, the angle is theoretically the first member to fail. However, the life predictions for Specimens 4.9-9, -11 and -12 are improved. The improved estimates are 18,000, 17,700 and 17,900 cycles, shown in Figure 109 by tick marks on the bars for the predictions.

With the improved analysis, the predicted critical member for Specimen 4.9-9 is corrected: For  $S_{\max} = 17$  ksi in both members, the angle is computed to be the first member to fail, whereas for  $S_{\max} = 20$  ksi in the skin, the skin is predicted to fail first in this specimen. The latter is correct, since stop-drilling of the skin crack became necessary before the angle failed.

The outside crack in the angle consistently grew faster than predicted. Figure 111 shows the prediction compared to data from five outside angle cracks from four different specimens. (Both angles of Specimen 4.9-6 were precracked and both cracks grew, providing the extra set of data.) In the

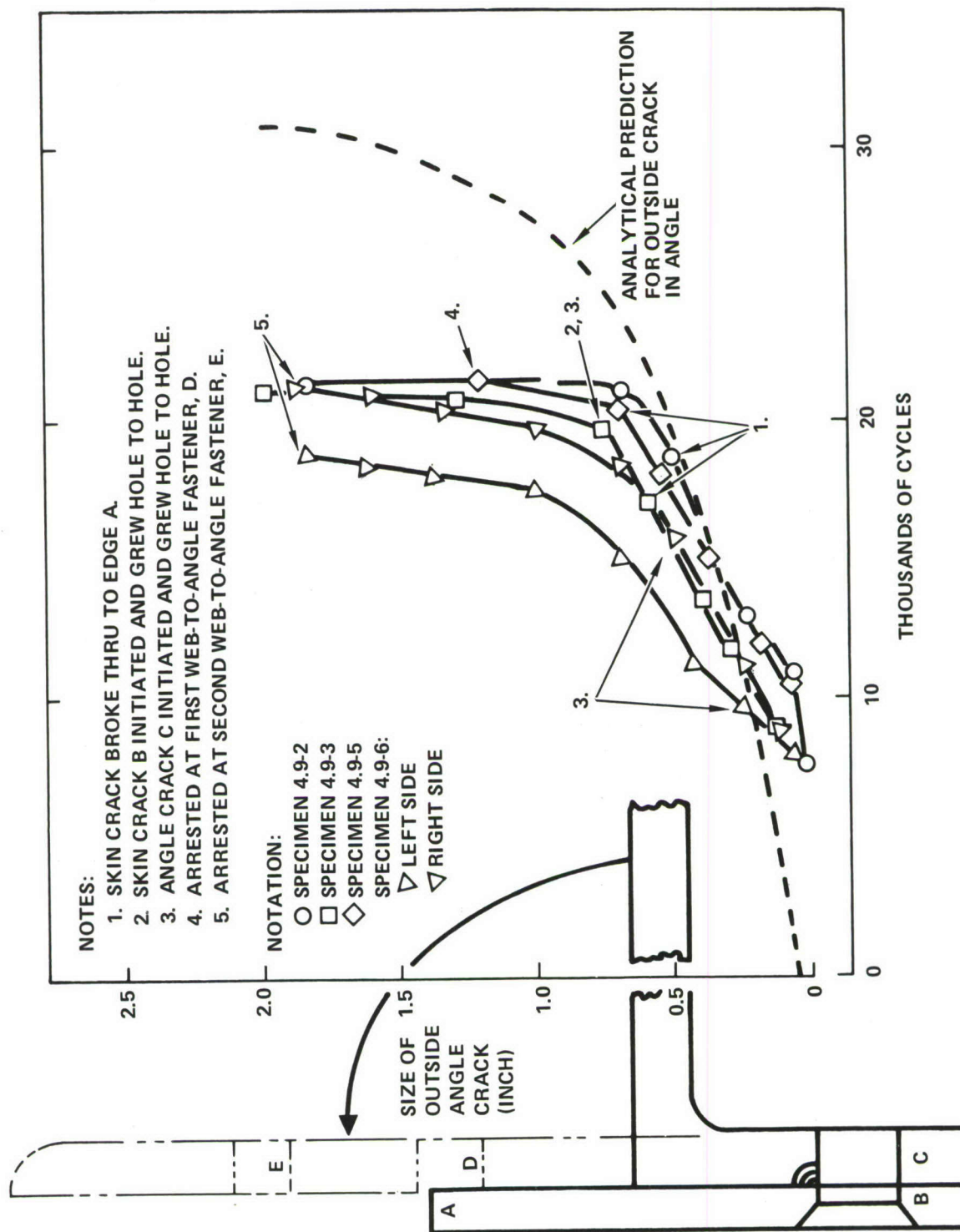


Figure 110. Prediction Compared to Five Outside Angle Cracks from Four Different Specimens

prediction, the angle was imagined to be unbent and was modeled as a planar strip, as indicated in the sketch in Figure 110. A uniform gross area stress of  $S_{\max} = 17$  ksi was assumed with no load transfer between the angle and either the skin or the simulated web. According to the prediction, the crack at point C in the angle (see Figure 110), should not have initiated until after the main crack had reached the top edge of the angle.

There are several possible sources of error in these analyses, but some of them should have tended to make the life predictions too short rather than too long. A listing of these sources of error follows:

- The nominal stresses are close to  $S_{\max} = 17$  ksi in the base of the angle, but are perhaps as much as ten percent lower halfway up the outstanding leg of the angle, according to the strain gage measurements (Figure 108). An adjusted analysis would have an increased error.
- Modeling the angle as an unbent (planar) strip as discussed in Section V, Paragraph 5.1 underestimates the width correction factor for the stress intensity. Furthermore, after the crack passes the corner of the angle it induces eccentricity like an edge crack, and the loss of area induces a crack-opening bending moment. Adjusted analyses to include these two effects would have a decreased error.
- For Specimens 4.9-2, -3 and -5 the outside skin crack broke through to the free edge just before the angle crack accelerated. (See Note 1 in Figure 110). With this extensive skin damage there should have been load transfer from the skin to the angle. If the analysis had included this the prediction for the angle would have been improved. However, in Specimen 4.9-6 the skin was uncracked and should have picked up load from the base of the angle. Furthermore, the web always remained uncracked and should have picked up load from the outstanding leg of the angle. An adjusted analysis to include effects of load transfer to the simulated web or the skin would have increased the error of the prediction.
- In both angles of Specimen 4.9-6 there were early crack initiations at point C in the sketch in Figure 110. According to the prediction and data from the other specimens these cracks should not have initiated. These early initiations may have resulted from residual predamage that was introduced during precracking and was not fully removed when the undersized holes for precracking were enlarged to final size. (As discussed in Section VI, Paragraph 1.2 there had been problems during precracking of outside angle cracks, and several angles had to be scrapped because a crack kept initiating on the wrong side of the hole. Thus the presence of undetected predamage on that side of

the hole in these two angles would not be surprising.) Whatever their origin, if the early occurrence of these secondary cracks had been considered in the prediction, the predicted growth rate of the outside crack would have been faster and more consistent with the test results.

Despite all the possible sources of error, the predictions were well within a factor of 2 of the test results on all 12 tests. Similar predictability was achieved on the 24 specimens with central tee stringers.

### 3. TWO-BAY SPECIMENS

Four two-bay specimens were precracked and constant amplitude tested at two stress levels to verify that the crack growth patterns for the center stringer and edge stringer specimens extrapolate to multiple stringer structure and to other stress levels.

#### 3.1 Strain Gage Results

Strain gages were placed on two of the two-bay specimens, 4.10-1 and 4.10-3. The purposes of taking the strain gage readings were:

- To check the uniformity of the stress distribution and estimate the extent of lateral bending.
- To ascertain whether the strain distributions in the two-bay specimens reproduce each other and those of the center-stringer and edge stringer specimens.
- To record how the strains change as a function of crack size.

Both strain-gaged specimens were tested at  $S_{\max} = 12$  ksi,  $R = 0.1$ . Figures 111 and 112 show the strain gage locations and results. The precracks in Specimen 4.10-1 were in the tee and skin at the location shown in the top sketch of Figure 111. The precracks in 4.10-3 were in the angle and skin as shown in Figure 112. The strains shown in parentheses are normalized values, equal to  $E \Delta \epsilon / \Delta S$ , where  $\Delta S = 10.8$  ksi.

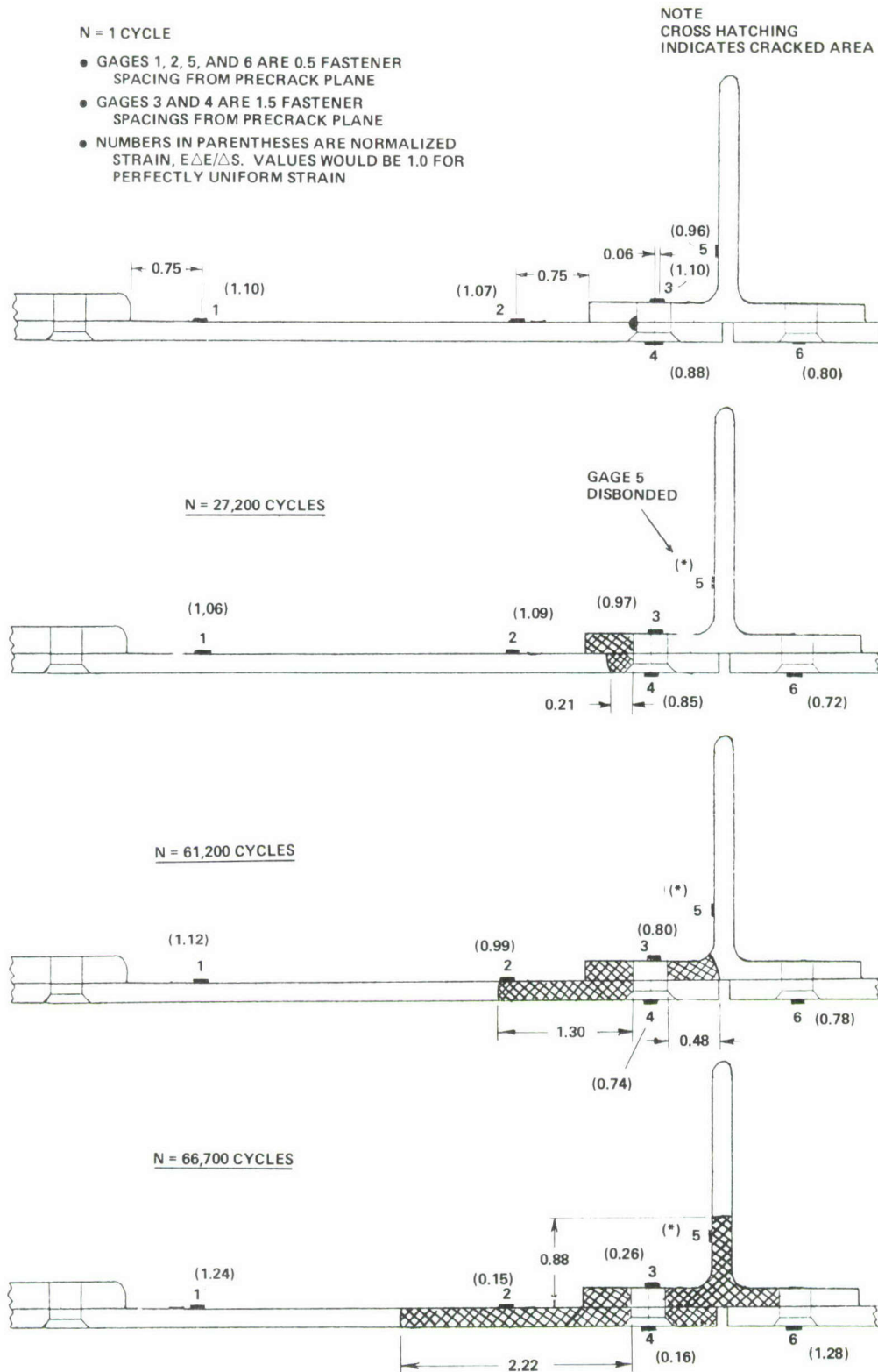


Figure 111. Summary of Strain Gage Data from Specimen 4.10-1

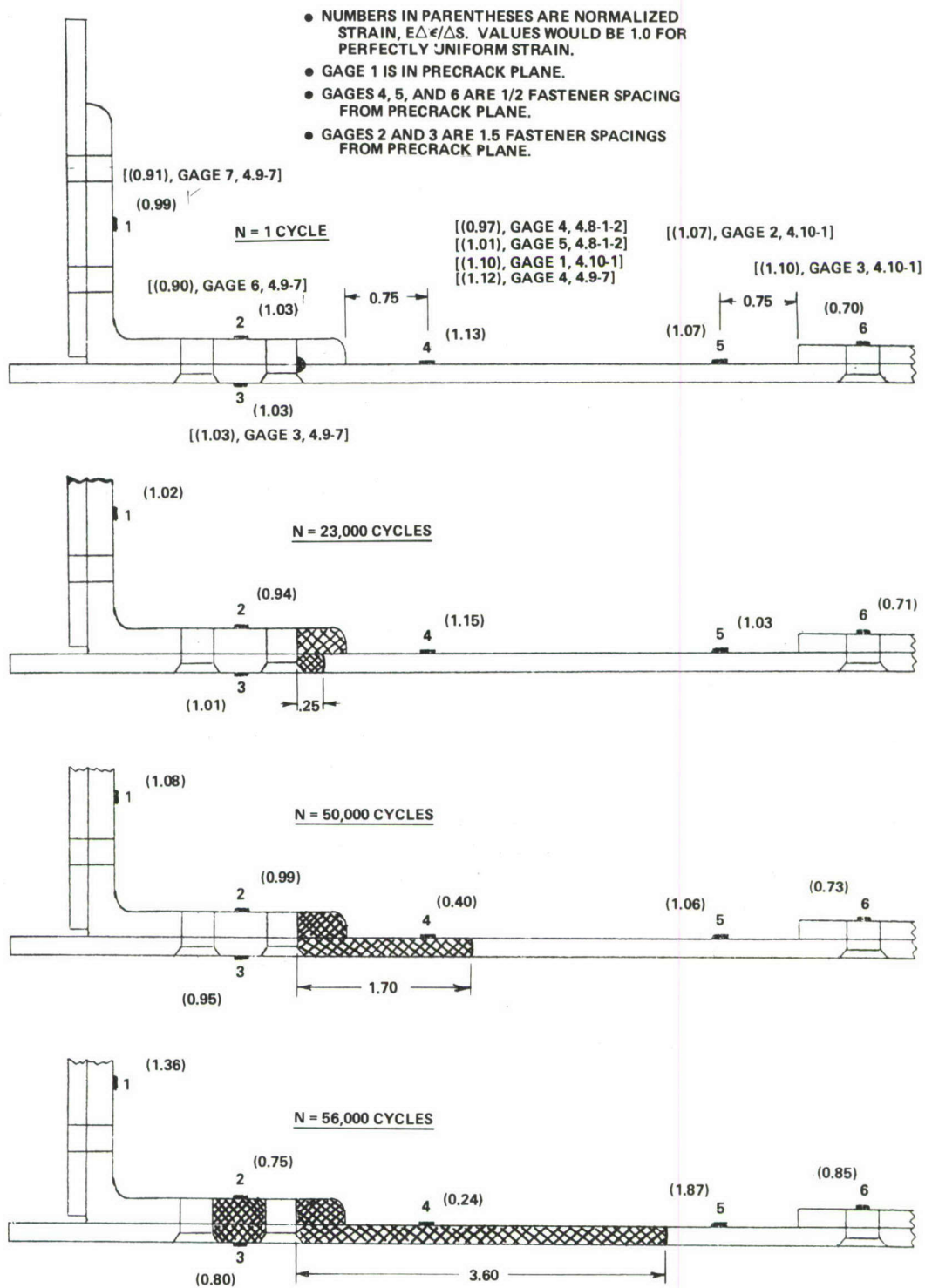


Figure 112. Summary of Strain Gage Data from Specimen 4.10-3

The dimensions and notes at the top of each figure are sufficient to locate the gages. When the gage is on a hole centerline, no dimension is shown.

Several of the gages on two-bay Specimens 4.10-1, 4.10-3, center stringer specimen 4.8-1-2, and edge-stringer specimen 4.9-7 were located in comparable positions. Quantities in square brackets at the top of Figure 113 provide these corresponding strain gage readings.

- Note that prior to crack growth the strains in the angle stringer were ten percent lower at gages 7 and 6 in edge stringer Specimen 4.9-7 than at corresponding gages 1 and 2 in two-bay Specimen 4.10-3. However the strains in the skin near the angle stringer were comparable in these two specimens (gages 3 and 4 in both Specimens).
- The initial strains at gages 4 and 6 in Specimen 4.10-1 differ by 10 percent.
- The initial strain at gage 3 of Specimen 4.10-1 is more than 1.5 times that at gage 6 in Specimen 4.10-3. No explanation is apparent. It appears (from gage 6 of 4.10-1 especially) that the stresses in the tee are lower than nominal, because the grips do not have direct stringer pickup.
- The strains at gages 1 and 2 on the skin of Specimen 4.10-1 are comparable to those at corresponding gages 4 and 5 in Specimen 4.10-3.
- The initial strains at gages 4 and 5, located on the skin 4 inches from the edge of center-stringer Specimen 4.8-1-2, are 10 percent lower than the corresponding strains at either gage 4 in Specimen 4.10-3 or gage 1 in Specimen 4.10-1.

Strains also change with crack length as shown in Figures 111 and 112. In particular, note the gradual increase in strain with crack length in gages 1 and 6, Figure 111; and 1 and 5, Figure 112.

### 3.2 Discussion of Test Results

Specimens 4.10-1 and 4.10-3 were tested at a maximum gross area stress of  $S_{\max} = 12$  ksi,  $R = 0.1$ . Specimens 4.10-2 and 4.10-4 were tested at  $S_{\max} = 17$  ksi,  $R = 0.1$ . Marking cycles were used in which  $S_{\max}$  was maintained while the stress ratio was increased to 0.82.

Specimens 4.10-3 and 4.10-4 were nominally identical, with 0.050-inch inside corner cracks in the angle and (at the same holes) the skin. Figure 113 is a plot of crack size versus time, with the time scale normalized by the number of cycles to failure. Thus, differences between the plots for the two specimens indicate different relative time periods for the various crack initiation and crack growth segments which sequentially combine to cause the final failure.

To understand the difference observed, consider the damage condition when 90 percent of the life has been consumed. Since failure occurs rapidly thereafter, this damage condition can be considered for practical purposes to be a critical (pre-failure) condition. For specimen 4.10-3 this damage is much more extensive, because the applied stress is lower. In order to achieve this damage condition, the cracks in Specimen 4.10-3 had to reach other lengths earlier than the cracks in 4.10-4. This tends to explain all the differences between these two tests results shown in Figure 114.

Thus the differences observed are exactly what would be expected to result from a stress level change. This is an important observation, since all specimens in this program were run at one stress level, 17 ksi. This comparison suggests that phenomena observed in the stringer reinforced tests run at 17 ksi would also be expected at different stress levels.

Comparison of the fracture surfaces of these two specimens also provides strong support for this argument. Figure 114 shows sawed-off midsegments of the bottom half of Specimen 4.10-3 and the top half of 4.10-4. The crack paths are so closely matched in every detail that these appear to have come from the same specimen.

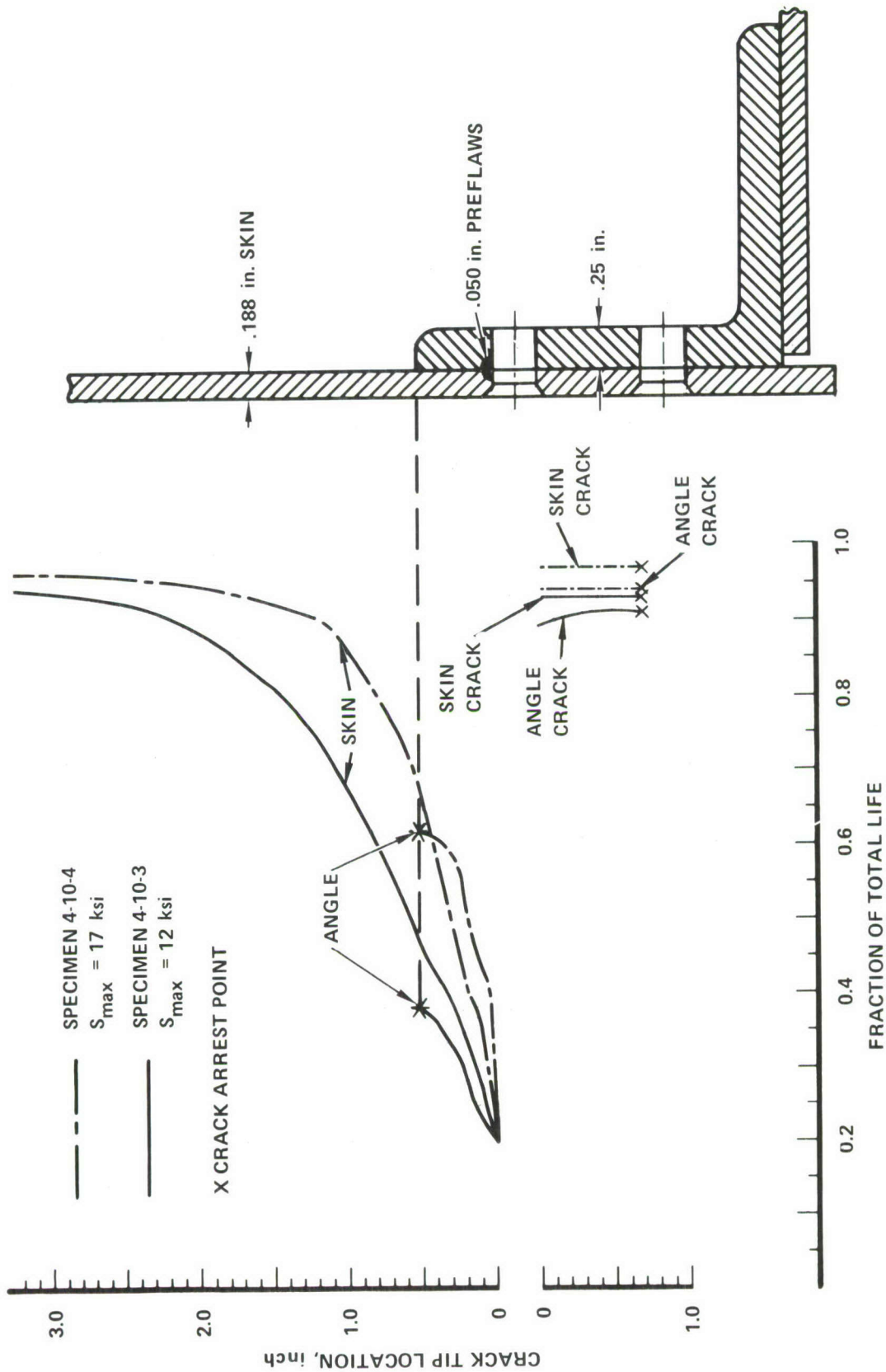


Figure 113. Stress Level Effect, Two-Bay Specimen with Precracked Edge Stringer and Skin

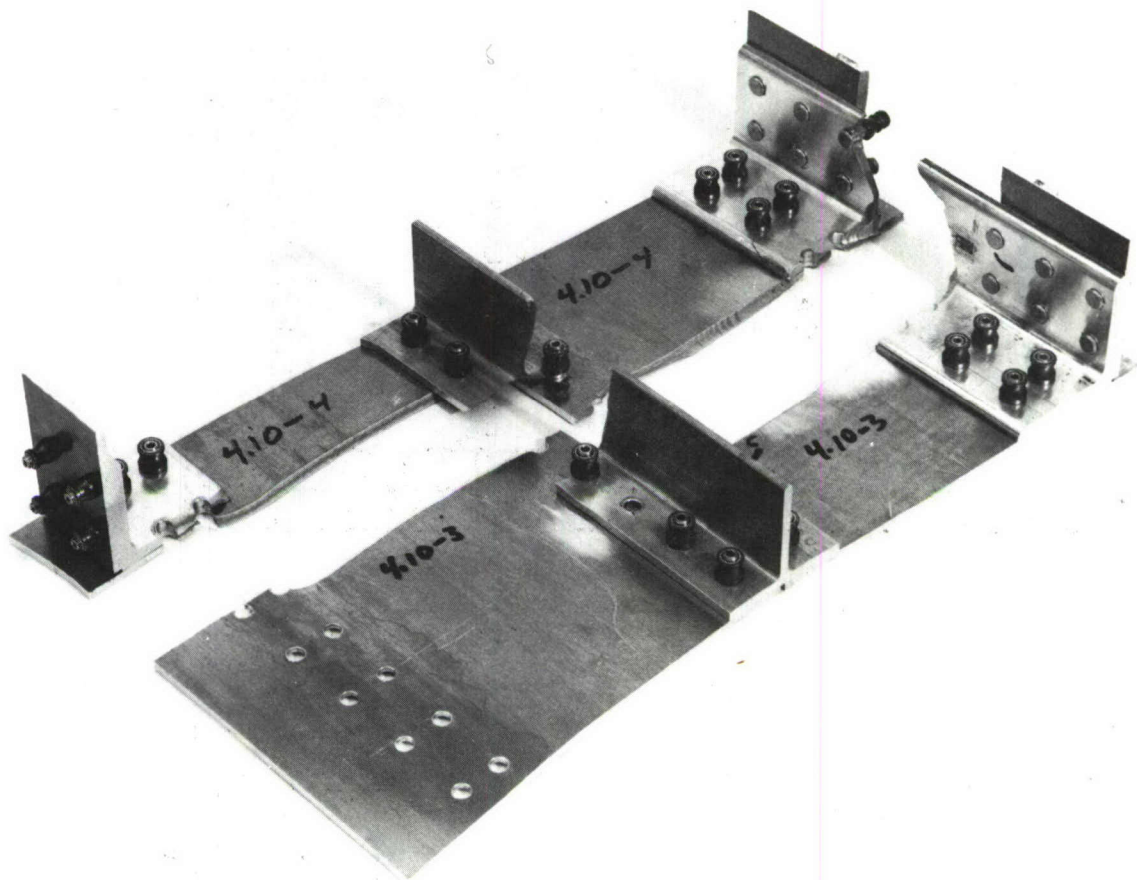


Figure 114. The Nearly Identical Crack Paths of Specimens 4.10-3 and 4.10-4

Note that as the crack grew across each specimen from member to member, the crack plane shifted from one fastener hole to the one immediately above or below. This shifting is expected in parallel-load-path structure because the stress severity factor is maximum at the location one fastener hole from the crack plane, where load is transferred from the cracked member. Fingertight, clearance-fit fasteners were used in all two-bay specimens all the way across the plane of the precrack. All other fasteners (including those one fastener hole from the crack plane) were interference fit, fully torqued. Nevertheless, the crack plane shifted in Specimens 4.10-3 and 4.10-4 to a plane of these torqued, interference-fit fasteners.

Specimens 4.10-1 and 4.10-2 were also initially identical, with 0.050-inch outside corner flaws located at the faying surface between the central tee and one sheet at the same fastener hole. Results of testing them at the two different stress levels are shown in Figure 115. The normalized

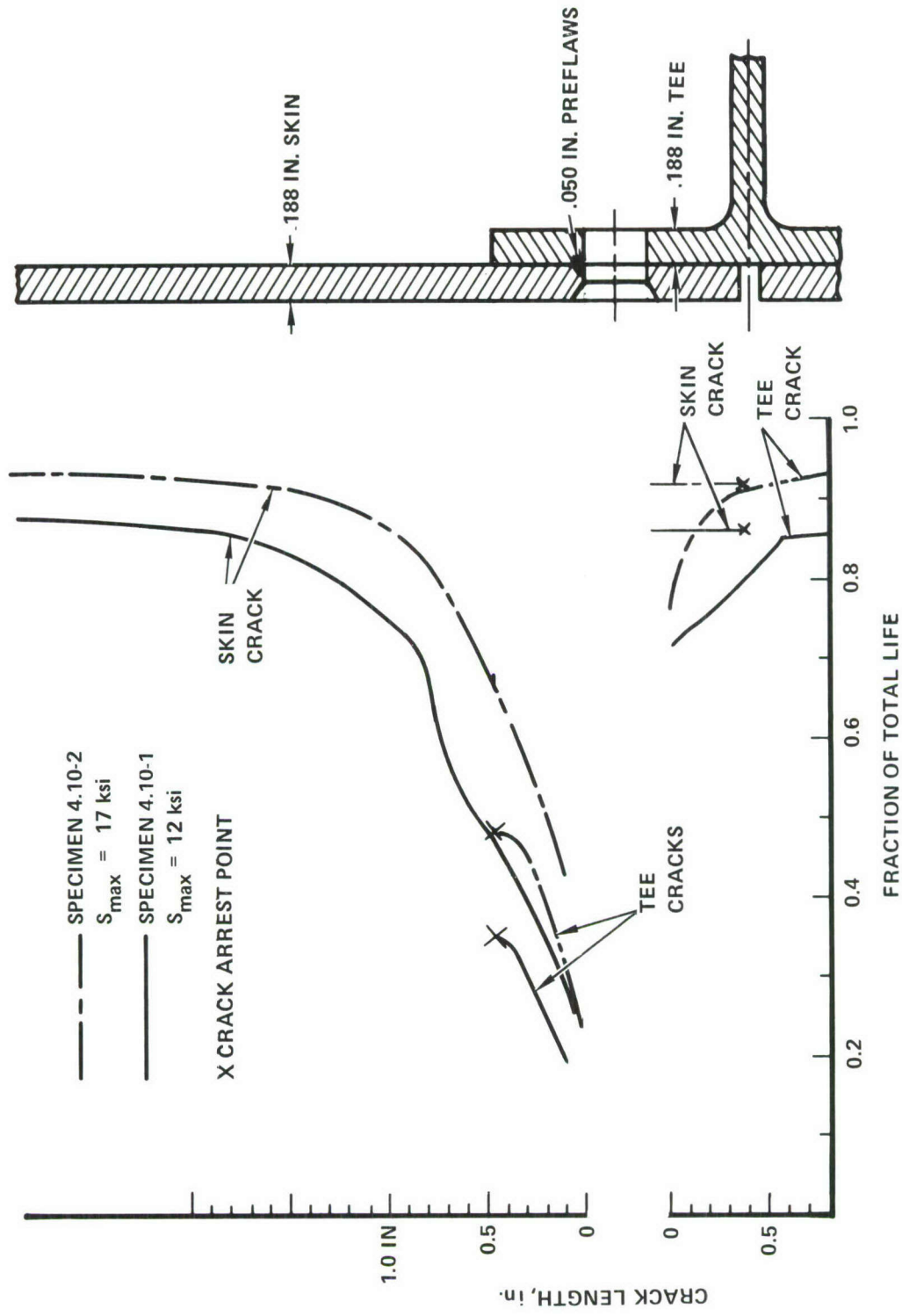


Figure 115. Stress Level Effect, Two-Bay Specimen with Precracked Tee and Skin

crack growth curve for Specimen 4.10-2, tested at  $S_{\max} = 17.0$  ksi, is to the right of the corresponding curve for Specimen 4.10-1, tested at  $S_{\max} = 12$  ksi. These two specimens show the same trend of differences as shown in Figure 114 for Specimens 4.10-3 and 4.10-4, due to the longer critical crack length for the lower stress level.

In contrast to Specimens 4.10-3 and 4.10-4, the crack paths of Specimens 4.10-1 and 4.10-2 were different from one another. In Specimen 4.10-1 the initial crack grew to the angle stringer and arrested in the first fastener hole it encountered. After subsequent failure of the tee, crack initiation in the initially-undamaged skin member occurred in the plane of the existing cracks, as it had in tee-reinforced split-skin Specimens 4.8-3-7 and 4.8-3-8. (These were tested at  $S_{\max} = 17.0$  ksi but had the same initial crack conditions, and the main skin cracks were stop-drilled at a length of about 1.6 inches.) In contrast to this, the initial crack in Specimen 4.10-2 bypassed the angle fastener and grew uninterrupted to the free edge. Subsequent to failure of the tee, a crack developed in the initially-undamaged skin member one fastener hole away from the existing crack plane.

It is not clear why one crack arrested at the fastener hole and one did not. However, the subsequent location of the initiated crack in the initially undamaged skin is rationally explainable. As suggested by the earlier discussion, the crack will shift planes if the load transfer is high enough to overcome the beneficial effects of fastener torque and interference on the stress severity factor of the hole. In Specimen 4.10-2 the unarrested crack and high stress level lead to a high-load-transfer situation in the plane adjacent to the existing crack. The result was static fracture in that plane. Because of the low stress level and the crack arrestment in Specimen 4.10-1, and because of the stop-drilling in the tee-reinforced split-skin specimens, the loads and the load transfer were lower and a fatigue crack initiated in the clearance fit, untorqued fastener in the plane of prior cracking.

Another purpose of testing the two-bay stringer specimens was to see whether the added structural complexity would result in significant differences in crack growth behavior. This assessment was accomplished by comparing test data from Specimens 4.10-2 and 4.10-4, which were tested at  $S_{\max} = 17$  ksi, to corresponding center stringer or edge stringer specimens previously tested at  $S_{\max} = 17$  ksi.

Tee-reinforced split-skin specimens 4.8-3-7 and 4.8-3-8 were comparable to Specimen 4.10-2. All three had double initial outside cracks in the tee and skin, no continuing damage, and all fasteners on the crack line installed with a clearance fit and low fastener torque.

Figure 116 shows the early crack growth histories of these three specimens. It can be seen that the added structural complexities did not significantly alter the early crack growth rates. Note that the growth of the initial skin cracks for all three specimens accelerated rapidly after the initiation of a new skin crack on the opposite side of the initial cracks.

Figure 117 compares the early crack growth histories for two-bay Specimen 4.10-4 and edge-stringer Specimen 4.9-9. Both had double initial inside cracks in the angle and skin, no continuing damage flaws, and clearance fit fasteners with low fastener torque in the plane of the precrack. The secondary cracks initiated about 4000 cycles earlier and the growth rates of the initial cracks were slightly faster in the two-bay specimen than in Specimen 4.9-9. However, these differences were small and it appears that no significant changes in crack growth result from the added structural complexity of the two-bay specimen.

#### 4. SUMMARY OF CONCLUSIONS FROM TESTS OF STRINGER-REINFORCED PANELS

From an overall review of Section VIII, a number of observations can be made. These are summarized in the following paragraphs.

For stringer reinforced specimens with 0.050-inch corner precracks in both the stringer and sheet at a common fastener hole, the crack growth predictions were accurate within a factor of about 1.6 without considering load shedding from cracked to intact members. Predictions could be farther off if load shedding were accounted for. It should be kept in mind that the conditions for predicting were close to ideal, in that

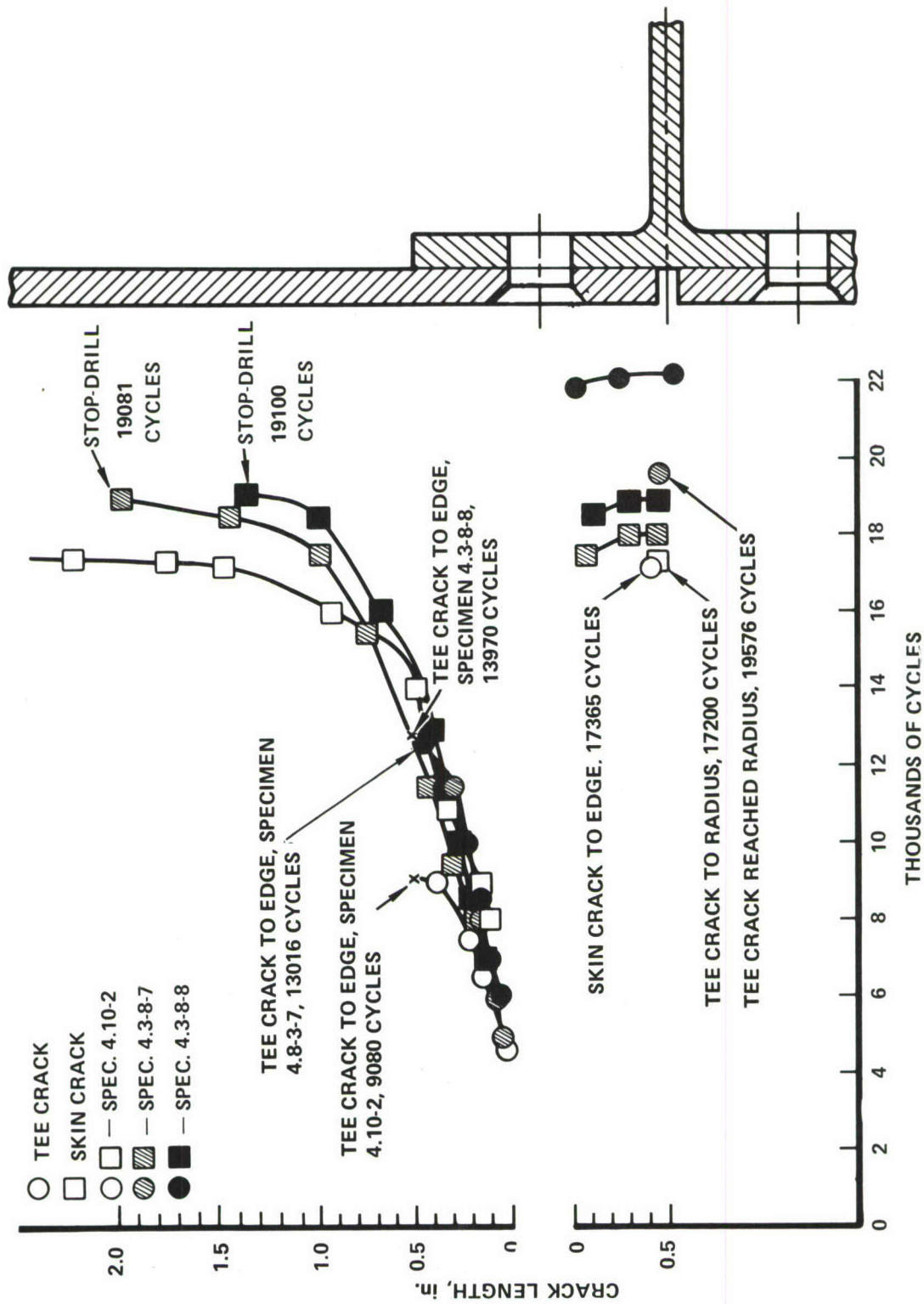


Figure 116. Early Crack Growth in Comparable Two-Bay and Center-Stringer Specimens

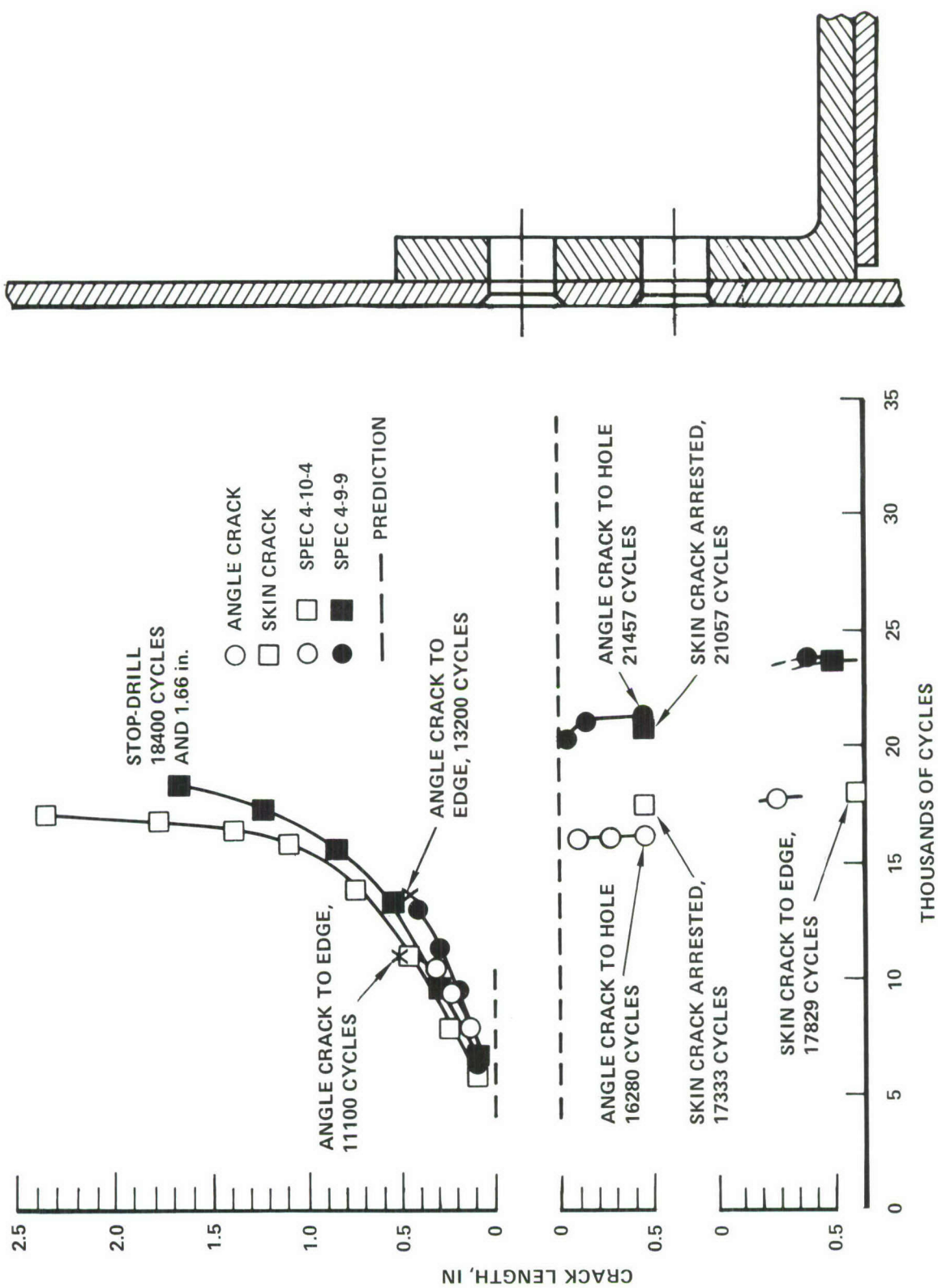


Figure 117. Early Crack Growth in Comparable Two-Bay and Edge-Stringer Specimens

- 7075-T6 Aluminum, a good fracture mechanics material, was used.
- One of the simplest of test conditions (uniaxial constant amplitude fatigue cycling,  $R = 0.1$ , controlled laboratory air environment) was used.
- A complete set of baseline data was generated specifically for predicting crack growth for these specimens.
- There were strict controls on specimen manufacture, precracking, and assembly procedures.

In making predictions for structure in service, where the above ideal conditions are not generally present and, in addition, the loads and environments are unknown and variable, the reliability of crack growth predictions could be substantially less than has been observed in this research program.

The crack growth life is significantly reduced when a simulated 0.005-inch continuing damage flaw is present on the opposite side of the hole containing the initial 0.050-inch corner flaw. At  $S_{\max} = 17$  ksi,  $R = 0.1$ , continuing damage flaws located at other locations had a negligible effect on life, although they did tend to grow as quarter-circular corner flaws.

Excluding cases with a continuing damage flaw and a primary crack on opposite sides of the same hole, variations in initial flaw multiplicity had little effect on early growth rates. However, single-crack specimens lasted longer because the crack had to initiate in the secondary member.

When no continuing damage flaws were present, the first new flaws to initiate were on the opposite side of the hole containing the precracks. The initiation occurred especially fast if the precrack grew to a free edge, creating a deep edge notch. Fatigue crack initiation data can be used to predict the nucleation of these secondary cracks.

For the inside crack in a tee stringer growing across the junction of the base and protruding leg of the tee, the crack front shape was approximately quarter-circular as sketched in Figure 55 for constant amplitude cycling at  $S_{\max} = 17.0$  ksi; whereas for spectrum loading where the maximum spectrum stress was 30 ksi, double crack tunneling occurred along the base and up the protruding leg as seen in Figures 105 and 106.

The lives of the split-skin tee reinforced specimens were shorter than the corresponding lives of the continuous-skin specimens. The split in the skin and the 0.062-inch increase in the fastener diameter slightly accelerate the crack growth process.

Crack growth in the angle-shaped edge stringer tended to be somewhat faster than predicted. It appears that in-plane and transverse bending effects occur which are not completely considered in the analysis used.

The practice of stop-drilling the skin crack proved to be an effective repair procedure for the stringer reinforced specimens when a fully torqued Hi-lok fastener was installed in the stop-drilled hole.

Spectrum loading using the 80-flight periodic loading sequence, marked the fracture surface so that the crack growth rates, crack front shape, and cracking sequence are clearly discernable on the fracture surface.

Although the two-bay specimens introduced more structural complexity, the crack growth lives and cracking sequence were similar to the comparable center stringer and edge stringer specimens.

Stress level had a predictable effect in the two-bay specimen. The critical crack length is shorter at the higher stress level so the growth of very short cracks encompasses a larger percentage of the crack growth life.

In stringer reinforced structure, there can be a tendency for cracks to nucleate in an undamaged member one fastener hole away from the plane of cracking of the adjacent member, because the load transfer is maximum at that fastener hole. In some specimens, the crack was biased to remain in the plane of the precrack, the only place where all fasteners are low-torqued clearance-fit.

APPENDIX A  
SUMMARY OF MIL-A-83444

The Air Force Damage Tolerance Specification MIL-A-83444 (Reference 1) requires that all primary aircraft structures be designed and qualified to comply with specific requirements of one of several categories of damage tolerant structures. This can be accomplished by providing acceptable combinations of initial quality, slow crack growth rates, and levels of detectability; and by use of multiple load path or crack arrest designs.

Figure A-1 is a flow diagram summarizing the requirements of MIL-A-83444. These requirements can be satisfied by successfully following any one path from the top of the flow diagram to the bottom. Alternative sets of requirements are established for slow crack growth structure and fail-safe structure. Any structure may qualify as slow crack growth structure, but single load path structure may not qualify as fail-safe structure.

Initial crack sizes  $a_{LT}$  at the beginning of the design lifetime are specified in Section 3.1.1 of MIL-A-83444. The specified length of the primary crack, for slow crack growth structure is 2.5 times larger than that for fail-safe structure. In addition to the primary crack, a multiplicity of small secondary cracks are specified to pre-exist throughout the structure.

As Figure A-1 indicates, the first step in evaluating a proposed design in terms of MIL-A-83444 requirements is to compute crack size versus time for the most critical initial crack location, using the specified initial crack sizes  $a_{LT}$ . (Here the term "crack size" includes the length of the primary crack and the length of any secondary crack that can have a possible bearing upon the failure process.) Typical crack-size-versus-time curves are shown schematically for slow crack growth structure in Figure A-2 and for fail-safe structure in Figure A-3. Once this curve has been established, all of the damage tolerance requirements can be considered in a routine manner.

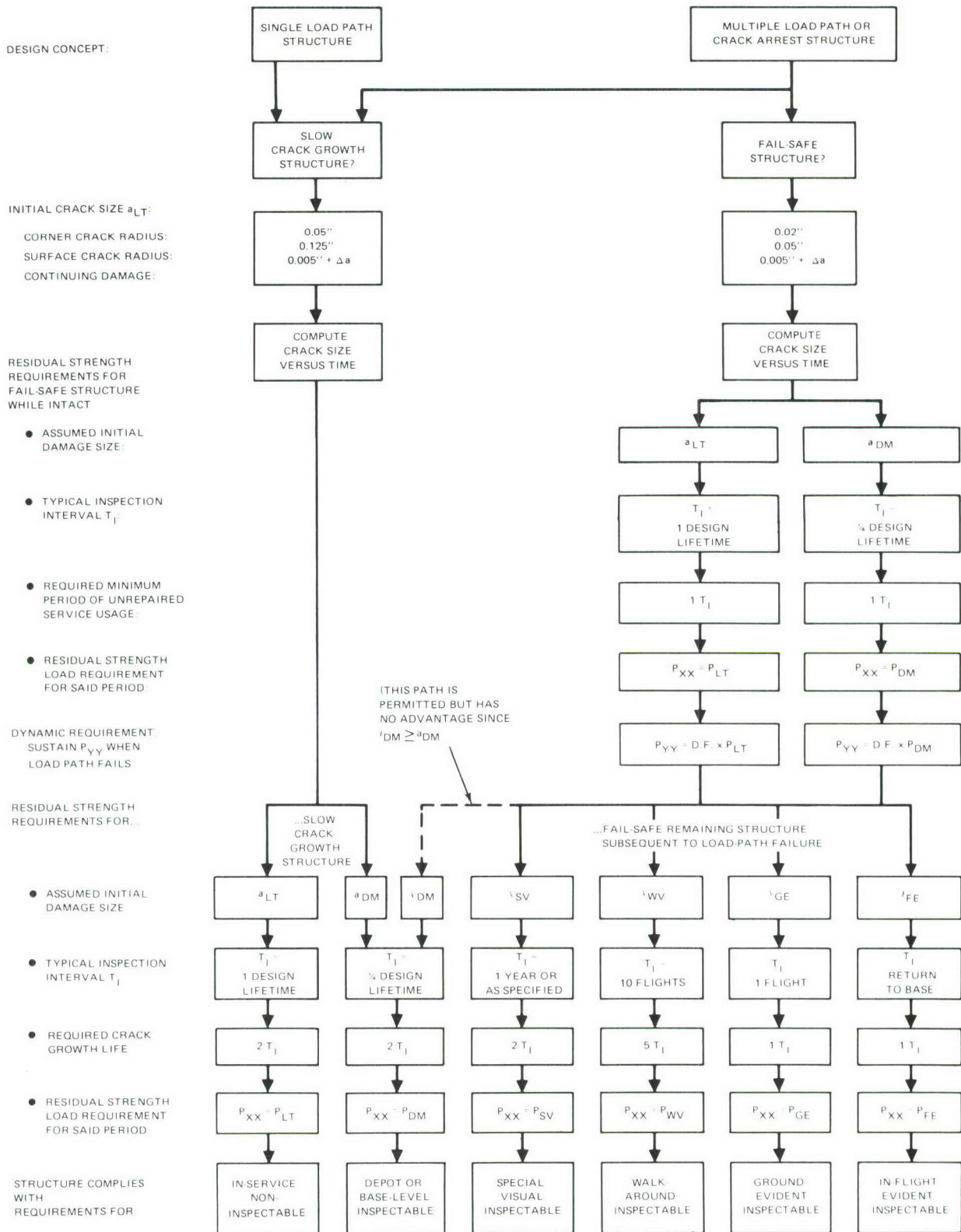


Figure A-1. Damage Tolerance Design Requirements

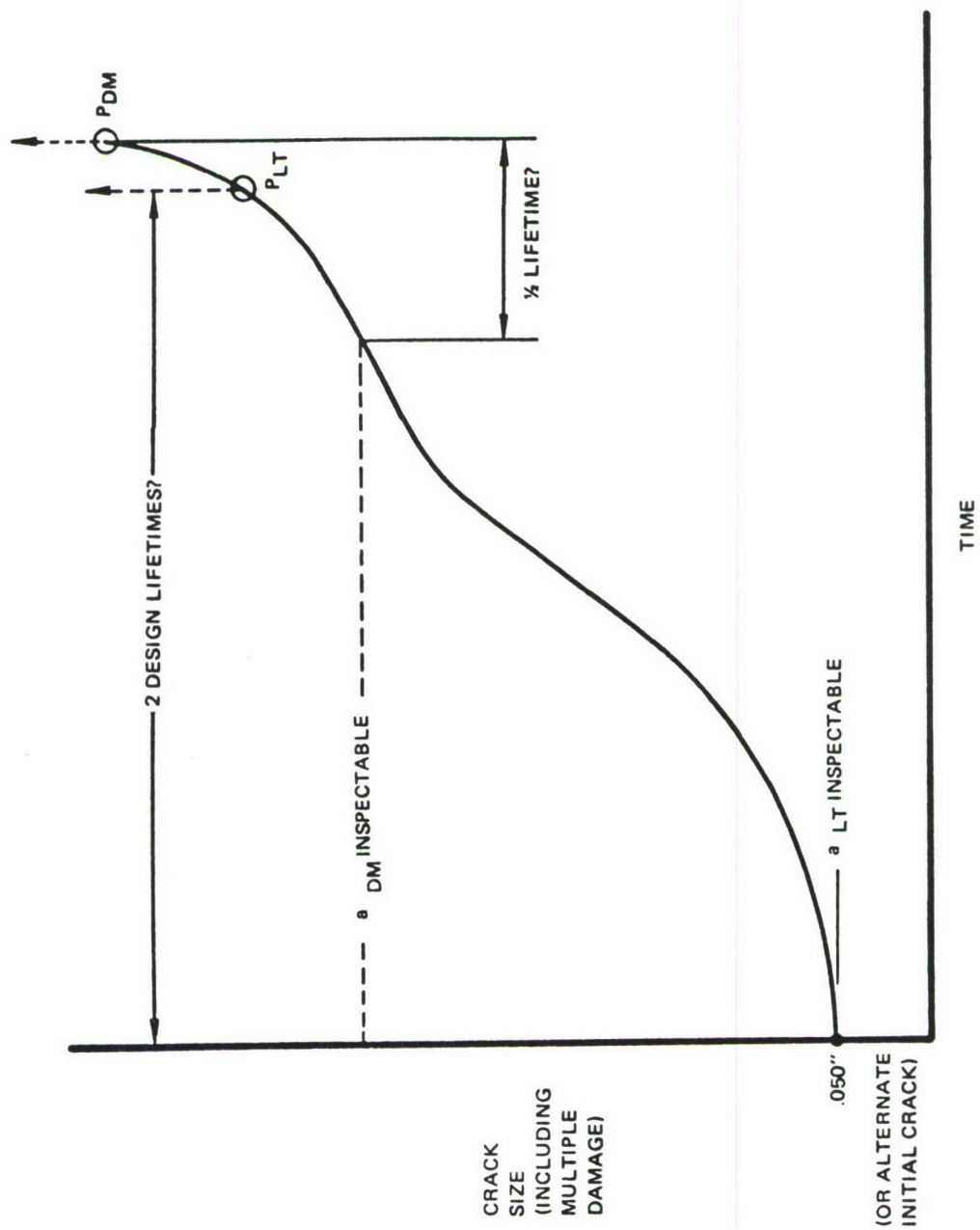


Figure A-2. Requirements for Slow Crack Growth Structure

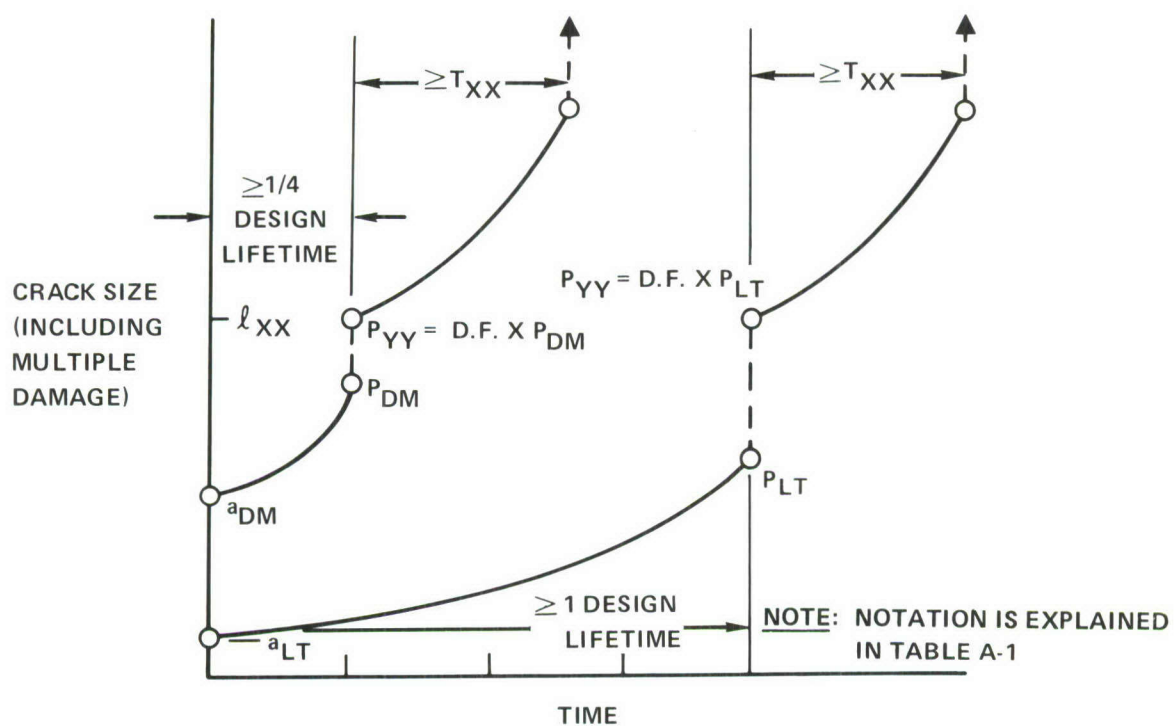


Figure A-3. Requirements for Fail-Safe Structure

TABLE A-1. ALTERNATIVE REQUIREMENTS FOR REMAINING STRUCTURE AFTER CRACK ARREST OR LOAD-PATH FAILURE

| INITIAL CRACK<br>$l_{XX}$ | DEGREE OF INSPECTABILITY | REQUIRED CRACK GROWTH PERIOD<br>$T_{XX}$ | REQUIRED RESIDUAL STRENGTH LOAD, $P_{XX}$ , THROUGH PERIOD $T_{XX}$ |
|---------------------------|--------------------------|--|---|
| $l_{FE}$                  | In-Flight Evident        | Return to Base                           | $P_{FE}$  |
| $l_{GE}$                  | Ground Evident           | 1 Flight                                 | $P_{GE}$  |
| $l_{WV}$                  | Walkaround               | 50 Flights                               | $P_{WV}$  |
| $l_{SV}$                  | Special Visual           | 2 Years                                  | $P_{SV}$  |
| $l_{DM}$                  | Depot or Base Level      | 0.5 Design Lifetimes                     | $P_{DM}$  |

Slow crack growth structure (Figure A-2) is the simpler type because only one requirement needs to be satisfied: The structure with an initial or inspectable extent of damage must be capable of sustaining a specified residual strength load at all times throughout two inspection periods. There are two alternative ways to satisfy this requirement. They differ only in the type of inspection used. For in-service noninspectable damage, the initial crack size is the assumed size  $a_{LT}$  at the start of the lifetime; the inspection interval is one design lifetime; and the residual strength requirement is  $P_{LT}$  as specified in Table I of MIL-A-83444. For depot- or base-level inspectable damage, the initial crack size  $a_{DM}$  is specified in Section 3.1.2 of MIL-A-83444; the typical inspection interval is 1/4 design lifetime; and the residual strength requirement is  $P_{DM}$  as specified in Table I of MIL-A-83444 (Note that  $P_{DM} \leq P_{LT}$ ; in fact, proceeding in order from left to right in Figure A-1 the initial crack sizes increase while the inspection intervals and residual strength requirements decrease for slow crack growth structure).

The requirements for fail-safe structure are somewhat more complex, because three requirements in all must be satisfied. As shown in Figure A-3, the crack-growth history for fail-safe structures consists of three parts. An initial period of stable crack growth is followed by a local crack instability when a load path fails (for fail-safe multiple load path structure) or unstable crack propagation occurs (for fail-safe crack-arrest structure). After the remaining members survive the initial load-path failure or the unstable crack is arrested, there is another period of stable crack growth.

Correspondingly, the three requirements for fail-safe structure are as follows. Prior to local crack instability the structure with a specified extent of initial or inspectable damage must be capable of sustaining the specified residual strength load at all times throughout one inspection period without load path failure or local crack instability. Secondly, when the load path fails or the crack becomes locally unstable, the remaining structure must have a static residual strength capable of sustaining the load path failure load times a specified dynamic factor. Thirdly, after load path failure the remaining damaged structure, with a specified degree of inspectability, must be capable of sustaining a specified residual strength load throughout a specified number of inspection periods without total failure of the structure.

The first two requirements for fail-safe structure may be satisfied in either of two ways, depending on the type of inspection selected. Both alternative ways are shown in Figure A-3. For in-service noninspectable damage the initial crack size is the size  $a_{LT}$  assumed at the start of the lifetime of the fail-safe structure; the inspection interval is one design lifetime; the residual strength load is  $P_{LT}$ ; and the dynamic load is  $P_{LT}$  times Dynamic Factor, D.F. (Section 3.1.3 of MIL-A-83444). For depot- or base-level inspectable damage the initial crack size is  $a_{DM}$ ; the typical inspection interval is 1/4 design lifetime; the residual strength load is  $P_{DM}$ ; and the dynamic load is  $P_{DM}$  times D.F.

The third requirement for fail-safe structure may be satisfied in any of five ways, depending upon the level of inspectability of the damage subsequent to load path failure or crack arrest. Inspectability depends not only upon damage size but also accessibility. Thus, the damage subsequent to load path failure or crack arrest may be in-flight evident ( $\ell_{FE}$ ), ground evident ( $\ell_{GE}$ ), walkaround inspectable ( $\ell_{WV}$ ), special visual inspectable ( $\ell_{SV}$ ), or depot- or base-level inspectable ( $\ell_{DM}$ ). Each of these inspectability levels is defined in Section 6.2 of Reference 1. Table A-1 shows the required crack growth period and residual strength load corresponding to each of these five alternatives. Both the required crack growth period and the required residual strength load are listed in order by increasing magnitude. Therefore, the more readily inspectable the remaining damage, the easier it is to satisfy this requirement.

APPENDIX B  
SPECIMEN DRAWINGS

The drawings of the structural specimens are included either in this appendix or in the main text of this volume, according to Table B-1.

TABLE B-1. DIMENSIONED DRAWINGS FOR STRUCTURAL SPECIMENS

| Specimen Type | Specimen Description         | Figure Number |
|---------------|------------------------------|---------------|
| 4.6A-X        | Thick Double Lap Joint       | 2             |
| 4.6B-X        | Thin Double Lap Joint        | 3             |
| 4.7-X         | Single Lap Joint             | 4             |
| 4.8-1-X       | Tee Stringer/Continuous Skin | B-1           |
| 4.8-3-X       | Tee Stringer/Split Skin      | B-1           |
| 4.9-X         | Edge Stringer                | B-2           |
| 4.10-X        | Two Bay                      | B-3           |



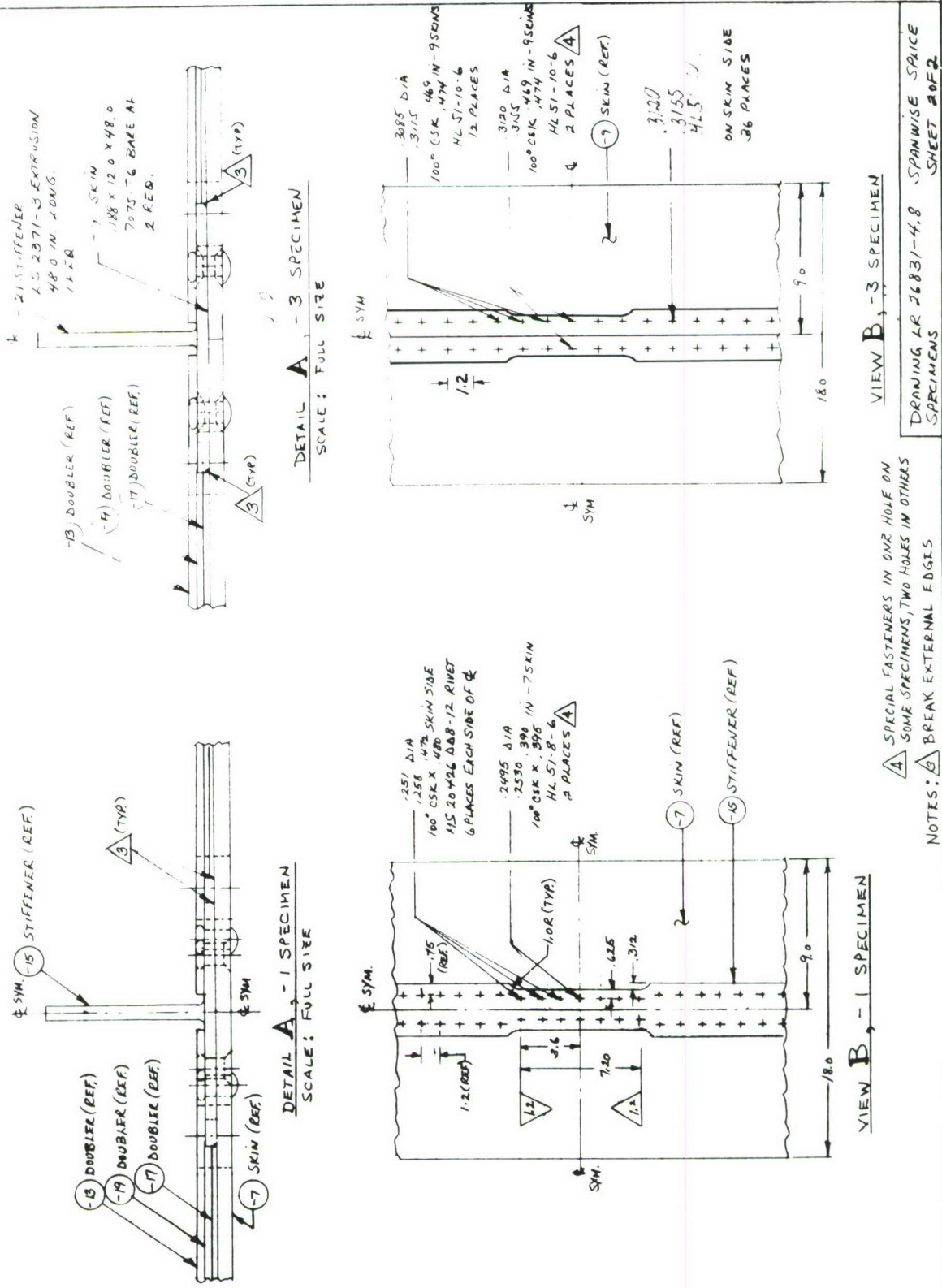


Figure B-1. Drawing for Tee-Reinforced Panel (Sheet 2 of 2)

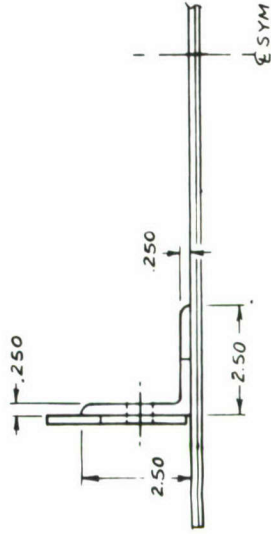


Figure B-2. Drawing for Edge Stringer Specimens

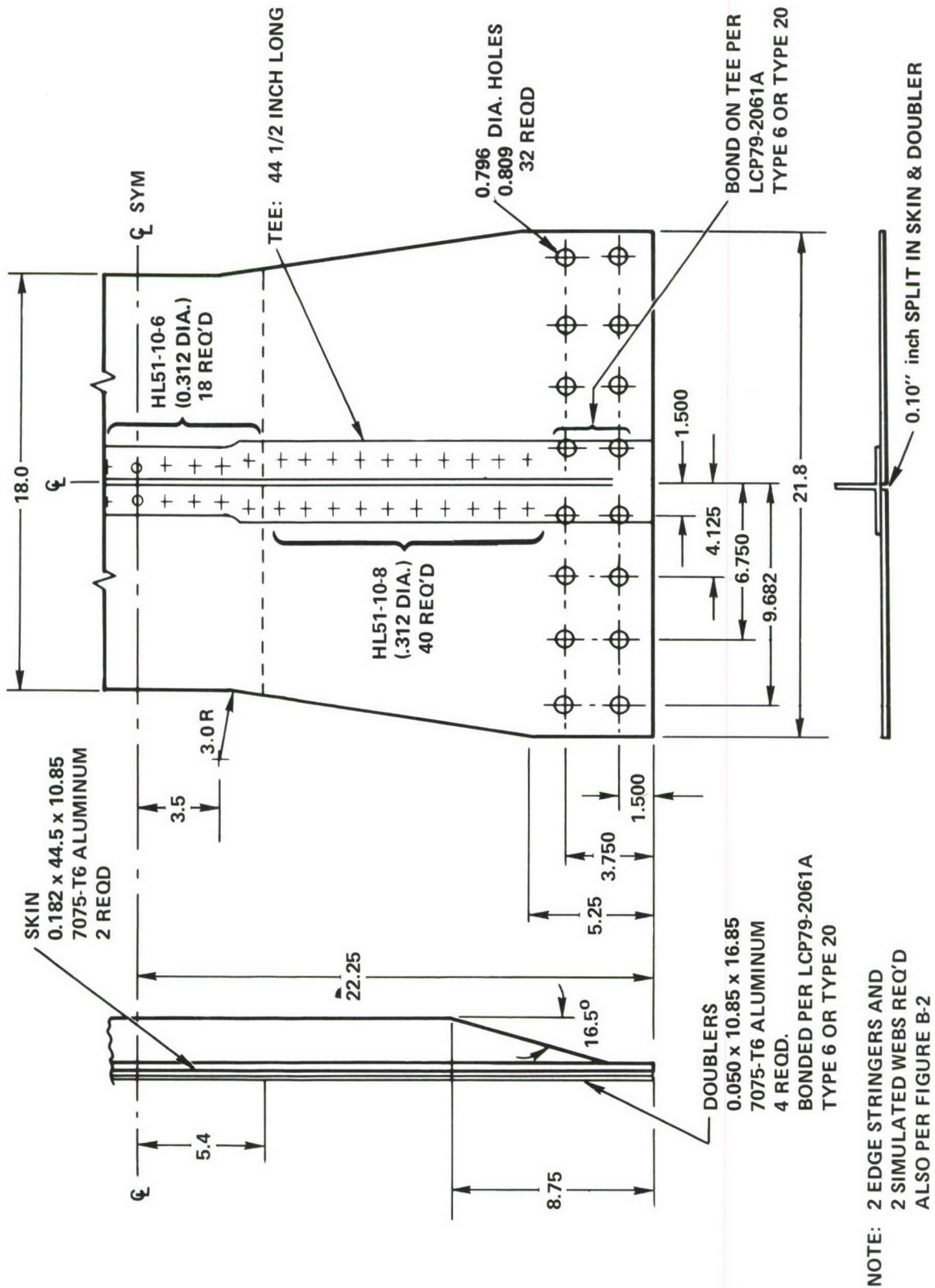


Figure B-3. Two-Bay Specimen, Type 4.10-X

## APPENDIX C

### FATIGUE TESTS OF CONTINUING DAMAGE FLAWS

(The work discussed in this appendix was conducted under other funding and reported in Reference 55. Because of the relevance of this work, the following is excerpted from Reference 55.)

For damage tolerance testing of complex structure it is not feasible to fatigue-induce a controlled precrack at more than one fastener hole per structural member. Therefore an alternate technique was required for complex structural specimens to induce continuing damage flaws equivalent to the 0.005 inch radius fatigue-induced cracks required in Reference 1.

Figure C-1 illustrates schematically what is meant by equivalent initial flaws. For two flaws to be equivalent, their growth histories must merge at some point in time. Furthermore, the crack size when the merging occurs must be fairly small (0.050 inch, for example) so that prior differences in flaw size do not significantly affect the nucleation or growth of neighboring cracks.

Preliminary spectrum fatigue tests were conducted on specimens with a razor-induced flaw at the edge of a 0.250-inch diameter hole. Data were obtained for 6 holes with 0.035-inch razor-induced flaws and 6 holes with 0.014-inch razor-induced flaws. A crack growth analysis was used to estimate the time required for a 0.005-inch fatigue-induced corner crack to grow to a length of 0.050 inch under the same loading spectrum. By interpolation, it was estimated that a 0.020-inch razor induced flaw would require the same time. Thereby it was hypothesized that a 0.020-inch razor-induced flaw is equivalent to a 0.005-inch fatigue-induced crack.

#### C.1 CONTINUING DAMAGE FLAW TEST PROGRAM

Following the preliminary tests, an extensive fatigue test program was conducted to compare the fatigue lives of fastener-hole specimens having 0.005-inch fatigue-induced initial cracks and 0.020-inch razor blade-induced

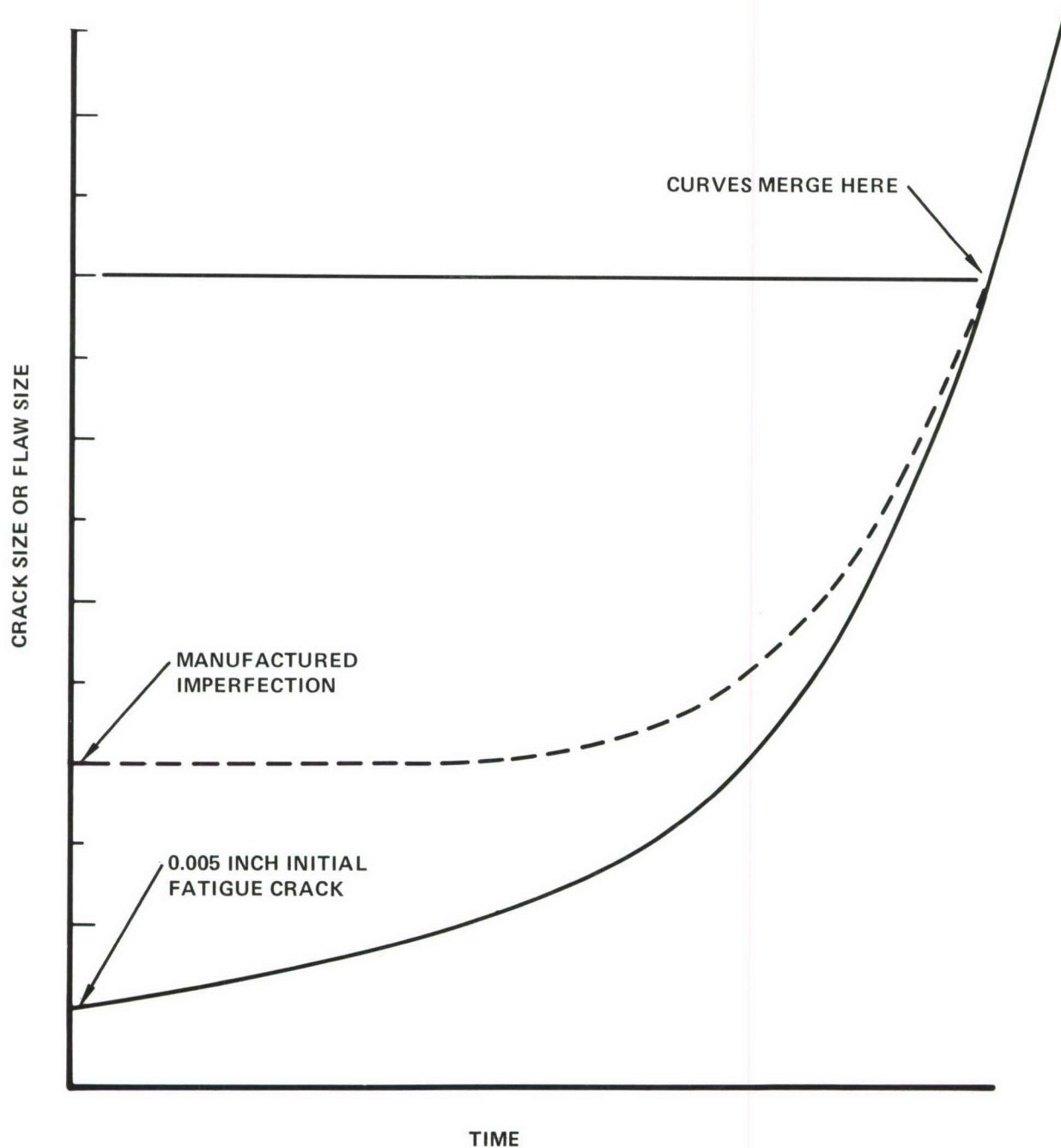


Figure C-1. Equivalence Between Manufactured Imperfections and 0.005-inch Fatigue Cracks

initial flaws. The objective was to verify the razor notch technique as an inexpensive method to introduce "continuing damage flaws" equivalent to 0.005-inch fatigue precracks.

The comparison of 0.005-inch fatigue cracks and 0.020-inch razor notches was made under the five conditions shown in Figure C-2. Three types of specimens were tested: an open hole specimen (gross area stress concentration factor of 3.1), a 1-1/2 dogbone specimen with a single fastener (medium load transfer), and a five-fastener single lap shear specimen with a slot connecting two fasteners to simulate an arrested crack (high load transfer). These specimens are shown in Figures 31, 33, and 34c of Section IV. The open hole specimen was tested under three different stress history conditions: constant amplitude,  $R = 0.1$ , maximum stress  $S_{\max} = 22.8$  ksi; constant amplitude,  $R = 0.1$ ,  $S_{\max} = 36.5$  ksi; and flight simulation loading with the 80-flight periodic loading sequence shown in Figure 8 of Section II. The 1-1/2 dogbone specimen was tested under constant amplitude loading,  $R = 0.1$  and maximum stress  $S_{\max} = 22.8$  ksi while the high-load transfer specimen was tested under constant amplitude loading,  $R = 0.1$ , and maximum stress  $S_{\max} = 12$  ksi. The five conditions were selected to cover a diverse range, and at the same time relate to the test conditions anticipated in complex aircraft structure.

The test specimens were fabricated from 0.187-inch-thick 7075-T6 sheet. Fasteners were 0.375-inch diameter protruding-head steel Hi-loks. Consistent with the requirements of Reference 1, a clearance fit was used for all fasteners and only a nominal torque was used (finger tight) to avoid beneficial clamping forces. Flaws in the fastened specimens were placed on the faying surface in the location of maximum stress.

The 0.005 inch fatigue cracks were induced in the following sequence of operations: (1) The piece was machined with a hole diameter 0.040 inch under-size. (2) A 0.014-inch razor notch was cut at one corner of the hole. (3) Cyclic bending was used to initiate a crack until the total length of the razor notch and crack was precisely 0.025 inch. Four-point bending was used as depicted in Figure C-3 (nominal stress = about 28 ksi). Great care was

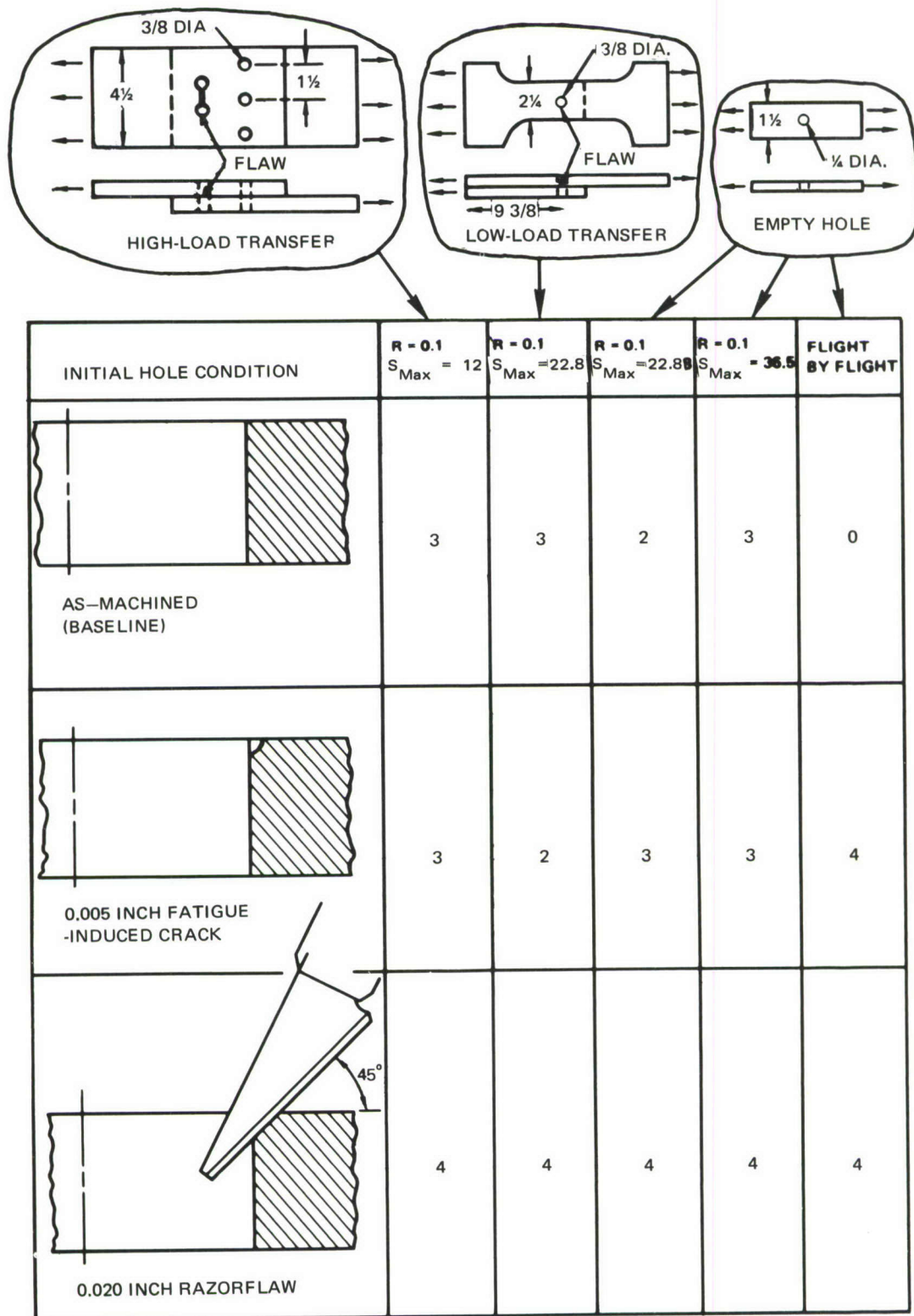
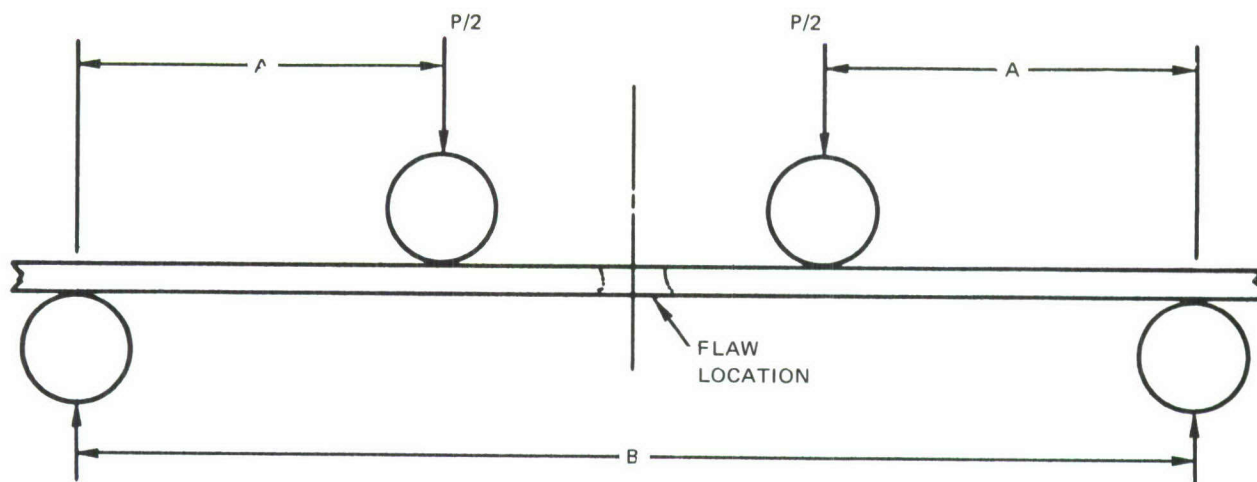


Figure C-2. Continuing Damage Flaw Tests Conducted



| SPECIMEN TYPE |             | A    | B    |
|---------------|-------------|------|------|
| FIGURE 31.    | OPEN HOLE   | 1.5" | 4.5" |
| FIGURE 34C.   | 1½ DOG BONE | 2.5  | 8.0  |
| FIGURE 33.    | LAP SHEAR   | 1.75 | 8.0  |

Figure C-3. Set-up for Inducing 0.005-Inch Cracks in Bending

needed here to keep the rejection rate under 25 percent. (4) The hole diameter was then enlarged 0.040-inch, leaving only a 0.005-inch corner crack at one edge of the hole.

The 0.020-inch razor notches were induced by hand as follows: A new X-ACTO blade No. 11 was coated with abrasive diamond paste. The blade was then oriented at a 45 degree angle to the specimen face and carefully located at the desired point. After seating the blade with a light sawing action, the pressure was increased to a constant maximum value. This pressure was maintained for 75 sawing strokes. (The actual notching of the specimen was preceded by several practice runs on a piece of scrap 7075-T6 aluminum to get the feel of the maximum pressure required to achieve a 0.020 notch in 75 strokes.) The pressure was then diminished and 25 to 50 strokes were made at a significantly reduced pressure to sharpen the flaw tip. Using this procedure no specimens were rejected, although one flaw was 0.027 inch instead of 0.020 inch.

Baseline fatigue tests without preflaws were run for the four constant amplitude loading test conditions. This allowed the data to be reviewed in terms of the reduction in fatigue life due to the flaws. No baseline spectrum fatigue data were run but tests run earlier on another heat of 3/16 inch thick bare 7075-T6 sheet showed an average life of 12,230 flights for this loading history .

A number of replications of each test condition were run to obtain a good estimate of the geometric mean life. The number of replications varied between two and four. In general, the first two tests were deemed adequate when nearly identical test lives were obtained.

## C.2 TEST RESULTS AND DISCUSSION

Tables C-1 through C-3 summarize the fabrication and testing history for each specimen and identify by number the laboratory data sheets on which the raw data were recorded.

The test lives are compared in Figure C-4. For each of the five test conditions the scale is normalized by the geometric mean fatigue life of the unflawed specimen. The individual data points are shown to indicate scatter.

For all five test conditions, the geometric mean lives for razor-flawed specimens and fatigue-flawed specimens were approximately equal. The ratio of these mean lives (life of razor-notched specimens divided by life of pre-cracked specimens) was bounded between 0.89 and 1.24.

The reduction in fatigue life due to precracking or notching is indicated in Figure C-4 by the difference between the length of the bar marked "no predamage" and the corresponding length for the precracked or razor-notched condition. The magnitude of this reduction in life is an indicator of the severity of the precrack or notch. The ratio of the mean reduction in life due to razor notching to that due to precracking was bounded between 0.89 and 1.14 for all five test conditions.

Figure C-5 shows the fracture surfaces from the spectrum tests. The fracture surface marking capability of the 80-flight loading sequence is utilized to demonstrate how the flaw shape develops. First note the

similarity in flaw shape histories for the 0.005-inch precracked specimens and the 0.020-inch razor-flawed specimens, both of which grew as quarter-circular corner flaws. Then contrast that to the flaw shape for the unflawed case. This flaw initiated at several points through the thickness on both sides of the hole and grew as a double through-the-thickness crack.

On the basis of these data, the 0.005-inch fatigue crack and the 0.020-inch razor notch were concluded to be equivalent in 7075-T6 Aluminum sheet.

TABLE C-1. SUMMARY OF DATA FOR UNFLAWED FATIGUE SPECIMENS

| Specimen Number | Geom. See Figure | Thickness t (Inch) | Width W (Inch) | Hole Diameter D (Inch) | Fastener Diameter (Inch) | Notes See Note No. | Type of Loading Spectrum OR C/A | Max Load P (Kip) | Max Stress P/Wt (Ksi) | Life to Failure $N_f$ (Cycles) | Data Sheet (Pg No.) |
|-----------------|------------------|--------------------|----------------|------------------------|--------------------------|--------------------|---------------------------------|------------------|-----------------------|--------------------------------|---------------------|
| 7B-3            | 31               | 0.1817             | 1.504          | [0.25]                 | -                        |                    | R = 0.1                         | 6.231            | 22.8                  | 64,957                         | 529065              |
| 7B-4            | 31               | 0.1805             | 1.505          | [0.25]                 | -                        |                    | R = 0.1                         | 6.192            | 22.8                  | 64,501                         | 529065              |
| 7B-1            | 31               | 0.182              | 1.502          | [0.25]                 | -                        | 1                  | R = 0.1                         | 9.692            | 35.45                 | 11,301                         | 529065              |
| 7B-5            | 31               | 0.1811             | 1.503          | [0.25]                 | =                        |                    | R = 0.1                         | 9.922            | 35.45                 | 7,155                          | 529065              |
| 7B-11           | 31               |                    |                |                        |                          |                    | R = 0.1                         |                  | 36.45                 | 6,798                          | 529066              |
| 4B              | 34c              | 0.1803             | 2.250          | 0.3753                 | 0.3738                   |                    | R = 0.1                         | 9.257            | 22.8                  | 16,460                         | 563307              |
| 3A              | 34c              | 0.1801             | 2.250          | 0.3764                 | 0.3742                   |                    | R = 0.1                         | 9.234            | 22.8                  | 18,280                         | 563308              |
| 2B-3            | 34c              | 0.1804             | 2.2557         |                        |                          | 2                  | R = 0.1                         | 9.277            | 22.8                  | 16,550                         | 555037              |
| 3A-2            | 33               | 0.1806             | 4.50           | 0.3750                 | 0.3739                   |                    | R = 0.1                         | 9.756            | 12.0                  | 7,000                          | 563304              |
| 3A-3            | 33               | 0.1807             | 4.50           | 0.3753                 | 0.3742                   |                    | R = 0.1                         | 9.756            | 12.0                  | 8,320                          | 563305              |
| 3A-4            | 33               | 0.1806             | 4.50           | 0.3754                 | 0.3750                   |                    | R = 0.1                         | 9.756            | 12.0                  | 8,110                          | 563306              |

## NOTES:

- (1) Stress 1 ksi lower than intended. Corrected life for 36.45 ksi would be
- $$N_f = 11,301 \times \left( \frac{35.45}{36.45} \right)^{4.3} = 10,030$$
- (2) This specimen was precracked, but precrack was placed on outer surface when assembled, so it did not affect the life. See Table C-2.

TABLE C-2. SUMMARY OF DATA FOR SPECIMENS WITH 0.005 INCH FATIGUE-INDUCED INITIAL CRACKS

| Specimen Description |             |             |              | Precracking: Geometry, Loading During Precracking, Flaw Size |                 |             |              |                       |             |            |                     |                    |                     | Geometry After Hole Enlargement For .005 <sup>th</sup> Crack |                    |                                     | Test Conditions And Results |             |                                  |                    |        |
|----------------------|-------------|-------------|--------------|--|-----------------|-------------|--------------|-----------------------|-------------|------------|---------------------|--------------------|---------------------|--|--------------------|-------------------------------------|-----------------------------|-------------|----------------------------------|--------------------|--------|
| Specimen Number      | Geom.       | Thickness   | Width        | Hole Diameter  | Razor Flaw Size | Max Load    | Moment Arm   | Bending Stress        | Range Ratio | Cycles     | Final Flaw Size     | Data Sht. Page No. | Dia. of Flawed Hole | Fastener Dia.  | Initial Crack Size | Type of Loading                     | Max. Load                   | Max. Stress | Life to Failure                  | Data Sht. Page No. |        |
|                      | See Figure: | t           | W            | d  | C <sub>O</sub>  | P'          | "A" (FIG. 4) | 3P'A/t <sup>2</sup> W |             |            | C <sub>O</sub> + ΔC |                    | D                   |  | a <sub>O</sub>     | Spectrum or C/A                     | P                           | P/Wt        | N <sub>f</sub> Cycles or Flights |                    |        |
| Tested               |             |             |              |  |                 |             |              |                       |             |            |                     |                    |                     |  |                    |                                     |                             |             |                                  |                    |        |
| 7A-1                 | 11          | .182        | 1.50         | [.2075]  | .0138           | .340        | 1.5          | 30.8                  | 0.1         | 11,572     | .0255               | 500377             | .251/.253 ②         | -  | .0045              | Spectrum                            | 11.47                       | 42          | 6439                             | 554822             |        |
| 7A-2                 | 11          | .1814       | 1.5025       | [.2075]  | .0135           | .275        | 1.5          | 25.0                  | 0.1         | 30,349     | .0275               | 500377             |                     | -  | .009               | Spectrum                            | 11.45                       | 42          | 5200                             | 554826             |        |
| 7A-3                 | 11          | .1815       | 1.5014       | [.2075]  | .0135           | .275        | 1.5          | 25.0                  | 0.1         | 59,590     | .047                | 500378             | .251                | -  | .007               | Spectrum                            | 11.45                       | 42          | 6060                             | 554824             |        |
| 7A-5                 | 11          | .1817       | 1.5027       | [.2075]  | .0130           | .300        | 1.5          | 27.2                  | 0.1         | 65,500     | .0247               | 500379             | .246                | -  | .007               | Spectrum                            | 11.47                       | 42          | 5750                             | 554825             |        |
| 7A-8                 | 11          | .1818       | 1.503        | [.2075]  | .013            | .300        | 1.5          | 27.2                  | 0.1         | 118,000    | .028                | 500381             | .252                | -  | .006               | R=0.1                               | 6.229                       | 22.8        | 11769                            | 554831             |        |
| 7A-9                 | 11          | .1812       | 1.504        | [.2075]  | .012            | .300        | 1.5          | 27.3                  | 0.1         | 79,000     | .0224               | 500382             | .2406               | -  | .007               | R=0.1                               | 6.218                       | 22.8        | 12585                            | 554829             |        |
| 7A-13                | 11          | .1817       | 1.503        | [.2075]  | .0165           | .280        | 1.5          | 25.4                  | 0.05        | 146,000    | .0255               | 500384             | .248                | -  | .004               | R=0.1                               | 6.227                       | 22.8        | 12219                            | 554830             |        |
| 7A-4                 | 11          | .1818/.1822 | 1.5022/1.504 | [.2075]  | .0130           | .300        | 1.5          | 27.1                  | 0.1         | 47,000     | .0260               | 500379             | .249/.256           | -  | .004               | R=0.1                               | 9.965                       | 36.45       | 3549                             | 554832             |        |
| 7A-10                | 11          | .1810/.1812 | 1.504        | [.2075]  | .0162           | .280        | 1.5          | 25.5                  | 0.05        | 36,900     | .0252               | 500382             | .252                | -  | .005               | R=0.1                               | 9.922                       | 36.45       | 4038                             | 554827             |        |
| 7A-14                | 11          | .1821       | 1.503/1.504  | [.2075]  | .013            | .280        | 1.5          | 25.3                  | 0.05        | 65,000     | .0253               | 500384             | .247                | -  | .006               | R=0.1                               | 9.984                       | 36.45       | 3228                             | 554828             |        |
| 2B-2                 | 12          | .1803       | 2.2509       | [.335]   | .014            | .275        | 2.5          | 28.2                  | 0.05        | 15,000     | .0275               | 529429             | .3820               | [.374]   | .0047              | R=0.1                               | 9.252                       | 22.8        | 9810                             | 555039             |        |
| 2B-4                 | 12          | .1812/.1807 | 2.253/2.2503 | [.335]   | .012            | .275        | 2.5          | 28.0                  | 0.05        | 43,750     | .0245               | 529431             | .3756               | [.374]   | .0056              | R=0.1                               | 9.270                       | 22.8        | 9290                             | 555036             |        |
| 3B-2                 | 13          | .1813/.1803 | 4.502        | [.335]   | .0136           | .750        | 1.75         | 26.8                  | 0.05        | 27,200     | .0235               | 500386             | .3742/.3752         | [.374]   | .0032              | R=0.1                               | 9.744                       | 12.0        | 2400+                            | 555040             |        |
| 3B-3                 | 13          | .182/.1802  | 4.502        | [.335]   | .018            | .800/.700 ③ | 1.75         | 28.4/24.9             | 0.05        | 30000/3200 | .021/.025           | 500385             | .3747               | [.374]   | .0050              | R=0.1                               | 9.732                       | 12.0        | 2498                             | 555041             |        |
| 3B-4                 | 13          | .1813/.1803 | 4.504        | [.335]   | .0156           | .700        | 1.75         | 25.0                  | 0.05        | 29,600     | .0242               | 500387             | .3750               | [.374]   | .0030              | R=0.1                               | 9.744                       | 12.0        | 2520                             | 555042             |        |
| Invalid Tests:       |             |             |              |  |                 |             |              |                       |             |            |                     |                    |                     |  |                    |                                     |                             |             |                                  |                    |        |
| 2B-1                 | 12          | .1808       | 2.2508       | [.335]   | [.014]          | .290        | 2.5          | 29.6                  | 0.05        | 18,000     | .0235               | 529427-9           | .3748               | [.374]   | .0041              | Doubler Cracked from Earlier Test.  |                             |             |                                  |                    | 555038 |
| 2B-3                 | 12          | .1807       | 2.254        | [.335]   | .0155           | .275        | 2.5          | 28.0                  | 0.05        | 56,000     | .025                | 529430             | .3765               | [.374]   | .0045              | Assembled Backwards. Crack Outside. |                             |             |                                  |                    | 555037 |
| Not Tested:          |             |             |              |  |                 |             |              |                       |             |            |                     |                    |                     |  |                    |                                     |                             |             |                                  |                    |        |
| 7A-6                 | 11          | [.181]      | [1.5]        | [.2075]  | .014            | .300        | 1.5          | 27.5                  | 0.1         | 35,510     | .081                | 500380             |                     |  |                    |                                     |                             |             |                                  |                    |        |
| 7A-7                 | 11          | [.181]      | [1.5]        | [.2075]  | .012            | .300        | 1.5          | 27.5                  | 0.1         | 115,000    | .012                | 500381             |                     |  |                    |                                     |                             |             |                                  |                    |        |
| 7A-11                | 11          | .1806       | 1.502        | [.2075]  | .013            | .280        | 1.5          | 25.7                  | 0.05        | 267,000    | .0395               | 500383             |                     |  |                    |                                     |                             |             |                                  |                    |        |
| 7A-12                | 11          | .1814       | 1.507        | [.2075]  | .016            | .280        | 1.5          | 25.4                  | 0.05        | 105,000    | .035                | 500383             |                     |  |                    |                                     |                             |             |                                  |                    |        |
| 3B-1                 | 13          | .1814       | 4.5          | [.335]   | .0125           | .900        | 1.75         | 31.9                  | 0.05        | 10,000     | .041                | 500385             | .4072               | [.374]   | .0039              |                                     |                             |             |                                  |                    |        |

NOTES:

- (1) Dimensions in brackets are nominal sizes where no laboratory measurements were recorded.  
(2) Double entries for the dimensions t, W and D denote different laboratory measurements made at different times.  
(3) In precracking specimen 3B-3 a .021 inch flaw was achieved at a load of 800 pounds. Precracking was completed at a reduced load of 700 pounds.

TABLE C-3. SUMMARY OF DATA FOR RAZOR-FLAWED SPECIMENS

| Specimen Number | Geom See Figure | Thickness $t$ (Inch) | Width $W$ (Inch) | Dia. of Flawed Hole $D$ (Inch) | Fastener Diameter (Inch) | Initial Flaw Size $A_o$ (Inch) | Type of Loading Spectrum or C/A | Max Load $P$ (Kip) | Max Stress $P/Wt$ (Ksi) | Life to Failure $N_f$ Cycles or Flights | Data Sheet (Pg No.) |
|-----------------|-----------------|----------------------|------------------|--------------------------------|--------------------------|--------------------------------|---------------------------------|--------------------|-------------------------|---|---------------------|
| 7B-17           | 31              | 0.1819               | 0.1503           | 0.248                          | -                        | 0.019                          | Spectrum                        |                    | 42.0                    | 5,320                                   | 554843              |
| 7B-20           | 31              | 0.1807               | 1.502            | 0.247                          | -                        | 0.018                          | Spectrum                        |                    | 42.0                    | 5,870                                   | 554844              |
| 7B-23           | 31              | 0.1808               | 1.502            | 0.245                          | -                        | 0.019                          | Spectrum                        |                    | 42.0                    | 5,920                                   | 554845              |
| 7B-26           | 31              | 0.1813               | 1.502            | 0.245                          | -                        | 0.023                          | Spectrum                        |                    | 42.0                    | 4,360                                   | 554846              |
| 7B-16           | 31              | 0.1812               | 1.502            | 0.248                          | -                        | 0.022                          | R = 0.1                         | 6.206              | 22.8                    | 13,390                                  | 554835              |
| 7B-19           | 31              | 0.1807               | 1.503            | 0.248                          | -                        | 0.017                          | R = 0.1                         | 6.192              | 22.8                    | 16,720                                  | 554836              |
| 7B-22           | 31              | 0.1810               | 1.502            | 0.245                          | -                        | 0.022                          | R = 0.1                         | 6.199              | 22.8                    | 13,030                                  | 554841              |
| 7B-25           | 31              | 0.1815               | 1.503            | 0.246                          | -                        | 0.024                          | R = 0.1                         | 6.221              | 22.8                    | 14,370                                  | 554842              |
| 7B-15           | 31              | 0.1816               | 1.503            | 0.248                          | -                        | 0.019                          | R = 0.1                         | 9.947              | 36.45                   | 3,440                                   | 554837              |
| 7B-18           | 31              | 0.1808               | 1.502            | 0.248                          | -                        | 0.022                          | R = 0.1                         | 9.899              | 36.45                   | 3,910                                   | 554838              |
| 7B-21           | 31              | 0.1821               | 1.502            | 0.247                          | -                        | 0.021                          | R = 0.1                         | 9.969              | 36.45                   | 4,170                                   | 554839              |
| 7B-24           | 31              | 0.1808               | 1.503            | 0.245                          | -                        | 0.020                          | R = 0.1                         | 9.903              | 36.45                   | 3,030                                   | 554840              |
| 2B-12           | 34c             | 0.181                | 2.253            | 0.375+                         | 0.3744                   | 0.0238                         | R = 0.1                         | 9.298              | 22.8                    | 5,760*                                  | 555043              |
| 2B-11           | 34c             | 0.1802               | 2.234            | 0.375+                         | 0.3740                   | 0.0206                         | R = 0.1                         | 9.179              | 22.8                    | 8,410*                                  | 555044              |
| 2B-13           | 34c             | 0.1807               | 2.252            | 0.375+                         | 0.3740                   | 0.0208                         | R = 0.1                         | 9.277              | 22.8                    | 8,990                                   | 563311              |
| 2B-14           | 34c             | 0.1803               | 2.253            | 0.375+                         | 0.3740                   | 0.0214                         | R = 0.1                         | 9.261              | 22.8                    | 8,700                                   | 563312              |
| 2B-15           | 34c             | 0.1802               | 2.254            | 0.3770                         | [0.374]                  | 0.021                          | R = 0.1                         | 9.257              | 22.8                    | 9,570                                   | 563315              |
| 3A-6            | 33              | 0.1812               | 4.502            | 0.375+                         | [0.374]                  | 0.0243                         | R = 0.1                         | 9.790              | 12.0                    | 7,810*                                  | 555045              |
| 3A-5            | 33              | 0.1805               | 4.501            | 0.375+                         | [0.374]                  | 0.021                          | R = 0.1                         | 9.749              | 12.0                    | 4,370*                                  | 555046              |
| 3A-7            | 33              | 0.181                | 4.501            | 0.375+                         | [0.374]                  | 0.0205                         | R = 0.1                         | 9.780              | 12.0                    | 3,760                                   | 563313              |
| 3A-8            | 33              | 0.181                | 4.501            | 0.375+                         | [0.374]                  | 0.027                          | R = 0.1                         | 9.776              | 12.0                    | 5,360                                   | 563314              |
| 3A-9            | 33              | 0.181                | 4.501            | 0.3770                         | [0.374]                  | 0.0227                         | R = 0.1                         | 9.776              | 12.0                    | 1,970                                   | 563316              |
| 3A-10           | 33              | 0.181                | 4.502            | 0.3770                         | [0.374]                  | 0.0240                         | R = 0.1                         | 9.779              | 12.0                    | 2,210                                   | 563317              |

\*Electronics problems with the load cell on these tests.

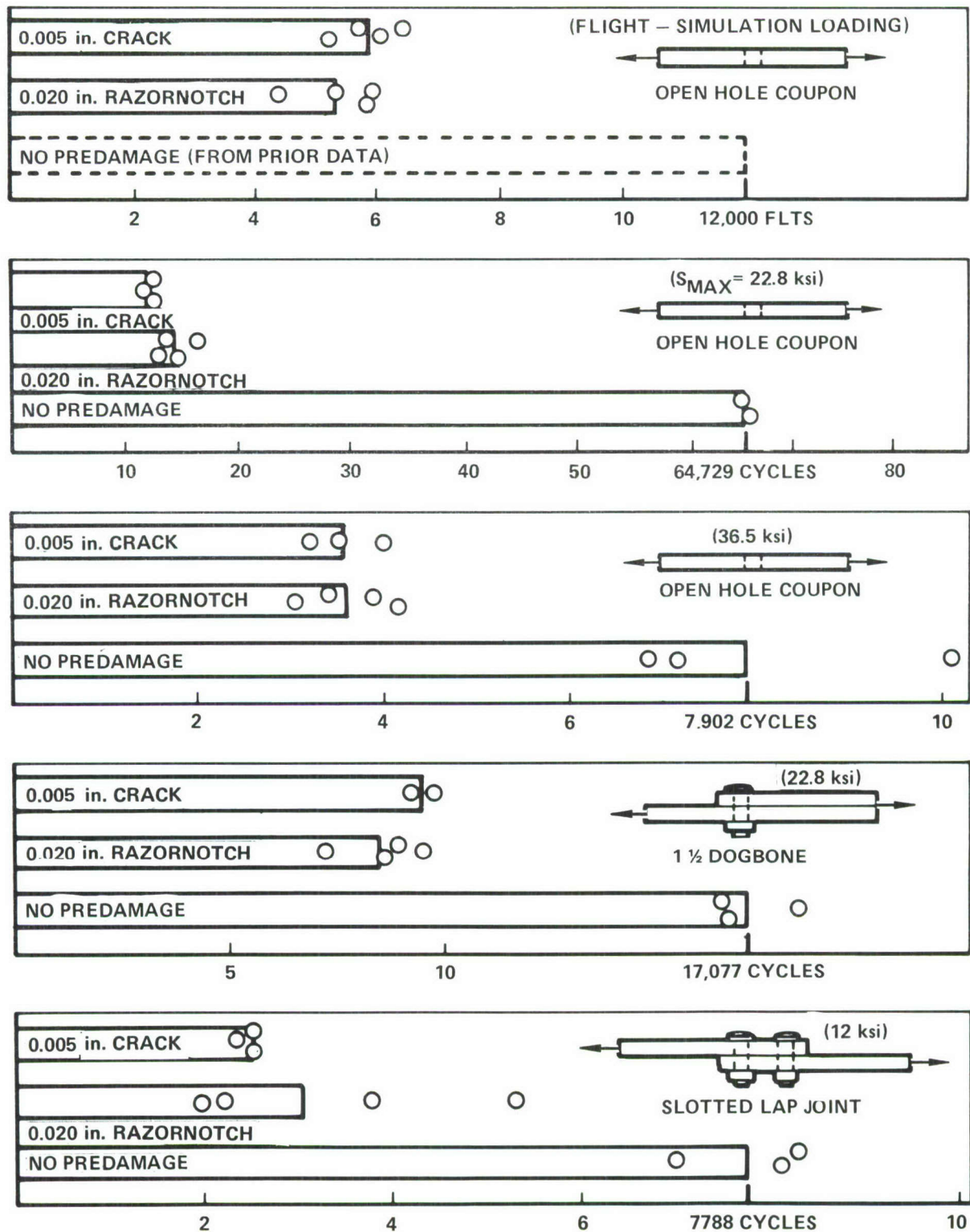


Figure C-4. Summary of Test Results for Continuing Damage Flaws

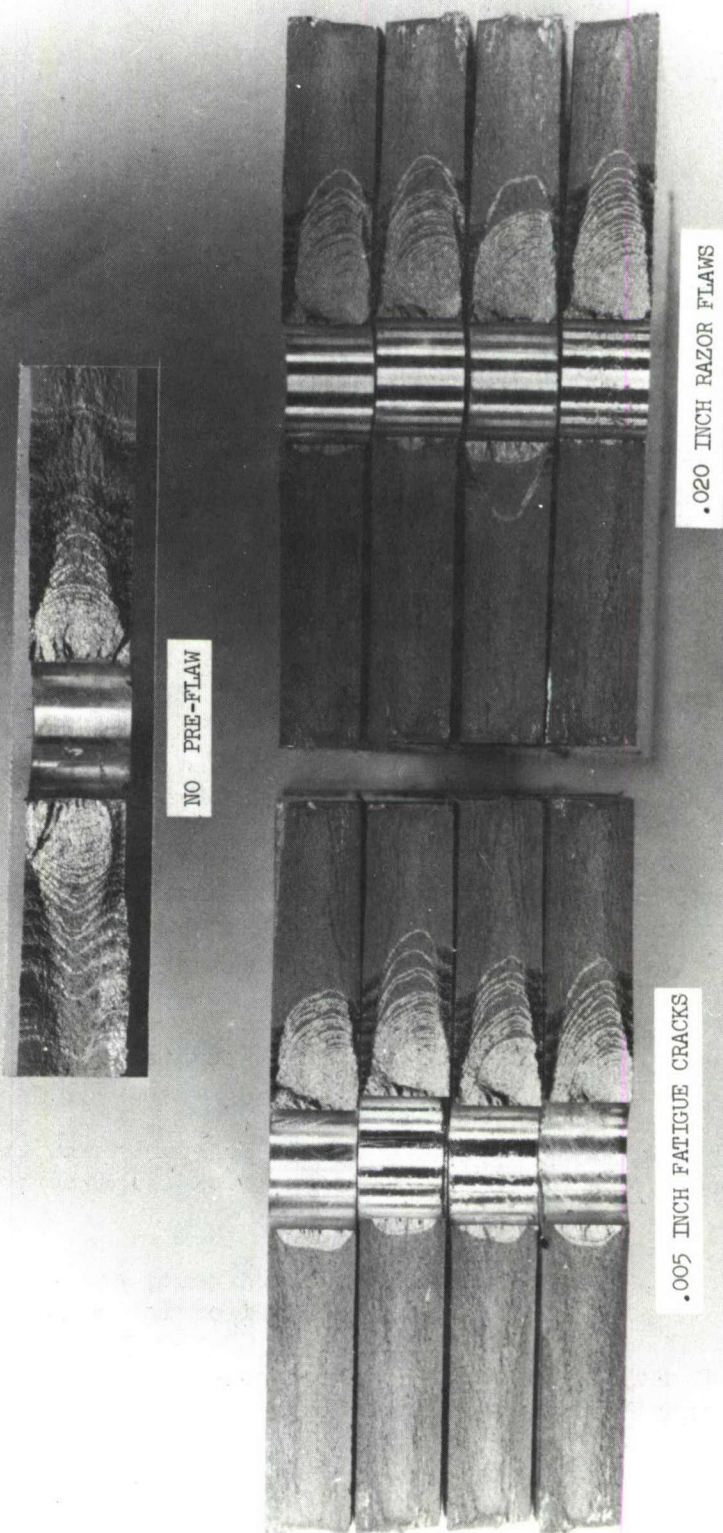


Figure C-5. Fracture Surfaces Showing Equivalent Flaw Front Shapes for 0.005-Inch Cracks and 0.020-Inch Notches

## REFERENCES

1. "Airplane Damage Tolerance Design Requirements," MIL-A-83444 (USAF), Military Specification, United States Air Force, May 1974.
2. Ekvall, J. C., Brussat, T. R., Liu, A. F. and Creager, M., "Engineering Criteria and Analysis Methodology for the Appraisal of Potential Fracture Resistant Primary Aircraft Structure," AFFDL-TR-72-80, Lockheed-California Company, Sept. 1972.
3. Rosenkranz, C., et al., "Advanced Lightweight Fighter Structural Concept Study," AFFDL-TR-72-98, Northrop Corporation, Aircraft Division, July 1972.
4. Pitman, W. A., et al., "Preliminary Design Technical Summary - Phase 1A, Wing Carrythrough Structure for an Advanced Metallic Air Vehicle," AFFDL-TR-72-65, Lockheed-Georgia Company, July 1972.
5. Staff Report, "Advanced Metallic Air Vehicle Structural Program," AFFDL-TR-72-75, General Dynamics, Convair Aerospace Division, June 1972.
6. Staff Report, "Preliminary Concept Evaluation for the Wing Carrythrough Structure of an Advanced Metallic Air Vehicle - Summary," AFFDL-TR-72-70, The Boeing Company, June 1972.
7. Brussat, T. R., "P-3 Service Life Evaluation -- Fatigue Crack Growth Analysis for W. S. 167," LR 26085, Lockheed-California Company, Nov. 1973.
8. Anon., "Final Report, F/RF-4C/D Damage Tolerance and Life Assessment Study," Report No. MDC A2883, Vol. 1, McDonnell Aircraft Company, June 1974.
9. Brussat, T. R., "Fatigue Crack Growth, Arrest, and Reinitiation Along a Row of Holes," LR 26806, Lockheed-California Company, Dec. 1974.
10. Hardrath, H. F., Leybold, H. A., Landers, C. B., and Hauschild, L. W., "Fatigue Crack Propagation in Aluminum Alloy Box Beams," NACA TN 3856, Aug. 1956.

11. Hardrath, H. F. and Leybold, H. A., "Further Investigation of Fatigue Crack Propagation in Aluminum Alloy Box Beams," NACA TN 4256, June 1958.
12. Foster, L. R. and Whaley, R. E., "Fatigue Investigation of Full-Scale Transport-Airplane Wings: Tests with Constant-Amplitude and Variable-Amplitude Loading Schedules," NASA TN D-547, Oct. 1960.
13. Van Beck, E. J., "Full-Scale Fatigue Tests on the Fokker 'Friendship'," in Full Scale Fatigue Testing of Aircraft Structures, edited by F. J. Plantema and J. Schijve, Pergamon, New York, 1961, pp 326-344.
14. Broek, D., "Crack Propagation and Residual Strength of Full-Scale Wing Center Sections," NLR-TM S-612, Amsterdam, Aug. 1964.
15. Schijve, J. and Broek, D., "Fatigue Test Results of Two Full-Scale Wing Center Sections Under Ground-to-Air Cycle Loading," NLR-TM S-635, Amsterdam, Apr. 1965.
16. Ketola, R. N., "Fatigue Test of Wing and Main Landing Gear," LR 13645, Lockheed-California Company, Apr. 1964.
17. Berman, L., "Fatigue Test of the Model TF-9J Airplane Wing," NAEC-ASL-1113, Aero. Structures Laboratory, Philadelphia, June 1967.
18. Bakow, L. "Fatigue Evaluation of L-1011-385-1-14/15 Airframe Flight Structure" LR 27219, Lockheed-California Company, July 1975.
19. Wood, H. A., Bader, R. M., Trapp, W. J., Hoener, R. F., and Donat, R. C., ed. Proceedings of the Air Force Conference on Fatigue and Fracture of Aircraft Structures and Materials, AFFDL-TR-70-144, Air Force Flight Dynamics Laboratory, Sept. 1970.
  - (a) Poe, C. C., "The Effect of Reveted and Uniformly Spaced Stringers on the Intensity Factor of a Cracked Sheet," pp. 207-216.
  - (b) Smith, S. H., Porter, T. R., and Engstrom, W. L., "Fatigue Crack Propagation Behavior and Residual Strength of Bonded Strap Reinforced, Lamellated and Sandwich Panels," pp. 611-634.
  - (c) Swift, T. and Wang, D. Y., "Damage Tolerant Design -- Analysis Methods and Test Verification of Fuselage Structure, pp. 653-683.
  - (d) Fitch, G. E., Jr., Jackman, R. E., and Horsfall, W. P., "The F-100 Aircraft Structural Integrity Program (ASIP)," pp. 723-753.
  - (e) Bryan, D. F., "The B-52G-H Wing Cyclic Test Program," pp. 755-778.

20. Kepert, J. L. and Payne, A. O., "Interim Report on Fatigue Characteristics of a Typical Metal Wing," NACA TM 1397, Mar. 1956.
21. Whaley, R. E., McGuigan, M. J., Jr. and Brian, D. F., "Fatigue Crack Propagation and Residual Static Strength Results on Full-Scale Transport-Airplane Wings," NACA TN 3847, Dec. 1956.
22. Whaley, R. E., "Fatigue Investigation of Full-Scale Airplane Transport Wings: Variable-Amplitude Tests with a Gust-Loads Spectrum," NACA TN 4132, Nov. 1957.
23. Broek, D. and DeRijk, P., "Fatigue Cracks in F-27 Wing Tension Skins Subjected to Random-Load Fatigue Tests," NLR Report M-2105, Amsterdam, Aug. 1962.
24. Wang, D. Y., "An Investigation on Fatigue Crack Propagation and Fail-safe Design of Stiffened Large Aluminum Alloy Panels with Various Crack Stoppers," Proceedings, AIAA/ASME 10th Structures, Structural Dynamics and Materials Conference, April 14-16, 1969, pp. 330-343.
25. Nelson, L. W., Melcon, M. A., and Simons, H., "The Lockheed L-1011 Tristar Fatigue and Fail-Safe Development Program" presented at the 7th Symposium of the International Committee on Aeronautical Fatigue, London, July 18, 1973.
26. Damage Tolerance in Aircraft Structures, ASTM STP 486, American Society for Testing and Materials, 1971.
  - (a) Poe, C. C., Jr., "Fatigue Crack Propagation in Stiffened Panels," pp. 79-97.
  - (b) Liu, A. F., and Ekvall, J. C., "Material Toughness and Residual Strength of Damage Tolerant Aircraft Structures," pp. 98-121.
27. Salvetti, A., Frediani, A., and Grassi, E., "Theoretical and Experimental Research on the Fatigue Behavior of Cracked Stiffened Panels," AD 769948, U. S. Army European Research Office, Feb. 1973.
28. Mackey, D. J. and Simons, H., "Structural Development of the L-1011 Tristar," AIAA Paper No. 72-776, Presented at the AIAA 4th Aircraft Design, Flight Test, and Operations Meeting, August 1972.
29. Jarfahl, L. E., "Optimum Design of Joints: The Stress Severity Factor Concept," Fifth ICAF Symposium, Melbourne, Australia, May 1967.
30. Creager, M. and Liu, A. F., "The Effect of Reinforcements on the Slow Stable Tear and Catastrophic Failure of Thin Metal Sheet," ASME Trans., J. Engrg. Mat. & Tech., Jan. 1974, pp. 49-55.

31. Vlieger, H. and Broek, D., "Residual Strength of Cracked Stiffened Panels," NLR-TN-653, National Aerospace Laboratory, The Netherlands, Dec. 1967.
32. Wang, D. Y., "An Investigation of Fatigue Crack Propagation and Fail-Safe Design of Stiffened Large Aluminum Alloy Panels with Various Crack Stoppers," in Proc. 10th ASME/AIAA Structures, Structural Dynamics and Materials Conference, New Orleans, Apr. 14, 1969.
33. Grandt, A. F., Jr., "Stress Intensity Factors for Some Throughcracked Fastener Holes," Int. J. Fracture, Vol. 11, 1975, pp. 283-294.
34. Byskov, E., "The Calculation of Stress Intensity Factors Using the Finite Element Method with Cracked Elements," Int. J. Fract. Mech., Vol. 6, 1970, pp. 159-167.
35. Creager, M., "Development of a Cracked Finite Element," LR 23996, Lockheed-California Company, Dec. 1970.
36. Chiu, S. T., "Formulation of Cracked Finite Elements," LR 25939, Lockheed-California Company, Sept. 1973.
37. Chu, C. S., Anderson, J. M., Batdorf, W. J., and Aberson, J. A., "Finite Element Computer Program to Analyze Cracked Orthotropic Sheets," NASA CR-2698, July 1976.
38. Pian, T. H. H., "Crack Elements," Proc. World Congress on Finite Element Methods in Structural Mechanics, Vol. I (edited by J. Robinson), Oct. 1975, pp. F.1-F.39.
39. Liu, A. F., "Stress Intensity Factor for a Corner Flaw," Engrg. Fracture Mech., Vol. 4, 1972, pp. 175-179.
40. Cartwright, D. J. and Rooke, D. P., "Approximate Stress Intensity Factors Compounded from Known Solutions," Engrg. Fracture Mech., Vol. 6, 1974, pp. 563-572.
41. Rooke, D. P. and Cartwright, D. J., "The Compounding Method Applied to Cracks in Stiffened Sheets," Engrg. Fracture Mech., Vol. 8, 1976, pp. 567-573.
42. Rooke, D. P. and Cartwright, D. J., Compendium of Stress Intensity Factors, Her Majesty's Stationery Office, London, 1976.
43. Tada, H., Paris, P., and Irwin, G., The Stress Analysis of Cracks Handbook, Del. Research Corp., Hellertown, Pa., 1973.

44. Pinckert, R. E., "Observations of Crack Origins in Aircraft Wing Structure," presented at meeting of Subcommittee 6 of Committee E-24, American Society for Testing and Materials, ASTM Headquarters, Phila., Pa., Oct. 9, 1974.
45. Irwin, G. R., "Analysis of Stresses and Strains Near the End of a Crack Traversing a Plate," ASME Trans., J. Appl. Mech., Vol. 24, 1957, pp. 361-364.
46. Rice, J.R., "Plastic Yielding at a Crack Tip," Proc. Int. Conf. Fracture, Sendai, Japan, 1965, pp. 283-308.
47. Tweed, J. and Rooke, D. P., "The Distribution of Stress Near the Tip of a Radial Crack at the Edge of a Circular Hole," Int. J. Engrg. Sci., Vol. 11, 1974, pp. 1185-1195.
48. Cornell, B. L. and Darby, L. G., "Correlation of Analysis and Test Data to the Effect of Fastener Load Transfer on Fatigue," AIAA Paper No. 74-983, Aug. 1974.
49. Peterson, R. E., Stress Concentration Factors, Wiley, 1974.
50. Isida, M., "On the Tension of a Strip with a Central Elliptic Hole," Trans. JSME, Vol. 21, 1955, pp. 507-518.
51. Bowie, O. L., "Analysis of an Infinite Plate Containing Radial Cracks Originating at the Boundaries of an Internal Circular Hole," J. Math. and Phys., Vol. 35, 1956, pp. 60-71.
52. Isida, M., "Stress Intensity Factors for the Tension of an Eccentrically Cracked Strip," ASME Trans , J. Appl. Mech., Vol. 33, 1966, pp. 674-675.
53. Feddersen, C. E., in Plane Strain Crack Toughness Testing, ASTM STP 410, 1967, p. 77.
54. Isida, M., "On the Determination of Stress Intensity Factors for Some Common Structural Problems," Engrg. Fract. Mech., Vol. 2, 1970, p. 61.
55. Young, L. and Brussat, T. R., "Summary of 1975 Independent Research in Fatigue and Fracture Mechanics Methods," LR 27298, Lockheed-California Company, Burbank, Ca., Dec. 1975.
56. Hall, L. R., Shah, R. C., and Engstrum, W. L., "Fracture and Fatigue Crack Growth Behavior of Surface Flaws and Flaws Originating at Fastener Holes; Vol. I - Results and Discussion," AFFDL-TR-74-47, Vol. 1, May 1974, p. 198.

57. Harris, H. G., Ojalvo, I. U., and Hoosen, R. E., "Stress and Deflection Analysis of Mechanically Fastened Joints," AFFDL-TR-70-49, May 1970.
58. Neuber, H., "Theory of Stress Concentration for Shear-Strained Prismatical Bodies with Arbitrary Nonlinear Stress-Strain Law," ASME Trans: J. Appl. Mech., Vol. 28, 1961, pp. 544-550.
59. Creager, M., "The Elastic Stress Field Near the Tip of a Blunt Crack," Masters Thesis, Lehigh University, Bethlehem, Pa., 1966.
60. Cyclic Stress-Strain Behavior - Analysis, Experimentation and Failure Prediction, ASTM STP 519, American Soc. for Testing and Materials, May 1973.
61. Pettit, D. E., and Pickel, F. M., "Experimental Techniques for Fracture Mechanics: R-Curve Test Procedures Evaluation," LR 27398, Lockheed-California Company, Nov. 1975.
62. Pettit, D. E., "Buckling Guide Considerations for CCT Specimens," Presented at ASTM Committee E24, Fall Meeting, Philadelphia, Pa., Oct. 1975.
63. "Proposed Recommended Practice for R-Curve Determination," 1975 ASTM Book of Standards, Part 10, Nov. 1975, pp. 811-825.
64. Irwin, G. R., "Fracture Testing of High Strength Sheet Materials Under Conditions Appropriate for Stress Analysis," NRL Report 5486, U. S. Naval Research Labs, July 27, 1960.
65. Eftis, J. and Liebowitz, H., "On the Modified Westergaard Equation for Certain Plane Crack Problems," Int. J. Fract. Mech., Vol. 8, No. 4., Dec. 1972, pp 383-391.
66. Newman, J. C., Jr., "Crack-Opening Displacements in Center-Crack, Compact, and Crack-Line Wedge-Loaded Specimens," NASA TN D 8268, July 1976.
67. Brussat, T.R., "An Approach to Predicting the Growth to Failure of Fatigue Cracks Subjected to Arbitrary Uniaxial Cyclic Loading," Damage Tolerance in Aircraft Structures, ASTM STP 486, 1971, pp. 122-143.
68. Walker, E. K., "The Effect of Stress Ratio During Crack Propagation and Fatigue for 2024-T3 and 7075-T6 Aluminum," Effects of Environment and Complex Load History on Fatigue Life, ASTM STP 462, Jan. 1970, pp. 1-14.
69. Lockheed Aircraft Company, Structural Life Assurance Manual, Section 16.

70. Ekvall, J. C., Young, L., and Bakow, L., "Fatigue Evaluation of Materials and Processes," Problems with Fatigue in Aircraft, Proc. 8th ICAF Symposium, Lausanne, Switzerland, June 2-5, 1975, p. 6.2/59.
71. Chiu, S. T. and Brussat, T. R. "Summary of 1976 Independent Research in Fracture Mechanics Analysis Methods," LR 27703, Lockheed-California Company, Dec. 1976.